Stromal Heterogeneity in Pancreatic Cancer

A thesis submitted to the University of Manchester for the degree of
Doctor of Philosophy
in the Faculty of Biology, Medicine and Health

2020

Colin Hutton

Cancer Research UK Manchester Institute

Table of Contents

Word count: 70,377 words

List of Figures

List of Tables

List of Abbreviations

Table 1. Abbreviations used in this document

Abbreviation	Meaning
αSMA	Alpha Smooth Muscle Actin
BEC	Blood Endothelial Cell
BrdU	5-Bromo-2′-deoxyuridine
CAF	Cancer-Associated Fibroblast
Cas-9	CRISPR Associated Protein 9
CC3	Cleaved-Caspase 3
CRISPR	Clustered Regularly Interspaced Short Palindromic Repeats
CyTOF	Cytometry by Time-of-Flight (akak. Mass cytometry)
DAMP	Damage-Associated Molecular Pattern Molecules
DES	Desmin
DNMT1	DNA Methyltransferase 1
DTR	Diphtheria Toxin Receptor
ECM	Extracellular matrix
EMT	Epithelial to Mesenchymal Transition
EndMT	Endothelial to Mesenchymal Transition
ENG	Endoglin (CD105)
EpCAM	Epithelial Cell Adhesion Molecule
FACS	Fluorescence-Activated Cell Sorting
FAP	Fibroblast Activation Protein Alpha
FFPE	Formalin fixed Paraffin Embedded
FGF	Fibroblast Growth Factor
FlowSOM	Flow Self-Organizing Maps
GEMM	Genetically Engineered Mouse Model
HSV	Herpes Simplex Virus
iCAF	Inflammatory Cancer-Associated Fibroblast
IdU	5-Iodo-2′-deoxyuridine
IFNβ	Interferon Beta
IFNγ	Interferon Gamma
IRF	Interferon Regulatory Factor
Ki67	Marker of Proliferation Ki-67
KRAS	Kirsten Rat Sarcoma Viral Oncogene Homolog
LEC	Lymphatic Endothelial Cell
LIF	Leukemia inhibitory factor
LOX	Lysyl Oxidase
MAPK	Mitogen-Activated Protein Kinase
MHCI	Major Histocompatibility Complex 1
MHCII	Major Histocompatibility Complex 2
MMP	Matrix Metallopeptidase
MSC	Mesenchymal Stem Cells
MyCAF	Myofibroblast Cancer-Associated Fibroblast
NFκB	Nuclear Factor Kappa-Light-Chain-Enhancer of Activated B Cells
NG2	Neuron-Glial Antigen 2 (aka. Chondroitin Sulfate Proteoglycan 4)
NOTCH	Notch (Drosophila) Homolog (Translocation-Associated)

PAMP	Pattern-Associated Molecular Pattern Molecules
PanIN	Pancreatic Intraepithelial Neoplasia
PCK	Pan-Cytokeratin
PCR	Polymerase Chain Reaction
PDA	Pancreatic Ductal Adenocarcinoma
PDGF	Platelet-Derived Growth Factor
PDGFRα	Platelet-Derived Growth Factor Receptor Alpha
PDGFRβ	Platelet-Derived Growth Factor Receptor Beta
PDPN	Podoplanin
RFP	Red Fluorescent Protein
RNAseq	Ribonucleic Acid Sequencing
ROCK	Rho-Associated Protein Kinase
ROS	Reactive Oxygen Species
scRNAseq	Single Cell Ribonucleic Acid Sequencing
SHH	Sonic Hedgehog
SMO	Smoothened
STING	Stimulator of Interferon Genes
TGFβ	Transforming Growth Factor Beta
TIMP	Tissue Inhibitor of Metalloproteinase
TLR	Toll-like Receptor
TME	Tumour Microenvironment
TNFα	Tumour Necrosis Factor
UMAP	Uniform Manifold Approximation and Projection
UV	Ultraviolet
VDR	Vitamin D receptor
VIM	Vimentin
WNT	Wingless-Type MMTV Integration Site Family
YAP	Yes-Associated Protein

Abstract

Fibroblasts are a mesenchymal cell type present in most mammalian tissues, that make a major contribution to ECM deposition and modification in health and disease. Pancreatic ductal adenocarcinoma (PDA) tumours are typically infiltrated with large numbers of fibroblasts but their functional contributions to tumour progression are poorly understood. Research into dermal fibroblasts has revealed at least two distinct fibroblast lineages in mammalian skin, that diverge during embryonic development and have different, non-overlapping functions in adult tissue homeostasis and wound-healing. Whether such distinct lineages of fibroblasts exist in other tissues or tumours is not known. A major barrier to understanding fibroblast heterogeneity in tumours is a lack of robust fibroblast surface markers, which has precluded the isolation of live subpopulations for functional characterisation. I sought to address this by developing a single cell mass cytometry analysis workflow to annotate the PDA tumour microenvironment (TME). The analysis reveals extensive fibroblast heterogeneity in PDA tumours and highlights potential associations between fibroblast abundance and proliferation rates of certain immune cell subsets. A notable feature of murine and human normal pancreatic and PDA fibroblasts is the presence of two major fibroblast populations, demarked by differential expression of CD105. Isolation of these populations reveals that differential CD105 expression is stable under extended passaging and under various activating conditions, suggesting CD105+ and CD105- pancreatic fibroblasts to be stable, distinct lineages. CD105+ pancreatic fibroblasts are more sensitive to TGFβ1 and Il1α stimulation *in vitro* but both populations have equal sensitivity to IFNγ stimulation. In a syngeneic subcutaneous co-transplant model, CD105+ pancreatic fibroblasts are tumour permissive, and do not alter PDA tumour growth, and CD105- pancreatic fibroblasts are found to be highly tumour suppressive. The mechanism for tumour suppression is entirely dependent on functional adaptive immunity, with a major contribution from cDC1-mediated CD8+ T cell cross-priming. Despite CD105- PDA fibroblasts consistently having a fraction of cells with evidence of expression of MHCII antigen presentation *in vivo*, fibroblast MHCII antigen presentation does not contribute to the enhancement of anti-tumour immunity in this model. In addition, CD105+ fibroblasts cannot be made to become tumour suppressive by deletion of CD105, suggesting that whilst CD105 is a useful marker for separating functionally distinct pancreatic fibroblast lineages, lack of CD105 does not functionally contribute to

the dominant *in vivo* phenotype of CD105- pancreatic fibroblasts. CD105+ and CD105- fibroblasts are found to be present in at least 12 other mammalian organs and 2 other spontaneous tumour types. This data highlights CD105 as marker of distinct fibroblast lineages in a large number of mammalian tissues and also indicates that fibroblast and immune cell interactions can drive dominant phenotypes *in vivo.*

Declaration

No portion of the work referred to in this thesis has been submitted in support of an application for another degree or qualification of this or any other university or other institute of learning.

Copyright Statement

Library's regulations (see http://www.library.manchester.ac.uk/about/regulations/) and in The University's policy on Presentation of Theses

Acknowledgements

I am deeply grateful to Claus, for the usual things a good boss does, discussion and debate, advice and support, but mainly for having confidence in a very eager but pretty clueless chemist that asked him for a job 5 years ago with no bioscience experience. I don't think many people would have done the same. Maybe electrons and cells have some similarities! I would also like to thank Claus for being a pillar of calm after the Paterson Building fire (and the move to Alderley Park) and after the coronavirus pandemic (and the move to home working!), for all the conferences I had the privilege to attend and for my training, that will hopefully take me on to new and exciting things. Systems Oncology is filled with great people and great scientists and its many various members have been a pleasure to work with over the years (and have been incredibly supportive of my weird soup-era!). I'm grateful to the CRUK-MI Core Facilities, that enable so many things to be done so quickly. In particular, Toni has been a champion of mass cytometry and it would simply not exist at CRUK-MI without her: so, thanks for enabling the technology that my whole project is based on (!) but mainly thanks for being a great friend. Thank you to 'KPC Jen' for giving me a scientific home after the fire, for supporting the majority of the GEMM work that drove the project and for being a top, no-nonsense scientist. Thank you Katherine, for always being caring and supportive, for working hard for so many years to make the distance feel like it didn't matter and for listening to my relentless grumbling about (many!) failed experiments. Lastly, I would like to thank the mighty and humble fibroblast… images of mysterious little 'spindle-shaped' monsters will be engrained into my memory for the rest of my life, I am sure!

I have enjoyed my PhD experience beyond words and am certain that I will now be a scientist, in some form or another, for the rest of my professional career. I got very lucky with my boss, my project and the people around me and whatever my next steps are, I will always be grateful for the things that came together during this time.

Chapter 1 - Introduction

1.1 – Fibroblasts in health and fibrosis

1.1.1 – Definition of fibroblasts as a discrete cellular entity

Fibroblasts are a loosely defined cell type with spindle-like morphology and mesenchymal features, that lack epithelial, immune and vascular features and are easily propagated by adherent cell culture (Kalluri, 2016). In healthy tissues, fibroblasts are typically found embedded within the interstitial ECM and the fibroblasts themselves and the surrounding ECM, are a major component of the tissue stroma that supports normal physical structure and functioning of the parenchyma (Furuya and Furuya, 2007). Fibroblasts in healthy tissues can be found in direct contact with or close proximity to, the basement membrane or a wide range of other cell types, including adipocyte, chondrocyte, smooth muscle, vascular, neural, endocrine or inflammatory cells (Powell et al., 2011). The principle role of fibroblasts in development and homeostasis appears to be extracellular matrix (ECM) synthesis, deposition and modification (Kalluri, 2016), although other cells types, for example macrophages, pericytes and keratinocytes, have been shown to also make major contributions to ECM generation and alterations (Alitalo et al., 1982; Ferland-McCollough et al., 2017; King and Pope, 1986; Simoes et al., 2020; Wang et al., 2020). In addition, a wide range of other, non-ECM functions have now been described for fibroblasts (see below).

1.1.2 – Defining fibroblast identity

Fibroblasts are typically defined by negative expression of epithelial (e.g. EpCAM, E-cadherin), endothelial (e.g. CD31, B-cadherin) and leukocyte (e.g. CD45, CD11b) markers, positive expression of mesenchymal markers and (where appropriate) their elongated, spindle-like morphology**.** The specific markers used for positive identification of fibroblasts from other mesenchymal cell types varies widely between studies. For example, pericytes are another major mesenchymal cell type in healthy tissues that broadly falls into this category. Typically, pericytes are defined by expression of αSMA, DES, PDGFRβ, MCAM, ITGα1, NG2 or RGS5 (Armulik et al., 2011; Paquet-Fifield et al.,

2009) but several of these are variably expressed by pericytes and can also be expressed by fibroblasts. In addition, tissue-specific differences in pericyte phenotypes are also known (Yamazaki and Mukouyama, 2018). The most commonly used markers to positively identify fibroblasts generally are PDGFRα, PDGFRβ, αSMA or FAP, but these are not expressed on all fibroblasts, several are only expressed on fibroblasts under activating/pathological conditions and some are expressed on other, related cell types, such as pericytes (Sugimoto et al., 2006). In addition, arguably the most widely used activated fibroblast marker, αSMA, is intracellular which excludes it use for live cell isolation. Currently, there is no consensus on the optimum markers to use to fully define fibroblasts and other mesenchymal cells in healthy and diseased tissues (Sahai et al., 2020). A lack of robust fibroblast surface markers has been suggested to result in studies reporting overlapping, incomplete or discrete populations of fibroblasts, as well as potential misannotation of other mesenchymal cell types (Kobayashi et al., 2019). This, combined with tissue-specific differences in fibroblast phenotypes (see below), makes interpretation of and comparability between fibroblast studies challenging. Collectively a lack of robust fibroblast markers has hindered detailed characterisation of this cell type.

1.1.3 – Developmental origin of fibroblasts

The majority of tissue-resident fibroblasts are thought to originally develop from the primary mesenchyme (Lawson et al., 1991). Epiblasts undergo epithelial to mesenchymal transition (EMT) during gastrulation to form the primary mesenchyme, which goes on to form the endodermal and mesodermal germ layers, of which the mesoderm goes on to form the true mesenchyme. It is from this compartment that the majority of tissue fibroblasts appear to derive (Hay, 2005). Many other related cell types share a similar developmental pathway, including chondrocytes, adipocytes, myocytes, pericytes and blood/lymphatic endothelial cells. Relatively little is known about how much fibroblast-like cells and other mesenchymal cells interconvert in healthy tissue development and homeostasis. The data available appears to indicate a high degree of plasticity, in both directions, between fibroblasts and other cell types, during development. For example, lineage tracing studies suggest that during formation of the mouse liver, the majority of fibroblast-like cells (the so called hepatic stellate cells) derive from mesothelial cell precursors (Li et al., 2016; Li et al., 2013) and during development of murine skin, a subset of fibroblasts differentiate into adipocytes (Driskell et al., 2013)

(described below). Furthermore, during development, fibroblasts show phenotypic changes at defined time points, for example early embryos heal surface wounds with no scarring yet in adult tissues, extensive fibrogenic responses are observed (Redd et al., 2004).

Another subset of mesoderm-derived cells, called mesenchymal stem cells (MSCs) retain pluripotency in adult tissues and are found in the bone marrow, peripheral blood and adipose tissue (Sheng, 2015). Because differentiation assays are conducted *ex vivo* and some studies report pluripotency potential of tissue-resident fibroblasts, the phenotypic boundary between what is and isn't an MSC in tissues, and their identification *in vivo,* is often not clear (Soundararajan and Kannan, 2018).

The majority of cell-of-origin studies focus on pathological tissues and a variety of cell types have been reported to convert into fibroblasts or fibroblast-like cells during pathogenesis (Haviv et al., 2009; LeBleu and Neilson, 2020). The extent to which these processes contribute to the fibroblast pool in disease is actively debated. Epithelial to mesenchymal transition (EMT) and endothelial to mesenchymal transition (EndMT) have been shown to variably contribute fibroblast-like cells during the development of fibrotic scarring in different organs (Lovisa et al., 2015; Zeisberg et al., 2008). Other cell types also appear to have the potential to convert to fibroblast-like cells, including pericytes (Di Carlo and Peduto, 2018; Lemos and Duffield, 2018; Rock et al., 2011), adipocytes (El Agha et al., 2017; Marangoni et al., 2015) and mesothelial cells (Li et al., 2013). Typically, transitions towards fibroblast phenotypes are graduated processes, such that hybrid, intermediate cell states are observed (Karacosta et al., 2019). Whether these transitions all share a common pattern of epigenetic re-programming or whether there are multiple mechanisms by which a cell can transition to a fibroblast-like phenotype is not known. Mesenchymal transitions are reported to contribute to fibroblast pool during cardiac (Zeisberg et al., 2007), renal (Lovisa et al., 2015), liver (Lee et al., 2014b; Rowe et al., 2011) and lung fibrosis (Willis et al., 2006) and targeting such processes appears to reduce the severity of fibrosis (Grande et al., 2015; Lovisa et al., 2015). Comparability between studies can be complicated by the use of different lineage tracing models, different methods for fibrosis induction and differing time points of analysis.

Lastly, cells of myeloid origin, often referred to as fibrocytes, have been suggested to be another source of fibroblasts under inflammatory or fibrotic conditions (Bucala et al., 1994; Phillips et al., 2004). For example, single cell analysis indicates a potential myeloid origin of fibroblasts and adipocytes during and after murine skin wounding (Phillips et al., 2004). Fibrocytes reportedly show many similarities to circulating monocytes and lose immune features on differentiation (Kuwana et al., 2003) making confident identification challenging. Interestingly, in a lung fibrosis model, bone-marrow derived cells are able to contribute to collagen I deposition in the fibrotic lung but do not act as source of αSMA+ myofibroblasts and cannot be converted to αSMA+ myofibroblasts *in vitro* (Hashimoto et al., 2004), potentially suggesting a limit in the ability of distal fibroblast-like cells to adopt specific fibroblast phenotypes. The method used for tracking bone marrow derived cells cannot differentiate between MSCs and so-called fibrocytes (Abe et al., 2001), and it is not clear what contributions each makes individually.

The cell of origin of fibroblasts in health and disease is still an active matter of debate and has generated conflicting opinions (Bartis et al., 2014; Galichon et al., 2013; Huang and Susztak, 2016; Kriz et al., 2011; Zeisberg and Duffield, 2010).This can be at least partially attributed to the different models of fibrosis used, different criteria used to define a cell as a fibroblast, non-perfect lineage tracing and depletion systems and differences in opinion regarding the best gene promoters or cell identity markers to use to successfully target the desired populations. Importantly, whether fibroblasts that derive from tissue-resident fibroblasts or from other cells of origin are functionally the same or functionally different, is not known.

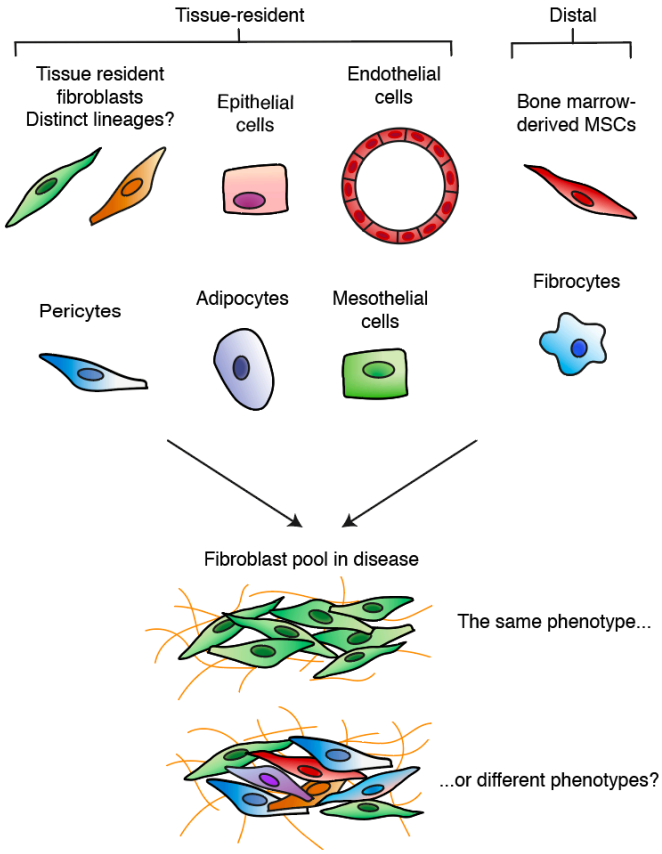

Figure 1. Proposed sources of fibroblasts in disease
Fibroblasts in fibrotic tissues and tumours have been suggested to derive from expansion of local fibroblasts as well as a variety of other cellular sources. Distinct lineages of tissue-resident fibroblasts have been demonstrated in murine skin but whether distinct fibroblast lineages exist in other organs is unknown. Lineage tracing studies have revealed the capacity of several mesenchymal and non-mesenchymal cell types to adopt fibroblast-like features during pathogenesis. It is not clear if fibroblasts from different cells of origin contribute the same or different functions during disease progression.

1.1.4 – Epigenetic control of fibroblast identity

Dermal fibroblasts isolated from different anatomical locations and from donors of different ages, have functional divergence in their ability to promote epidermal differentiation and the wound healing response (Hausmann et al., 2019). In addition, dermal fibroblasts isolated from different anatomical positions, retain transcriptomic differences, even after extended *in vitro* culture (Chang et al., 2002; Rinn et al., 2006). These gene expression signatures and epigenetic positional 'memory' have been associated with specific DNA methylation patterns in fibroblasts, that are retained through culture and cell divisions (Ivanov et al., 2016). DNA methylation remodelling also occurs during fibroblast activation *in vivo* and is a commonly observed feature of many

human diseases, including chronic obstructive pulmonary lung disease (COPD) (Clifford et al., 2018), rheumatoid arthritis (Karouzakis et al., 2018) and systemic sclerosis (Bergmann and Distler, 2017). Methylation changes to the protomer regions of specific genes in fibroblasts have been directly linked to sustained activation and enhanced pathology. For example, hypermethylation and silencing of the *Rasal1* gene promoter, maintains renal fibroblast activation and drives kidney fibrosis (Bechtel et al., 2010).

Targeting activated fibroblasts with epigenetic modifiers has demonstrated an ability to alter fibroblast activation status *in vitro* and *in vivo*. For example, inhibition of the acetyl-histone binding protein, BRD4 using JQ1, suppresses *Acta2* and *Postn* expression in fibroblasts during cardiac fibrosis (Stratton et al., 2019), inhibition of histone deacetylase using Vorinostat (suberoylanilide hydroxamic acid, SAHA), suppresses collagen expression in lung fibroblasts during lung fibrosis (Zhang et al., 2013) and treatment of fibroblasts from human tumours with dual JAK and DNMT1 inhibitors reverts their invasive phenotype (Albrengues et al., 2015).

As well as the epigenetic stability observed as 'positional memory' and 'memory of activation', fibroblasts also have a well-documented capacity to undergo epigenetic and phenotypic re-programming. Fibroblasts are the most widely used cell type for reprogramming and iPSC studies (although this is partly due to their ease of *in vitro* expansion) (Liebau et al., 2013; Raab et al., 2014) and fibroblasts isolated from different tissues have distinct and well-defined capacities to undergo epigenetic reprogramming (Sacco et al., 2019).

1.1.5 – Fibroblast heterogeneity and functions in the development and homeostasis of healthy organs

During healthy organ development and homeostasis, fibroblasts are thought to be a major contributor to the synthesis, maintenance and modification of the bulk of tissue ECM networks, as well as the basement membrane, which itself has a well-established role in supporting normal epithelial and endothelial cell function (Kalluri, 2003; LeBleu et al., 2007). Fibroblasts also have an increasing number of reported non-ECM functions during development and homeostasis, such a paracrine signalling to other cell types (Werner and Smola, 2001). To date, the most detailed fibroblast functional studies

conducted have focussed on the roles of fibroblasts in the development, homeostasis and response to injury in mammalian skin. Using a variety of lineage tracing and transplantation models, these studies have provided detailed evidence of heterogeneous lineages of fibroblasts (see below). These dermal fibroblast lineages have distinct differentiation pathways, locations, markers and functions, highlighting a 'division of labour' within the fibroblast compartment of the skin, that is imprinted during organ development.

Murine dermal fibroblasts derive from a multipotent mesenchymal cell population seen at E12.5, which expresses PDGFRα, delta-like homolog 1 (DLK1) and leucine-rich repeat protein (LRIG1) (Driskell et al., 2013). This shared precursor then differentiates at around E16.5 into fibroblasts that reside in the upper and lower dermis. During development, the upper dermis precursor expresses ITGα8, CD26, LRIG1 and B lymphocyte-induced maturation protein (BLIMP1). This upper dermis precursor goes on to form papillary dermal fibroblasts that support the function of the epidermis and basement membrane, the dermal papilla that supports hair follicle morphogenesis and the arrector pili muscle cells required for piloerection (Egawa et al., 2009; Fujiwara et al., 2011). Associated with each of these stages are defined changes in marker expression, for example the arrector pili begin to express *Acta2* (αSMA). The lower dermis precursor continues to expresses PDGFRα and DLK1 and goes on to form reticular dermal fibroblasts (DLK1+), that generate the bulk of the fibrillar ECM network of the thicker lower dermis, as well as pre-adipocytes and adipocytes (Sca1+Lipids+) of the hypodermis, collectively required for insulation, energy storage, ECM production and paracrine signalling to epidermal stem-cell niches (Donati et al., 2014; Driskell and Watt, 2015; Festa et al., 2011; Sorrell and Caplan, 2004; Wojciechowicz et al., 2013). At specific time points, lineage commitment is found to become irreversible, for example upper dermal fibroblasts isolated at E16.5 can be made to differentiate into adipocytes in culture but do not do so from P2 isolations (Driskell et al., 2013). After wounding of adult murine skin, the lower lineage mediates the initial wave of dermal repair via extensive ECM deposition, that is characteristic of fibrosis. The upper lineage is recruited later, during re- epithelialization and is required for hair follicle formation. Subsequently, use of an irreversible *Engrailed-1* (*En1*) lineage tracing model identified distinct murine skin fibroblast lineages that are present during embryonic development (Rinkevich et al., 2015). Dermal fibroblasts with historical *Eng1* expression appear to make a larger

contribution to connective tissue deposition during development, fibrosis and cancer stroma formation. Heterogenous fibroblast populations have now also been observed in human skin samples and several of the markers noted in the murine experiments (e.g. CD26), show uneven distribution across different human skin fibroblast clusters (Philippeos et al., 2018; Tabib et al., 2018). CD39 can be used to isolate the human papillary population and CD36 can isolate the human lower reticular/hypodermal population in human skin (Philippeos et al., 2018). Although these markers are lost on culture, phenotypic differences between the populations are still apparent, with the CD39+ papillary fraction better supporting *ex vivo* epidermal growth and the papillary CD36+ lower dermis/hypodermal populations having higher sensitivity to IFNγ. Interestingly, related to the DLK1+ lower dermis fibroblast precursor seen during murine skin development, a subset of DLK1+ fibroblasts have also recently been observed in breast cancer samples (Kieffer et al., 2020). Collectively, these results suggest that specific fibroblast populations may be conserved across species and also potentially present in multiple different mammalian organs.

Little is known about whether functionally distinct fibroblast lineages contribute to tissue development and homeostasis of other organs. However, a rapidly increasing number of single cell RNA sequencing (scRNAseq) studies are revealing fibroblast transcriptional heterogeneity in healthy and diseased mammalian tissues, including in the lung ((Tsukui et al., 2020; Valenzi et al., 2019; Xie et al., 2018), liver (Dobie et al., 2019; Xiong et al., 2019), kidney (Park et al., 2018), mammary tissue (Bartoschek et al., 2018), skin (Vorstandlechner et al., 2020), synovial joints (Croft et al., 2019), bone marrow (Baryawno et al., 2019) and lymph nodes (Rodda et al., 2018). Several scRNAseq studies not principally aimed at understanding fibroblast diversity, have also inadvertently demonstrated extensive fibroblast heterogeneity in mice, non-human primates and humans and provide additional resources to better characterise gene expression differences between fibroblast subsets across tissues and species (Ziegler et al., 2020). Such single cell analysis is providing substantial evidence that transcriptional heterogeneity exists within fibroblasts of mammalian tissues. However, further work is needed to understand whether these equate to functionally distinct populations and if so, what their specific impact is on development, homeostasis and pathogenesis. For example, it is typically not known whether the transcriptionally distinct fibroblast populations identified in these scRNAseq studies represent the same parental

fibroblast in different phenotypic states or represent distinct, non-interchangeable fibroblast lineages. The studies of functional fibroblast heterogeneity in mammalian skin described above suggest that a detailed understanding of fibroblast heterogeneity will an essential prerequisite to accurately assigning fibroblast function *in vivo*.

1.2 - Fibroblasts in tumours

1.2.1 – Defining fibroblasts in tumours

Typically, fibroblasts in tumours (also termed cancer-associated fibroblasts (CAFs)) are defined in a similar manner to fibroblasts in healthy organs: negative expression of epithelial, endothelial and leukocyte markers, positive expression of mesenchymal markers and with, where applicable, spindle or elongated morphology. As for healthy tissues, this fraction of cells will also contain other mesenchymal cell types, such as pericytes. Moreover, in tumours this broad definition of fibroblasts will also include any cancer cells that have undergone an epithelial to mesenchymal transition (EMT) (Karacosta et al., 2019). Indeed, lineage tracing experiments in mice have shown that EMT can be a major contributor to what appears to be the mesenchymal compartment of tumours (Rhim et al., 2012). Because mesenchymal cancer cells contribute to disease progression in a very different manner to fibroblasts, it is vitally important to be able to separate fibroblasts from EMT cancer cells when analysing tumours. There is no known single, complete marker that can separate non-transformed and transformed mesenchyme in tumours and therefore care needs to be taken when assigning fibroblast identity generally, but particularly so in tumours.

Several factors have likely contributed to the lack of clarity on the optimal markers required to accurately identify fibroblasts in tumours, including tissue-specific differences between fibroblasts (Lemos and Duffield, 2018), the plasticity of the fibroblast phenotype (Ohlund et al., 2017), the heterogeneity of human cancers (Consortium, 2020), the intense and variable ‘wound’ and inflammatory conditions of the TME (Ohlund et al., 2014) and the misclassification of mesenchymal cancer cells or other stromal cell types as fibroblasts (Rhim et al., 2012). Indeed, the fact that fibroblasts may derive from a diverse range of other cell types and graduated nature of such transitions, may mean

precisely defining the boundary between a fibroblast and another cell type may be inherently challenging.

1.2.2 – The origin of fibroblasts in tumours

The origin of fibroblasts in human tumours is largely unknown. A detailed understanding of changes to the TME during progression of human tumours is lacking because biopsies are normally taken long after tumour initiation and taking serial biopsies of the same lesion is rare, although longitudinal tumour studies are increasingly being conducted (Nature Research TRACERx Collection, 2020). As such, mouse models are the main source of information regarding various contributions to the fibroblast pool in tumours, even though it is not clear how well mouse model systems recapitulate fibroblast behaviour in human tumours (discussed in Chapter 10). As for tissue fibrosis, local tissue-resident fibroblasts are thought to be a major contributor to fibroblasts in tumours. This is because they are present in most healthy organs and fibroblast expansion is seen early during tumourigenesis, at a time point when conversion of large numbers of other cells types or sufficient recruitment of precursors from distal locations seems unlikely (Collins et al., 2012). However, a lack of robust lineage tracing models for tissue-resident fibroblasts, applied in the context of spontaneous tumour formation, has precluded formal proof of this (Sahai et al., 2020). Also, in line with observations in fibrotic conditions described above, lineage-tracing methods have been used to demonstrate that other tissue-resident cell types have the potential to undergo transitions towards mesenchymal and fibroblast-like phenotypes in tumours and other fibrotic conditions. As for fibrosis, these include endothelial cells (Potenta et al., 2008), pericytes (Di Carlo and Peduto, 2018; Lu and Shenoy, 2017), adipocytes (Bochet et al., 2013; El Agha et al., 2017) and mesothelial cells (Rynne-Vidal et al., 2015).

Bone-marrow derived MSCs have been suggested a possible distal source of fibroblasts in tumours but current evidence indicates a minor contribution. Analysis of cancer patients that have previously received sex-mismatched bone marrow transplantation indicates that between 1-5% of fibroblast-like cells in human tumours are bone marrow-derived (Kurashige et al., 2018). Another study using bone-marrow chimeric mouse models, indicates ~10% of the fibroblasts in murine skin tumours derive from bone-marrow stromal cells (Lecomte et al., 2012) and a second similar study suggests the

bone marrow contribution to tumour fibroblasts is <1% (Arina et al., 2016). As for fibrosis studies, such bone marrow chimera experiments would be expected to simultaneously measure a contribution from MSCs and so-called fibrocytes (Abe et al., 2001). As for fibrosis, it is currently not known if fibroblasts that originate from different cell types, are functionally different to each other and to tissue-resident fibroblasts in tumours.

1.2.3 – The accumulation of fibroblasts in tumours

Some of the first evidence that fibroblasts may be important to tumour biology, was the demonstration by the Stokers laboratory that fibroblasts can inhibit growth of polyoma-transformed cells, over 50 years ago (Stoker et al., 1966). 20 years later, seminal experiments conducted by the Bissell laboratory demonstrated that local tissue wounding promotes Rous sarcoma virus-mediated tumour formation (Dolberg et al., 1985). Even within just these two early studies, a dichotomous role for the fibrotic tumour microenvironment in tumour formation and progression was beginning to emerge. Mouse models indicate that expression of oncogenic KRAS in the epithelial compartment results in activation of adjacent, non-transformed mesenchymal cells and this single genetic transformation on its own, is capable of initiating a local wound-like, fibrotic response (Collins et al., 2012). Indeed, fibroblast expansion is commonly observed within premalignant or early primary and metastatic lesions of these models (Aiello et al., 2016; Hingorani et al., 2003). ~90% of human cancers are defined as carcinomas, with epithelial features (Rogalla and Contag, 2015) and a generic wound healing response initiated by oncogenic processes, such as mutant KRAS, presumably reflects the continuous engagement of processes that have evolved to detect and contain epithelial tissue damage and initiate complex repair processes. The ability of cancer cells to persist, means there is no resolution phase of the ‘cancer-wound’ and the fibroblast-mediated processes occurring in tumours may show parallels with those occurring in chronic, and perhaps to a lesser degree, acute fibrotic conditions. Indeed, the notion of tumours as ‘wounds that do not heal’ has become a central concept in the field of the TME (Bissell and Hines, 2011; Dvorak, 2019). Notably, there are far more published studies on either fibroblast functions in fibrosis or fibroblast functions in cancer, than there are studies that directly compare the two pathologies. Therefore, a detailed, quantitative understanding of how similar tumour and non-tumour fibroblast-mediated processes are is lacking.

Fibroblast accumulation is a common feature of many tumours and consistent differences are observed between different tumour types. For example, breast, prostate and pancreatic tumours typically show higher fibroblast abundance than brain, renal and ovarian cancers (Aboussekhra, 2011; Augsten et al., 2009; Neesse et al., 2011; Ohlund et al., 2014; The Human Protein Atlas, 2020). Oncogenic processes that have been linked to fibroblast activation, such as KRAS and MAPK pathway hyperactivation, are a shared feature of many cancer types, yet not all tumours with these mutations accumulate fibroblasts to similar magnitudes, suggesting factors beyond just the specific identity of oncogenic mutations regulates fibroblast abundance in tumours. Indeed, even within a single tumour type, a wide variation in 'tumour fibrosis' is observed. The key factors that determine whether a tumour will accumulate many or few fibroblasts are poorly defined.

1.2.4 – Fibroblast recruitment and activation in tumours and other pathologies

Expansion of the fibroblast compartment is observed in several tumour types and fibroblasts in tumours are found to be epigenetically and metabolically distinct from fibroblasts in normal tissues (Albrengues et al., 2015; Zhang et al., 2015). Expansion of fibroblasts in tumours is associated with increased deposition of type I, III and IV collagens, laminins, elastin, fibronectin, tenascin and water holding glycoproteins (Kalluri, 2016), as well enhanced ECM modification, for example through altered collagen crosslinking via lysyl oxidases (Cox et al., 2013). Moreover, fibroblasts play a key role in dictating ECM degradation dynamics and turnover rates, for example via expression of matrix metalloproteinases (MMPs) or tissue inhibitor of metalloproteinases (TIMPs) (Gong et al., 2013). A state of high ECM expression and modification is thought to be a major activation phenotype of fibroblasts in tumours. However, non-fibrotic, inflammatory states have now also been described (Erez et al., 2010), suggesting fibroblasts can exist in a complex array of phenotypes in tumours, some of which may or may not be analogous to those observed in fibrotic conditions.

As described above, mouse models have indicated that fibroblast activation is downstream of oncogenic transformation, such that if essential driver mutations are removed, the stroma normalises and the fibroblast compartment returns to a state

indiscernible from that of the normal tissue (Collins et al., 2012). Thus, sustained fibroblast activation in tumours, is an active, continuous process, driven by factors either derived directly from the tumour cells themselves or indirectly from other cells or environmental conditions that are only present in the tissue because of the tumour cells. This supports the concept that fibroblast activation is a dynamic state and that it may be a viable therapeutic strategy to target key fibroblast activation processes, if they contribute to tumour progression and treatment failure.

Fibroblasts exposed to TGFβ undergo metabolic reprogramming (Guido et al., 2012) and activate towards a phenotype that most closely matches that described as the 'myofibroblast' phenotype, or 'MyCAFs' in tumours. Typically the myofibroblast state is defined as increased αSMA expression and increased stress fibre formation (Ohlund et al., 2017) and is associated with increased ECM expression and a capacity to transmit contractile forces via the actin cytoskeleton and ECM network (Vennin et al., 2017). This increases tissue stiffening, which itself has a variety of complicated downstream effects, including increased proliferation of the epithelium (Provenzano and Keely, 2011). Increased environmental stiffening has also been shown to induce the myofibroblast phenotype and sustain it in a feed-forward loop, in a process that is dependent on YAP- and ROCK-mediated signalling (Calvo et al., 2013). TGFβ is secreted in a latent form and requires covalent attachment to the ECM prior to release of the active ligand, a process in itself that is facilitated by other ECM components (e.g. thrombospondin-1) or cell surface integrins (e.g. αvβ6) (Annes et al., 2003). The exact relationship and sequence of events between TGFβ activation, ECM deposition, the myofibroblast phenotype, cell contractibility and microenvironmental stiffness is not clear, and is further complicated by the fact that fibroblasts secrete TGFβ-family ligands that can act in an autocrine manner (Ohlund et al., 2017) and that TGFβ1, TGFβ2 and TGFβ3 appear to have different functions *in vivo* (Gilbert et al., 2016). Activation of the vitamin D receptor (VDR) in fibroblasts is antagonistic to the TGFβ1-induced pro-fibrotic response via competition at SMAD binding sites (Ding et al., 2013) and synthetic agonists of the VDR (e.g. calcipotriol) suppress the myofibroblast-like phenotype (Sherman et al., 2014). IL1α activation induces a phenotype distinct from the myofibroblast phenotype (Ohlund et al., 2017) and because of increases in expression of several cytokines (with known roles in inflammation (e.g. *Il6*)), this phenotype has been named the 'inflammatory fibroblast', or 'iCAF' phenotype. Interestingly, TGFβ1 antagonises the IL1-induced phenotype,

suggesting the MyCAF- and iCAF-like states are to some extent distinct and competitive polarisations (Biffi et al., 2019).

Oncogenic KRAS in PDA cancer cells directly upregulates SHH expression, which induces hedgehog signalling and secretome changes in co-cultured fibroblasts (Tape et al., 2016). In addition, PDA cancer cell-derived SHH is a major driver of fibroblast expansion in GEMM tumours *in vivo* (Lee et al., 2014a; Rhim et al., 2014; Shin et al., 2014). LIF is capable of inducing expression of multiple inflammatory genes in fibroblasts via STAT3-signalling and can act in a paracrine manner from PDA cancer cells (Shi et al., 2019) or in a self-sustaining autocrine manner in fibroblasts of specific inflammatory polarisations (Nguyen et al., 2017). Interestingly, LIF is part of the iCAF-like gene expression program, suggesting autocrine LIF signalling may be one way in which an inflammatory fibroblast phenotype is reinforced and sustained *in vivo* (Biffi et al., 2019). FGF-family and PDGF-family ligands are also known activators of fibroblasts in tumours and have mainly been described as fibroblast mitogens (Bhattacharyya et al., 2020; Zhou et al., 2018). In addition, WNT and NOTCH signalling have established roles in skin and synovial fibroblast activity, respectively (Driskell and Watt, 2015; Wei et al., 2020) but these activation pathways are less studied in tumour fibroblasts. How SHH-, PDGF, FGF, LIF, WNT and NOTCH pathway-induced fibroblast phenotypes overlap or contrast with the more established MyCAF and iCAF phenotypes is not clear, although, for example, FGF ligands appear to have the potential to antagonise TGFβ-mediated activation (Bordignon et al., 2019), highlighting the interactive nature of these signalling networks.

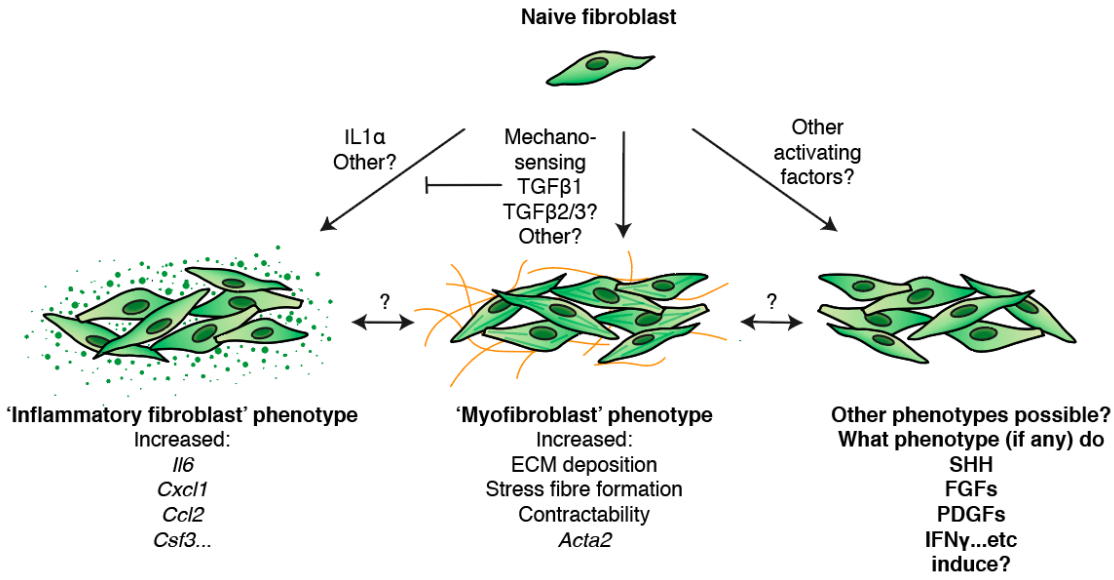

Figure 2. Fibroblast activation in PDA tumours
Naïve pancreatic fibroblasts can be activated towards a myofibroblast phenotype by TGFβ receptor activation or local tissue stiffening. The myofibroblast phenotype is characterised by increased *Acta2* expression, αSMA stress fibre formation, and deposition of ECM proteins, particularly collagens. IL1α is able to induce an inflammatory fibroblast state, characterised by reduced expression of *Acta2* and increased expression of variety of soluble chemokines, including *Il6*, *Cxcl1*, *Ccl2* and *Csf3* (GCSF). TGFβ signalling has been shown to antagonise the inflammatory phenotype (Biffi et al., 2019). It is not clear what other factors can induce the two major phenotypes. In addition, it is poorly understood whether other known fibroblast activators are able to modulate the myo- or inflammatory-fibroblast phenotype or whether they induce distinct phenotypes.

Reactive oxygen species (ROS) (Bocchino et al., 2010) and hypoxia (Madsen et al., 2015) have also been shown to alter fibroblast activity and phenotype, although whether the key processes that occur under these conditions are generic responses (as for other cell types) or fibroblast-specific responses, is not well established. Understanding of fibroblast activation generally and comparisons between different ligands and different studies is complicated because of the use of various *in vitro* and *in vivo* assays, different end point measurements (e.g. proliferation versus gene expression), different ligand concentrations used, different time points for measuring a response and the presence of multiple paralogs within several of the protein families, often with different receptor affinities and functions.

Fibroblast activation, fibrosis and inflammation are highly intertwined and possibly inseparable biological processes (Croft et al., 2019) and thus the more general terminology of a 'fibroinflammatory' state may be more reflective of the range of phenotypic states occurring in tumours and fibrotic tissues. For example, deletion of the interleukin receptor, *Il17ra* in cardiac fibroblasts, reduces fibroblast secretion of the

potent myeloid cytokine, GM-CSF and limits cardiac fibrosis and tissue damage. As well as responding to common inflammatory signals, fibroblasts can act as immune-like sentinels to initiate early inflammatory responses to pattern-associated molecular patterns (PAMPs) and damage-associated molecular patterns (DAMPs), for example via expression of toll-like receptors (TLRs) (Bautista-Hernandez et al., 2017; Bhattacharyya et al., 2017). In addition, fibroblasts are able to sense genomic stress in adjacent cancer cells via cytoplasmic transfer and fibroblast STING/IRF3-pathway activation, which results in IFNβ expression (Arwert et al., 2020). Fibroblasts as innate-like sentinels may take advantage of their wide distribution throughout tissues and close proximity to a variety of pathogen entry sites, such as the epithelium, basement membrane and vasculature.

Targeting fibroblasts via blockade of activation processes has been proposed as a therapeutic strategy in cancer (Chen and Song, 2019). Two key factor needs to be considered when targeting any fibroblast activation process. Firstly, these activating factors influence the behaviour of many other cells types in the TME (including cancer cells themselves) and systemically, therefore targeting such pathways will likely have complex results. Secondly, fibroblasts have pleotropic effects on the TME, so targeting a single activation pathway, even if specific to fibroblasts only, may have both pro- and anti-tumourigenic effects, with an unknown net result. Much more work is needed to better characterise fibroblast activation in the context of tumour biology.

1.2.5 – Pancreatic ductal adenocarcinoma (PDA)

Pancreatic cancer is the 14th most common cancer and 7th highest cause of cancer mortality in the world (Frere et al., 2018). The lifetime risk of pancreatic cancer is ~1% (Del Chiaro et al., 2014). >450,000 diagnosis and >400,000 deaths are reported each year (Bray et al., 2018; Ferlay et al., 2019; Rahib et al., 2014; Zafar et al., 2019), with incidence and death rates increasing in Western countries by ~1% year on year (Saad et al., 2018). Rising incidence of pancreatic cancer and improved outcomes in other cancer types have meant that pancreatic cancer is projected to become the 2nd leading cause of cancer-related death in the United States by 2030 (Rahib et al., 2014). Pancreatic ductal adenocarcinoma (PDA) accounts for >90% of all pancreatic cancers

and carries the worst prognosis (Feldmann et al., 2007), with an average 5-year survival of 8-9% (American Cancer Society, 2019).

80-85% of PDA patients are not eligible for surgical resection because PDA is typically detected late, when locally advanced or overt metastatic disease is radiographically detectable (Hong et al., 2012). Even if surgical resection is able to remove the entire macroscopic tumour with clean surgical margins, recurrence occurs in the vast majority of PDA patients that undergo surgery.

Patients with metastatic disease often receive FOLFIRONOX (a combination of high dose 5-fluorouracil, irinotecan, leucovorin and oxaliplatin) which improves overall survival (OS) to 11.1 mo, compared to 6.8 mo for gemcitabine alone, but is associated with multiple adverse effects and is often poorly tolerated (Vaccaro et al., 2011). For patients who are too unwell for FOLFIRINOX treatment (as often occurs due to rapid disease progression), elect not to receive it or experience dose-limiting toxicities, there are a limited number of better tolerated but less efficacious chemotherapy regimens. For example, the MPACT trial demonstrated that gemcitabine plus an albumin-bound paclitaxel formulation (Abraxane) was better tolerated and improved OS to 8.7 mo compared to 6.6 mo with gemcitabine alone (Goldstein et al., 2015; Von Hoff et al., 2013).

The PDA mutational spectrum is dominated by high frequency mutations in a currently undruggable oncogene (*KRAS*, >90%) and loss of function mutations of a range of tumour suppressors (*TP53*, *CDKN2A*, *SMAD4,* typically each *>60%*), with a long 'tail' of additional low frequency mutations in genes involved in a variety of cellular processes (Bailey et al., 2016; Cancer Genome Atlas Research Network, 2017). As such, the majority of PDA patients do not have an obvious druggable oncoprotein or vulnerability that can be targeted and the targeted therapies, that have become integrated into patient care in many other cancer types, have had no impact to the standard of care for most PDA patients (Drilon et al., 2018; Golan et al., 2019). Single agent immune checkpoint blockade has also failed in PDA (Brahmer et al., 2012; Henriksen et al., 2019), although the small minority of pancreatic cancer patients with defects in the DNA mismatch repair pathway (~1% for PDA) show benefit with anti-PD-1/PD-L1 therapy (Le et al., 2017; Le

et al., 2015). Alternative therapies with improved efficacy and reduced toxicities are urgently needed to improve the quality of life of PDA patients.

The healthy adult pancreas consists of predominantly acinar cells, which are exocrine cells responsible for digestive enzyme production, and a network of ductal cells responsible for digestive enzyme transport to the duodenum. Interspaced among the acinar structures are the pancreatic islets, responsible for endocrine functions, such as glucose regulation through insulin and glucagon release, and a network of blood and lymphatic vessels. Mesenchymal, fibroblast-like cells, which are present throughout the organ, are in close contact with all of these structures (Wang et al., 2016). Autopsy analysis of apparently healthy adult human pancreas samples indicates that within the normal pancreatic tissue, non-invasive microscopic lesions with duct like morphology, called pancreatic intraepithelial neoplasia (PanINs) can frequently be observed and are surprisingly common in older people (Andea et al., 2003; Hruban et al., 2001; Hruban et al., 2008). It is from PanINs that human PDA is thought to develop, an observation supported by mouse models (Kozuka et al., 1979). Notably, experiments using transgenic mice have suggested that a major cell of origin for PanINs is transformed acinar cells, that undergo acinar to ductal metaplasia (ADM) (Hingorani et al., 2003). It is unknown if acinar cells are the precursor cell of origin for human PDA. The frequency of PanIN lesions has been shown to increase with age (Schwartz and Henson, 2007) and modelling has suggested that progression from early stage PanINs to PDA takes >10 years (Peters et al., 2018; Yachida et al., 2010). Typically, the development of PDA is associated with the formation of an abundant stromal reaction and in particular, the accumulation of activated fibroblasts in the TME (Mueller et al., 2018). The lack of longitudinal studies have meant that how the TME and the fibroblast compartment evolves as PDA progresses in humans, is largely unknown, although stromal desmoplasia is observed at both primary and metastatic PDA sites and where matched samples are available, there does appear to be some concordance with the level of stromal reaction (Whatcott et al., 2015). It is still a matter of debate whether this extensive desmoplastic stromal reaction has a net pro- or anti-tumourigenic effect on disease progression (Bissell and Hines, 2011). A minority of PDA tumours do not show this desmoplastic reaction and the key molecular drivers that dictate whether one PDA tumour has more or less fibroblast accumulation than another and the clinical consequences of the fibroblast accumulation, are not well defined.

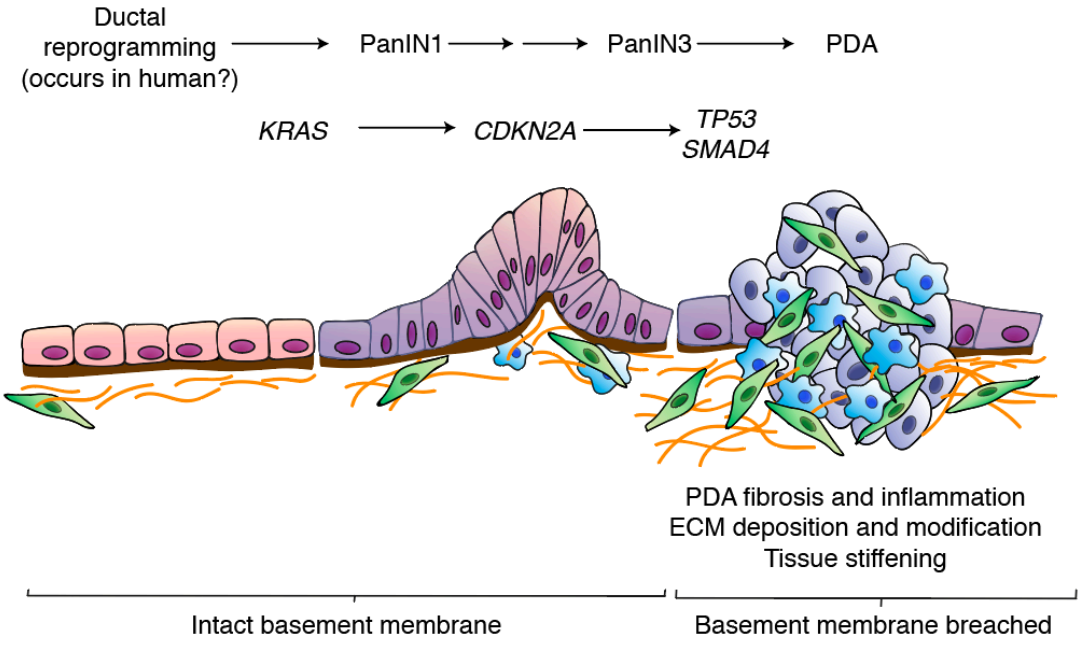

Figure 3. The progressive stages of PDA development
Mouse models have shown that oncogenic *Kras* is sufficient to initiate PanIN formation. Increasing levels of cellular atypia and increasing numbers of mutations occur with time. In parallel to changes in the epithelium, a desmoplastic stroma develops, containing altered fibroblast accumulation, immune cell infiltrate and ECM deposition and modification. Subsequent LOF mutations in key tumour suppressors (or often epigenetic silencing, in the case of the *Cdkn2a* locus), is sufficient to result in overt adenocarcinoma, characterised by invasive and metastatic potential.

1.2.6 – Modelling the PDA tumour microenvironment

The low resection rates of PDA have greatly limited the availability of surgical biopsies for research purposes. This, combined with poor human PDA engraftment potential, have also limited the use of patient-derived xenografts (PDXs) to study PDA (Xu et al., 2019). In addition, transplantation of 2D *in vitro* cultured human and murine PDA cell lines into mice does not induce the stromal response that is typical of the human disease (Baker et al., 2016). Therefore, the majority of researchers have turned to genetically engineered mouse models (GEMMs) of PDA for preclinical modelling. By far the most frequently used model is the *Pdx1-Cre; Kras*$^{LSL\text{-}G12D/+}$*; Trp53*$^{LSL\text{-}R172H/+}$ (KPC) GEMM. In this model, a conditional oncogenic *Kras* transgene is inserted into the endogenous Kras locus, replacing a single wild-type (WT) *Kras* allele. Importantly, this allows physiologically relevant gene expression when oncogenic *Kras* is expressed. In addition, a single allele of WT *Trp53* is replaced with a conditional *Trp53* transgene that mainly functions through loss of function (LOF) but also appears to have some gain of function

(GOF) oncogenic properties (Weissmueller et al., 2014). Oncogenesis is induced in the pancreas during embryonic development by Cre-recombinase expression in epithelial cells with active *Pdx1* expression. The Cre-recombinase, recombines *loxp* sites that flank stop codons in the transgenes and oncogene expression is irreversibly initiated. Primary tumours develop that match several clinical, histopathological and genomic hallmarks of human PDA, including local invasion followed by metastatic spread to predominantly the liver, cancer-associated cachexia, primary drug resistance, progression through increasingly dysplastic PanIN stages to adenocarcinoma, a highly stiffened and hypovascular microenvironment with abundant ECM deposition, αSMA+ fibroblasts and genomic instability with features of complex, nonreciprocal translocations without telomere erosion (Gopinathan et al., 2015; Hingorani et al., 2005; Singh et al., 2010). Whilst matching these aspects of the human disease, several important aspects regarding the accuracy of the KPC GEMM for human PDA modelling, remain to be fully explored. These include a lack of clarity on the relevance of using this predominantly-primary tumour model to explore human PDA, which is typically a metastatic disease and whether the KPC can model the range of classical and squamous PDA differentiations seen in humans. In addition, transgene activation and inflammation occurs throughout the entire pancreas, the resulting tumours are often multifocal and all non-transformed cells in the mouse have only one copy of WT *Kras* and *Trp53*, all with unknown consequences. Moreover, there is a lack of clarity on how well the model predicts therapeutic sensitivity and there is a notable lack of direct comparisons of the cellular composition of the TME between murine and human tumours, particularly with respect to fibroblast composition (Gengenbacher et al., 2017; Gopinathan et al., 2015; Ireson et al., 2019).

1.2.7 – Transcriptional and surface marker heterogeneity of PDA fibroblasts

As for many other tissues and tumour types, scRNAseq has revealed extensive transcriptional heterogeneity within fibroblasts from PDA tumours (Bernard et al., 2019; Dominguez et al., 2020; Elyada et al., 2019; Hosein et al., 2019). Elyada et al. observe 3 distinct fibroblast-like clusters from KPC GEMM tumours and 2 distinct fibroblast-like clusters in human PDA samples. Domingeuz et al. observe a total of 6 distinct clusters of fibroblast-like cells across normal murine pancreas and KPP GEMM (*Pdx1-Cre; Kras*$^{LSL\text{-}G12D/+}$*; p16/p19*$^{fl/fl}$) tumours (Dominguez et al., 2020). In both studies, several of

the clusters have differential expression of selected MyCAF and iCAF genes and thus polarisation between myofibroblast-and inflammatory-like fibroblast states appears to be a common and major driver of transcriptional differences in PDA fibroblasts. Compatibility between the studies is complicated by different analytical workflows, different selected MyCAF/iCAF genes and the use of the KPC GEMM in the former and an alternative, less characterised PDA GEMM, the KPP, in the later.

Elyada et al. go on to isolate fibroblasts with iCAF-like features using surface Ly6C expression, a second fibroblast-like population based on an MHCII expression reporter and a third population that lacks these markers and is suggested to overlap with the MyCAF-like phenotype. Domingeuz et al. isolate a MyCAF-like population based on LRRC15. Both studies show divergent functions of these fibroblast-like cells in co-culture experiments, with CD4 T cells and PDA cancer cells respectively, but the stability of the fibroblast phenotypes *in vitro* was not assessed and the relevance of these phenotypes *in vivo* are not known. The authors suggest that the LRCC15+ fibroblast signature predicts immunotherapy failure, but because this signature is effectively a myofibroblast signature (that can be induced in TGFβ-rich environments) and TGFβ is potently immunosuppressive, it is hard to determine if immunotherapy response is in any way related to fibroblasts or is simply a downstream readout for a high-TGFβ and immunosuppressed environment.

FAP was identified as a putative marker of a subpopulation of fibroblasts in PDA tumours over 10 years ago (Feig et al., 2013; Kraman et al., 2010) and has also since been observed to be expressed on fibroblasts in other tumour types (Costa et al., 2018; Kieffer et al., 2020) and in other fibrotic pathologies (Aghajanian et al., 2019). There is conflicting data on the distribution of FAP on fibroblasts in PDA: one study has suggested FAP protein expression overlaps with the myofibroblast phenotype by IHC in PDA tumours (Ohlund et al., 2017), whilst one scRNAseq study suggests that the *Fap* gene it is equally expressed in all activated fibroblasts in PDA (Elyada et al., 2019) and a second scRNAseq study suggests that normal pancreatic fibroblasts have equally high expression of *Fap* as fibroblasts in PDA (Dominguez et al., 2020). The reasons for the differences between these studies and the exact population that FAP expression identifies are not clear.

As mentioned above, surface expression of PDGFRα and PDGFRβ are used as fibroblast markers but appear to have variable expression depending on the tissue/tumour being analysed and the activation state of the fibroblasts (Dominguez et al., 2020; Ohlund et al., 2017; Sugimoto et al., 2006). A study in breast cancer samples suggests GPR77 and CD10 demarks a fibroblast population with high NFkB signalling (Su et al., 2018). Interestingly, C5a signalling via GRP77 was functionally important for the pro-tumourigenic function of this fibroblast population in an immune deficient PDX model. Whether GPR77/CD10 also identifies a fibroblast subpopulation in PDA is not known.

1.2.8 – Evidence for tumour-promoting and tumour-suppressive functions of PDA fibroblasts

Laser capture microdissection of human PDA tumours has identified ECM-rich and immune-rich environments, with the ECM-rich being associated with reduced survival, especially within the squamous PDA cancer subtype (Maurer et al., 2019). A second study of human PDA samples indicates that lower levels of stroma are associated with metastatic disease and that high levels of stroma are predictive of improved survival (Torphy et al., 2018). Such studies may support the idea that different TME environments can influence disease progression in humans but tell us little about whether these stromal elements are driving tumour progression or are simply a downstream product of the key processes that are. For example, as for the findings from Dominguez et al., a TGFβ-rich environment is known to drive cancer cell EMT and invasion and also support an immunosuppressed environment (all features of aggressive disease) but would also induce an myofibroblast- and ECM-rich microenvironment. In a similar manner, the immune-rich environment reported, may simply represent ongoing T cell-mediated cancer killing that is important for tumour progression but is largely independent of fibroblasts. The difficulty of inferring the role of fibroblasts from bulk stromal measurement of human tumours has meant that most understanding of direct functions of fibroblasts in tumours has mainly come from *in vitro* assays or mouse modelling.

A large number of pro-tumourigenic functions of fibroblasts in PDA have been described. Fibroblasts can provide mitogenic and survival paracrine signals to PDA cells (Shi et al., 2019; Tape et al., 2016) and can inactive the cytotoxicity of gemcitabine (Dalin et al.,

2019). In addition, fibroblasts have the capacity to support PDA cell metabolism through amino acid and lipid release (Auciello et al., 2019; Olivares et al., 2017; Sousa et al., 2016). FAP+ fibroblasts have been reported to exclude CD8+ T cells from PDA tumours (Kraman et al., 2010), in a mechanism based on altered stromal T cell trafficking due to CXCL12 secretion (Feig et al., 2013), a pleotropic soluble factor, known to have strong lymphocyte chemotactic properties (Bleul et al., 1996). The abundant ECM in PDA tumours appears to change molecular diffusion dynamics, altering pharmacodynamics of drug delivery (Jacobetz et al., 2013; Olive et al., 2009; Provenzano et al., 2012), and collagen networks produced by fibroblasts are found to influence T cell migration, in what is thought to be a non-productive manner (Hartmann et al., 2014). IL6 secreted by PDA fibroblasts is able to promote the formation of immature myeloid cells, with a phenotype associated with immune-suppressive properties (Mace et al., 2013) and IL6 released from PDA primary tumours (possibly from iCAF-like fibroblasts) is found to contribute to metabolic changes in the liver, systemic cachexia and immune suppression (Flint et al., 2016). An ability for fibroblasts to mediate angiogenesis and cancer cell invasion and migration have been demonstrated in other cancer types (Calon et al., 2012; Fukumura et al., 1998; Gaggioli et al., 2007; O'Connell et al., 2011) but it is not clear if these fibroblast functions contribute to PDA progression, although fibroblast depletion appears to improve PDA tumour vascularisation (Rhim et al., 2014).

Notably, several of the studies that report pro-tumourigenic features of fibroblasts utilize reductionist *in vitro* experiments to infer *in vivo* function or do not account for the impact fibroblast heterogeneity may have on the conclusions. For example, of all the studies cited above, only those exploring FAP+ fibroblasts take fibroblast heterogeneity into account when studying fibroblast function. Unfortunately, in this regard there is still little consensus on what fibroblast population FAP identifies in PDA tumours and what the population's role is *in vivo* (Aghajanian et al., 2019; Busek et al., 2018; Dominguez et al., 2020; Elyada et al., 2019; Kakarla et al., 2013; Ohlund et al., 2017; Tran et al., 2013).

However, several lines of preclinical and clinical evidence suggest a net anti-tumourigenic role for fibroblasts in PDA progression. Early studies of the PDA TME, provided compelling evidence that SHH paracrine signalling from cancer cells to PDA fibroblasts was a key determinant of the expansion and maintenance of the fibroblast-rich stroma in PDA tumours and that targeting the canonical Hedgehog signalling

receptor, smoothened (SMO), reduces fibroblast accumulation (Bailey et al., 2008; Fendrich et al., 2011; Nolan-Stevaux et al., 2009; Olive et al., 2009; Tian et al., 2009). Based on this preclinical data, some of the first stromal targeting clinical trials were initiated, using SMO inhibitors (SMOi) in PDA patients (Rosow et al., 2012). Unfortunately, not only did these studies fail to show efficacy, there was evidence that treating PDA patients with SMOi accelerated tumour progression. For example, interim analysis of a phase 2 double-blind placebo-controlled study, indicated that OS in the SMOi plus gemcitabine cohort was less than 6 mo, compared to greater than 6 mo in the gemcitabine only cohort, resulting in termination of the clinical trial (Businesswire.com, 2012).

Such studies widened an appreciation that fibroblasts in the PDA TME may have tumour restrictive properties. Three subsequent, seminal studies, using several spontaneous PDA GEMMs, have also suggested a net tumour restrictive effect of fibroblasts in PDA tumours. In two studies, pharmacological blockade of Hedgehog signalling or genetic deletion of *Shh* in PDA tumour cells, reduces paracrine activation of fibroblasts, reduces fibroblast accumulation and reduces tumour cell differentiation, accelerates tumour progression, increases metastasis and reduces survival (Lee et al., 2014a; Rhim et al., 2014). Paracrine SHH signalling in these models appears to be highly restricted to occur from PDA cancer cells to fibroblasts, thus, conditional *Shh* deletion in PDA cancer cells should have minimal direct effects on other components of the TME and allow fibroblast-regulated processes to be measured. The SMOi-induced reduction of fibroblasts, is associated with a less-differentiated cancer cell phenotype and a highly altered composition of the TME, with vascular and immune components changing, further highlighting the complex heterocellular interactions of fibroblasts in tumours. Conversely, dosing PDA tumour-bearing mice with an activating SMO agonist, induces stromal hyperplasia and fibroblast accumulation, increases cancer cell differentiation, reduces tumour progression and growth and is found to induce aggregates of immune cells around lesions (Lee et al., 2014a). Notably, a similar restrictive function of SHH-activated fibroblasts in bladder cancer has been reported (Shin et al., 2014). A third study generated a transgenic mouse in which herpes simplex virus-1 thymidine kinase (HSV-TK) expression is driven by the αSMA gene promoter, which allows for active depletion of proliferating myofibroblasts on dosing with ganciclovir (Ozdemir et al., 2014). Crossing this model with several different PDA GEMMs (including the KPC), indicates that

depletion of proliferating myofibroblasts at both an early and late timepoint, was associated with reduced fibroblast accumulation, reduced ECM deposition, reduced stiffness but increased tumour cell invasion and decreased survival. A key caveat with this study is that other cells in the TME express αSMA, such as pericytes and smooth muscle cells. Because the HSV-TK system can only deplete proliferating cells, the authors suggest this minimises the impact on the vasculature, however minimally evidence to support this is given. Importantly, not all αSMA+ fibroblasts are proliferative and some are observed to remain in the tumours after depletion, so the exact population that is targeted by this strategy is also not clear. Interestingly, whilst in both the hedgehog signalling and αSMA+ cell depletion studies disease is accelerated, loss of fibroblasts results in sensitisation of the tumour to therapies that the fibroblast-rich tumours are refractory to. The studies demonstrate increased sensitivity to targeted therapies (vascular endothelial growth factor inhibitors (VEGFRi)) and immune checkpoint blockade, respectively, suggesting that fibroblast abundance can directly modulate response to therapies that target other TME components (Ozdemir et al., 2014; Rhim et al., 2014).

The idea of 'normalising' fibroblasts rather than finding therapies that deplete them, has gained traction in the PDA research field, mainly based on the ability of vitamin D receptor agonists to attenuate the myofibroblast-like state (Sherman et al., 2014). However, interpretation of the *in vivo* results in this study are complicated by the expression of the receptor by many other cell types and its involvement in a huge array of biological processes (Bhattacharjee et al., 2014; Takahashi and Morikawa, 2006). The idea of fibroblast modulation over fibroblast depletion is supported by studies of fibrosis: depletion of PDGFRβ+ cells fails to alter kidney fibrosis progression (LeBleu et al., 2013) but inhibition of PDGFRβ signalling is efficacious (Chen et al., 2011).

A variety of methods aimed at therapeutically targeting fibroblasts in tumours are currently being explored (Chen and Song, 2019; Ho et al., 2020; Hosein et al., 2020) but apparent fibroblast heterogeneity and their ability to regulate multiple microenvironmental processes in parallel, suggests a highly targeted approach will be required to yield clinical benefits.

1.3 – Advances in novel single cell technologies for mapping cellular heterogeneity and phenotypes

Understanding of the role of fibroblasts in PDA will likely be greatly enhanced by an improved understanding of fibroblast heterogeneity in tumours and subsequent functional interrogation of individual fibroblast populations. In recent years, advances in single cell technologies have been a major driver for improved understanding of cellular heterogeneity in complex tissues (Spitzer and Nolan, 2016; Stuart and Satija, 2019) and application of such technologies to fibroblasts in tumours may lead to a more detailed understanding of fibroblast heterogeneity and its consequences. Whilst traditional flow cytometry and tissue imaging methods are well established techniques that retain single cell resolution, they typically measure only a limited number of parameters at a time and therefore require detailed *a priori* knowledge about the system of interest.

1.3.1 – Single cell RNA sequencing

scRNAseq has been the most widely adopted novel single cell technology, particularly since the introduction of droplet-based methods. ScRNAseq has revolutionised the ability of researchers to assess the gene expression patterns of complex, heterogenous cell mixes in an unbiased, discovery fashion (Vieth et al., 2019). scRNAseq is unmatched by any other technique in its genome-wide coverage and new advances are improving the accuracy of gene detection and sample to sample comparability (Gaublomme et al., 2019; McGinnis et al., 2019). Disadvantages of scRNAseq include high cost, high levels of gene dropout, lack of detection of specific genes or detection of low to intermediately expressed genes, poor expression quantification, batch effects and a lack of consensus on analytical workflows. In addition, RNA measurements show incomplete correlation with protein levels, such that on average, variation in RNA accounts for only ~40% of protein level variation (Liu et al., 2016) and can be substantially lower for proteins that are under extensive post-translational regulation, such as cell surface molecules (Dong et al., 2015).

1.3.2 – Mass cytometry

Mass cytometry (or cytometry by time-of-flight, CyTOF) is another single cell technology, that shares many similarities to flow cytometry. Single cell suspensions are labelled with antibodies that enable protein levels to be measured. Instead of being conjugated to fluorophores, mass cytometry antibodies are labelled with heavy metal ions via specialised chelation chemistry (Spitzer and Nolan, 2016). The antibody-metal complexes that are bound to target cells are quantified using a time of flight (TOF) mass spectrometer. Signal spill over between different mass channels in a TOF is small and therefore the cross-talk between different antibody channels is low. This, combined with the fact that the TOF mass spectrometer can detect metal ions across a mass range of 79-209 Da, means up to 60 markers can now be simultaneously measured at single cell resolution and the number of parameters is increasing as new metal/chelation chemistries are developed (Han et al., 2018). The output file format for mass cytometry is an FCS file which is the same format used for flow cytometry data analysis and many of established flow cytometry analytical pipelines and principles can be used for mass cytometry data analysis. In addition, once a mass cytometry panel has been developed and optimised, dozens to hundreds of samples can be tested and use of sample barcoding can minimise batch effects and allow accurate quantification of protein levels. The technology can be used to measure extracellular and intracellular lineage and phenotypic markers and can be adapted to quantify aspects of cell cycle (Behbehani et al., 2012), cell signalling (Bodenmiller et al., 2012), metabolism (Hartmann et al., 2020) or epigenetic modifications (Cheung et al., 2018). However, mass cytometry has several key limitations, including high setup costs, a dependence on available/robust antibodies for targets of interest, limitation to measurement of selected markers only (and the bias that introduces) and lower acquisition speed and signal flux than for current flow cytometry platforms (Spitzer and Nolan, 2016).

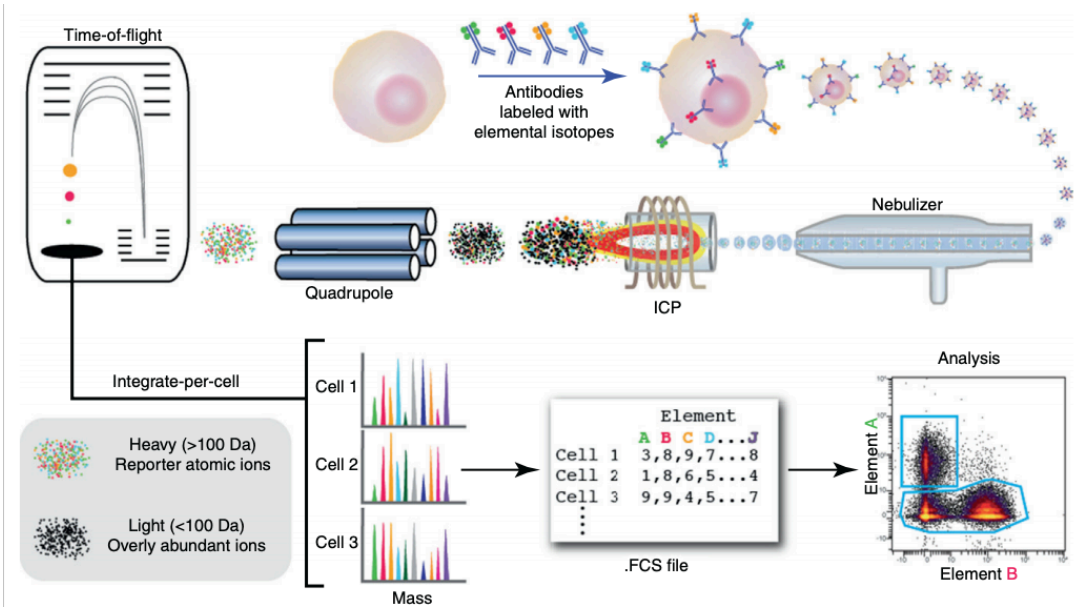

Figure 4. Analysis of heavy metal tagged cells by mass cytometry (CyTOF)
Schematic illustrating how mass cytometry allows single-cell atomic mass spectrometry of heavy elements (>79 Da). Antibodies tagged with heavy metal isotopes bind cellular epitopes. The cell is introduced to the inductively coupled plasma (ICP) torch by droplet nebulisation. Each cell is vaporised, atomised and then ionised, low mass ions (such as those of carbon, oxygen, hydrogen and nitrogen) are removed by quadrupole filter and the remaining heavy metal ions are measured by a highly precise time-of-flight (TOF) mass spectrometer. Signals of the elemental tag are integrated across the entire ion cloud for each cell and correspond to the abundance of the epitope on that particular cell. The process is repeated for the others cells in the sample at a sample acquisition rate of ~500 events/s. Quantification data is stored as an FCS file, allowing application of standard cytometry analysis. Reproduced from (Bendall et al., 2012)

1.3.3 – Hybrid technologies

Another aspect to consider when picking a tool for single cell analysis of heterogenous tissues, is that the boundaries between different single cell technologies are blurring. mRNA measurements can now be done with mass cytometry detection, using mass tagged mRNA-probes (Mavropoulos et al., 2017). Cellular indexing of transcriptomes and epitopes by sequencing (CITE-seq) technology, which uses oligo-tagged antibodies, is allowing protein measurements using droplet based scRNAseq platforms (Maier et al., 2020; Mimitou et al., 2019; Stoeckius et al., 2017). Lastly, new spectral un-mixing flow cytometry platforms, in which the entire emission profile of each fluorochrome is measured and quantified, are allowing for >20 parameters to be routinely measured by flow cytometry methods with minimized channel spill over (Ferrer-Font et al., 2020).

Chapter 2 - Project aims

Fibroblasts are abundant in PDA tumours but understanding of their contributions to PDA progression and treatment response is limited. This may be in part due to their heterogeneity, with fibroblast phenotypic plasticity reported in PDA tumours and functionally distinct fibroblast lineages well established in other mammalian tissues. In particular, a lack of robust surface markers for isolating live fibroblast populations for functional analysis, has hindered detailed interrogation of their contributions to PDA tumour progression. I sought to address this by mapping the heterogonous PDA TME at single cell resolution and isolate fibroblast populations for characterisation. Specifically, my aims are as follows:

Aim 1 – Develop a single cell analysis workflow to map the PDA TME

Aim 2 – Analyse fibroblast heterogeneity within the PDA TME

Aim 3 – Isolate distinct fibroblast populations and characterise their functions

Aim 4 – Apply the single cell analysis workflow to other tissues and tumour types

Chapter 3 – Materials and methods

3.1 – Tissue samples, processing and mass cytometry analysis

3.1.1 – Mice

All animal experiments were performed under a UK Home Office Licence and in accordance with the 'Animal (Scientific Procedures) Act of 1986' under Project Licence Number 70/8745 and 70/8375. Experiments adhered to Animal Research: Reporting of In Vivo Experiments (ARRIVE) guidelines and were subject to review by the Animal Welfare and Ethical Review Boards of the University of Manchester (UoM) and the University of Glasgow (UoG). *Pdx1-Cre; Kras*$^{LSL\text{-}G12D/+}$*; Trp53*$^{LSL\text{-}R172H/+}$ (KPC) mice (Hingorani et al., 2005) have been described previously. KPC colonies on mixed backgrounds were bred in-house in individually ventilated cages, under pathogen-free conditions at CRUK Beatson Institute (CRUK-BI) and maintained in conventional caging with environmental enrichment, access to standard chow and water *ad libitum*. Genotyping was performed by Transnetyx (Cordoba, TN, USA). Mice of both sexes were monitored 3 times weekly and when a diagnosis of pancreatic cancer was made by abdominal palpation, tumour growth was monitored by ultrasound imaging (Fujifilm VisualSonics, Vevo 3100 preclinical imaging system). Mice were culled by Schedule 1 method, as per institutional guidelines, when exhibiting moderate symptoms of PDA, such as swollen abdomen, loss of body conditioning resembling cachexia or reduced mobility. 'RFP+ KPC' mice were generated by crossing KPC and *Rosa26*$^{LSL\text{-}tdRFP/LSL\text{-}tdRFP}$ mice (Luche et al., 2007). RFP+ KPC colonies on a mixed background were maintained under pathogen-free conditions at the UoM and monitored as described above. Female C57BL/6 (B6) mice were purchased from Envigo and used at ages specified for each experiment. Female NOD-scid.*Il2rg*$^{-/-}$ (NSG) mice were purchased from Charles River and used at 14 weeks of age. B6.*Rag1*$^{-/-}$ mice (Mombaerts et al., 1992) and B6.*Batf3*$^{-/-}$ mice (Hildner et al., 2008) have been described previously, were maintained at the UoM and both sexes used at >12 weeks of age. B6.*Villin::CreER; Kras*$^{LSL\text{-}G12D/+}$*; Trp53*$^{fl/fl}$*; Rosa26*$^{Notch1icd/+}$ (KPN) mice (Jackstadt et al., 2019) have been described previously. KPN mice of both sexes at 6-12 weeks age were injected intraperitoneally with a single dose of 2 mg tamoxifen (Sigma Aldrich, T5648) and primary colorectal tumours collected

at clinical end point, defined as animal weight loss and/or hunching and/or cachexia. *MMTV-PyMT* mice (Guy et al., 1992) have been described previously. Female *MMTV-PyMT* mice were monitored for tumour growth by calliper measurement and tumours collected when total tumour volume was >900 mm^3, typically across multiple foci. B6.*Kras*$^{LSL\text{-}G12D/+}$*; Trp53*$^{fl/fl}$ ('KP') mice were generated by crossing B6.*Kras*$^{LSL\text{-}G12D/+}$ mice (Jackson et al., 2001) and B6.*Trp53*$^{fl/fl}$ mice (Marino et al., 2000), both of which have been described previously. KP mice of both sexes at 8-14 weeks of age were anaesthetized using isoflurane and intranasally administered with 50ul of $1x10^6$ PFU replication-deficient Cre-expressing adenovirus, as per standard protocols (Meuwissen et al., 2001) and monitored for tumour formation by computerized tomography scans. Resulting lung tumours were collected 16 weeks after adenoviral induction. B6.*Tyr::CreER; Braf*$^{LSL\text{-}V600E/+}$ (BRAFV600E) mice (Dhomen et al., 2009) have been described previously and were generated by crossing B6.*Tyr::CreER* (Mercer et al., 2005) and B6.*Braf*$^{LSL\text{-}V600E/+}$ mice (Yajima et al., 2006), both of which have been described previously. 8-12-week-old female mice had 1 mg freshly prepared tamoxifen in ethanol applied to their shaven back. 4 weeks after transgene induction, the back skin was UV irradiated with a UV6 lamp (UV280-380 nm) every week for 4 weeks. Once tumours were visible, tumour volume was measured weekly and collected at a minimum volume of 500 mm^3.

3.1.2 – Human tissue samples

Formalin fixed paraffin embedded (FFPE) human pancreatic, colorectal, breast and lung tumour samples were obtained with informed patient consent by the Manchester Cancer Research Centre (MCRC) Biobank in accordance with the Human Tissue Act 2004. The MCRC Biobank is licensed by the Human Tissue Authority (license number: 30004) and is ethically approved as a research tissue bank by the South Manchester Research Ethics Committee (Ref: 07/H1003/161+5). The role of the MCRC Biobank is to distribute samples. For more information see www.mcrc.manchester.ac.uk/Biobank/Ethics-and-Licensing. Human breast tumours were selected for triple negative status and human lung tumours selected for adenocarcinoma classification.

3.1.3 – Mass cytometry antibodies and antibody conjugation

Supplier, clone and heavy-metal isotope tag of each mass cytometry antibody used in this study is listed in Table 2-5. Where possible targets were allocated to heavy-metal channels of appropriate sensitivity of detection and spill over, placing low abundance targets in higher sensitivity channels with minimal spill over from more abundant channels. The dedicated panel builder at dvssciences.com was used to estimate isotope and oxide spill-over and guide channel selection. Particular antibody clones were selected based on widespread use and extensive evidence of specific staining in the literature or from our own flow cytometry analysis. Where indicated antibodies were purchased pre-conjugated (Fluidigm). All other antibodies were purchased in carrier protein-free format and labelled with the indicated heavy-metal tag using Maxpar X8 Antibody Conjugation Kits (Fluidigm) (Han et al., 2018). 200 µg of each antibody was washed twice with 400 µL R buffer (Fluidigm) in a 50 kDa Microfilter (Merck Millipore, UFC505096) by centrifuging at 12,000 g at room temperature (RT) for 6 minutes. Antibodies were partially reduced using 200 µL of a 4 mM solution of tris(2-carboxyethyl)phosphine hydrochloride (TCEP) (Thermo Fisher, 77720) in R-buffer. After 25 min of TCEP reduction, antibodies were washed twice with C-buffer (Fluidigm). In parallel to antibody reduction, metal chelation was performed by adding 10ul of 50 µM lanthanide metal solutions to two equivalents of Maxpar X8 chelating polymer (Fluidigm) in 190 µL of L-buffer (Fluidigm) and incubating for 1 h at RT. The metal loaded polymers were washed once with L-buffer then once with C-buffer in 3 kDa Microfilters (Merck Millipore, UFC500324), by centrifuging at 12,000 g for 20 min. The metal loaded polymer in C-buffer was added to the partially reduced antibody and incubated at 37 °C for 90 min. Conjugated antibodies were washed six times with W-buffer (Fluidigm), suspended in 100ul W-buffer, vortexed and left for 5 min at RT before being reverse centrifuged into a fresh 1.6 mL collection tube. Protein content was assessed using a Nanodrop One/One Spectrophotometer (Thermo Fisher) and then 300 µL of PBS-based Antibody Stabilization Buffer (Candor Biosciences, 13150) containing 0.6 mg/mL sodium azide (Sigma Aldrich, S8032) was added and the conjugated antibodies stored at 4 °C. To generate cisplatin conjugates, 200 µg of antibody was reduced as described above and incubated with 200 µL of 400 µM monoisotopic cisplatin (BuyIsotope, custom order) in C-buffer at 37 °C for 90 min and washed and stored as for the polymer/lanthanide conjugates. For any antibody that showed low final protein content (<40% recovery), the process was repeated but with a 10 min TCEP reduction. If significant degradation was still observed, an alternative antibody clone was tested or the target was not included in

the panel. Antibodies were titrated in panels by staining samples of known positive and negative controls. These included mixes of established and in-house cell lines, with and without recombinant protein stimulations and disaggregated murine normal tissues and tumours. If the lowest antibody concentration tested resulted in overstaining the antibody was diluted further with antibody stabilization buffer and re-titrated.

Table 2. Antibodies used for mesenchymal stroma mass cytometry analysis

Mesenchymal stroma panel - extracellular						
Target	**Metal**	**Clone**	**Pre-conjugated/custom**	**Supplier**	**Identifier**	**Comment**
Fc block	-	2.4G2	-	BD Biosciences	558636	5 min before mastermix
CD44	89Y	IM7	Custom	Biolegend	103002	
EpCAM	113In	G8.8	Custom	Biolegend	118202	
CD86	139La	GL-1	Custom	Biolegend	105002	
MCAM	141Pr	ME-9F1	Pre-conjugated	Fluidigm	3141016B	
ITGA5	142Nd	5H10-27(MFR5)	Custom	Biolegend	103801	
CD81	143Nd	Eat-2	Custom	Biolegend	104902	
CD87	144Nd	109801	Custom	Thermo Fisher	MA5-23853	
PE (ITGA1)	145Nd	PE001	Pre-conjugated	Fluidigm	3145006B	
ITGAV	146Nd	RMV-7	Custom	Biolegend	104102	
ITGA2	147Sm	Hma2	Custom	Biolegend	103501	
PDGFRA	148Nd	APA5	Pre-conjugated	Fluidigm	3148018B	
PDPN	149Sm	8.1.1	Custom	Biolegend	127402	
CD24	150Nd	M1/69	Pre-conjugated	Fluidigm	3150009B	
PDGFRB	151Eu	APB5	Pre-conjugated	Fluidigm	3151017B	
ICAM1	153Eu	YN1/1.7.4	Custom	Biolegend	116102	
CD63	155Gd	NVG-2	Custom	Biolegend	143902	Not used for RFP+ tumours
CD73	156Gd	TY/11.8	Custom	Biolegend	127202	
FITC (CD26)	160Gd	FIT-22	Pre-conjugated	Fluidigm	3160011B	
ITGB3	161Dy	Cc9.G2 (HMB3-1)	Custom	Biolegend	104302	
CD34	162Dy	MEC14.7	Custom	Biolegend	119302	
ITGA6	164Dy	GoH3	Custom	Biolegend	313602	
Biotin (CD105)	165Ho	1D4-C5	Pre-conjugated	Fluidigm	3165012B	
CD14	166Er	Sa14-2	Custom	Biolegend	123302	
CD74	167Er	In1/CD74	Custom	Biolegend	151002	
CD80	168Er	16-10A1	Custom	Biolegend	104702	
CD31	170Er	MEC13.3	Custom	Biolegend	102502	
CD38	171Yb	90	Pre-conjugated	Fluidigm	3171007B	
ITGB1	172Yb	HMB1-1	Custom	Biolegend	102202	
VCAM1	173Yb	429 (MVCAM.A)	Custom	Biolegend	105702	
CD45	175Lu	30-F11	Pre-conjugated	Fluidigm	3175010B	
APC (CD90)	176Yb	APC003	Pre-conjugated	Fluidigm	3176007B	
MHCI	194Pt	28-14-8	Custom	Biolegend	114502	
MHCII	209Bi	M5/114.15.2	Pre-conjugated	Fluidigm	3209006B	
Mesenchymal stroma panel - intracellular						
Target	**Metal**	**Clone**	**Pre-conjugated/custom**	**Supplier**	**Identifier**	**Comment**
Fc block	-	2.4G2	-	BD Biosciences	558636	5 min before mastermix
Cytokeratin-7	115In	RCK105	Custom	Abcam	Ab9021	
PDPN	149Sm	8.1.1	Custom	Biolegend	127402	
Pan-cytokeratin	152Sm	C-11	Custom	Biolegend	628602	
VIM	154Sm	D21H3	Pre-conjugated	Fluidigm	3154014A	
CD63	155Gd	NVG-2	Custom	Biolegend	143902	Not used for RFP+ tumours
RFP	155Gd	8E5.G7	Custom	Rockland Inc	200-301-379	Only for RFP+ tumours
DES	158Gd	Y66	Custom	Abcam	ab271829	
aSMA	159Tb	1A4	Custom	Abcam	ab240654	
Cleaved caspase-3 (CC3)	163Dy	D3E9	Custom	Cell Signaling Technology	9579	
CD74	167Er	In1/CD74	Custom	Biolegend	151002	
Ki67	169Tm	So1A15	Custom	Thermo Fisher	14-5698-82	
Collagen-4	174Yb	n/a (pAb)	Custom	Abcam	ab6586	

Table 3. Antibodies used for myeloid/NK/B cell mass cytometry analysis

Myeloid/NK/B cell panel - extracellular						
Target	**Metal**	**Clone**	**Pre-conjugated/custom**	**Supplier**	**Identifier**	**Comment**
CD64	151Eu	X54-5/7.1	Pre-conjugated	Fluidigm	3151012B	10 min before mastermix
CD16/32	145Nd	93	Custom	Biolegend	101302	5 min before mastermix
CD11b	89Y	M1/70	Custom	Biolegend	101202	
PDCA-1	113In	927	Custom	Biolegend	127002	
CD68	115In	FA-11	Custom	Biolegend	137002	
CD14	139La	Sa14-2	Custom	Biolegend	123302	
Ly6G	141Pr	1A8	Pre-conjugated	Fluidigm	3141008B	
Siglec-F	143Nd	E50-2440	Custom	BD Biosciences	552125	
PD-L1	144Nd	10F.9G2	Custom	Biolegend	124302	
F4/80	146Nd	BM8	Pre-conjugated	Fluidigm	3146008B	
MHCI	147Sm	28-14-8	Custom	Biolegend	114502	
CD3e	148Nd	17A2	Custom	BD Biosciences	555273	
CD19	149Sm	6D5	Pre-conjugated	Fluidigm	3149002B	
CD1d	150Nd	1B1	Custom	Biolegend	123502	
CD11c	154Sm	N418	Custom	Biolegend	117302	
CD63	155Gd	NVG-2	Custom	Biolegend	143902	
XCR1	156Gd	ZET	Custom	Biolegend	148202	
TCRb	157Gd	H57-597	Custom	Biolegend	109202	
CD45	158Gd	30-F11	Custom	Biolegend	103102	
CX3CR1	159Tb	SA011F11	Custom	Biolegend	149002	
CXCR2	160Gd	SA044G4	Custom	Biolegend	149302	
CSF1R	162Dy	AFS98	Custom	Biolegend	135502	
CD40	163Dy	HM40-3	Custom	Biolegend	102902	
CD103	164Dy	2E7	Custom	Biolegend	121402	
PD-L2	165Ho	TY25	Custom	Biolegend	107202	
VISTA	166Er	MIH63	Custom	Biolegend	150202	
SIRPa	167Er	P84	Custom	Biolegend	144002	
IL-4Ra	168Er	I015F8	Custom	Biolegend	144802	
CD206	169Tm	C086C2	Pre-conjugated	Fluidigm	3169021B	
CD49b (ITGA2)	170Er	HMa2	Pre-conjugated	Fluidigm	3170008B	
CD80	171Yb	16-10A1	Pre-conjugated	Fluidigm	3171008B	
CD86	172Yb	GL1	Pre-conjugated	Fluidigm	3172016B	
CD101	173Yb	Moushi101	Custom	Biolegend	Custom order	
NKp46	174Yb	29A1.4	Custom	Biolegend	137602	
CD38	175Lu	90	Pre-conjugated	Fluidigm	3175014B	
Ly-6C	176Yb	HK1.4	Custom	Biolegend	128002	
CD24	194Pt	M1/69	Custom	Biolegend	101802	
MHCII	209Bi	M5/114.15.2	Pre-conjugated	Fluidigm	3209006B	
Myeloid/NK/B cell panel - intracellular						
Target	**Metal**	**Clone**	**Pre-conjugated/custom**	**Supplier**	**Identifier**	**Comment**
Fc block	-	2.4G2	-	BD Biosciences	558636	5 min before mastermix
CD68	115In	FA-11	Custom	Biolegend	137002	
Cleaved caspase-3 (CC3)	142Nd	D3E9	Custom	Cell Signaling Technology	9579	
CD3e	148Nd	17A2	Custom	BD Biosciences	555273	
Ki67	152Sm	So1A15	Custom	Thermo Fisher	14-5698-82	
Galectin-9	153Eu	9M1-3	Custom	Thermo Fisher	16-9116-85	
CD63	155Gd	NVG-2	Custom	Biolegend	143902	
iNOS	161Dy	CXNFT	Pre-conjugated	Fluidigm	3161011B	
CD206	169Tm	C086C2	Pre-conjugated	Fluidigm	3169021B	

Table 4. Antibodies used for T cell mass cytometry analysis

T cell panel - extracellular						
Target	**Metal**	**Clone**	**Pre-conjugated/custom**	**Supplier**	**Identifier**	**Comment**
Fc block	-	2.4G2	-	BD Biosciences	558636	5 min before mastermix
Ly-6C	89Y	HK1.4	Custom	Biolegend	128002	
TCRb	115In	H57-597	Custom	Biolegend	109202	
CXCR3	139La	CXCR3-173	Custom	Biolegend	126502	
GITR	143Nd	DTA1	Pre-conjugated	Fluidigm	3143019B	
CD44	144Nd	IM7	Custom	Biolegend	103002	
CD69	145Nd	H1.2F3	Pre-conjugated	Fluidigm	3145005B	
TIGIT	146Nd	1G9	Custom	Biolegend	142102	
4-1BB	148Nd	17B5	Custom	Biolegend	106107	
CD101	149Sm	Moushi101	Custom	Biolegend	Custom order	
CD27	150Nd	LG.3A10	Pre-conjugated	Fluidigm	3150017B	
LAG3	151Eu	C9B7W	Custom	Biolegend	125202	
CD8a	153Eu	53-6.7	Pre-conjugated	Fluidigm	3153012B	
CTLA4	154Sm	UC10-4B9	Pre-conjugated	Fluidigm	3154008B	
CD4	155Gd	RM4-5	Custom	Biolegend	100506	
CD11c	157Gd	N418	Custom	Biolegend	117302	
CD45	158Gd	30-F11	Custom	Biolegend	103102	
PD-1	159Tb	29F.1A12	Pre-conjugated	Fluidigm	3159024B	
CD62L	160Gd	MEL-14	Pre-conjugated	Fluidigm	3160008B	
TIM3	162Dy	RMT3-23	Pre-conjugated	Fluidigm	3162029B	
CD49b	163Dy	HMa2	Custom	Biolegend	103501	
CD103	164Dy	2E7	Custom	Biolegend	121402	
OX40	166Er	OX-86	Custom	Thermo Fisher	14-1341-82	
KLRG1	167Er	2F1	Custom	BD Biosciences	562190	
ICOS	168Er	C398.4A	Pre-conjugated	Fluidigm	3168024B	
CD39	169Tm	24DMS1	Custom	Thermo Fisher	14-0391-82	
NKp46	170Er	29A1.4	Custom	Biolegend	137602	
SLAM	171Yb	TC15-12F12.2	Custom	Biolegend	115902	
CD25	172Yb	PC61	Custom	Biolegend	102002	
CD3e	173Yb	17A2	Custom	BD Biosciences	555273	
CD127	174Yb	A7R34	Pre-conjugated	Fluidigm	3174013B	
CD38	175Lu	90	Pre-conjugated	Fluidigm	3175014B	
TCRgd	176Yb	UC7-13D5	Custom	Biolegend	107502	
CD11b	194Pt	M1/70	Custom	Biolegend	101202	
MHCII	209Bi	M5/114.15.2	Pre-conjugated	Fluidigm	3209006B	
T cell panel - intracellular						
Target	**Metal**	**Clone**	**Pre-conjugated/custom**	**Supplier**	**Identifier**	**Comment**
Fc block	-	2.4G2	-	BD Biosciences	558636	5 min before mastermix
GATA3	113In	L50-823	Custom	BD Biosciences	558686	
GZMB	141Pr	GB11	Custom	Thermo Fisher	MA1-80734	
Cleaved caspase-3 (CC3)	142Nd	D3E9	Custom	Cell Signaling Technology	9579	
TCF1	147Sm	C63D9	Custom	Cell Signaling Technology	2203	
Ki67	152Sm	So1A15	Custom	Thermo Fisher	14-5698-82	
CTLA4	154Sm	UC10-4B9	Pre-conjugated	Fluidigm	3154008B	
EOMES	156Gd	Dan11mag	Custom	Thermo Fisher	14-4875-82	
TBET	161Dy	4B10	Pre-conjugated	Fluidigm	3160010B	
FOXP3	165Ho	FJK-16s	Pre-conjugated	Fluidigm	3165024A	
CD3e	173Yb	17A2	Custom	BD Biosciences	555273	

Table 5. Antibodies used for signalling mass cytometry analysis

Phospho panel - all intracellular						
Antibody target	**Metal**	**Clone**	**Pre-conjugated/custom**	**Supplier**	**Identifier**	**Comment**
Fc block	-	2.4G2	-	BD	558636	5 min before mastermix
RFP	89Y	8E5.G7	Custom	Rockland Inc	200-301-379	
pMARPKAPK2 [T334]	139La	27B7	Custom	Cell Signaling Technology	3007	
pTAK1 [S412]	141Pr	pAb	Custom	Cell Signaling Technology	9339	
Cleaved caspase-3 [D175]	142Nd	D3E9	Custom	Cell Signaling Technology	9579	
pAMPKa [T172]	143Nd	40H9	Custom	Cell Signaling Technology	2535	
pPLCg2 [Y759]	144Nd	K86-689.37	Pre-conjugated	Fluidigm	3144015A	
pFAK [S910]	145Nd	K73-480	Custom	BD Biosciences	Custom order	
pp90RSK [S380]	146Nd	D5D8	Custom	Cell Signaling Technology	12032	
B-catenin	147Sm	D10A8	Pre-conjugated	Fluidigm	3147005A	
pSTAT4 [Y693]	148Nd	38/p-Stat4	Pre-conjugated	Fluidigm	3148006A	
p4EBP1 [T37/T46]	149Sm	236B4	Pre-conjugated	Fluidigm	3149005A	
pSTAT5 [Y694]	150Nd	47/Stat5	Pre-conjugated	Fluidigm	3150005A	
pGSK3B [S9]	151Eu	D85E12	Custom	Cell Signaling Technology	5558	
pAKT [S473]	152Eu	D9E	Pre-conjugated	Fluidigm	3152005A	
pSTAT1 [Y701]	153Eu	58D6	Pre-conjugated	Fluidigm	3153003A	
pSMAD1/5/9 [S463]/465]/[S463/465]/[S465/467]	154Sm	D5B10	Custom	Cell Signaling Technology	13820	
p70S6K [T389]	155Gd	1A5	Custom	Cell Signaling Technology	9206	
pp38 [T180/182]	156Gd	D3F9	Pre-conjugated	Fluidigm	3156002A	
pSTAT3 [Y705]	158Gd	4/P-STAT3	Pre-conjugated	Fluidigm	3158005A	
pMEK1/2 [S221]	159Tb	166F8	Custom	Cell Signaling Technology	2338	
pAKT [T308]	160Gd	D25E6	Custom	Cell Signaling Technology	13038	
pSRC [Y418]	161Dy	SC1T2M3	Custom	Thermo Fisher	12-9034-82	
pMKK3/6 [S189]/[S207]	162Dy	D8E9	Custom	Cell Signaling Technology	12280	
CyclinB1	163Dy	V152	Custom	Cell Signaling Technology	4135	
IkBa (Amino-terminal Antigen)	164Dy	L35A5	Pre-conjugated	Fluidigm	3164004A	
pCREB [S133]	165Ho	87G3	Pre-conjugated	Fluidigm	3165009A	
pJAK2 [Y1007/1008]	166Er	E132	Custom	Abcam	ab219728	
pERK1/2 [T202]/[Y204]	167Er	D1314.4E	Pre-conjugated	Fluidigm	3167005A	
pIKKa/b [S176/180]	168Er	16A6	Custom	Cell Signaling Technology	2697	
pSMAD2/3 [S465/467]/[S423/425]	169Tm	D27F4	Custom	Cell Signaling Technology	8828	
pNFkBp65 [S536]	170Er	92H1	Custom	Cell Signaling Technology	3033	
pMKK4 [S257]	171Yb	C36C11	Custom	Cell Signaling Technology	4514	
pRelB [S552]	172Yb	D41B9	Custom	Cell Signaling Technology	5025	
pPDK1 [S241]	173Yb	J66-653.44.22	Custom	BD Biosciences	558395	
pRB [S807/S811]	174Yb	J112-906	Custom	BD Biosciences	558389	
pS6 [S235/S236]	175Lu	N7-548	Pre-conjugated	Fluidigm	3175009A	
pHH3 [S28]	176Yb	HTA28	Custom	Biolegend	641002	
GFP	198Pt	FM264C	Custom	Biolegend	338002	

3.1.4 – Tumour disaggregations

For tumour samples that would be analysed by mass cytometry, all buffers and reagents used in tissue processing and cell staining were checked for heavy-metal ion contamination, particularly barium contamination, and buffers were made up in non-glass containers that had not been detergent washed. 5-iodo-2'-deoxyuridine (IdU) (Sigma Aldrich, 17125) was solubilized overnight at RT under mixing, in a minimally basic solution of 0.01 M sodium hydroxide (NaOH) (Sigma Aldrich, 757527) in water, to 10 mg/mL concentration and filtered through a 0.22 µm pore mesh. To label cells in S-phase for mass cytometry studies, mice were injected intraperitoneally with 200 µL of IdU solution 2 h before the mouse was culled by Schedule 1 method and tissues collected. Tumour samples were quickly transferred into ice-cold phosphate-buffered saline (PBS) (Fisher Scientific, 10091403) on ice. From all tumours, care was taken to dissect away all non-tumour tissue that was attached to the outer edge of the denser tumour core. The surface of the tumour samples was dried with sterile paper and tumour weight recorded. Samples were washed once with ice-cold RPMI media and minced with disposable scalpels in 2 mL of disaggregation buffer (DB), consisting of 2 mg/mL Collagenase Type IV (Thermo Fisher, 17104019), 1 mg/mL DNase1 (Sigma Aldrich, 10104159001) and 0.5 mg/mL Hyaluronidase (Sigma Aldrich, H3757) in RPMI. Once no tumour piece was bigger than 3 mm in length, the fragments and buffer were transferred to a C-tube (Miltenyi Biotech, 130-096-334) and a further 3 mL of DB added. If tumours were >600 mg, the disaggregation was carried out in two C-tubes, each with a total of 5 mL DB. The C-tube was placed in a GentleMACS Octo Dissociator (Miltenyi Biotech), heating blocks fitted and tumours disaggregated using the automated 37C_m_TDK1 program. Once complete, the C-tube was centrifuged at 100 g for 2 min, to ensure the contents were gathered at the bottom of the tube. The sample was diluted with a further 5 mL of fresh and warmed DB, mixed well by pipetting and filtered into a 50 mL tube through a 70 µm strainer, which was then washed with 10 mL ice-cold RPMI to quench the digestion. The single cell suspension was pelleted at 300 g for 6 min and used for mass or flow cytometry staining.

3.1.5 – Mass cytometry live/dead and extracellular staining

Because mass cytometry staining involves multiple steps, all spins used a swinging bucket centrifuge with the braking speed reduced to avoid disruption to the cell pellet. Aspirations were done carefully and always left at least 50 µL of void volume above the pellet. Live cells were spun at 300 g for 6 min and fixed cells spun at 1000 g for 6 min. Particular care was taken during PBS-only washes to ensure that cells had pelleted completely. The disaggregated tumour cell pellet was resuspended in 300 µL of ice-cold PBS, vortexed well and 300 µL of 1 µM 198Pt monoisotopic cisplatin (Fluidigm, 201198) in PBS added, followed by vortexing. After exactly 1 min incubation, the staining was quenched with 20 mL of CSM-E (Cell Staining Buffer – Extracellular) consisting of 5 mg/ml Bovine Serum Albumin (BSA) (Sigma Aldrich, A3294), 0.5% v/v Fetal Bovine Albumin (FBS) (Thermo Fisher, 10270106) and 0.2 mg/mL DNAse1 in PBS. The cells were resuspended and counted using a Luna Cell Counter (Logosbio) on fluorescence mode. The propidium iodide and acridine orange staining allows for improved cell counting of disaggregated tissues compared with trypan blue-based methods. $3x10^6$ cells were aliquoted into a 5 mL polypropylene FACS tube, washed with 3 mL CSM-E and pelleted. 20 µL of 100 U/mL heparin sodium salt (Sigma Aldrich, H3393) solution in PBS and 1 µL Fc block (BD Biosciences, 558636) was added. The contents were mixed by gentle rocking but no vortexing and incubated on ice for 5 min. A master mix of fluorophore-conjugated antibodies (see Table 6) in 50 µL CSM-E was added, mixed by gentle rocking and incubated on ice in the dark. After 20 min the mixture was vortexed. After a total incubation of 45 min, the cells were washed once with 4 mL of CSM-E. A master mix of extracellular targeting, metal-conjugated antibodies (see Table 2-4) in 50 µL of CSM-E was added, mixed by gentle rocking and incubated on ice in the dark. After 20 min the mixture was vortexed. After a total incubation of 45 min, the cells were washed twice with 4 mL of CSM-E. The cell pellet was resuspended in 100 µL of PBS and vortexed and 1 mL of FOXP3 Fixation/Permeabilization Kit (Thermo Fisher, 00-5523-00) 1x FOXP3 Fixation Buffer added, followed by thorough vortexing. After 30 min incubation at RT, 2 mL of 1x FOXP3 Permeabilization Buffer was added and the cells pelleted. The cell pellet was resuspended in 1 mL of 10% v/v DMSO (Sigma Aldrich, D2650) in CSM-I (Cell Staining Buffer – Intracellular), consisting of 5 mg/ml BSA and 0.2 mg/ml sodium azide in PBS, vortexed and frozen at -80 °C. For staining the sample with the Myeloid/NK/B cell (MNB) panel, no extracellular Fc block was used. Instead, the cells were incubated with heparin solution for 5 min, followed by metal-conjugated anti-CD64 antibody for 10 min on ice, followed by metal-conjugated anti-CD16/32 antibody for 5

min on ice, before adding the remaining master mix of extracellular antibodies. This ensured strong metal labelling of Fc-receptors, which contributed to accurate sub-setting of the mononuclear phagocyte lineage.

Table 6. Fluorophore conjugated antibodies used for mass cytometry

Fluorophore conjugated antibodies					
Target	**Conjugate**	**Clone**	**Supplier**	**Product code**	**Comment**
Fc block	-	2.4G2	BD Biosciences	558636	5 min before mastermix
CD90	APC	G7	Abcam	ab25322	
CD105	Biotin	MJ7/18	Biolegend	120404	
ITGA1	PE	HMa1	Biolegend	142604	
CD26	FITC	H194-112	Biolegend	137806	

3.1.6 – Mass cytometry barcoding, pooling and intracellular staining

Once the samples for an entire study had been collected, all the frozen aliquots were allowed to thaw at RT and washed once with 4 mL PBS. Each of the cell pellets were resuspended in a unique barcoding aliquot from the Cell-ID 20-plex Pd Barcoding Kit (Fluidigm, 201060) in 1 mL of cold PBS, vortexed and incubated at RT for 15 min. After the incubation, the mixtures were diluted in 3 mL of CSM-I, pelleted and washed once more with 4 mL CSM-I. Each of the cell pellets from the samples to be included in the study were resuspended in 200 µL of 1x FOXP3 Permeabilization Buffer each, pooled into a 5 mL polypropylene FACS tube and pelleted. For each sample included in the pooled sample, 10 µL of 100 U/mL heparin sodium salt in PBS and 0.5 µL of Fc block was added and the sample mixed by gently rocking. After incubating for 5 min at RT in the dark, a master mix of intracellular targeting, metal-conjugated antibodies (see Table 2-4) in CSM-I was added. For each sample included in the pooled sample, one equivalent of antibody and 25 µL of CSM-I was used and scaled up as required. The sample was mixed by gentle rocking and incubated on ice in the dark. After 20 min the mixture was vortexed. After a total incubation of 45 min the cells were washed twice with 4 mL of CSM-I. The cell pellet was resuspended in 1 mL of PBS and vortexed well. For every individual sample included in the pooled sample, a minimum of 500 µL of 4% Paraformaldehyde (PFA) (Thermo Fisher, 28908) in PBS was added to ensure complete fixation, using larger tubes as needed. If during sample acquisition, the heavy-metal markers are seen to ‘streak’, this is an indication the cells were not sufficiently fixed at this stage. The sample was vortexed and stored overnight at 4 °C in the dark.

3.1.7 – Mass cytometry DNA staining and acquisition

On the day of acquisition, 0.5 µL of 125 µM of Cell-ID Iridium Intercalator (Fluidigm, 201192A) for each individual sample included in the pooled sample was added to the cells/PFA mixture and vortexed well. After 1 h of incubation at RT the cells were washed once with PBS, aliquoting across multiple tubes to allow staggered acquisition over a long run time. Typically, a pooled sample containing >15 individual samples was stored as x4 cell pellets, each prepared just before running. Each cell pellet was washed twice with water and resuspended at a concentration of $1x10^6$ cells/mL in 15% EQ Four Element Calibration Beads (Fluidigm, 201078) in water, filtered twice through 70 µm Filcons (BD Biosciences, 340633) and acquired on a Helios Mass Cytometer (Fluidigm), using a Super Sampler (Victorian Airship & Scientific Apparatus LLC) to improve the consistency of sample delivery. The sample was acquired at a maximum of 500 events/s and sample lines and nebulizers were replaced each time an additional $5x10^6$ events had been recorded. If marker 'streaking' during acquisition was seen to occur, the PFA step can be quenched with CSM-I to further cross-link the cells and the sample kept on ice during acquisition.

3.1.8 – Mass cytometry data processing

FCS files were normalized for signal-drift during the acquisition run using the in-built Helios normalization tool (Fluidigm) and individual sample events deconvoluted using either the in-built debarcoder (Fluidigm) or a stand-alone debarcoder (Zunder et al., 2015), typically using a Mahalanobis distance of 10 and 15 respectively and a minimum barcode separation of 0.26 for both. Individual sample FCS files were uploaded to the cloud-based cytometry platform Cytobank (www.cytobank.org, Beckmann Coulter) and checked for consistent signal across the entire acquisition period, as well as clean and correct barcode deconvolution. As per standard methods, live cell events were selected based on 191Ir positivity and 198Pt negativity. Because samples were stained with cisplatin separately, this step was conducted using sample tailored gating. 191Ir+ debris and cell doublets and aggregates were removed based on event length. If possible, target cells were selected by manual biaxial gating: MNB cell events were selected as CD45+CD3ε- and T cell events selected as CD45+CD3ε+. Target cells were exported

as FCS files and uploaded to the Cytofkit2 package (version 2.0.1). Cells were clustered using FlowSOM (Van Gassen et al., 2015) and visualized using UMAP projections and expression overlays (Becht et al., 2018), exporting cell data with annotated clusters for further downstream analysis. For target cells that consist of cell populations that are difficult to separate cleanly from non-target cells by simple biaxial gating, such as tumour mesenchymal stromal populations, an initial analysis of high-dimensional clustering and visualization was carried out which allowed usage of the full dataset to cluster and annotate events. This was particularly effective at separating mesenchymal cancer cells from non-cancer mesenchymal cells, including robust identification of fibroblasts and pericytes away from cancer cells which, un-like CD31 on endothelial cells, lack a single, canonical marker for identification (see RFP+ KPC data discussion). Clusters of target cells were exported and then re-uploaded for analysis free of non-target cells. Three KPC tumours could not be weighed (mouse #16,17 and 18) and one mouse did not receive an IdU injection (mouse #16), so this data is not present in the respective analysis. KPC mouse #19 was only stained using the mesenchymal stroma (S) antibody panel but not the MNB and T cell panels, which gave n=18 KPC PDA tumours in which each sample was stained with all three antibody panels.

3.1.9 – Mouse organ disaggregations and *in vitro* expansion of primary fibroblasts

To expand primary fibroblasts, we took advantage of the fact that fibroblasts survive and expand using standard *in vitro* culture methods much more efficiently than other, non-transformed cell types. Primary fibroblast/fibroblast-like cells were expanded from the following mouse organs: pancreas, colon, small intestine, mammary tissue, shaved back skin, stomach, mesentery adipose tissue, spleen, thymus, lungs, liver, kidneys, bladder, oesophagus and heart. The entire hind legs were collected and bone marrow processed separately (see below). Unless stated the tissues were isolated from female 8-week-old B6 mice. In parallel, the prostate was isolated from 8-week-old male B6 mice. The number of organs required for successful fibroblast expansion from each tissue is detailed in Table 7. All tissues were transferred to ice-cold sterile PBS on ice. The stomach, small intestine and colon were flushed clear with PBS. Some tissues were processed manually and others were disaggregated using a GentleMACS Dissociator: previous experiments had indicated which method yielded the most fibroblasts from each tissue (for a full list of methods used, see Table 7). Each tissue was transferred to a 10

cm cell culture dish and washed once with ice-cold RPMI. For some specific tissues, DB was supplemented with 0.5 mg/mL Dispase II (Thermo Fisher, 17105041) to aid disaggregation (also noted in Table 7). For manual disaggregation, 3 mL of RT DB was added and the tissue minced using disposable scalpels. Once the tissue had been reduced to pieces no bigger than 3 mm in length, a further 17 mL of DB was added and the dish incubated at 37 °C for 25 min. The cells, tissue fragments and buffer were transferred to a centrifuge tube and the contents allowed to settle for ~10 s. The settled tissue pieces in ~5 mL of buffer was collected with a 5 mL pipette and transferred to a separate centrifuge tube. Using the same pipette, the tissue pieces were repeatedly mixed to break up the fragments as much as possible. The contents of both centrifuge tubes were combined and quenched with 20 mL of cell culture media (CCM), consisting of 20% v/v FBS, 1% v/v HyClone Antibiotic/Antimycotic (Fisher Scientific, 11536481) and 0.2% v/v Primocin (InvivoGen, ant-pm-1) in DMEM with glucose and L-glutamine (Thermo Fisher, 41966052). Cells and remaining tissue fragments were centrifuged at 300 g for 6 min and resuspended in 40 mL CCM and transferred to a 225 cm^2 culture flask. For GentleMACS tissue disaggregations, a similar method as used for the KPC PDA tumours was applied but a specific automated program was used for each tissue (listed in Table 7). Once the program was complete the C-tube was centrifuged at 100 g for 2 min, to ensure contents were gathered at the bottom of the tube. The sample was diluted with a further 15 mL of fresh DB, mixed by pipetting and quenched with 20 mL CCM. Cells and remaining tissue fragments were centrifuged at 300 g for 6 min and resuspended in 40 mL CCM and plated into a 225 cm^2 flask. For isolation of bone marrow stromal cells, muscle was removed from each pair of intact tibias and fibias, the ends of the bones cut with a disposable scalpel and the bone marrow flushed out with 5 mL DB using a needle and syringe. The combined bone marrow extracts were vortexed to break up clumps, quenched with 20 mL CCM, pelleted, resuspended in 40 mL CCM and transferred to a 225 cm^2 culture flask. Frozen B6 primary mouse embryonic fibroblasts (MEFs) (Generon, C57-6028) were thawed and resuspended in 40 mL CCM and transferred to a 225 cm^2 culture flask. All primary cell cultures were grown in an incubator at 37 °C with 5% CO2, humidified air. Media was carefully replaced at 24 h and 48 h, taking care not to dislodge attached tissue fragments. Each primary fibroblast isolation resulted in different yields depending on the tissue of origin, so were used for downstream assays in batches when the cells reached ~50% confluence, which varied between 6-15 d. The time for each isolation to expand to sufficient cell number for each

tissue is described in Table 7. For isolations to be analysed by mass cytometry, the day before analysis the cells were lifted by aspirating media, washing with sterile PBS (Thermo Fisher, 10010023) and incubating with 10 mL of Accutase Cell Detachment Solution (Sigma Aldrich, A6964) at 37 °C for 10 mins. The dissociation buffer was quenched with 30 mL CCM and the cells allowed to settle in the same flask (without washing out the dissociation buffer). This step removes many non-fibroblast cell types that do not survive detachment well. The following day 40 µL of 10 mM IdU solution in 0.2 M NaOH/water was added directly to the media, mixed by swirling and the cells incubated at 37 °C for 20 min. Media was aspirated, cells lifted with 10 mL Accutase Cell Detachment Solution, diluted with 20 mL PBS and centrifuged at 300 g for 6 min at 4 °C. The cell pellet was resuspended in 100 µL PBS, vortexed and 100 µL of 1 µM 198Pt cisplatin in PBS added, followed by vortexing. After exactly 1 min incubation, the staining was quenched with 10 mL of CSM-I, cells pelleted, resuspended in 2 mL CSM-I, counted and $3x10^6$ cells aliquoted into a 5 mL polypropylene FACS tube. The remaining staining, acquisition and analysis steps were as described above for the *ex vivo* analysis.

Table 7. Mouse organ disaggregations

Mouse organ disaggregations and primary fibroblast expansion details						
Organ/tissue	Female/male BL6	Age (wk)	Number of organs combined before expansion	Dispase in disaggregation buffer?	Manual or GentleMACS disaggregation?	GentleMACS program	Number of days in culture before suffcient cell number for analysis
Pancreas	F	8	1	N	Manual	n/a	6
Mammary tissues (all)	F	8	1	N	Manual	n/a	6
Lung	F	8	1	N	GentleMACS	37C_m_LDK_1	10
Kidney (both)	F	8	1	N	GentleMACS	37C_Multi_B	6
Bladder	F	8	5	N	Manual	n/a	6
Thymus	F	8	5	N	Manual	n/a	6
Bone marrow (flushed)	F	8	2 (x4 tibia, x4 femur pooled)	N	Manual	n/a	6
Prostate	M	8	5	Y	Manual	n/a	6
Small intestine	F	8	1	Y	Manual	n/a	8
Colon	F	8	1	Y	Manual	n/a	8
Shaved back skin (~1.5cmx1.5cm)	F	8	1	N	Manual	n/a	8
Stomach	F	8	1	N	Manual	n/a	15
Spleen	F	8	1	N	GentleMACS	37C_m_SDK_1	15
Esophagus	F	8	1	N	Manual	n/a	15
Heart	F	8	1	N	GentleMACS	37C_Multi_G	15
Mesentery adipose tissue	F	8	1	N	Manual	n/a	15
Liver	F	8	1	N	GentleMACS	37C_m_LIDK_1	15
Commerical MEFs (Generon, C57-6028)	Not given	n/a	n/a	n/a	n/a	n/a	6 (since thaw)

3.1.10 – Mass cytometry cell signalling antibody conjugations and barcode generation

Supplier, clone and heavy-metal isotope tag of each antibody used in the cell signalling mass cytometry analysis are listed in Table 5. Where indicated antibodies were purchased pre-conjugated (Fluidigm). All other antibodies were labelled with the indicated metal tag using the Maxpar X8 antibody conjugation kit (Fluidigm), as described above. Cell signalling antibodies were titrated in panels against *in vitro* cell lines stimulated with recombinant cytokines and growth factors. Antibody clones were prioritized based on extensive prior validation (Kumar et al., 2020; Lun et al., 2019; Lun et al., 2017; Rapsomaniki et al., 2018) or confirmation of expected signal node activation during the antibody titration step. A custom 6-choose-3 barcode scheme using enriched isotopes of 105Pd, 106Pd, 108Pd, 110Pd, 113In and 115In (Trace Sciences) was generated using established methodology (Zunder et al., 2015). Stocks of 10 mM palladium/indium salt solutions in L-buffer were diluted 1:10 in 20 mM ammonium acetate ($NH_4CH_3CO_2$) (Sigma Aldrich, 372331). 127 µL of these 1 mM palladium/indium nitrate solutions were added to 2 mg of 1,4,7,10-tetraazacyclododecane-1,4,7-tris-acetic acid-10-maleimidoethylacetamide (mDOTA) (Macrocyclics, B-272) in a 1.5 mL polypropylene tube giving a 2:1 ratio of chelator:metal. Volumes were adjusted based on the accurate weight of mDOTA. After 1 min of vortexing the tube was snap frozen in dry ice/ethanol bath and stored at -80 °C. Tubes were opened and lyophilized overnight in a cooled Alpha 2-4 Benchtop Lyopholizer (MartinChrist Freeze Dryers), working quickly to ensure the contents did not thaw before being desiccated. The resulting powder was dissolved to 10 mM in dry DMSO (Sigma Aldrich, D2650) and an aliquot diluted 5000x to give a 2 µM working stock. This was titrated against PFA fixed and methanol permeabilized *in vitro* cells, to mimic final assay conditions as closely as possible. Once an optimal dilution for each of the six barcodes was found 1:1:1 mixture was generated in a 6-choose-3 barcode scheme (Zunder et al., 2015) and each of the 20 possible combinations was titrated to ensure optimal staining, before being aliquoted and stored at -20 °C.

3.1.11 – Mass cytometry cell signalling staining and analysis

$1.5x10^6$ mCherry+ CD105+ pancreatic fibroblasts and $1.5x10^6$ GFP+ CD105- pancreatic fibroblasts were combined in 30 mL of reduced-serum cell culture media (CCM(0.5)), consisting of 0.5% v/v dialyzed FBS (dFBS) (Thermo Fisher, 26400044) and 1% v/v HyClone Antibiotic/Antimycotic in DMEM with glucose and L-glutamine, and plated into a 225 cm^2 cell culture flask. After 24 h, 40 µL of 10 mM IdU solution in 0.2 M NaOH/water

was added directly to the media, mixed well and the cells incubated at 37 °C for a further 20 min. The media was aspirated and replaced with 28 mL of warmed CCM(0.5) containing cytokine or growth factors, as detailed in Table 5. The conditions consisted of x1 no stimulation control and x19 recombinant cytokine or growth factor stimulations. After exactly 5 min of stimulation at 37 °C, 4 mL of 16% PFA was added to the media, to give a final PFA concentration of 2%, and immediately swirled over the cells to fix. After 30 min of fixation, the media was aspirated, and the attached cells washed with PBS, CSM-I, and then PBS. 15 mL of Accutase Cell Detachment Solution was added and the flasks incubated at 37 °C for 15 min. Because buffer-mediated detachment is less efficient for fixed cells, a cell scraper was used to further detach the cells from the flask and collected in a centrifuge tube and diluted with 20 mL PBS. Cells were centrifuged at 1000 g for 6 min with reduced braking, aspirated and resuspended in 2 mL PBS, vortexed and permeabilized by slowly adding 5 mL of -20 °C methanol (Fisher Scientific, 10767665) with vortexing, followed by incubation at -20 °C for 20 min. The methanol-permeabilized cells were diluted with 10 mL PBS and then a further 10 mL CSM-I and pelleted. Cells were resuspended in PBS, counted and a maximum of $3x10^6$ cells aliquoted into separate 5 mL polypropylene FACS tubes. After washing with 4mL of PBS and resuspending the cell pellets in void volume, one aliquot of each unique 6-choose-3 barcode dissolved in 1mL of ice-cold PBS was added to each sample and vortexed. Once a 30 min incubation at RT was complete, the cells were washed twice with 4 mL CSM-I, pooled into a single 5 mL polypropylene FACS tube in CSM-I and pelleted. The 20-sample pooled cell pellet was resuspended in the void volume and 200 µL of 100 U/mL heparin sodium salt solution and 10 µL of Fc block added. After 5 min at RT a master mix containing 20 equivalents of each antibody from the cell signalling panel (Table 5) in 500 µL of CSM-I was added and vortexed. After staining for 2 h at RT with regular vortexing, the sample was washed three times with 4 mL CSM-I and resuspended in 1 mL PBS, transferred to a larger centrifuge tube and fixed in 10 mL of 4% PFA in PBS. The sample was vortexed and stored at 4 °C in the dark overnight. After the overnight fixation, the PFA/PBS was washed out with PBS and the cells incubated in 1mL of 100 µg/mL bis(2,2′-bipyridine)-4′-methyl-4-carboxybipyridine-ruthenium *N*-succinimidyl ester-bis(hexafluorophosphate) (ASCQ_Ru) (Sigma Aldrich, 96631) in 0.1 M sodium bicarbonate ($NaHCO_3$) (Sigma Aldrich, 31437) solution for 1 h at RT, before continuing with the PBS and water washes and acquisition, as described above.

3.2 – Immunohistochemistry, flow cytometry and gene expression analysis

3.2.1 – Multiplexed Tyramide Signal Amplification (TSA) immunofluorescence

Multiplexed Tyramide Signal Amplification (TSA) immunofluorescence staining was performed using the BOND RX automated platform (Leica Microsystems). 4um sections of FFPE tumours were cut and mounted on charged slides. Dewaxing and heat induced epitope retrieval of slides was automated on the Bond RX, using Epitope Retrieval Solution 1 (ER1) (Leica Microsystems, AR9961) for 20 min at 100 °C. Using the Research Detection System 2 (Leica Microsystems, DS9777), endogenous peroxidase was blocked using 3% v/v hydrogen peroxide (VWR, 23622.260) in Tris Buffer Saline with Tween 20 (TBST) (VWR, J77500.K8) for 10 min and the slides further blocked with 10% w/v casein (Vector, SP5020) in TBST. Antibody application, detection and TSA amplification was conducted in three sequential rounds following the same general procedure: incubation with the primary antibody in Bond Antibody Diluent (Leica Microsystems, AR9352) for 30 min, followed by detection using EnVision HRP (Agilent, K4001/4003) for 30 min, followed by a specific premixed TSA reagent (Perkin Elmer) at 1/200 for 30 min. Antibody sequence and TSA-fluorophore selection were optimised to reduce non-specific staining and tyramide binding site competition. The first staining round used mouse anti-human CD105 antibody (CST clone 3A9) at 1/200 and TSA570 (FP1488001KT). The second round used rabbit anti-human pan-CK antibody (Abcam ab9377) at 1/200 and TSA520 (FP1487001KT). The third round used mouse anti-human podoplanin antibody (Dako cloneD2/40) at 1/100 and TSA650 (FP1496001KT). Following labelling with TSA, antibodies were removed using a heat stripping step in ER1 for 10 min at 100 °C. This was not applied following application of the third antibody. Finally, nuclei were counterstained with 0.33 µg/ml 4′,6-diamidino-2-phenylindole (DAPI) (Thermo Fisher, 62248) for 15 min and coverslipped with ProLong Gold Antifade Mountant (Thermo Fisher, P36930). Slides were scanned using a VS120 microscope (Olympus Lifescience) at 20x and analysed using QuPath (v0.2.0-m9) (Bankhead et al., 2017).

3.2.2 – Immunohistochemistry of subcutaneous tumours

Subcutaneous co-transplant tumours were collected at 7 and 30 d after implantation. Large tumours were cut in half. Samples were fixed for 24h in 10% v/v Neutral Buffered Formalin (Genta Medical, BIB10L), processed and paraffin embedded (Leica Microsystems). 4um cut sections were mounted onto charged glass slides and stained manually. Slides were dewaxed by x3 5 min xylene washes and rehydrated in 100%, 90% then 70% ethanol for 1 min each. Heat induced epitope retrieval was conducted using a Biocare Declocker at 110 °C for 15 min and allowed to cool for 15 min using Low pH Target Retrieval Buffer Ph6 (Agilent, S236984). Slides were cooled in running water for 2 min and endogenous peroxidases blocked using 3% v/v hydrogen peroxide in TBST for 10 min. Following further washing in TBST, slides were blocked with 10% w/v casein in TBST for 20 min. Staining was conducted using chicken anti-GFP antibody (Abcam, ab13970) at 1/500 in TBST for 1 h at RT, followed by x2 5 min TBST washes. Detection of the primary antibody used a biotinylated goat anti-chicken IgG antibody (Abcam, ab207998) at 1/200 in TBST for 30 min at RT, followed by Vectastain Elite ABC HRP Kit (Vector, PK-6100) for 30 mins at RT, x2 5 min TBST washes and 3,3'-diaminobenzidine (DAB) (Agilent, K3467) for 5 min. Finally, nuclei were counterstained with 1x Shandon Gill Haematoxylin (Thermo Fisher, 6765005) and then dehydrated and coverslips applied before being scanned using an SCN400 (Leica microsystems) and analysed using QuPath.

3.2.3 – FACS and flow cytometry

To isolate CD105+/- CAFs directly from PDA tumours, single cell suspensions were prepared as described above for analysis by mass cytometry. Red blood cells (RBCs) were lysed using 5 mL of ice-cold 1x RBS Lysis Buffer (Biolegend, 420301) for 2 min on ice. The lysis was quenched with 20 mL FACS buffer (FB), consisting of 2% v/v FBS and 2 mM ethylenediaminetetraacetic acid (EDTA) (Thermo Fisher, 15575020) in PBS and pelleted by centrifugation at 300 g for 6 min with reduced braking. Cells were counted using a Luna Cell Counter on fluorescence mode, washed once with 20 mL PBS and stained with Live/Dead Fixable Near-IR Dead Cell Stain Kit (Thermo Fisher, L10119), using 0.25 µL of reagent in 0.5 mL of ice-cold PBS per $1x10^6$ cells. After 20 min on ice, the staining was quenched with 20 mL FB and cells pelleted. 0.25 µL of Fc block per $1x10^6$ cells was added to the void volume and cells gently mixed. After 5 min on ice, a master mix containing anti-EpCAM-FITC, anti-CD45-FITC, anti-CD31-FITC, anti-PDPN-

APC (all Biolegend), anti-CD90-PE (Abcam) and anti-CD105-BV421 (BD Biosciences) was added at 0.25 µL of each antibody in 20 µL FB per 1x10^6 cells. Cells were vortexed, stained on ice in the dark for 45 min, washed once with 20 mL FB, resuspended to 5x10^6 cells/mL, filtered through 70 µm Filcons into 5 mL polypropylene FACS tubes and sorted on a BD FACS AriaIII (BD Biosciences) using the gating strategy described in the manuscript. FACS sorted CD105+ and CD105- fibroblasts in CCM were centrifuged, aspirated and cells lysed in RLT buffer (QIAGEN) and RNA isolated using a RNeasy Micro Kit (QIAGEN, 74004), according to the manufacturer's instructions. For flow cytometry analysis or FACS of *in vitro* cells (e.g. isolation and surface marker analysis of CD105+/- pancreatic fibroblasts), a similar protocol was used without the RBC lysis and dead cell staining steps, and alternative fluorophore conjugates were applied. For a full list of antibodies used for flow cytometry/FACS see Table 8. For flow cytometry/FCAS analysis all samples were analysed on a BD LSRFortessa (BD Biosciences). Flow cytometry/FACS plots were generated in Cytobank.

Table 8. Antibodies for flow cytometry or FACS

For flow cytometry/FACS with mouse cells					
Target	**Conjugate**	**Clone**	**Supplier**	**Product code**	**Comment**
Fc block	-	2.4G2	BD Biosciences	558636	5 min before mastermix
EpCAM	FITC	G8.8	Biolegend	118208	
CD45	FITC	30-F11	Biolegend	103108	
CD31	FITC	MED13.3	Biolegend	102506	
PDPN	APC	8.1.1	Biolegend	127410	
PDPN	PE-Cy7	8.1.1	Biolegend	127412	
CD90	PE	G7	Abcam	ab24904	
CD105	BV421	MJ7/18	BD Biosciences	562760	
CD105	PE	MJ7/18	Biolegend	120408	
CD105	PE-Cy7	MJ7/18	Biolegend	120410	
CD105	APC	MJ7/18	Biolegend	120414	
CD74	AF647	In1/CD74	Biolegend	151004	Intracellular staining
MHCII	PE-Cy7	M5/114.15.2	Biolegend	107630	
MHCII	BV421	M5/114.15.2	Biolegend	107632	
For flow cytometry/FACS with human cells					
Target	**Conjugate**	**Clone**	**Supplier**	**Product code**	**Comment**
CD90	AF746	5E10	Biolegend	328116	
CD105	PE	43A3	Biolegend	323206	

3.2.4 – Bulk RNA sequencing, Gene Set Enrichment Analysis and Differential Gene Expression analysis

RNA-sequencing projects were conducted with assistance from the CRUK-MI Molecular Biology Core Facility. Indexed PolyA libraries were prepared using 50 ng of total input RNA and 16 cycles of amplification with the Agilent SureSelect Strand Specific RNA Library Prep Kit for Illumina Sequencing (Agilent, G9691B). Libraries were quantified by qPCR using a Kapa Library Quantification Kit for Illumina Sequencing Platforms (Kapa

Biosystems Inc., KK4835). Paired-end 75 base-pair sequencing was carried out by clustering 1.9-2.0 pM of the pooled libraries on a NextSeq 500 Sequencer (Illumina Inc.) Pre-alignment quality control was performed using the FASTQC tool (version 0.11.3). Raw sequencing reads were aligned to the mouse reference genome GRCm38/mm10 using STAR aligner (version 2.5.1b) and gene annotation was taken from Ensembl build 92. Read counts were determined by using the *featureCounts* function from the Bioconductor package Rsubread (version 1.28.1). For analysis of pancreatic fibroblast transcriptional response to recombinant protein stimulations, a similar protocol was applied but only single-end reads were measured. Differential gene expression analysis was performed using the Bioconductor package DESeq2 (Love et al., 2014). For the *ex vivo* KPC CAF analysis, a gene was called as significantly differentially expressed if its abundance changed more than 2-fold between populations of interest, with a Benjamini-Hochberg(BH)-adjusted p-value <0.05. For the *in vitro* pancreatic fibroblast stimulation analysis, batch effect correction was performed using DESeq2 as recommended by DESeq2 workflow guidelines, batch occupancy was fed to the generalized linear model via the design formula and the same BH-adjusted p-value was used but no fold change cut-off was applied. For single gene expression comparisons, values were calculated either as TPM or scaled/normalized expression values directly from the DEseq2 analysis. For TGFβ and IL1 receptor and signalling mediator gene expression comparisons, read counts from the baseline and stimulation conditions were combined for comparison of gene expression between CD105+ and CD105- fibroblasts (these genes were not significantly differentially expressed between baseline and stimulation samples). Gene Set Enrichment Analysis (GSEA) (Subramanian et al., 2005) was carried out using the GSEA stand-alone software (version 4.0.3) (Subramanian et al., 2007), using default settings and the Hallmark Gene Set (Liberzon et al., 2015). Due to the relatively small number of samples for each condition, gene sets were permutated according to the software recommendations.

3.2.5 – BioMark HD multiplex qPCR

BioMark qPCR analysis was conducted with assistance from Felix Heider, Systems Oncology. Assay primers and probes were designed using the Roche Universal Probe Library Assay Design Centre Tool (https://lifescience.roche.com/en_gb/brands/universal-probe-library.html). Where

possible, primers were selected to span different exons to minimize amplification of genomic DNA. See Table 9 for primer sequences and TaqMan probe numbers. New primers and probes were validated by qPCR using Universal Mouse Reference RNA (Thermo Fisher, QS0640). cDNA was synthesized from 500 ng of RNA in a 50 µL reaction mixture of 1x Reverse Transcription Buffer (Thermo Fisher, 18067017), 1.75 mM Mg_2Cl_2 (Thermo Fisher, R0971), 2 mM dNTP Mix (Thermo Fisher, R0191), 5mM DL-Dithiothreitol (DTT) (Sigma Aldrich, 43815), 100 U/mL RNAse Inhibitor (Thermo Fisher, N8080119), 2.5 µM Random Hexamers (Thermo Fisher, N8080127) and 2500 U/mL Multiscribe Reverse Transciptase (Thermo Fisher, 4311235). Reverse transcription was carried out at 25 °C for 10 min, 37 °C for 60 min, 95 °C for 5 min and 4 °C indefinitely before being stored at -20 °C. A pre-amplification of 2.5 µL of the cDNA mixture was conducted in 10 µL of 1x TaqMan Pre-Amp Master Mix (Applied Biosystems, 4391128) and a pool of all assay-specific primers at 5 nM (see Table 9), by temperature cycling at 95 °C for 10 min for 1 cycle, 95 °C for 15 s and 60 °C for 4 min for 14 cycles and 4 degree indefinitely until being diluted with 40 µL RNAse-free water (Thermo Fisher, 10977035) and storage at -20 °C. Assay mixes for the qPCR reactions were made using 8 µM of each primer and 1 µM of the appropriate hydrolysis probe in 1x Assay Loading Reagent (Fluidigm, 85000736). Sample mixes were made by diluting the amplified cDNA 1:1 in TaqMan Universal PCR Master Mix (Applied Biosystems, 4304437) and GE Sample Loading Reagent (Fluidigm, 85000746). Samples and assays were carefully loaded on a 96x96 Dynamic Array Chip (Fluidigm, BMK-M-96.96) and analysed according to manufacturer's instructions using standard settings, auto-exposure settings and with ROX as the passive reference dye. Raw qPCR data was analysed using the BioMark Real-Time PCR Analysis Software (Fluidigm). Assay dependent thresholds were used to calculate cycle threshold (Ct) values and relative expression calculated as: relative expression = $2^{-\Delta Ct}$, where: ΔCt = (Ct value gene A) – (Geometric mean (Ct values house-keeping genes)). A combination of house-keeping genes (Actb, Gapdh, Pgk1, Ppia, Tbp, Tubb4a) was used for normalization to mitigate potential confounding issues caused by differential housekeeping-gene expression between cell lines.

Table 9. List of qPCR primers and probe numbers

qPCR primer target	Source	Sequence	TaqMan probe
Actb F	Sigma Aldrich	aaggccaaccgtgaaaagat	56
Actb R	Sigma Aldrich	gtggtacgaccagaggcatac	
Gapdh F	Sigma Aldrich	gggttcctataaatacggactgc	52
Gapdh R	Sigma Aldrich	ccattttgtctacgggacga	
Pgk1 F	Sigma Aldrich	tacctgctggctggatgg	108
Pgk1 R	Sigma Aldrich	cacagcctcggcatatttct	
Ppia F	Sigma Aldrich	gccaccctccctaactgc	103
Ppia R	Sigma Aldrich	gcgggctcctactagatggt	
Tbp F	Sigma Aldrich	ggcggtttggctaggttt	107
Tbp R	Sigma Aldrich	gggttatcttcacacaccatga	
Tubb4a F	Sigma Aldrich	gacctatcatggggacagtga	55
Tubb4a R	Sigma Aldrich	cggctctgggaacatagttt	
Acta2 F	Sigma Aldrich	ctctcttccagccatctttcat	58
Acta2 R	Sigma Aldrich	tataggtggtttcgtggatgc	
Col1a1 F	Sigma Aldrich	caggcaagcctggtgaac	80
Col1a1 R	Sigma Aldrich	aacctctctcgcctcttgc	
Ctgf F	Sigma Aldrich	tgacctggaggaaaacattaaga	71
Ctgf R	Sigma Aldrich	agccctgtatgtcttcacactg	
Fndc1 F	Sigma Aldrich	tggtcctcaaggaacaaagtg	85
Fndc1 R	Sigma Aldrich	ttctgcattcaacaccaagc	
Il6 F	Sigma Aldrich	gctaccaaactggatataatcagga	6
Il6 R	Sigma Aldrich	ccaggtagctatggtactccagaa	
Cxcl1 F	Sigma Aldrich	gactccagccacactccaac	83
Cxcl1 R	Sigma Aldrich	tgacagcgcagctcattg	
Ccl2 F	Sigma Aldrich	catccacgtgttggctca	62
Ccl2 R	Sigma Aldrich	gatcatcttgctggtgaatgagt	
Csf3 F	Sigma Aldrich	ccaccttggacttgcttcag	77
Csf3 R	Sigma Aldrich	ccacccctaggttttccatc	

3.3 – Cell lines, gene editing, subcutaneous co-transplant studies and data plotting

3.3.1 – *In vitro* fibroblast and cancer cell lines

Where possible the same frozen stock of each cell line was used for all experiments within the study, to limit culture-induced phenotypic changes. For the same reason, all cells were used within one month of thawing. All cell lines were negative for mycoplasma infection, as regularly assessed by PCR through the CRUK MI Molecular Biology Core facility. The murine PDA cancer cell lines used in this study (designated as 'PDA' and 'PDA#2' in the manuscript) are BL6KPC-TB32043 and BL6KPC-TB32047 and were a kind gift from Dr. Kris Frese at CRUK MI and were cultured in Cell Culture Media 10% (CCM(10)), consisting of 10% v/v FBS and 1% v/v HyClone Antibiotic/Antimycotic in DMEM with glucose and L-glutamine. Primary pancreatic fibroblasts (PaFs) were expanded *in vitro* from the pancreas of 8-week-old female B6 mice, as described above. At 7 d, the cells were FACS sorted into LIN(CD45/CD31/EpCAM)-PDPN+CD90+CD105+ and LIN-PDPN+CD90+CD105- populations. Cultured fibroblasts were never allowed to become confluent and were detached for splitting using Accutase Dissociation Solution. All transformations were performed in NEB 5-Alpha Competent *E.*

coli (New England BioLabs Inc., C2987I) using standard methods and DNA isolated using QIAGEN Plasmid Midi Kits (QIAGEN, 12145X4). Complexes of 144 µL Lipofectamine2000 (Thermo Fisher, 11668019), 18 µg pBABE-puro SV40 LT plasmid (Addgene, 13970) and 18 µg pCL-Eco plasmid (Addgene, 12371) in 18 mL of Optimem Reduced Serum Media (Thermo Fisher, 31985070) were allowed to form for 20 min at RT and added to $7.5x10^6$ Phoenix Cells (Pear et al., 1993) in a 15 cm dish, plated 24 h prior. After 6 h the media was aspirated and replaced with 22 mL CCM. After 24 h this media was collected, filtered through a 0.22 µm pore mesh and stored at 4 °C. 22 mL of fresh CCM was added to the dish and after another 24 h of incubation the media was collected, combined with the previous day's supernatant, polybrene (Sigma Aldrich, 107689) added to a final concentration of 8 µg/mL, filtered through a 0.22 µm pore mesh and used neat to transduce target cells. 24 h later the media was replaced with fresh CCM. After 3 d in culture, cells were selected using CCM containing 1 µg/mL puromycin (Sigma Aldrich, P8833) for 7 d. After selection cells were re-sorted to ensure high purity, expanded, frozen stocks made and used for downstream functional assays. To generate GFP and mCherry expressing target cells, a second-generation lentiviral system was used. $4.5x10^6$ HEK293FT cells were plated in 10 mL CCM(10) in a 10 cm dish. The following day 4 µg of SFFV-eGFP or SFFV-mCherry expression plasmid (Harris et al., 2012), 2ug of pCMV delta R8.2 packaging plasmid (Addgene 12263), 1 µg pMD2.G envelope plasmid (Addgene, 12259) and 21 µL Polyethylenimine (PEI) (Sigma Aldrich, 764647) (3:1 PEI:plasmids) were combined and mixed in 1 mL of serum-free DMEM and incubated at RT for 30 min. The plasmid/PEI mixture was added directly to the HEK293FT media, gently swirled to mix and incubated overnight, after which the media was replaced taking care not to dislodge cells. Media at 24 h (stored at 4 °C) and 48 h was combined, polybrene added to a final concentration of 8 µg/mL, filtered through 0.22 µm pore mesh and stored at -80 °C. Target cells were transduced with neat virus-containing media for 24 h. No puromycin selection was carried out and GFP/mCherry expressing cells were isolated by FACS. For cancer cell and fibroblast co-culture experiments $2x10^6$ mCherry+ PDA cells and 2x10^6 GFP+ PaFs were plated in 20 mL CCM(10) in a 225 cm^2 flask and analysed after 48 h. To analyse the primary PaF surface marker changes under recombinant protein stimulation, primary PaFs were expanded *in vitro* as described, and incubated in 75 cm^2 flasks with recombinant proteins in CCM(10) at concentrations listed in Table 10 for 3 d. Cells were analysed by mass cytometry as described above. To analyse the transcriptomic responses of CD105+ and CD105- PaFs

to recombinant protein stimulation, 10^5 CD105+ and CD105- PaFs were plated into 6 well plates in 2 mL CCM(0.5), taking care not to swirl the media. The following day the media was replaced with CCM(0.5) containing recombinant cytokines or growth factors (see Table 10 for details) and after 6 h, cells were aspirated, washed with ice-cold PBS and lysed using RLT buffer, fully detached with a cell scraper and RNA isolated using RNeasy Mini Kit (QIAGEN, 74104), according to the manufacturer's instructions. Human pancreatic fibroblasts (hPaFs) (Generon, H-6201) were cultured in CCM, CD105+ and CD105- cells separated by FACS and cell lines generated using the lentiviral system described above with a pCSII-IRES2-hygro plasmid containing an hTERT expression inset, which was a kind gift from Dr. Farnando Calvo at the Institute of Cancer Research London, followed by 50 µg/mL hygromycin B (Thermo Fisher, 10687010) selection for 7 d.

Table 10. Recombinant proteins used for fibroblast stimulations

Primary pancreatic fibroblast stimulation for surface marker analysis at 3 d			
Recombinant protein	**Source**	**Identifier**	**Final concentration used (ng/mL)**
Recombinant mouse TGFB1	RnD Systems	7666-MB-005	2
Recombinant rat PDGF-BB	RnD Systems	520-BB-050	60
Recombinant mouse FGF2	RnD Systems	3139-FB-025	20
Recombinant human/mouse Activin-A	RnD Systems	338-AC-010	20
Recombinant mouse BMP2	RnD Systems	355-BM-010	20
Recombinant mouse BMP4	RnD Systems	5020-BP-010	20
Recombinant mouse BMP9	RnD Systems	5566-BP-010	20
Recombinant mouse MIF	Biolegend	599504	200
Recombinant mouse IFNg	PeproTech	315-05	20
Recombinant mouse TNFa	Peprotech	315-01A	15
Recombinant mouse IL1a	RnD Systems	400-ML-005	10
Recombinant mouse IL1b	PeproTech	211-11B	10
Recombinant mouse IL4	PeproTech	AF-214-14	20
Recombinant mouse IL13	RnD Systems	413-ML-005	20
Recombinant mouse IL22	RnD Systems	582-ML-010	20
Recombinant mouse LIF	PeproTech	250-02	5
Pancreatic fibroblast stimulation for qPCR analysis at 3 d			
Recombinant protein	**Source**	**Identifier**	**Final concentration used (ng/mL)**
Recombinant mouse TGFB1	RnD Systems	7666-MB-005	2
Recombinant mouse IL1a	RnD Systems	400-ML-005	10
Pancreatic fibroblast stimulation for RNAseq analysis at 6 h			
Recombinant protein	**Source**	**Identifier**	**Final concentration used (ng/mL)**
Recombinant mouse TGFB1	RnD Systems	7666-MB-005	2
Recombinant mouse IL1a	RnD Systems	400-ML-005	10
Recombinant mouse IFNg	PeproTech	315-05	20
Pancreatic fibroblast stimulation for phospho mass cytometry analysis at 5 min			
Recombinant protein	**Source**	**Identifier**	**Final concentration used (ng/mL)**
Recombinant mouse TGFB1	RnD Systems	7666-MB-005	2
Recombinant rat PDGF-BB	RnD Systems	520-BB-050	60
Recombinant mouse FGF2	RnD Systems	3139-FB-025	20
Recombinant human/mouse Activin-A	RnD Systems	338-AC-010	20
Recombinant mouse BMP2	RnD Systems	355-BM-010	20
Recombinant mouse BMP4	RnD Systems	5020-BP-010	20
Recombinant mouse BMP7	RnD Systems	5666-BP-010	20
Recombinant mouse BMP9	RnD Systems	5566-BP-010	20
Recombinant mouse BMP10	RnD Systems	6038-BP-025	20
Recombinant mouse IFNg	PeproTech	315-05	20
Recombinant mouse TNFa	Peprotech	315-01A	15
Recombinant mouse IL1a	RnD Systems	400-ML-005	10
Recombinant mouse IL1b	PeproTech	211-11B	10
Recombinant mouse IL6	PeproTech	216-16	5
Recombinant mouse LIF	PeproTech	250-02	5
Recombinant mouse MIF	Biolegend	599504	200
Recombinant mouse IL13	RnD Systems	413-ML-005	20
Recombinant mouse IL22	RnD Systems	582-ML-010	20

3.3.2 – Subcutaneous co-transplant model

The majority of subcutaneous co-transplant studies in this study used female B6 mice of 14 weeks of age. Previous experiments had shown that tumour formation in female mice younger than 10 weeks old was regularly associated with tumour ulceration, requiring mice to be euthanized before study completion. Where indicated female 14-week-old NSG mice were used. Both male and female *Rag1*$^{-/-}$ and *Batf3*$^{-/-}$ mice of mixed ages >12 weeks old were used where indicated and sex/age matched across cohorts. During optimization, cells were injected in 100 µL PBS (Thermo Fisher, 10010056) but this fails to retain fibroblasts within the growing tumour (see manuscript). For all subsequent transplants Growth Factor Reduced Matrigel (Corning, 356231) was used. Where possible, a single Matrigel lot was used for experiments to minimize the impact of lot-to-lot variation. Cancer cells and fibroblasts were lifted 20-24 h before the day of injection using Accutase Cell Detachment Solution and $6x10^6$ and $3x10^6$ cells plated, respectively into 225 cm^2 flasks. Cancer cells were cultured in CCM(10) and fibroblasts in CCM. One the day of injection, cells were lifted again using Accutase Cell Detachment Solution, washed twice with ice-cold PBS and counted in triplicate using a Luna Cell Counter on bright-field mode. The required number of cancer cells and fibroblasts were combined in 5 mL polypropylene FACS tubes, washed once more with PBS and carefully and fully aspirated. Accurate volumes of ice-cold Matrigel were added using pre-cooled pipette tips to obtain an accurate concentration of each cell type at 5000 cells/µL, taking care not to introduce air bubbles. Samples were well mixed be gentle pipetting and kept on ice. Before each injection, the sample was carefully mixed by pipetting using pre-cooled tips. Braun Omnican 50 Insulin Syringe/Needles (VWR, 9151117) were used to accurately measure 20 µL of cell/Matrigel mix with no dead-volume, which was injected subcutaneously into the right flank of the mouse (therefore giving $10x10^5$ cancer cells and $10x10^5$ fibroblasts). Larger injection volumes showed evidence of necrosis in the centre of the polymerized Matrigel at 7 d. 20 µL injection volume was found to be the optimal balance between generating plugs of Matrigel containing healthy cells throughout the early phase of tumour engraftment and being able to measure the liquid volume accurately. Tumour width and length were measured by callipers and tumour volume (V) calculated as V = (2xwidth)xlength)/2. Study end point was V>900 mm^3, if the mouse lost >10% body weight or if a mouse's health showed any other signs of deterioration e.g. loss of activity, altered breathing, behavioural changes.

3.3.3 – CRISPR/Cas-9 gene editing

The described CRISPR/Cas-9 gene editing protocol was initially optimised by Felix Heider, Systems Oncology. For *in vitro* fibroblasts, nucleofection-based CRISPR/Cas-9 methods are superior to other methods to generate efficient gene knockouts. For each target gene, three separate gRNAs were designed (Synthego 'Mulit-Guide' platform), such that their spatial distribution favoured large (>50bp) genomic deletions rather that small indels, resulting in improved knockout efficiency and consistency. gRNAs were synthesized and chemically modified to improve stability and reduce intracellular immune responses. Ribonucleoprotein (RNP) complexes were formed by diluting 2 µL of 100 µM of multi-gRNA (Synthego) (Table 11) in Tris-EDTA (TE) (Synthego) and 1 µL of 20 µM recombinant Cas-9 (Integrated DNA Technologies (IDT), 1081059) in RNase-free PBS in 12 µL Primary Cell P3 Nucleofector solution (Lonza, V4XP-3032) and incubating at RT for 20 min. To $2.5x10^5$ cells in 5 µL Nucelofector solution, 0.8 µL of Electroporation Enhancer Solution (IDT, Alt-R Cas9 Electroporation Enhancer, 2 nmol) was added, followed by 15 µL of the RNP solution and mixed by pipetting. This was transferred to a well of a 100 µL Nucleocuvette Strip (Lonza, V4XP-3032) and transfected using a 4D-Nucleofector Core Unit (Lonza), using the CM-137 program and filling empty wells with PBS. Cells were allowed to rest for 3 min before being plated in CCM and cultured as normal. Transfection with a pool of x2 separate non-targeting (NT) gRNAs (Synthego) was used to generate control cells. Gene knockout was confirmed in a split of the cells at the protein level by flow cytometry after 7 d, using IFNγ stimulation to induce expression of *H2Ab1* and *Cd74*. Surface MHCII expression was measured and CD74 expression was measured by intracellular staining (CD74 is predominantly located in the ER/endosomes), using the FOXP3 Fixation/ Permeabilization kit. Cells were not purified further as gene knockout was consistently >95% for all targeted genes.

Table 11. CRISPR/Cas-9 gRNA sequences

CRISPR/Cas-9 gRNA target	Source	Sequence
Scrambled non-targeting 1	Synthego	gcacuaccagagcuaacuca
Scrambled non-targeting 2	Synthego	guacgucgguauaacuccuc
Mouse Eng 1	Synthego	cucuuucugcgagaccugcu
Mouse Eng 2	Synthego	cggcugugaucuacagccug
Mouse Eng 3	Synthego	ucaccccuuugugggguccac
Mouse H2Ab1 1	Synthego	ucucauccacacagcuuauu
Mouse H2Ab1 2	Synthego	gaaccagcgcacuuugaucu
Mouse H2Ab1 3	Synthego	ugagggccucuguccuggac
Mouse Cd74 1	Synthego	auuucggaagcuucaugcga
Mouse Cd74 2	Synthego	uuacuuccuguaccagcaac
Mouse Cd74 3	Synthego	ugagggccucuguccuggac

3.3.4 – General data analysis and plotting

Some plotting and statistical tests were conducted with assistance from Alex Kononov, Systems Oncology. Plotting and statistical tests were performed in Prism (version 7, GraphPad Software Inc.) or R Statistical Software. For RNAseq data visualization, differentially expressed genes (DEGs) from DESeq2 were scaled by library size using the function *estimateSizeFactors*, the data transformed by the function *normTransform* and the obtained expression values used for visualization. Heatmap plots were drawn using the R package ComplexHeatmap. Heatmap visualization of CyTOF data was achieved by first processing the data using the R package flowCore (Hahne et al., 2009). According to best practices, data was transformed by hyperbolic arc-sine with cofactor = 5 by the function *asinh*. The z-score was calculated by the function *scale* and heatmaps drawn using the R package ComplexHeatmap. Principle Component Analysis (PCA) plots were generated using the *pcaplot* function. For the abundance/phenotype cross-cluster correlation analysis, the number of cells in each FlowSOM cluster as a percentage of the total number of gated cells from each sample was used as the abundance input data. To calculate the fraction of proliferating and dying cells in each cluster, FCS files containing all target cells, including FlowSOM cluster annotation were exported from Cytofkit2 and uploaded to FlowJo (version 10.6.2, BD Life Sciences). S-phase cells were defined as cells with both Ki67 mass intensity signal ≥ 20 and IdU mass intensity signal ≥ 20. Dying cells were defined as cells with cleaved caspase-3 (CC3) mass intensity signal ≥ 8. The abundance of each FlowSOM cluster and the percentage of S-phase and dying cells within each FlowSOM cluster for each sample was exported and used as the phenotypic input data for the cross-correlation analysis. Since all antibody panels were measured on each of the 18/19 PDA samples, the abundance, proliferation and apoptosis data for each of the 20 FlowSOM clusters from each of the three panels (60 total clusters) was concatenated into one data frame for these 18

samples. Correlation analysis was performed on selected abundance, proliferation and apoptosis comparisons (see manuscript for specific comparisons), using Spearman correlation measurement. The correlation results were visualized by the R package corrplot.

Chapter 4 – Results – Single cell analysis of the PDA TME

4.1 – Results

4.1.1 – Development of a mass cytometry antibody panel to analyse mesenchymal cell types from mouse tissues

One of the major limiting factors for understanding the consequences of fibroblast heterogeneity in tumours, is an incomplete understanding of surface protein markers that can be used to isolate pure, live fibroblast subpopulations for characterisation and functional analysis. I hypothesised that a better understanding of the fibroblast surface proteome would allow us to better clarify the distinct fibroblast populations and activation states in PDA tumours and allow us more precisely characterise the PDA microenvironment. To address this, I sought to develop a single cell proteomic workflow by developing a novel mass cytometry panel, predominantly focussed on measuring known and putative surface markers of mesenchymal cells. Mass cytometry was the selected single cell technique because it enables the measurement of large numbers of protein markers simultaneously, providing a detailed picture of cellular surface marker expression and phenotype. Such high parameter mass cytometry analysis would allow me to maximise the data collected from each *ex vivo* sample and also avoid the requirement for *in vitro* fibroblast expansion. This is important because the expression of fibroblast markers are known to be dramatically and rapidly altered after *in vitro* culture (even though they may retain phenotypic features) (Philippeos et al., 2018). Additionally, once a mass cytometry antibody panel is established, a large number of samples can be analysed and this would give me a flexible tool to interrogate the mesenchymal stromal compartment across varied samples. I identified a list of >50 potential markers based on an extensive literature search (see Table 12). The aim was to include as many of these as possible in the complete mass cytometry panel. I also included a reduced number of intracellular markers that are widely used for histological identification of fibroblasts or other mesenchymal cells (e.g. VIM and αSMA). Whilst these markers would not be useful to isolate live cells, they would aid in accurately annotating the different cell types/phenotypes within complex tumour samples.

Table 12. Markers for inclusion in mesenchymal stroma mass cytometry panel, reasons for inclusion and example reference

Included:		
Marker	**Reason for inclusion**	**Example reference**
CD44	Hyaluronic acid-binder, contributes to fibroblast activation	(Spaeth et al., 2013)
EpCAM	Epithelial/PDA marker	(Rhim et al., 2012)
CD86	T cell co-stim	(Pechhold et al., 1997)
MCAM	Pericyte marker, upregulated on subset of fibroblasts and functional wrt activation	(Zheng et al., 2016)
ITGα5	Overexpressed on PDA mesenchyme, inhibition attenuates desmoplasia	(Kuninty et al., 2019)
CD81	Distributed expression observed on lung fibroblasts	(Heinzelmann et al., 2018)
CD87	Reported marker of activated fibroblasts	(Agorku et al., 2019)
ITGα1	Pericyte marker	(Armulik et al., 2011)
ITGαV	Reported expression on subset of melanoma CAFs, integrin contributes to TGFβ activation	(Davidson et al., 2020)
ITGα2	Reported marker of activated fibroblasts	(Agorku et al., 2019)
PDGFRα	Widely used marker of fibroblasts	(Chen and Song, 2019)
PDPN	Widely used marker of fibroblasts	(Dominguez et al., 2020)
CD24	Distributed expression in passaged MEFs	(Singhal et al., 2016)
PDGFRβ	Reported upregulation on fibroblast activation, pericyte marker	(Chen and Song, 2019)
ICAM1	Fibroblast expression induced by pro-inflammatory cytokines and mediates T cell interactions	(Musso et al., 1999)
CD63	Broad marker of cells with similar endocytic properties	(Pols and Klumperman, 2009)
CD73	Reported marker of fibroblast subset	(Costa et al., 2018)
CD26	Marker of distinct fibroblast lineages in murine skin	(Driskell et al., 2013)
ITGβ3	Major integrin subunit for fibronectin binding, reported to mediate EndMT	(Wang et al., 2018)
CD34	Reported subset of fibroblasts in PanIN/PDA	(Feig et al., 2013)
ITGα6	Laminin-binding integrin subunit	(Humphries et al., 2006)
CD105	Endothelial and pericyte marker, canonical marker of BM-MSCs, distributed expression in passaged MEFs	(Dominici et al., 2006)
CD14	Reported expression on fibroblasts regulated by IFNγ, lack of expression defining feature of BM-MSCs	(Sugawara et al., 1998)
CD74	MHCII antigen presentation reported on fibroblasts	(Elyada et al., 2019)
CD80	T cell co-stim and reported expression on fibroblasts, distributed expression in passaged MEFs	(Pechhold et al., 1997)
CD31	Canonical endothelial cell marker	N/A
CD38	Distributed expression in passaged MEFs	(Singhal et al., 2016)
ITGβ1	Reported marker of subset of breast CAFs	(Costa et al., 2018)
VCAM1	Fibroblast expression induced by pro-inflammatory cytokines and mediates T cell interactions	(Musso et al., 1999)
CD45	Canonical immune cell marker	N/A
CD90	Fibroblast subset marker in RA, canonical BM-MSC marker, distributed expression in passaged MEFs	(Wei et al., 2020)
MHCI	MHCII antigen presentation reported on fibroblasts	(Lakins et al., 2018)
MHCII	MHCII antigen presentation reported on fibroblasts	(Elyada et al., 2019)
Cytokeratin-7	Epithelial/PDA marker	(Schussler et al., 1992)
Pan-cytokeratin	Epithelial/PDA marker	(Rhim et al., 2012)
VIM	General mesenchymal marker	(Sahai et al., 2020)
DES	Widely used fibroblast marker and pericyte marker	(Chen and Song, 2019)
αSMA	Myofibroblast marker	(Ohlund et al., 2017)
Intracellular collagen-4	Indicator of basement membrane synthesis and reported increased expression under fibrotic conditions	(Mak and Mei, 2017)
Not included:		
Marker	**Reason could not be included**	**Example reference**
FAP	During panel development, no robust monoclonal antibody successfully validated	(Kraman et al., 2010)

FSP1	During panel development, no robust monoclonal antibody successfully validated	(Sugimoto et al., 2006)

For the markers that had commercially available antibodies, carrier protein-free (e.g. BSA-free) formulations of the antibodies were purchased and conjugated to chelating polymers pre-loaded with specific heavy-metal isotopes, using commercially available kits (see Materials and methods section). Each different antibody was allocated to a unique heavy-metal channel. Mass cytometry has significantly reduced channel spill over compared to fluorescence-based methods but low levels do still exist and should be mitigated where possible. Thus, a dedicated panel-builder was used to ensure markers with known high expression (and therefore 'bright' signal) were allocated into 'dim' channels with minimal spill over into less highly expressed markers. For improved reproducibility antibodies with extensive validation in the literature or by commercial vendors were prioritised and monoclonal antibodies were selected over polyclonal where possible. Several antibodies failed during conjugation because the step to partially reduce the disulphide-bridges that covalently link the two heavy chains (which act as the attachment point for the polymer), caused the antibody to degrade/decompose. In these cases, an alternative antibody clone was tried and if no other suitable antibody clone was available, an antibody targeting another protein was included in the panel instead. The final mesenchymal stroma mass cytometry panel is detailed in Table 2.

4.1.2 – A multi-parameter mass cytometry analysis is able to clearly separate fibroblasts from mesenchymal cancer cells and other non-transformed mesenchymal cell types

To test how effective the final 41-marker mass cytometry panel was at mapping mesenchymal heterogeneity in complex cellular systems such as tumours, I needed a system in which I could confidently identify mesenchymal cancer cells from non-transformed mesenchymal stromal cells. To achieve this, I incorporated an antibody targeting Red Fluorescent Protein (RFP) into the panel and stained and analysed the single cell suspensions of late stage PDA tumours from *Pdx-1-Cre; Kras*$^{LSL\text{-}G12D/+}$*; Trp53*$^{LSL\text{-}R172H/+}$; *Rosa26*$^{LSL\text{-}tdRFP/+}$ (RFP+ KPC) mice. In these mice, Cre-recombinase is expressed in pancreatic epithelial cells during embryogenesis which, as well as driving oncogenic KRAS expression and mutant P53 expression, also allows expression of RFP, permitting positive identification of transformed cancer cells. It has previously been

demonstrated that the penetrance of such fluorescent protein expression systems is not complete in all target cells (Cabeza-Cabrerizo et al., 2019; Luche et al., 2007), probably due to incomplete recombination and lack of selective pressure for RFP expression compared with oncogenic proteins. However, the model would enable positive identification of cancer cells and, by association, other phenotypically similar RFP- cancer cells. End stage RFP+ KPC tumours were disaggregated, stained with a dead cell marker (198Pt cisplatin), surface proteins labelled with metal-conjugated antibodies, cells fixed and permeabilised, intracellular targets labelled with metal-conjugated antibodies and the cells further fixed and acquired on a Helios mass cytometer. The resulting single cell data from an RFP+ KPC tumour is plotted as a UMAP projection, a 2D representation of the high dimensional data, in which each dot represents a single cell and cells with similar phenotypes are more closely associated. In this UMAP projection, all markers including RFP are used to determine clustering (Figure 5). Expression of selected individual markers are plotted as an overlaid colour intensity, where blue through yellow through red indicates increased protein levels.

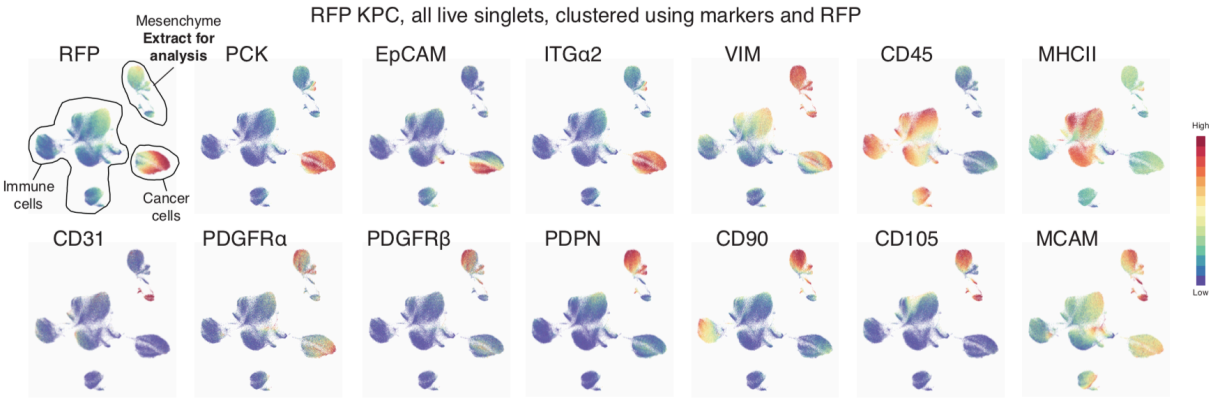

Figure 5. UMAP projection of all live, single cells from an RFP KPC tumour sample using all phenotypic markers, including RFP to drive clustering

UMAP plots for each listed marker are shown. Each single dot represents one cell and the overlaid signal intensity depicts the detected level of each protein. A total of $1.5x10^5$ randomly downsampled cells are displayed. Major cell clusters are annotated in the first UMAP plot.

High pan-cytokeratin (PCK) expression is observed predominantly in one cluster. The cells in this cluster mostly (but not completely) stain for RFP and thus this cluster consists of cancer cells, approximately half of which have expression of the transmembrane cell-cell adhesion glycoprotein EpCAM, which denotes epithelial status. Vimentin (VIM) is a type III intermediate filament associated with mesenchymal morphology and cell functions. It can be seen that within the RFP+ cancer cell clusters, a large number of

cancer cells that are EpCAM low are VIM high, thus these cells appear to be cancer cells that have undergone EMT. Interestingly, the integrin alpha subunit, ITGα2, is a very complete marker of the cancer cell clusters regardless of EMT status. Notably, a fraction of cancer cells have some PDGFRα expression, a marker widely used to isolate fibroblasts from tumours. The protein tyrosine phosphatase receptor type C (PTPRC), also known as CD45, is a complete and canonical marker of all major immune cell types. Here, its expression clearly identifies multiple immune cell clusters, the majority of which are positive for major histocompatibility complex II, MCHII. The remaining clusters are non-transformed, mesenchymal stromal cells. Within these two clusters, a major and minor cluster, are positive for platelet endothelial cell adhesion molecule 1 (PECAM-1), also known as CD31, the canonical marker of endothelial cells. This leaves the remaining clusters as predominantly fibroblasts and pericytes (see below for detailed discussion). The fibroblast and pericyte clusters are RFP-, EpCAM- but surprisingly show some low-level expression of PCK expression in a minority of cells. Cytokeratin expression in mesenchymal cell types has been reported by others (von Koskull and Virtanen, 1987). This demonstrates that established markers associated with the epithelium and cancer cells can have some restricted expression in non-transformed mesenchymal cells and supports the concept that using multiple markers to identify cell types in an unbiased manner leads to more accurate annotation in complex cell mixtures. High expression of the immunoglobulin superfamily glycoprotein, CD90 is particularly useful in positively identifying fibroblasts, pericytes and a minor endothelial cluster. Expression of the mucin-type protein podoplanin, PDPN is restricted to fibroblasts and the minor endothelial cell cluster. It is well established in the literature that PDPN demarks lymphatic endothelial cells (LECs) (Fletcher et al., 2010).

Importantly, repeating the clustering analysis without using RFP to inform clustering, still enables complete separation of RFP+ cancer cells from RFP- mesenchymal cells (Figure 6). This demonstrates that the other markers used in the panel carry enough information about cell identity to fully separate fibroblasts from other mesenchymal stromal populations and from cancer cells, even in models that don't have lineage tracing proteins and in which cancer cells have undergone extensive EMT. This enabled me to use the standard KPC model (with no RFP) for our subsequent analysis. Such a workflow, of using all of the available markers to separate cells into clusters of phenotypically similar cells, allowed me to cleanly separate mesenchyme cells away

from other cells in the tumour (particularly from mesenchymal cancer cells) and extract these pure clusters for further downstream analysis, without prior-knowledge or bias about which markers to use for selection.

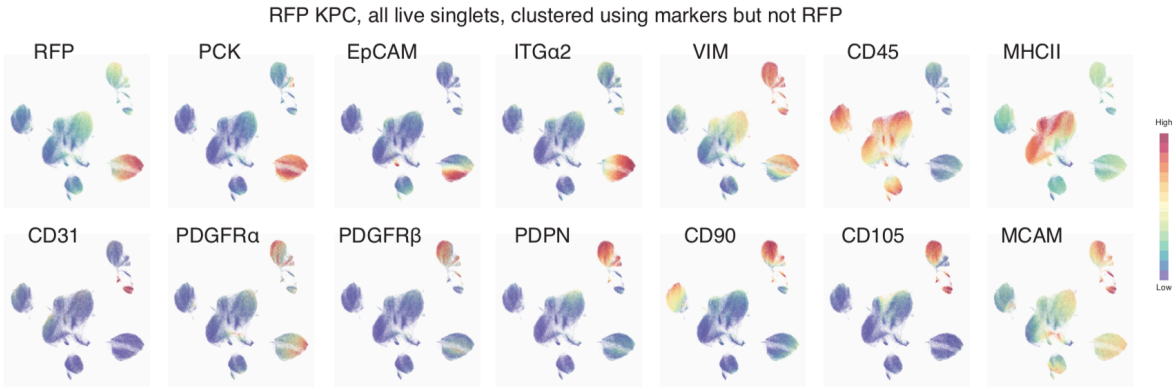

Figure 6. UMAP projection of all live, single cells from an RFP KPC tumour sample using all phenotypic markers other than RFP to drive clustering
UMAP plots for each listed marker are shown. Each single dot represents one cell and the overlaid signal intensity depicts the detected level of each protein. A total of $1.5x10^5$ randomly downsampled cells are displayed.

4.1.3 – Extensive inter- and intra-tumoural heterogeneity exists in the composition of the mesenchymal stromal compartment of spontaneous murine pancreatic tumours

To better understand fibroblast heterogeneity in the PDA TME, I applied the novel mesenchymal stromal mass cytometry panel to single cell suspensions from n=19 different KPC tumours. I anticipated that this analysis would clearly define the abundance and phenotypic variability across a large number of tumours. The KPC, like other spontaneous GEMMs is a highly stochastic model. For example, despite all tumours in this cohort having the same $KRAS^{G12D}$ and $TP53^{R172H}$ driver point mutations and the same induction time point (embryogenesis), tumour progression and time to advanced, symptomatic disease takes a highly variable length of time and tumours show a wide range of sizes. Although a broad positive correlation is observed between mouse age and weight of tumours used in this study (Figure 7) (Spearman correlation method, $\rho=0.531$, $p=0.04$), the data shows a wide range in length of time to advanced disease (88 - 220 days) and the final tumour weight (213 – 1380 mg).

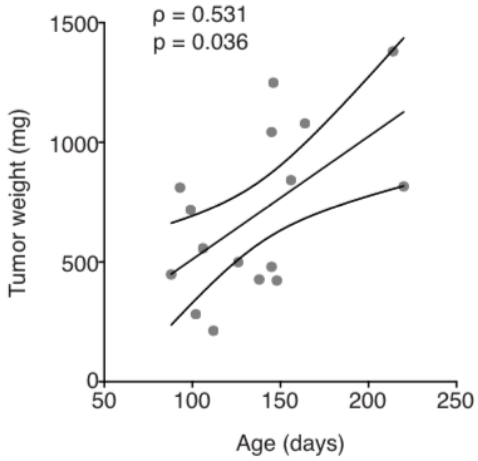

Figure 7. Correlation between KPC mouse age and tumour weight.
ρ=Spearman correlation coefficient, 90% confidence intervals displayed.

To focus the analysis on the mesenchymal stroma only, I first selected CD45- cells only to remove all immune cells. I then ran high dimensional analysis on the remaining cells (cancer cells and mesenchymal stroma) using all cell markers to allocate every cell to a cluster, as for the RFP+ KPC example above. I extracted all mesenchymal clusters (for example, as highlighted in Figure 5). This cleanly removed epithelial cancer cells and importantly, mesenchymal cancer cells from the samples. The data, containing target cells only (endothelial cells, pericytes, fibroblasts and any other non-cancer mesenchymal cells) was then exported. This methodology also removes rare doublet events containing fibroblast and cancer cells that were not excluded in the initial gating. Across all 19 PDA tumours, the mesenchymal stroma made up 23.0±11.5% of all viable, CD45- single cells. ~26,000 randomly down-sampled mesenchymal stromal cells from each sample were combined to give a total of 500,000 cells for analysis. These were plotted using UMAP visualisation and cell clusters determined by unsupervised FlowSOM analysis (Figure 8A) (Van Gassen et al., 2015). For both UMAP and FlowSOM analysis, markers of cancer cells (EpCAM, CK7, PCK) and immune cells (CD45) were not used to drive visualisation/clustering, as most of these cell types had been removed from the mesenchymal dataset in the prior step. Also, in this instance, markers of cell proliferation (Ki67 and IdU) and cell death (cleaved caspase-3 (CC3)), that are included in the panel, were not used to drive visualisation and clustering. These proteins are rapidly and dynamically regulated and their use in visualisation and clustering would fragment all clusters into proliferative and dying sub-clusters and complicate the analysis. Instead, cell proliferation and apoptosis were analysed separately (see section 4.1.4). The relative abundance of each FlowSOM cluster within the total mesenchymal

compartment is plotted as stacked bar graphs in Figure 8B, a heatmap showing the median expression of each marker used in the analysis along with the putative annotation of the corresponding cluster is shown in Figure 8C and UMAPs of selected individual markers are shown in Figure 8D. In addition, the mean relative abundance of each cluster is shown in Figure 9, plotted with the standard deviation to show variation across samples. Collectively these visualisations allow us to navigate the high dimensional data and begin to annotate mesenchymal clusters.

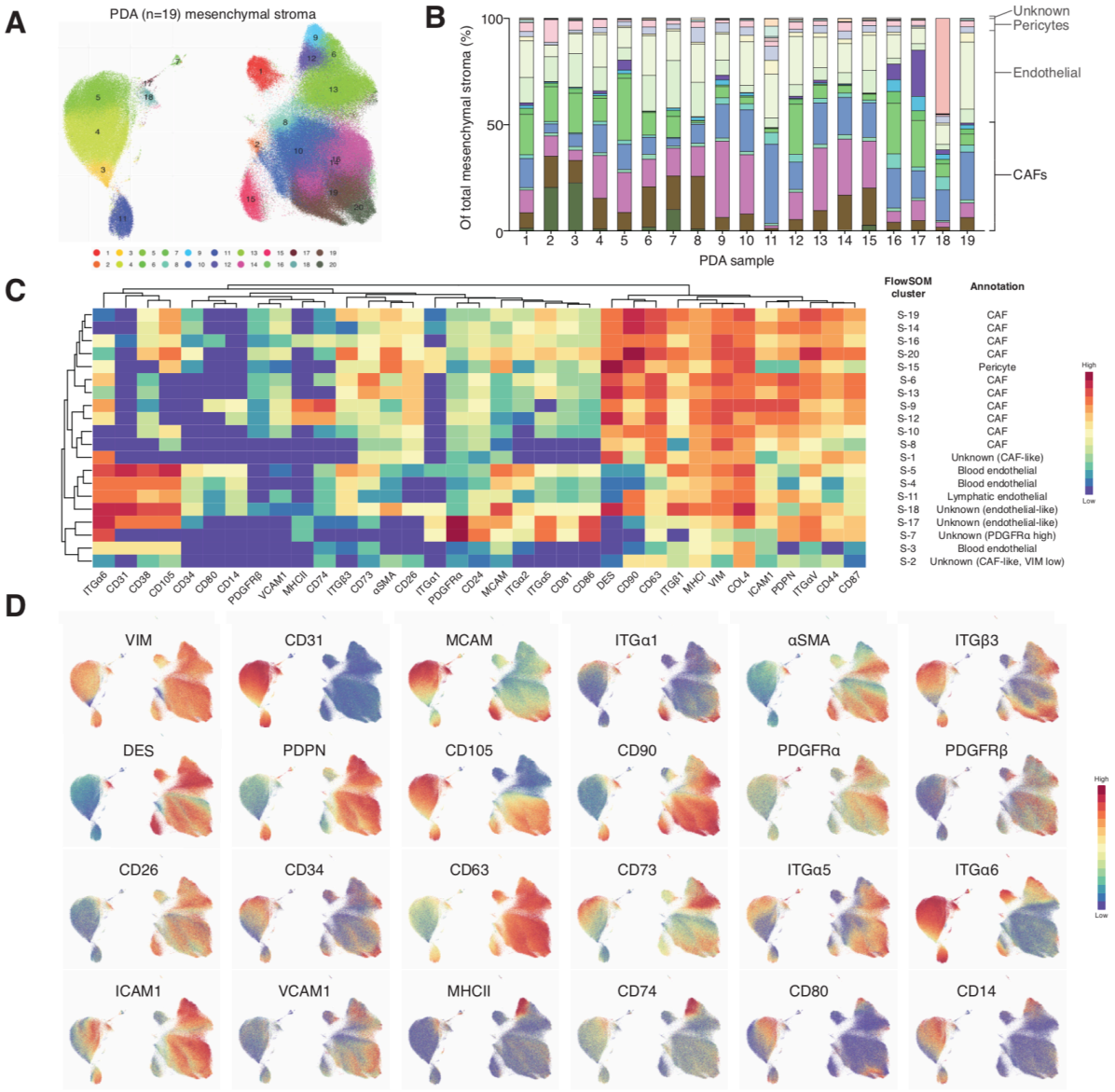

Figure 8. Phenotypic and compositional heterogeneity of pancreatic cancer-associated mesenchymal cells

(A) UMAP projection of single mesenchymal stromal cells from end-stage KPC PDA tumors (n=19 samples) with color-coded FlowSOM clusters. Each tumor sample contributes an equal number of cells to the dataset. (B) Stacked bar graph displaying relative abundance of KPC PDA mesenchymal stromal FlowSOM clusters, with clusters grouped into mesenchymal sub-types. CAF clusters are emphasized. (C) Heatmap displaying marker median mass intensities (MMIs) for each FlowSOM mesenchymal stroma

cluster. Phenotypic markers and mesenchymal stromal clusters are grouped using unsupervised hierarchical clustering based on marker MMIs. Cell-type annotations based on canonical phenotypic markers are listed. (D) UMAP projection from (A) displaying overlaid signal intensity of example phenotypic markers.

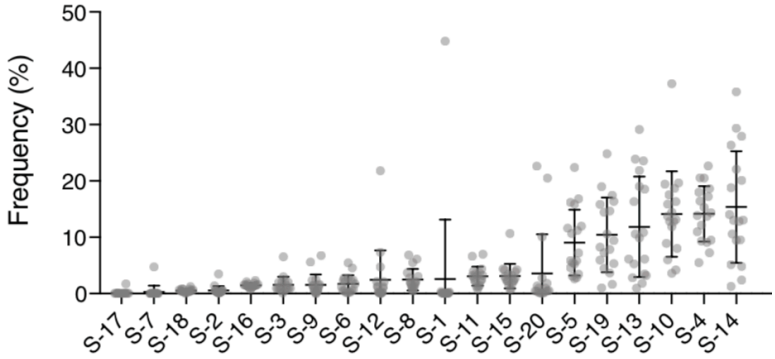

Figure 9. Variability of abundance of pancreatic cancer mesenchymal stromal subsets
The relative frequency of FlowSOM-determined PDA mesenchymal cell subsets. Data displayed as mean+/-standard deviation.

The analysis shows that the mesenchyme of these PDA tumours is a complicated mixture of discrete cell clusters, and within these discrete clusters, a graduated continuum of phenotypes is also observed. The variation in relative abundance of each FlowSOM cell cluster across the n=19 tumours is striking, with some clusters, such as cluster S-14, present to high amounts in all tumour samples and some clusters, such as cluster S-20, lowly abundant in the majority of samples but highly abundant in two tumour samples. In addition, one cluster, S-1, is highly abundant in just one sample, where is contributes 44.8% of all mesenchymal cells, yet present at <1% in all other samples.

To annotate clusters, I surveyed the marker expression of each cluster, plotting the median expression of each marker as a heatmap (Figure 8C). The vast majority of cells are VIM positive, indicative of a mesenchymal phenotype. CD31 expression identifies 6 endothelial cell clusters, with all endothelial clusters expressing CD105, a co-receptor for the TGFβR complex. Additional expression of PDPN and CD90 identifies S-11 as lymphatic endothelial cells (LECs), which represent 3.1±1.64% of all mesenchymal cells. Endothelial clusters S-3, S-4 and S-5 form a continuum of phenotypes. Based on abundance, positive expression of CD31, CD105 and the cell surface glycoprotein, MCAM and negative expression of PDPN, CD90 and the intracellular microfilament protein αSMA, these cells most closely resemble blood endothelial cells (BECs), in various phenotypic states. The expression levels of canonical endothelial cell markers, such as CD31, MCAM and CD105, increases from the minor cluster S-3, through the

most abundant cluster S-4 (relative abundance 14.2±7.4% of all mesenchymal cells), to the most highly expressing cluster S-5 (9.1±5.7%), which may represent increasing differentiation/maturation of BECs or potentially distinct local microenvironmental niches. All 19 PDA samples contained all 3 BEC clusters and the single LEC cluster, albeit to widely varying levels (see discussion later regarding abundance variation).

S-17 and S-18 are minor clusters representing 0.1±0.4% and 0.5±0.3% of mesenchymal cells respectively. Both have CD31 staining suggesting an endothelial-like phenotype but further definitive annotation with this dataset is not possible.

S-15 (3.1±2.1%) forms a single discrete cluster that has high and uniform expression of CD105, CD90, MCAM and αSMA and lacks CD31 and PDPN expression. This cluster also expresses consistently high levels of the intermediate filament protein, DES and the integrin alpha subunit, ITGα1, identifying these cells as pericytes (Armulik et al., 2011; Kosyakova et al., 2020). Three minor clusters, S-2 (relative abundance of 0.55±0.66%), S-3 (1.5±1.4%) and S-7 (0.3±1.1%) have low expression of VIM, yet still show expression of other known mesenchymal markers. Lack of VIM staining may be a technical artefact or be genuine and VIM may not be a fully complete mesenchymal marker.

The remaining clusters fall under the broad definition of cancer-associated fibroblasts (CAFs), as non-cancer mesenchymal cells in tumours that lack expression of canonical markers of other cells types. All these fibroblast-like clusters, except for S-1, share common features such as high and consistent expression of PDPN, DES and CD90 and lack of CD31. The clusters show variable levels of widely used fibroblast markers such as αSMA and the growth factor receptor tyrosine kinase (RTK) PDGFRα. Interestingly, αSMA and PDGFRα show inverse expression across several clusters, with cells showing high expression of one or the other but not both at the same time. Levels of αSMA, the canonical marker of the so called myofibroblastic (MyCAF) phenotype, are highest in four closely-related fibroblast clusters positive for CD105 expression: S-20 (3.6±6.8%), S-19 (10.4±6.4%), S-16 (1.5±0.4%) and S-14 (14.2±4.8%) and a more distinct fibroblast cluster that lacks CD105 expression, S-13 (11.9±8.7%). ICAM1, a glycoprotein that regulates leukocyte binding, is present on most of the mesenchymal cell populations but shows variable expression. In the fibroblast clusters, like PDGFRα, ICAM1 also shows an inverse expression pattern to αSMA. The type 1 membrane cell adhesion

sialoglycoprotein, VCAM1 (also known to play a role in leukocyte binding) shows a similar expression pattern but is mostly restricted to fibroblasts. Whilst high and consistent expression of MCAM, ITGα1 and αSMA is a hallmark feature of pericytes, minor CAF clusters also share this phenotype but with the co-expression of several other proteins (e.g. PDPN, CD90), highlighting the need for multiple markers to be used if clusters of distinct mesenchymal lineages are to be confidently annotated.

The surface peptidase, CD26 has been shown to be a marker of distinct lineages of fibroblasts in human and murine skin (Driskell et al., 2013). However, in these PDA samples, CD26 is highly expressed across all major fibroblast clusters with some graduated expression seen. The sialomucin adhesion protein, CD34 and the growth factor RTK, PDGFRβ have all previously been shown to identify subpopulations of fibroblasts in tumours and tissues (Table 12). In this dataset, we observe graduated expression of all of these markers but their expression is present in multiple discrete fibroblast clusters. For example, CD34 is co-expressed in 3 distinct regions of fibroblast cells, in clusters that also have the highest αSMA and MCAM expression, established markers of myofibroblast phenotype. The integrin subunits, ITGα5 and ITGβ3, whose complexes are involved in fibronectin, osteopontin and thrombospondin binding, also follow a similar pattern, with increased expression in αSMA+ fibroblasts, although none of these markers have expression profiles that perfectly overlap. The multivesicular transport tetraspanin, CD63 shows broad and uniform expression in fibroblasts and pericytes, lower expression in LECs and very little expression in BECs.

The majority of the markers tested show some form of graduated expression patterns and are present in multiple clusters in different regions of the uMAP plot. In comparison, CD105 shows clear binary expression, in which cells either express high levels or CD105 or have none/very minor expression of CD105. Within the fibroblast clusters there are clear, distinct groups of CD105+ and CD105- clusters. Within both these groups, there are regions of αSMA and MCAM expression, and regions of PDGFRα, ICAM1 and VCAM1 expression. Regardless of their CD105 status, all these fibroblast clusters show positive expression of PDPN and CD90.

The AMP nucleotidase, CD73 and the lamin-binding integrin subunit, ITGα6, both show much higher expression on CD105- fibroblast clusters compared to CD105+ fibroblast

clusters. Interestingly, ITGα6 is present on all other mesenchymal cell types apart from CD105+ fibroblast clusters. Two proteins involved in MHCII antigen presentation, MHCII complex itself and the MHCII stabiliser and transporter invariant chain, CD74, as well as the bacterial lipopolysaccharide co-receptor, CD14, all show high expression in specific fibroblast clusters. Interestingly, MHCII, CD74 and CD14 are almost exclusively expressed in specific CD105- clusters only, with little or no expression in CD105+ fibroblasts. The minor CD105- cluster S-9 (relative abundance 1.6±1.8%) has the highest median expression levels of MHCII, CD74 and CD14 of all mesenchymal stromal clusters. The MHCII and CD74 expression levels in this cluster and a related CD105- cluster S-12 (2.5±5.0%) are far higher than that on BECs, cell types well known to express MHCII antigen presentation machinery under inflammatory conditions (Pober et al., 2017). Two T cell co-stimulatory molecules, CD80 and CD86 are expressed on the endothelial cell cluster S-5 and a minority of fibroblast clusters but interestingly, are expressed in a non-overlapping pattern.

Cluster S-1, which is a major fibroblast fraction in just one PDA sample and very rare in other samples, has high expression of ITGα6, CD63, DES and VIM but low to intermediate expression of PDPN, αSMA and CD90 and does not match any other mesenchyme phenotype in these tumours. Whilst this cluster resembles fibroblast-like cells, its identity is hard to confidently annotate within this dataset. It is possible that this is a technical or biological artefact specific to PDA sample 18.

To try and link variation in stromal composition with macroscopic features of the tumour, I compared the relative abundance of all FlowSOM stromal clusters with tumour weight across the PDA tumours, using the Spearman correlation method to quantify relatedness. 2/20 (10%) comparisons showed statistically significant correlations between cluster abundance and tumour weight (Figure 10). The largest BEC cluster, S-4 showed an inverse correlation with tumour weight (ρ=-0.582, p=0.020) and the minor PDPN+CD105-MHCII+ fibroblast cluster S-12, showed a positive correlation with tumour weight (ρ=0.597, p=0.017).

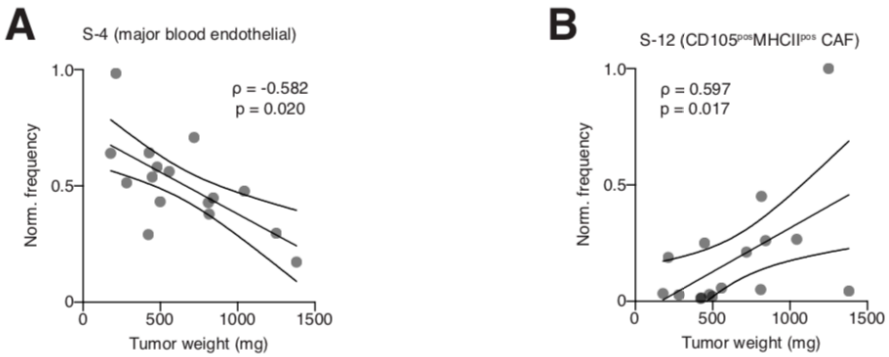

Figure 10. Correlations between pancreatic cancer mesenchymal stromal subsets and tumour weight

(A) Spearman correlation analysis between the relative frequency of the endothelial cell subset, S-4 and PDA tumor weight. ρ=Spearman correlation coefficient, 90% confidence intervals displayed. (B) As for (A), comparing relative frequency of CAF subset, S-12 and tumor weight

To better understand how the abundance of one stromal cluster was related to the abundance of all other stromal clusters, Spearman correlation analysis was again used but this time plotting all pair-wise abundance comparisons as a heatmap, where the Spearman coefficient (1 to -1) is displayed as either positive correlation (red) or negative correlation (blue), estimated statistical significance ($p<0.05$) denoted with an asterisk and the clustering of the row/column by unsupervised hierarchical clustering (Figure 11).

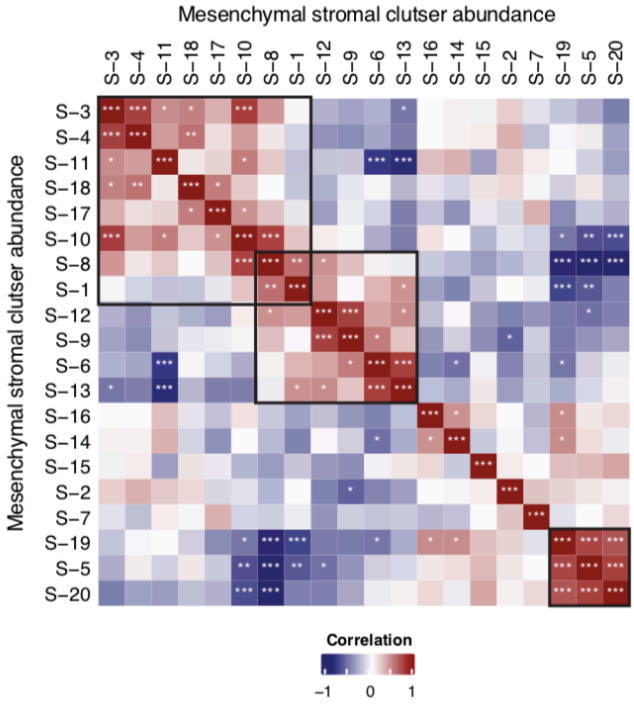

Figure 11. Pancreatic cancer mesenchymal stromal subset abundance correlations

Correlation matrix displaying Spearman correlation coefficients of all pairwise mesenchymal stroma cluster frequency comparisons. *p<0.05, **p<0.01, ***p<0.001.

37/190 (19%) of the unique pairwise comparisons show significant correlations ($p<0.05$) i.e. across the 19 PDA samples as one cluster increases/decreases, the abundance of another cluster shows the same/opposite pattern in a statistically significant manner. The most striking feature of the analysis is that clusters that show coordinated variation across the 19 samples, organise into 3 distinct modules by unsupervised hierarchical clustering. Module 1 consists of two of the BEC clusters, the single LEC cluster, the two endothelial-like clusters S-17 and S-18 and several CD105+ fibroblast clusters, which show positive abundance associations with each other across the 19 samples. This suggests a PDA tumour that has low numbers of one cluster, is likely to have low numbers of the other clusters. Interestingly, the distinct module 2 contains all four of the CD105- fibroblast clusters. The third and smallest module, module 3, consists of the BEC cluster S-5 and the two CD105+αSMAhi clusters S-19 and S-20. Some of these associations show notably strong correlations, despite being unrelated cell types, for example BEC S-5 and fibroblast S-20 ($\rho= 0.78$, $p <0.001$). I choose to avoid interpretation of the negative abundance correlations: the measurement used here is relative abundance, so as a major cell cluster increases, others will proportionally decrease and this is expected to introduce non-real negative correlations.

4.1.4 – Distinct mesenchymal stromal cell clusters have different proliferation and apoptotic characteristics

The tumour microenvironment is a dynamic cellular ecosystem that changes over time with certain cell populations expanding or contracting as the tumour progresses and grows. To capture these changes occurring in the stromal compartment at the chosen sampling time point (i.e. advanced end-stage disease), I incorporated markers of proliferation and apoptosis into the mass cytometry panel. The ribosomal RNA-transcription enhancer protein, Ki-67 is highly expressed during the G1, S and G2 phases of the cell cycle and is a widely accepted marker of cells in an active proliferative state (regardless of which part of the cell cycle they are in). Mice in this study were also injected with an IdU solution 2 h before they were culled. IdU works in a similar manner to the more widely used BrdU, but the bromine atom is replaced by an iodine atom. IdU is rapidly taken up by cells throughout the body and tumour, though transporters of the structurally similar natural nucleoside, thymidine. All cells in S-phase of the cell cycle that are actively replicating DNA, take up and incorporate IdU into their genome and this can be measured in the 127I channel of the mass cytometer. All IdU+ cells (S-phase) are

Ki67+ (G1, S and G2 phase) but not all Ki67+ cells are IdU+ (proliferating but not in S-phase) (see example plot in Figure 12). Every single cell in the mass cytometry analysis, had Ki67 and IdU measurements recorded and these two proteins give a remarkable snapshot of the rate of proliferation of each different stromal cell cluster. Figure 13 plots the mean fraction (± standard deviation (SD)) of proliferating and actively cycling cells (Ki67+/IdU+), across all 20 clusters ordered by increasing average proliferation rates.

Across all PDA tumour mesenchymal clusters, the mean fraction of S-phase cells was 2.8±2.4%. 5/20 (25%) mesenchymal cell clusters had high proliferation rates, with >5% of all cells in the cluster in active S-phase of the cell cycle (S-12, -6, -18, -9 -5). Interestingly, despite being minor populations in terms of relative abundance at this sample collection time point, 3/5 of these clusters were CD105- fibroblasts. This includes both CD105- fibroblast populations with high MHCII expression (S-9 and -12), with cluster S-12 (S-phase fraction = 6.8±3.4%) being the most proliferative of all mesenchymal stromal clusters in PDA tumours. Notably, all CD105- fibroblast clusters had >3% cells in S-phase and conversely, all CD105+ fibroblast clusters had <2% of cells in S-phase, with many much lower. The least proliferative cluster was S-3 (0.2±0.4%), the smallest BEC cluster that has the lowest expression of canonical endothelial cell markers possibly reflecting an immature endothelial state. As for abundance measurements, the rates of proliferation for all clusters showed high variability across the 19 PDA samples, shown in (Figure 13).

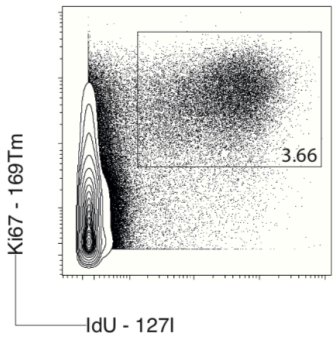

Figure 12. Example Ki67 v IdU plot illustrating how the S-phase fraction is measured for each cluster

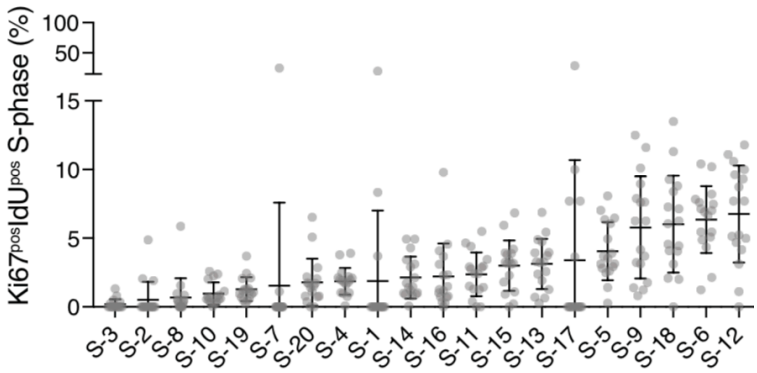

Figure 13. Variability of proliferation rates of pancreatic cancer mesenchymal stromal subsets
The proliferative fraction of FlowSOM-determined PDA mesenchymal cell subsets. Data displayed as mean+/-standard deviation.

Cleaved caspase-3 (CC3) is the most widely used marker of the programmed cell death process known as apoptosis. Caspase-3 is an inactive proenzyme that is activated by cleavage at a conserved aspartate residue by upstream caspases 8, 9 and 10, which themselves are regulated by a vast array of pro- and anti-apoptotic signalling pathways. Cleaved caspase-3 goes on to cleave many proteins required for normal cellular homeostasis (Fernandes-Alnemri et al., 1994), which results in controlled cell death and degradation and release of degraded cell components. Measurement of CC3 with single cell resolution across all 20 mesenchymal stromal clusters, showed a very distinct pattern compared to the proliferation analysis. As for abundance and proliferation measurements, the apoptosis measurements for all clusters across the 19 PDA samples showed a wide range of values. The mean CC3+ fraction across all clusters was 15.5±6.9%, although the average was highly skewed by the high CC3+ fractions seen in endothelial cells: all four of the mesenchymal stromal clusters with the highest fractions of CC3+ cells (S-5, S-11, S-4 and S-18) are endothelial cells, including the two largest BEC clusters and the single LEC cluster. It is not clear from published studies whether different cell-types, like the endothelial cells here, have higher baseline levels of CC3 or whether this high CC3+ fraction represents genuinely high levels of endothelial cell apoptosis occurring in PDA tumours. Fitting with the later idea, is the observation mentioned above, that larger tumours have a reduced abundance of the BEC cluster S-4, compared to small tumours (Figure 10A) and that PDA tumours are well known to be hypovascular (Provenzano et al., 2012; Rhim et al., 2014). Compared to endothelial cells, all fibroblast clusters had much lower CC3+ fractions, ranging from S-9 (5.8±3.6% CC3+), down to S-8 (0.7±1.4% CC3+). This lower level of apoptosis may be one of the

reasons why fibroblasts are able to persist in PDA tumours and accumulate to the high numbers seen in advanced stage lesions.

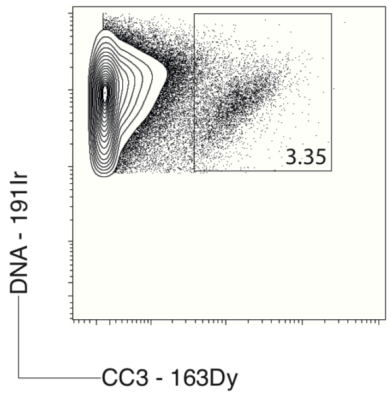

Figure 14. Example cleaved-caspase 3 (CC3) plot illustrating how the apoptotic fraction is measured for each cluster

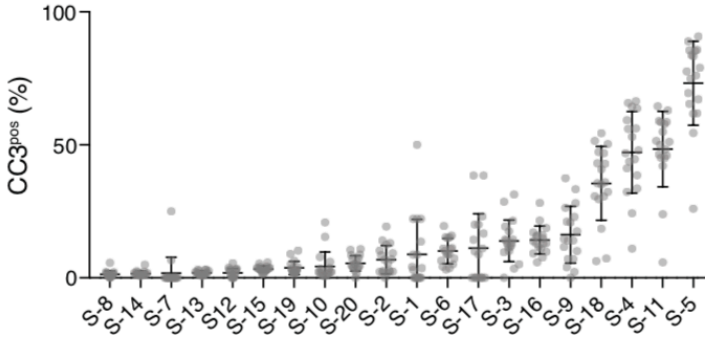

Figure 15. Variability of apoptotic rates of PDA mesenchymal stromal subsets
The apoptotic fraction of FlowSOM-determined PDA mesenchymal cell subsets. Data displayed as mean+/-standard deviation.

4.1.5 – Additional mass cytometry panels to map heterogeneity across immune cells allows for complete mapping of the cellular composition of the PDA TME – Myeloid/NK/B cell (MNB) analysis

The compositional and phenotypic analysis of the mesenchymal stromal compartment by mass cytometry described above, was highly effective and I hypothesised a similar approach could be used to map inflammatory cells, with the aim to assess relationships between mesenchymal and immune cell subsets in a non-biased, discovery manner. In order to map the immune compartment, I developed two further mass cytometry panels. One panel was designed to map CD45+CD3ε- cells, which consist of all myeloid cells,

natural kill (NK) cells (or other innate lymphoid cells (ILCs)) and B cells ('MNB' panel). The other panel aimed to map the CD45+CD3ε+ compartment, consisting entirely of CD3ε+ T cells ('T' panel). Together with the mesenchymal stromal data, this gave complete coverage of all non-tumour cells in the PDA tumours. Because mass cytometry has been extensively used by other researchers to map murine immune cell heterogeneity, many of the key markers to include in panels had already been disclosed in publications. I assessed data from a range of mass cytometry publications and selected the key lineage and phenotypic markers and combined them into MNB and T cell targeting panels. Antibody conjugations were conducted as for the mesenchymal stromal panel. The same PDA tumour samples for which the mesenchyme was measured (described above), were stained with the MNB and T cell panels. One tumour (PDA-19) only had the mesenchyme panel applied, but the remaining n=18 other tumours, were all stained with the mesenchymal stromal (S) panel, the MNB panel and the T cell panel. The resulting matched data for all 18 PDA tumours gives coverage of all TME, non-cancer cells in these 18 different PDA tumours.

In a similar manner to the mesenchymal stromal analysis, the MNB analysis of the CD45+CD3ε- fraction for the 18 PDA samples is shown in Figure 16. Across all 18 PDA tumours, the CD45+CD3ε- fraction accounted for 35.7±11.8% of all viable, single cells. Using well established canonical markers, we are able to annotate the MNB clusters (canonical markers for major immune cell subsets are described in Table 13). All major CD45+CD3ε- immune cell types are observed in the dataset. Cluster MNB-4 is CD19+MHCII+ B cells (7.0±7.8%). Two CD11b+Ly6G+ neutrophil clusters, MNB-1 and -5, are present with MNB-1 (19.8±9.2%) matching a mature neutrophil phenotype (Ly6GhiCXCR2hi) and MNB-5 (1.1±0.6%) matching an immature neutrophil phenotype (Ly6intCXCR2-) (Evrard et al., 2018). MNB-13 (11.3±6.8%) and MNB-17 (0.4±0.6%) are both CD11b+Ly6C-SiglecF+ and therefore are the remaining granulocyte lineages (eosinophils, basophils and mast cells). CD68 is found to be a uniformly expressed by the mononuclear phagocyte lineage, that consists of monocytes, macrophages and dendritic cells (DCs). DC clusters are identified as CD11c+MHCII+CD64-, and within this is MNB-10 (1.3±1.0%) matching a cDC1 phenotype (CD24+CD103+XCR1+) and MNB-9 (1.4±0.8%) matching a cDC2 phenotype (higher CD11b, MHCII and SIRPα expression and lack of cDC1 markers). MNB-7 (0.5±0.4%) are plasmacytoid DCs (pDCs) (SIRPα+PDCA1+).

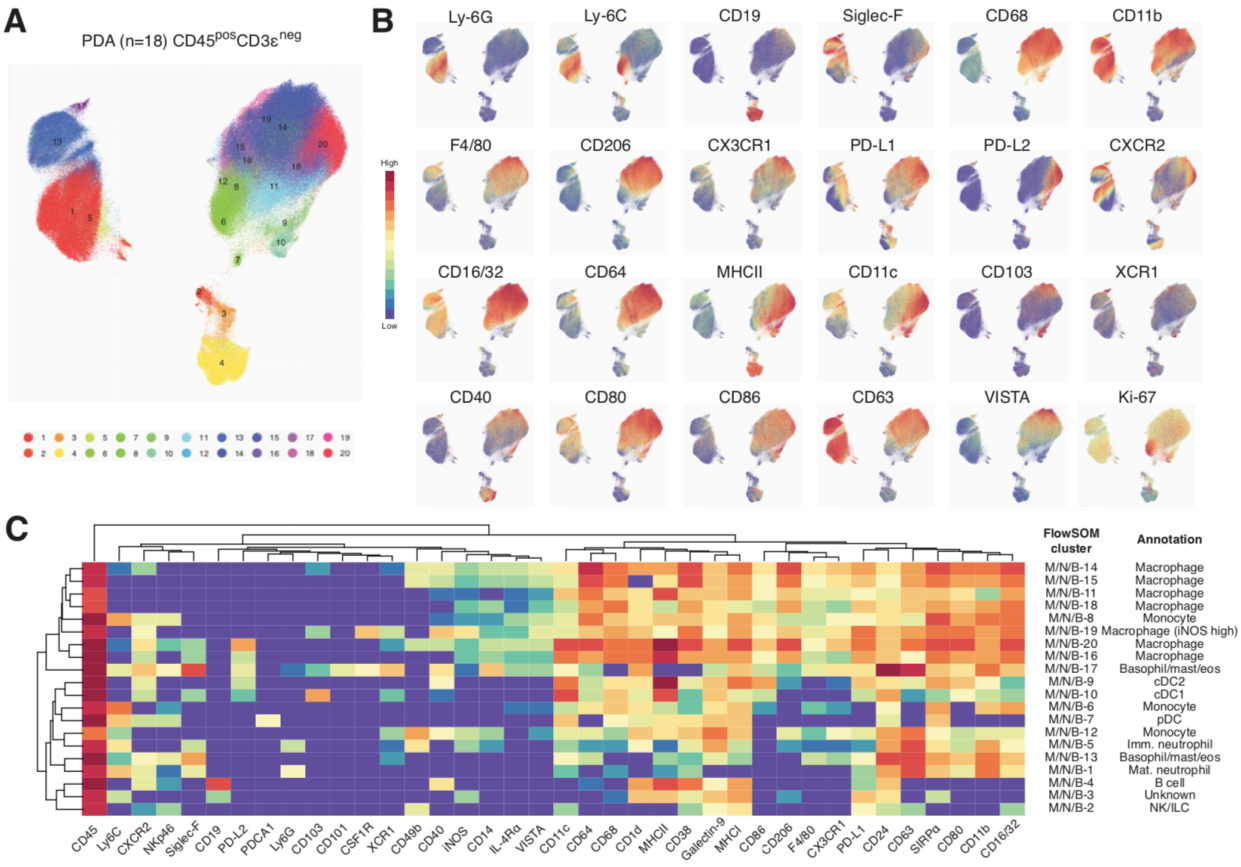

Figure 16. Phenotypic and compositional heterogeneity of pancreatic cancer-associated myeloid, NK and B cells (MNB)

(A) UMAP projection of single MNB stromal cells from end-stage KPC PDA tumors (n=18 samples) with color-coded FlowSOM clusters. Each tumor sample contributes an equal number of cells to the dataset. (B) UMAP projection from (A) displaying overlaid signal intensity of example phenotypic markers. (C) Heatmap displaying marker median mass intensities (MMIs) for each FlowSOM MNB stromal cluster. Phenotypic markers and MNB stromal clusters are grouped using unsupervised hierarchical clustering based on marker MMIs. Cell-type annotations based on canonical phenotypic markers are listed.

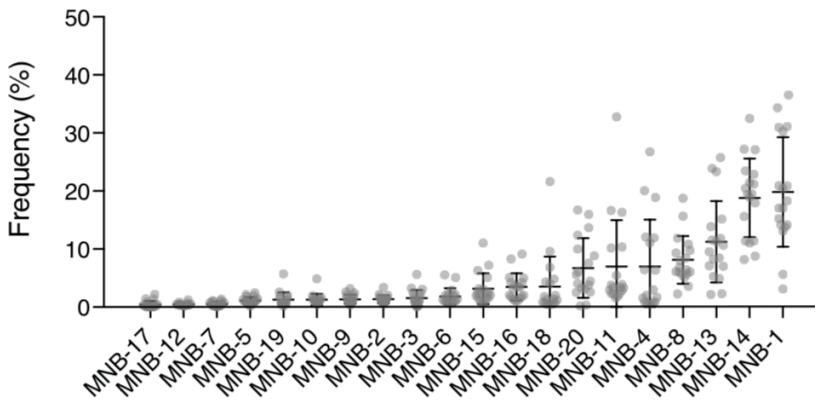

Figure 17. Variability of abundance of pancreatic cancer myeloid, NK and B cell (MNB) stromal subsets

The relative frequency of FlowSOM-determined PDA MNB stromal subsets. Data displayed as mean+/- standard deviation.

Table 13. List of phenotypic markers identifying major immune cell subsets

Cell type	Key markers for identification
Monocyte	CD11b+, Ly6C+, Ly6G-
Macrophage	CD68+, CD16/32+, CD64+, F4/80+
M1 macrophage	As above, CD206+
M2 macrophage	As above, iNOS+
Eosinophil/basophil/mast cell	CD11b+, CD68-, Ly6C-, SiglecF+
cDC1	MHCII+, CD11c+, CD64-, CD24+, CD103+
cDC2	MHCII+, CD11c+, CD64-, CD11b+, SIRPα+
pDC	CD68+, CD11cint, SIRPα+, Ly6C+, PDCA1+
Immature neutrophil	CD11b+, Ly6G+, CXCR2-
Mature neutrophil	CD11b+, Ly6G+, CXCR2+
B cell	CD19, MHCII
NK/innate lymphoid cell	Lack of other lineage markers, CD49b+
Th1 CD4+ T cell	TCRβ+, CD3ε+, CD4+, TBET+
Th2 CD4+ T cell	TCRβ+, CD3ε+, CD4+, GATA3+
Treg CD4+ T cell	TCRβ+, CD3ε+, CD4+, FOXP3+
Antigen experienced CD8+ T cell	TCRβ+, CD3ε+, CD8+, PD1+, CD39+
Bystander CD8+ T cell	TCRβ+, CD3ε+, CD8+, PD1-, CD39-
γδ T cell	TCRγδ+, CD3ε+

A striking feature of this data set is the abundance and heterogeneity of the monocytes/macrophages present in the PDA TME. Cluster MNB-6, -8 and -12 are monocyte clusters (CD11b+CD68+Ly6C+Ly6G-) and show graduated differentiation into a wide variety of phenotypically divergent macrophage clusters. The majority of these cells express F4/80, the canonical marker of tumour associated macrophages (TAMs). Almost all macrophage clusters in these samples have high expression of the mannose receptor, CD206, a widely used marker of the so called alternatively activated (M2) phenotype. Only a minor macrophage cluster MNB-19 (relative abundance 1.3±1.3%) show expression of iNOS, the canonical marker of the so called classically activated (M1) macrophages. However, these cells also show some level of CD206 expression, so definitive M1/2 annotation is not clear. Various gradients of expression of several other proteins results in a patchwork of macrophage phenotypes. These variable proteins include the T cell inhibitory checkpoint molecules PD-L1, PD-L2 and VISTA, the stimulatory receptor CD40, the T cell co-stimulatory ligands CD80 and CD86, the chemotactic receptors CXCR2 and CX3CR1, the Fc receptors CD16/32 and CD64, the 'don't eat me' signal receptor SIRPα, the Th2-related interleukin receptor IL4Ra and the

non-classical MHCI protein, CD1d. Many of these proteins have well established roles in macrophage biology and function in tumours (Cassetta and Pollard, 2018; DeNardo and Ruffell, 2019). On average, these heterogenous monocyte and macrophage clusters make up 52.7±11.2% of all MNB cells in PDA tumours. Of the remaining two minor clusters, MNB-2 has features of NK or ILCs (lack of myeloid and B cell markers and expression of CD49b and Nkp46) and MNB-3 has a mixed phenotype and is unknown/unannotated.

The mature neutrophil cluster MNB-1 shows the highest abundance of any single MNB cluster (19.8±9.2%). This is possibly due to its relatively homogenous phenotype, especially compared to the heterogenous and fragmented macrophage clusters. The standard deviation from the average abundance of this cluster was also the highest of all MNB clusters, with the relative abundance ranging >10-fold from 3.1-36.5%, suggesting neutrophils accumulate to wildly different degrees across PDA tumours. Other cell types also vary widely, being very rare or highly abundant in some PDA tumours. For example, B cells can make up between 0.5-26.8% of all the CD45+CD3ε- cells (average 7.0±7.8%), depending on the particular PDA tumour. Because B cells rarely infiltrate tumours, these cells may be part of tertiary lymphoid structures or less coordinated immune cell aggregates.

The average proliferation rate of all the MNB clusters was 2.9±1.9% and was very similar to the average proliferation rate of all the stromal cell clusters (2.8±2.4%). Even though Ki67 is not used to drive clustering in this analysis, we can see that it shows uneven distribution among clusters, for example with high expression in monocyte clusters and little expression in B cell clusters, which fits with the known proliferation behaviour of these cell types in tumours (Gabrilovich et al., 2012; Sarvaria et al., 2017). Detailed analysis of the proliferative and apoptotic fractions of each cluster is given in Figure 18-19. As for the mesenchymal stromal cell analysis, a wide range of proliferation and apoptosis rates are observed both between different MNB clusters in the same PDA tumour and also between the same cluster in different PDA tumours, highlighting the heterogenous nature of this spontaneous tumour model.

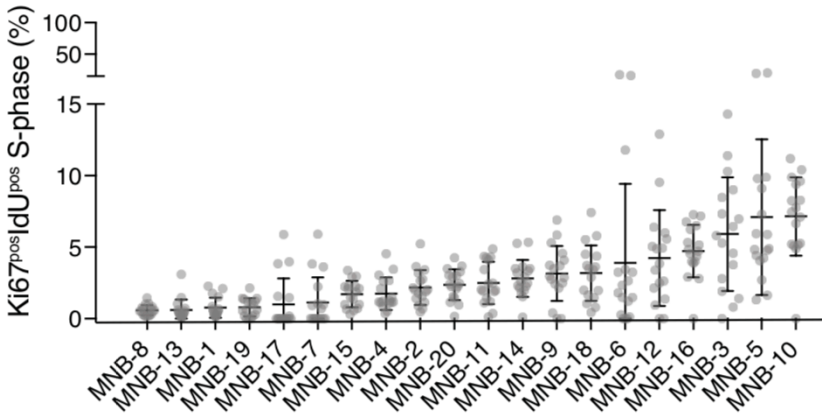

Figure 18. Variability of proliferation rates of pancreatic cancer Myeloid, NK, B cell (MNB) stromal subsets.
The proliferative fraction of FlowSOM-determined PDA MNB stromal subsets. Data displayed as mean+/- standard deviation.

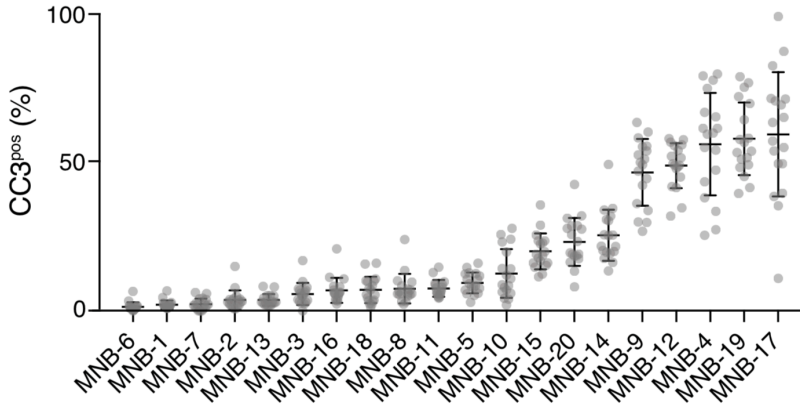

Figure 19. Variability of apoptotic rates of pancreatic cancer Myeloid, NK, B cell (MNB) stromal subsets
The apoptotic fraction of FlowSOM-determined PDA MNB subsets. Data displayed as mean+/-standard deviation.

Surprisingly, the rare cDC1 cluster, MNB-10, is the most proliferative MNB cluster, with an average S-phase occupancy of 7.2±2.7%. Despite rapid cDC1 proliferation, cDC1s are a minor cell type here (and in other tumours). Suppressive effects can restrain them to the tumour margins and reduce cell survival (Bottcher et al., 2018; Bottcher and Reis e Sousa, 2018). In addition, antigen capture and DC maturation initiates a CCR7-dependant migrational program that transports them away from the tumour to the tumour-draining lymph node (TDLN) (Bottcher and Reis e Sousa, 2018; Roberts et al., 2016). Notably, PDA tumours are known to secrete high levels of GM-CSF (Bayne et al., 2012), a key growth factor for cDCs in the periphery (Greter et al., 2012). For unknown reasons, despite this high cDC1 proliferation, these tumours are clearly not being controlled effectively by adaptive immunity.

The least apoptotic of all MNB clusters is the immature monocyte cluster, MNB-6, consistent with the fact that healthy monocytes derive directly from the blood and begin to differentiate into macrophages (and lose their monocyte phenotype) as they travel into tissues and encounter inflammatory ligands and environmental stresses, before dying as terminally differentiated macrophages (DeNardo and Ruffell, 2019).

4.1.6 – Additional mass cytometry panels to map heterogeneity across immune cells allows for complete mapping of the cellular composition of the PDA TME – T cell (T) analysis

Next, I applied a similar analysis to the CD45+CD3ε+ compartment of the 18 PDA samples, using the mass cytometry T cell panel (Figure 20). Across all 18 PDA tumours, the CD45+CD3ε+ fraction accounted for just 4.0±3.9%% of all viable, single cells. As for the mesenchyme and CD45+CD3ε- immune cells, extensive cellular heterogeneity is observed among the T cells in these PDA samples. As expected from the pre-gating strategy, all cells are positive for CD3ε. Lack of TCRβ expression and positive TCRγδ expression identifies three small and distinct γδ T cell clusters (T-11, -13 and -15). Three other minor clusters show zero/very low expression of TCRβ, TCRγδ, CD4 or CD8a (T-8, 9, 18). These cells possibly represent genuine 'double negative' T cells that others have reported in tumours (Brandt and Hedrich, 2018; Yao et al., 2019), blood circulating thymocytes that have been brought into the tumour under inflammatory gradients or are in the blood vessels at the time of tumour collection (Anderson et al., 1996). Alternatively, some of these clusters may be NKT cells or possibly myeloid cells that have taken on CD3ε protein by trogocytosis or phagocytosis (Ahmed et al., 2008), causing them to fall within the CD45+CD3ε+ gate used to select these target cells. In support of this, clusters T-18 and T-9 have much lower median expression of CD3ε than the other *bone fide* T cell clusters. Alterative markers would be needed to better characterise these minor clusters. TCRβ expression and CD4 and CD8a expression identifies the two main groups of clusters as CD4+ T cells (MHCII-peptide targeting) and CD8a+ T cells (MHCI-peptide targeting), respectively. I focussed further detailed annotation on these major CD4+ and CD8a+ T cells clusters, as they make up a combined average of 84.2±8.7% of all T cells in these PDA tumours and have well-established roles in the regulation and execution of anti-tumour immunity.

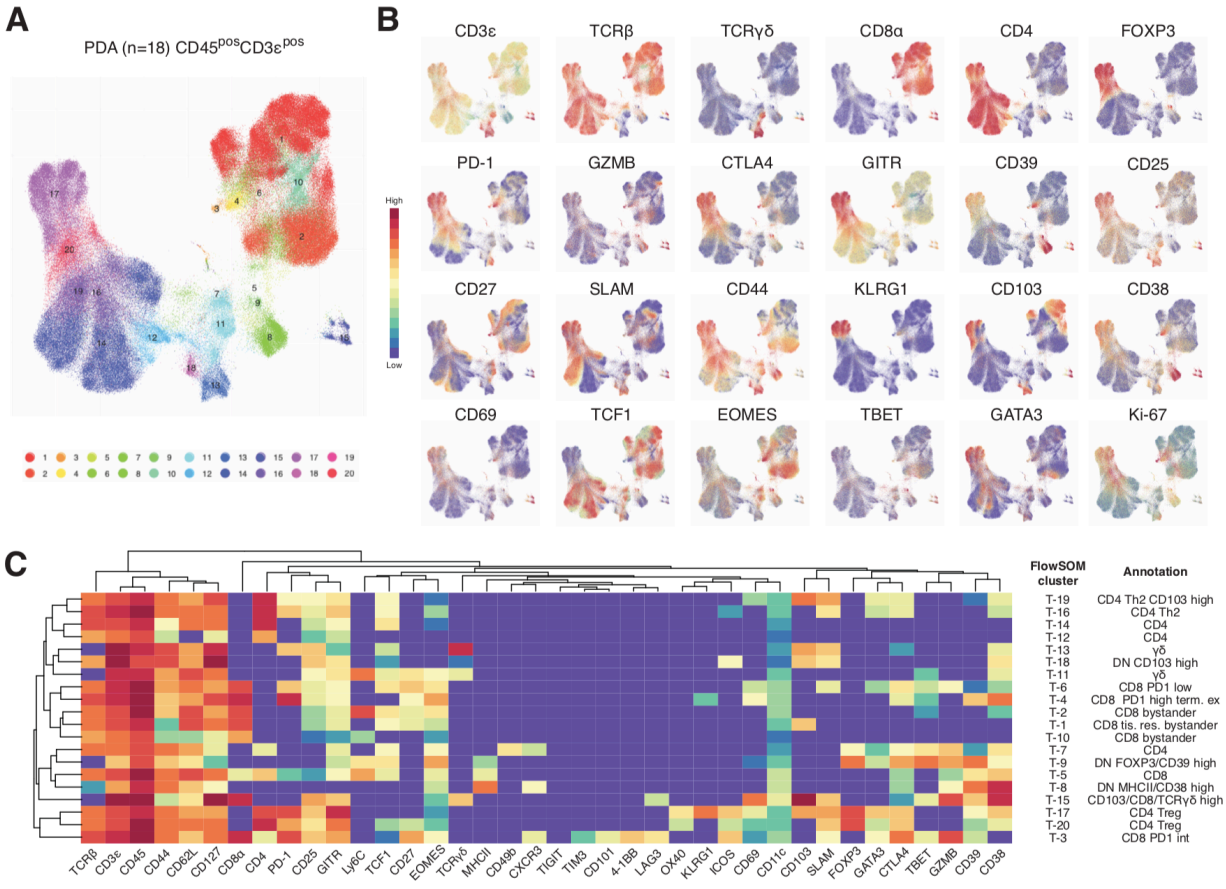

Figure 20. Phenotypic and compositional heterogeneity of pancreatic cancer-associated T cells (T)
(A) UMAP projection of single T cells from end-stage KPC PDA tumors (n=18 samples) with color-coded FlowSOM clusters. Each tumor sample contributes an equal number of cells to the dataset. (B) UMAP projection from (A) displaying overlaid signal intensity of example phenotypic markers. (C) Heatmap displaying marker median mass intensities (MMIs) for each FlowSOM T cell cluster. Phenotypic markers and T cell clusters are grouped using unsupervised hierarchical clustering based on marker MMIs. Cell-type annotations based on canonical phenotypic markers are listed.

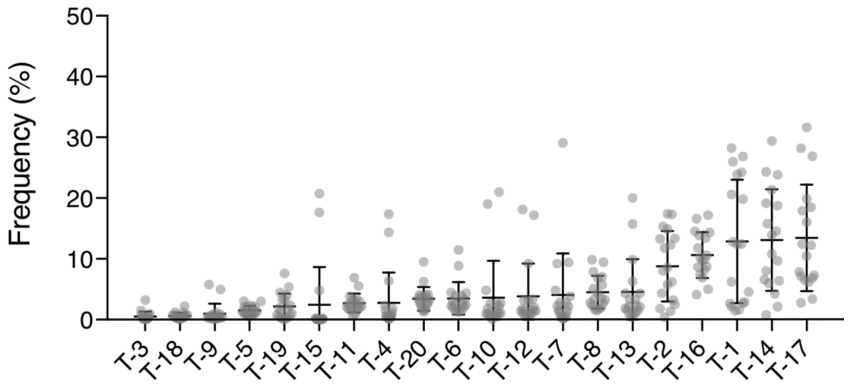

Figure 21. Variability of abundance of pancreatic cancer T cell (T) subsets
The relative frequency of FlowSOM-determined PDA T cell subsets. Data displayed as mean+/-standard deviation (SD).

Within the CD4+ group of T cell clusters, the transcription factor FOXP3 identifies two regulatory T cell (Treg) populations: T-17 (13.5±8.5% of all T cells) and T-20 (3.4±1.9%). Both have expression of the checkpoint receptor PD-1 and the C-Type lectin, CD69, proteins both rapidly and positively regulated by TCR engagement. Cluster T-17 has the highest levels of PD-1 and also the Tumour necrosis factor receptor superfamily (TNFRSF) members GITR and OX40, the E- and N-cadherin targeting lectin-like receptor KLRG1 and the E-cadherin binding integrin CD103. All of these proteins have known functions in Treg biology in tissues and tumours (Togashi et al., 2019). Of the remaining five CD4+ T cell clusters, T-16 (10.6±3.7%) and T-19 (2.2±2.1%) express GATA3, the canonical lineage-defining transcription factor of Th2 cells. These Th2 cells also express PD-1 and other markers of activation including CTLA4, a key negative regulator of antigen-dependant activation that is increased after TCR signalling, suggesting recent antigen-recognition by these Th2 cells. Two other CD4+ T cell clusters, T-12 (3.8±5.3%) and T-14 (13.1±8.1%), lack expression of the T effector lineage defining markers used in the panel. These cells are not Th1 cells because they lack expression of the transcription factor, TBET, so they may be Th17 cells. However, an antibody targeting the Th17-defining transcription factor, RORγT would be needed to clarify this annotation. These unclassified effector T cell clusters have no expression of PD1 and CD69, thus are unlikely to be interacting with their cognate antigen in the TME and may be less relevant to tumour biology than the PD1+ Treg and Th2 cells. Thus, the CD4+ T cell compartment in the PDA tumours is dominated by Tregs and Th2-polarized CD4+ T cells with minimal Th1 cells, which matches the tumour-promoting CD4+ T cell composition of PDA tumours noted in recent publications (Dey et al., 2020; Hegde et al., 2020).

CD8+ T cell clusters make up 33.9±6.2% of all T cells in these samples. A wide variety of distinct phenotypes are seen. However, the most striking observation within the CD8+ T cell clusters, is that the largest clusters (T-1, T-2 and T-10), which contain the vast majority of total CD8+ T cells, show no expression of markers associated with TCR activation. For example, they completely lack expression of PD1, CD69 and CTLA4. They also have no expression of the ATP ectonucleotidase, CD39. Lack of CD39 expression has recently been shown to denote bystander CD8+ T cells in human and mouse tumours, that have microbial antigen-specificity and are likely brought into the tumour under inflammatory gradients and irrelevant to tumour control (Simoni et al.,

2018). Remarkably, this indicates that >70% of all the CD8+ T cells in these PDA tumours, likely do not have the antigenic potential to target and kill tumour cells. Three minor CD8+ T cell clusters do have evidence of PD1, CD69 and CTLA4 expression, suggestive of antigen stimulation and tumour-specificity: T-3 (0.5±0.8%), T-4 (2.7±4.9%) and T-6 (3.5±2.6%). Of the three PD1+CD8+ T cell clusters, T-4 fits the classical phenotype of the so called 'terminally differentiated exhausted' or 'late dysfunctional' CD8+ T cells (Thommen et al., 2018; van der Leun et al., 2020). This cluster has the highest median levels of PD1, CD39, and the cyclic ADP ribose hydrolase, CD38, all of which have been shown to consistently mark terminally differentiated CD8+ T cells (Philip et al., 2017; Simoni et al., 2018). T-4 cells also express the highest levels of EOMES, a T-box transcription factor shown to play a role in enforcing the terminally exhausted phenotype (Li et al., 2018). T-4 also lacks expression of GZMB, a key effector molecule required for target cell killing. In other human and mouse studies, the terminally differentiated/late dysfunctional CD8+ T cell phenotype is characterised by a lack of clonal expansion potential and reduced effector function within the TME (Khan et al., 2019; Thommen et al., 2018; van der Leun et al., 2020). In contrast, another PD1+CD8+ T cell cluster, T-3 shows evidence of tumour antigen-specificity but with a very distinct phenotype. It has intermediate expression of PD1, CD39 and lacks CD38 expression, suggesting an active but not terminally exhausted phenotype. It has the highest expression of GZMB and CTLA4 and has the highest level of TBET, a transcription factor suggested to mark the early CD8+ T cell exhausted state, capable of rapid expansion and tumour control (van der Leun et al., 2020). This is the only PD1+CD8+ cluster to express some level of the co-stimulatory receptor, TNFSF member 4-1BB, co-stimulatory molecule ICOS, and the immune checkpoints, LAG3 and TIM3. The expression of these proteins has been associated with cells experiencing ongoing TCR engagement and effector activity, as well as having a role themselves in directly regulating effector function (Chen and Flies, 2013). Interestingly, this T-3 population is also the only CD8+ T cell cluster to express CXCR3, a key chemotactic receptor responsible for T cell migration to APCs (Groom and Luster, 2011). The final PD1+CD8+ T cell cluster, cluster T-6, has intermediate expression of PD-1 but little expression of CD39, so its antigen relevance is not clear. T-6 is the only one of these PD1+CD8+ clusters to express the transcription factor TCF-1, associated with T cell stem/progenitor-like functions and long-term self-renewal capacity during immunotherapy (Miller et al., 2019; Siddiqui et al., 2019; Yost et al., 2019).

Analysis of the proliferative and apoptotic fractions of each T cell cluster is given in Figure 22-23. The most proliferative T cell clusters are far more rapidly cycling than any mesenchymal stromal or MNB cluster. Of all T cells, the rare PD1+CD8+ T cell clusters, T-3 and T-6, have the highest proliferation. The proliferation levels of T-3 are particularly remarkable, with an average S-phase occupancy of 31.8±21.3%. Because S-phase is only one phase the cell must go through to achieve complete division, these levels are suggestive of almost constant cell cycling within this cluster. Knowledge of the relative lengths of G0/1, S, G2 and M-phase for CD8+ T cells would need to be known to asses this accurately. Interestingly, as well as being highly proliferative in many of the PDA samples, this cluster (T-3), has the second-highest average apoptosis rate of all T cell clusters (24.8±22.1%). However, this apoptosis rate is highly variable across the different PDA tumours, with the T-3 cluster in several samples having <1% CC3+ cells. Thus T-3 appears to be a highly dynamic tumour-specific CD8+ T cell population, with a phenotype of an early exhaustion/tumour-killing potential and proliferation/apoptosis rates that vary widely across the 18 PDA tumours. Interestingly, the terminally exhausted CD8+ T cell cluster, T-4 still appears to retain a low level of proliferation (2.5±2.6%), albeit much lower than that for cluster T-3. Of all the CD4+ T cell clusters, the Treg cluster T-20 has the highest proliferation (10.9±6.5%) supporting the concept that in late stage PDA the T helper phenotype is skewed towards being highly suppressive (Dey et al., 2020; Hegde et al., 2020). In general, all CD4 T cell clusters, including Tregs, show low levels of apoptosis.

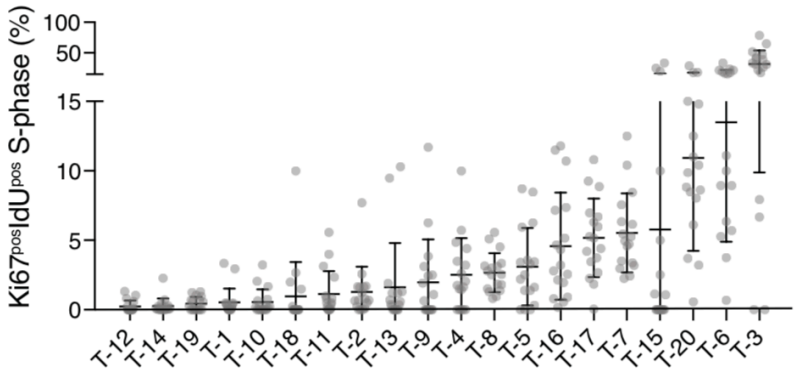

Figure 22. Variability of proliferation rates of pancreatic cancer T cell (T) subsets
The proliferative fraction of FlowSOM-determined PDA T cell subsets. Data displayed as mean+/-standard deviation.

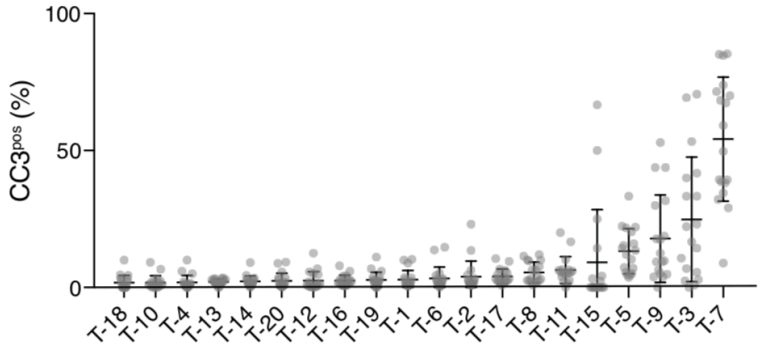

Figure 23. Variability of apoptotic rates of pancreatic cancer T cell (T) subsets
The apoptotic fraction of FlowSOM-determined PDA MNB subsets. Data displayed as mean+/-standard deviation.

4.2 – Summary

In this chapter, I outline the development and application of three separate mass cytometry panels, each focussing on deep phenotyping of a different cellular compartment in PDA GEMM tumours. Two panels map the immune landscape of these tumours and a third, novel mass cytometry panel, maps the mesenchyme. Importantly, all panels included markers of proliferating cells (Ki67 and IdU) and apoptotic cells (CC3) and this data provides a detailed 'snapshot' of the state of the PDA TME at the time the tumours are collected (advanced, late stage disease), both in terms of cellular abundance and cell phenotype. The hypothesis of this section was that novel single cell technologies could provide a detailed analysis of the TME and I believe in this regard, the methodology was successful in revealing details of a complex, highly variable and dynamic PDA tumour ecosystem. A notable feature of the data is the range of heterogenous fibroblast phenotypes observed.

4.3 – Discussion

In an attempt to improve understanding of the PDA TME, I developed a single cell analysis workflow that maps the abundance and phenotype of cells in the KPC PDA TME. Using mouse tumours was required: high quality human PDA biopsy samples are difficult to obtain in sufficient number for this type of analysis. In addition, the huge heterogeneity (genetic and non-genetic) present in human tumours, the fact that single, small biopsies do not capture processes occurring throughout the tumour (Rosenthal et al., 2019) and the variable treatment history of patients, would likely complicate and

confound the identification of common patterns of behaviour of cells in the PDA TME ecosystem, as has been done here. This study acts as a proof of principle, illustrating the vast information that can be gathered from such experiments and is a useful basis for any potential future equivalent study with human PDA samples. It is striking that even though the initiating mutations and timing of oncoprotein expression are the same for all KPC tumours, the end composition and properties of the TME are highly variable across the cohort. The factors that drive this divergence are largely unknown. In particular, an understanding of how individual mutations and the cancer cell epigenome contributes to shaping the TME is poorly understood, although recent work has shown that epigenetic regulation of TP63 in PDA cells, can influence the phenotype of adjacent fibroblasts via IL1α secretion (Somerville et al., 2020). Whilst tumour genetic heterogeneity is now a well-established driver of therapeutic resistance, it is unclear what contribution the heterogeneity of the TME infiltrate and phenotype makes to the failure of clinical interventions in cancer patients.

It is notable that immune cells constitute a large fraction of the single cell suspensions in this study (mean 39.3±14.7%). Although PDA is a highly inflammatory tumour type, preferential release of immune cells may act to confound the analysis, as different cell types are released with differing efficiencies during tumour during disaggregation. Generally, immune cells have more transient cell-cell interactions and are less embedded in the tumour extracellular matrix (ECM) than epithelial and mesenchymal cells. In support of this, the mesenchyme appears to be particularly under-represented generally in this analysis and also in published single cell analysis of PDA (Elyada et al., 2019), compared with histological analyses. The disaggregation protocol used here is highly optimised and this different ‘efficiency of release’ might be an inherent problem with any assay that requires single cell suspensions to be generated from a tissue (e.g. mass cytometry, flow cytometry and scRNAseq). Because the disaggregation protocol was followed consistency across all samples, I reason the relative abundance of each cell type is comparable between PDA samples within this cohort, even if the absolute number of cells of each cell type has been skewed by the isolation process (that is, the abundance quantitation in the analysis is precise, but may not be accurate of the actual numbers in the intact tumour).

I believe the experiment was successful in mapping the murine PDA TME: I identified all known major immune and mesenchymal cell types with expected distribution of canonical markers. The analysis of the mesenchyme with mass cytometry was particularly novel: no reports of such analysis are currently present in the literature. The fact that most major immune cell subsets are present in the analysis, provides confidence that the detailed analysis within the less-well characterised mesenchymal stroma compartment, identifies genuine, phenotypically distinct clusters of fibroblasts. The expression of PDPN and CD90 and lack of CD31 expression separates the general fibroblast population reasonably well from other cell types in these PDA tumours, including clean separation from cancer cells. It should be noted that CD90- fibroblasts are seen in other pathologies, such as rheumatoid arthritis (Croft et al., 2019; Wei et al., 2020). This may indicate that fibroblast phenotypes are distinct between different diseases/tissues and that useful markers in one disease/tissue may not be appropriate to use in others. Within this pure fibroblast population, a wide range of phenotypes are observed, highlighting the need to measure multiple protein targets simultaneously. In particular, the most striking result was the clear separation of two major groups of CD105+ or CD105- fibroblast clusters. Each contained a continuum of phenotypes with gradients of known activation markers, such as αSMA, PDGFRα, PDGFRβ, ICAM1, VCAM1, ITGβ3 and ITGα5. In this regard, CD105 is the only fibroblast marker that shows such a bimodal, discontinuous expression pattern.

Pair-wise comparison of the abundance of all mesenchyme clusters revealed that the abundance of CD105+ fibroblast clusters was associated with the abundance of other CD105+ fibroblast clusters, and CD105- fibroblast clusters to other CD105- fibroblast clusters. This possibly suggests that the abundance of total CD105+ and CD105- fibroblasts is variable across the different PDA tumours and that the clustering within these groups, simply represents splitting of these parent populations into phenotypically different subpopulations, hence they show a positive correlation with each other. CD105- fibroblasts are particularly distinct in that despite generally being less frequent than the CD105+ fibroblast clusters, they show high levels of proliferation at the time point these tumours were collected. This possibly reflects distinct proliferative ques in early versus late tumour progression. In addition, expression of proteins involved in antigen-presentation (such as MHCII and CD74), co-stimulation such as CD80 and other proteins such as ITGα6, are only seen on CD105- fibroblast clusters. Other proteins such as

CD73 are seen in both CD105+ and CD105- clusters but are more highly and more widely expressed in CD105- fibroblast clusters. Many of these proteins have known functional roles in regulation of immunity and inflammation. This suggests CD105+ and CD105- fibroblasts may have distinct phenotypes or functions or may be occupying distinct niches in the TME. 'Antigen presenting' CAFs (apCAFs) have previously been noted in KPC tumours by scRNAseq, based on MHCII loci gene expression (Elyada et al., 2019). Indeed, apCAFs may correspond to the same cluster of MHCII+ fibroblasts identified here, although the CD105 status was not described in the scRNAseq study. It is still unclear if the expression of antigen presentation machinery or co-stimulatory molecules by fibroblasts plays any functional role in the PDA TME (discussed further in chapter 8).

FlowSOM clustering and UMAP visualisation is successful in ordering known cellular differentiation trajectories in the datasets, in an unsupervised manner (for example monocyte to mature macrophage differentiation is apparent). A consistent feature in the mesenchyme analysis across all samples, is that fibroblast clusters appear to be ordered with varying expression of several markers. For example, αSMA and PDGFRα show a prominent inverse staining pattern on fibroblast clusters, marking MyCAF and iCAF-like phenotypes, respectively. In addition, ICAM1 and to lesser degree VCAM1, appear to largely, but not completely, overlap with the PDGFRαhi phenotype. CD26 expression identifies distinct populations of murine skin fibroblasts but appears broadly expressed across most PDA fibroblast clusters, as well as the single pericyte cluster. These differing results highlight the need for a better understanding of the similarities and differences of fibroblast phenotypes across different tissues and pathologies.

The current analysis lacks annotation of several rare CD45- cell types that would be expected to be in the various datasets, including smooth muscle cells, pancreatic islet cells, neurons and cell types associated with lymph node/immune cell aggregates, such as fibroblastic reticular cells, follicular dendritic cells and high endothelial venules (HEVs). It is likely that several of the minor, unannotated clusters in this analysis represent one or more of these rare cell types. Additional antibodies would be needed for this to be properly assessed. For example, there are several unannotated CD31 endothelial cell-like clusters and an anti-PNAd antibody could positively identify these as HEVs. Interestingly, cluster S-1 is a very rare cluster in most samples (>1%) but makes

up >40% of the mesenchyme in sample PDA-18. It is unclear if this is a technical artefact or it may possibly be an unusual mesenchymal cancer cell phenotype that only expands in a minority of tumours.

FlowSOM cluster annotation was used to derive many of the quantitative features in this chapter. This method of clustering is relatively new and best practices for its application are lacking. For example, I arbitrarily selected n=20 FlowSOM clusters because it largely matched the orthogonal cluster annotation provided visually by UMAP projections. In addition, this level of clustering also clearly separated cell subsets from the same major cell-type, that have established functional differences (e.g. cDC1 and cDC2s). Despite this, some clusters show discordance between FlowSOM and UMAP analysis, for example the putative NK/ILC cluster is split in the UMAP projection. Cluster accuracy and downstream analysis could likely be improved with better cluster number selection and/or inclusion of other markers for rarer lineages. Thus, the identification and accurate annotation of cell phenotypes, will likely improve as best practices for UMAP visualisations and FlowSOM clustering emerge.

Hierarchies of self-renewal, progenitor and terminally differentiated states are well established in several epithelial tissues (e.g. the intestinal epithelium). Very little is known about whether any such trajectories exist in mesenchymal cells, such as endothelial cells, pericytes or fibroblasts. Because an analysis such as the one described here contains a wealth of phenotypic information (surface receptors, transcription factors and proliferation and apoptosis rates), it provides an ideal platform to study such trajectories in mesenchymal cells in the future. For example, the endothelial cell clusters show progression from S-3, S-4 to S-5, with increasing canonical markers of endothelial maturation and increasing levels of both proliferation and apoptosis. Whether or not this represents an actual, uni-directional differentiation trajectory that occurs during tumour vasculogenesis is unclear. Studying such processes in systems less chaotic than growing tumours, may be more appropriate and provide clearer results.

The most striking feature of the immune cell datasets was the lack of PD1+CD39+ tumour-specific CD8+ T cells and highlights the need to measure cell phenotype (e.g. PD1/CD39/CD69/GZMB) status and not just count cells from different lineages (i.e. CD8+ T cells). Low numbers of antigen-specific T cells in the KPC model have recently

been reported by others (Hegde et al., 2020) and has been attributed to the very low mutational burden of these murine tumours relative to the human disease (Mueller et al., 2018), which in turn is expected to result in fewer MHCI-binding neoantigens. In addition, PDA tumour cells have recently been shown to downregulate MHCI via increased autophagy, which reduces CD8+ T cell expansion (Yamamoto et al., 2020). A recent publication has also described the OG-KPC GEMM, a KPC-based model that allows for Cre-recombinase-dependant expression of full-length OVA (a model antigen), in pancreatic cancer cells and generation of immunity to the dominant H2Kb-restricted SIINFEKL epitope (Hegde et al., 2020). The OG-KPC model has been shown to have large numbers of tumour-specific, CD8+ T cells and the authors suggest the model more closely mimics the antigenicity seen in the human disease, although a lack of direct mouse to human comparisons in the study is notable. It would be interesting to apply the TME phenotype mapping analysis described here, to this new PDA model system to see which features of the TME (immune and non-immune) are dependent on tumour cell antigenicity.

Chapter 5 – Results – Cell abundance and phenotypic associations in the PDA TME

5.1 – Results

5.1.1 – Proliferation correlation analysis

Two most striking features, common across the analysis of the mesenchyme and CD45+CD3ε+/- immune compartments are:

1) the complexity of cellular phenotypes present in each compartment and
2) the extensive variability observed of cellular abundance and phenotypes across the 18 tumours.

As the dataset provides a detailed map of the different states the KPC PDA TME can occupy, I hypothesised that by analysing this variability across the samples in a systematic, pairwise manner, putative associations between cell clusters could be identified. Such an analysis identifies pairs or groups of cell subsets that may be either coordinated by common upstream regulators or possibly regulate each other. A similar method has been used to compare the variation in abundance of major immune cell types during effective vs ineffective immunotherapy (Spitzer et al., 2017). Whilst such an analysis is imperfect, and will contain both potential false positives and false negatives, such an approach still offers a novel way to identify putative cell-cell relationships in complex cellular ecosystems, without any *a priori* knowledge about the actual mechanisms driving co-regulated behaviour. Such a non-biased method may provide starting points for further mechanistic studies.

The first 'cross-correlation' analysis compared the cellular proliferation rates across all 60 clusters, consisting of the 20 mesenchymal stroma (S) cell clusters, 20 Myeloid/NK/B (MNB) cell clusters and 20 T (T) cell clusters. The fraction of S-phase cells in one cluster was compared to the fraction of S-phase cells in a second cluster, across the different PDA samples and this was repeated for all unique pairs of clusters (n=1770 unique pairwise comparisons). I hypothesised that this analysis would highlight clusters whose proliferation is coordinated by a common upstream factor (e.g. growth factor or cytokine)

or for pairs of clusters that reciprocally regulate each other's proliferation. The data presented in Figure 24 plots each comparison with the Spearman coefficient (1 to -1) displayed as either positive correlation (red) or negative correlation (blue), estimated statistical significance ($p<0.05$) denoted with an asterisk and the clustering of the row/column by unsupervised hierarchical clustering.

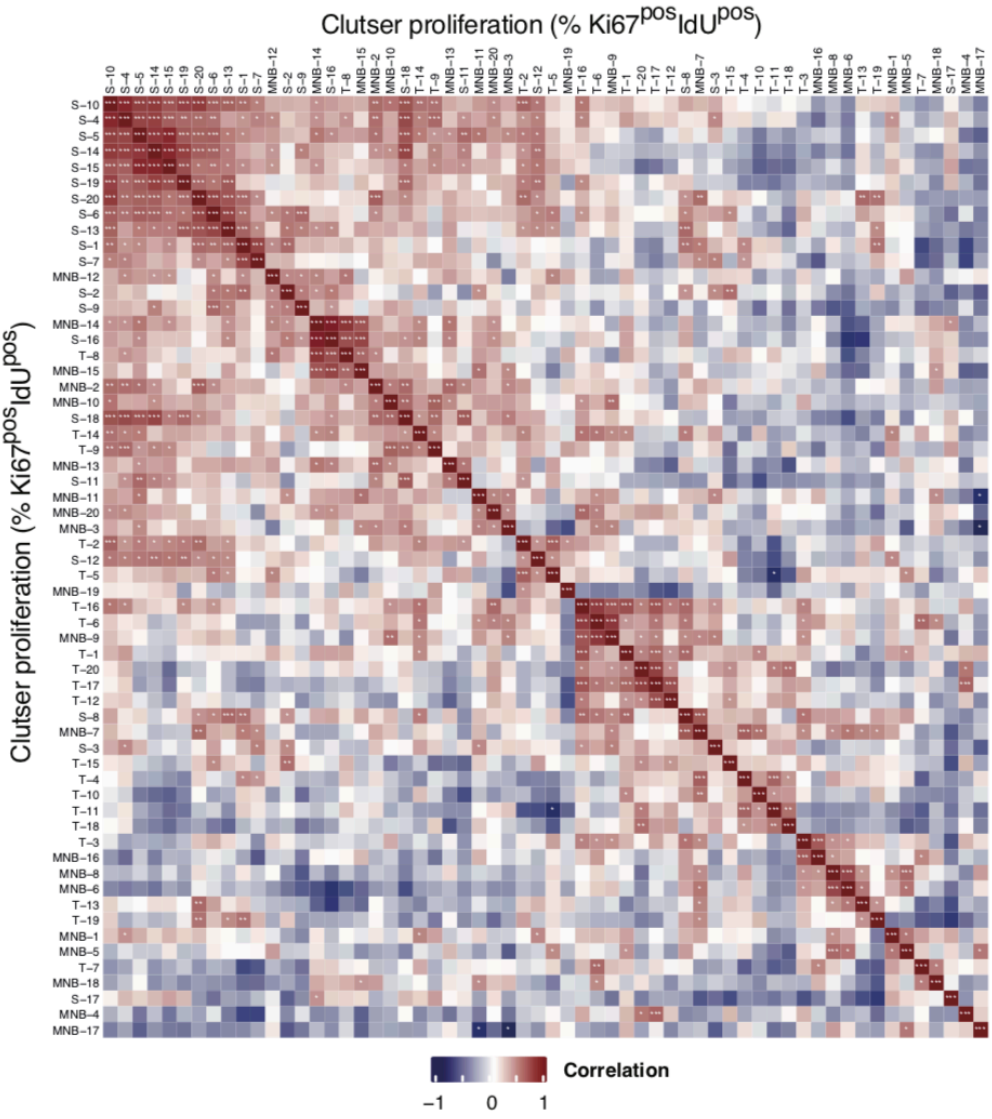

Figure 24. Pancreatic cancer stromal subset proliferation correlations
Correlation matrix displaying Spearman correlation coefficients of all pairwise stroma subset proliferative fraction comparisons. *p<0.05, **p<0.01, ***p<0.001.

1492 of the total 1770 unique pairwise comparisons (84.4%) show no associated proliferation between clusters, which would be consistent with the concept that much of the proliferation in the TME is controlled through a wide range of cell-subset specific, unconnected mechanisms. In addition, several clusters show little proliferation (see

previous chapter), so it is not possible for them to have correlated proliferation with other clusters. 277/1770 unique pairwise comparisons (15.6%) show a significant association of the S-phase fractions between pairs of clusters. A large module of clusters (Proliferation Module 1), containing 123/1770 (6.9%) of all unique pairwise comparisons, shows significant associations of S-phase fractions (such that if the proliferation for cluster X is high in one sample, it is likely that the proliferation of cluster Y will also be high in the same PDA sample). The proliferation rate of some clusters in this module, such as S-10, shows positive associations with the proliferation rates of almost all other clusters in the module. The most striking feature of the cell clusters that make up this module, is that 26/31 (83.9%) of them are either S or MNB clusters, with only five T cell clusters present in the entire module. Within this module, there is group of 11 mesenchymal stromal clusters that show particularly correlated proliferation rates with each other across the PDA samples. An example of a correlation from this module is between the proliferation of the 'mature' BEC cluster S-5 and proliferation of the pericyte cluster S-15, which aligns with the known reciprocal and co-regulated proliferation of these two vascular cells (Sweeney and Foldes, 2018).

Another notable example in the module is the coordinated proliferation rates of MNB-10 (cDC1s) and MNB-2 (NK-like) clusters. This reciprocal interaction has been reported in several recent publications and centres on the ability of NK cells to provide cDC1s with factors such as FLT3L and XCL1 and cDC1s to provide NK cells with factors such as IL-12 and IL-15 (Barry et al., 2018; Cabeza-Cabrerizo et al., 2019).

This analysis indicates that cell proliferation in the PDA TME is coordinated in discrete modules, with a major module consisting of coordinated proliferation among many mesenchymal stromal subsets and to a lesser extent, some specific macrophage, dendritic cell and NK cell clusters, potentially indicating shared upstream regulators of proliferation. T cell proliferation appears to be regulated distinctly. Indeed, the second notable module in the data (Proliferation Module 2) consists of 25/1770 unique pairwise comparisons (1.4%) and is mainly made up from correlated T cell clusters: 11/16 (69.8%) of these clusters are T cell clusters.

Within the whole analysis there is a prominent lack of negative associations of proliferation rates between one cluster and another: there are only 3 significant negative correlations out of all 1770 unique pairwise comparisons (0.2%).

5.1.2 – Apoptosis correlation analysis

The second 'cross-correlation' analysis compared the cellular apoptosis rates across all 60 clusters, as measured by CC3+ fraction. The majority of pairwise apoptosis rate comparisons (1540/1770, 87.0%) show no significant associations. Three small modules, Apoptosis module 1, 2 and 3 contained comparisons that did show significant associations between cluster apoptosis rates. Interestingly, these were predominantly made up of comparisons within T, S and MNB only clusters, respectively. This suggests firstly, that apoptosis rates of TME cells are regulated in a less organised manner in PDA tumours than proliferation rates and that secondly, where evidence of coordination exists (apoptosis Modules 1-3), apoptosis rates are regulated in a cell type specific manner (S, MNB or T), with little coordination between different cell types. Notably, as for proliferation, only a minority of the significant correlations were negative correlations. Curiously, those negative correlations that were present were almost entirely between the apoptosis rates of MNB and T clusters.

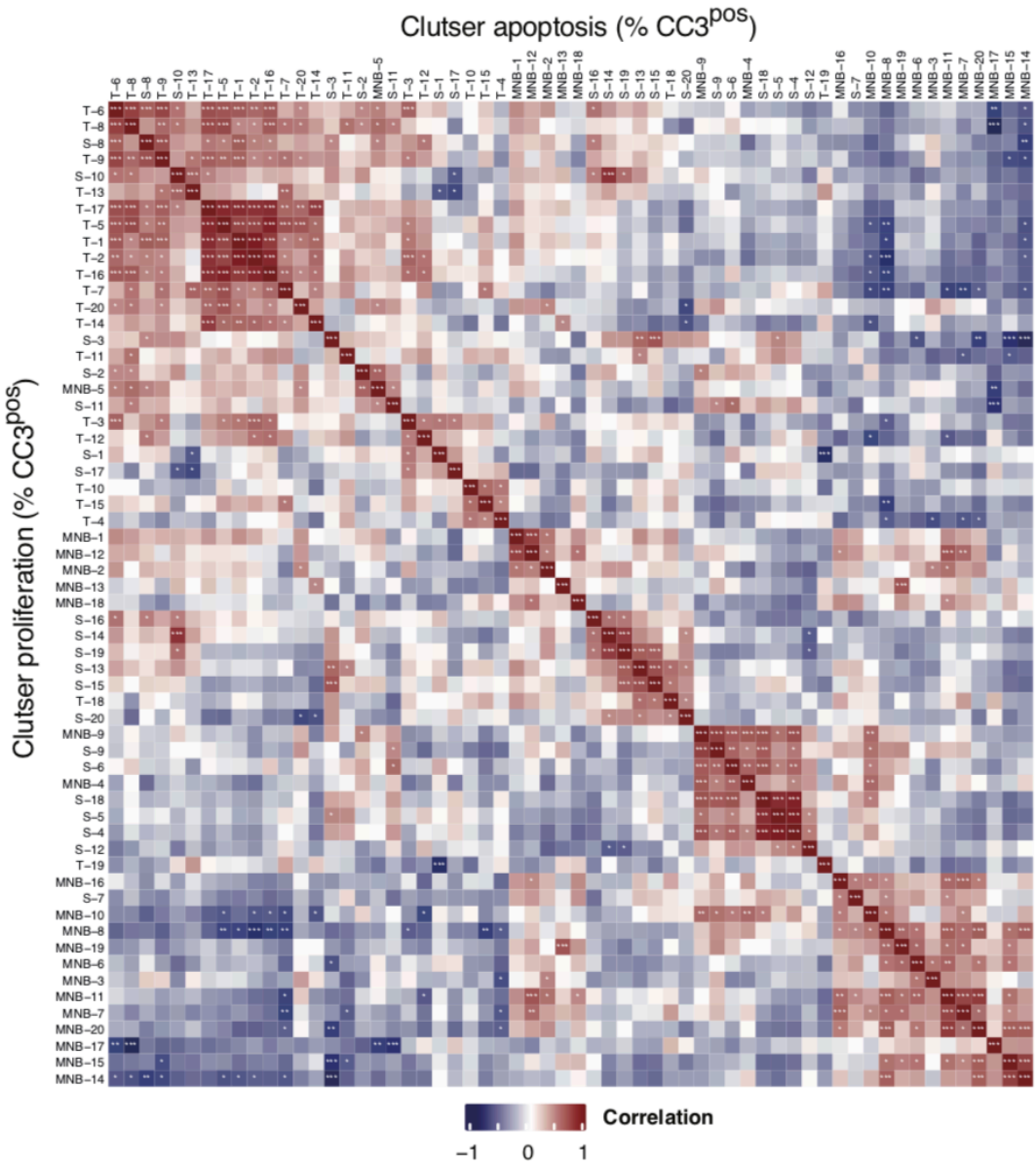

Figure 25. Pancreatic cancer stromal subset apoptosis correlations
Correlation matrix displaying Spearman correlation coefficients of all pairwise stromal subset apoptotic fraction comparisons. *p<0.05, **p<0.01, ***p<0.001.

5.1.3 – Mesenchymal stromal cell abundance and immune cell proliferation correlation analysis

Whilst the analysis described above is expected to provide associations between clusters that show common regulation of proliferation or apoptosis (i.e. factor X regulates the proliferation of cell type A and cell type B) or reciprocal interactions (cell type A regulates cell type B that regulates cell type A), conceptually it is hard to imagine how it would provide any information when the abundance of one cell type directly promotes the proliferation or survival of another cell type in uni-directional manner (i.e. cell type A

is the source of factor X that regulates cell type B but there is no reciprocal interaction). To explore this concept, I compared the variability of the cluster abundance with the fraction of proliferating cells from other clusters. Because I was particularly interested in how the abundance of (or lack of) mesenchymal stromal subsets may regulate the expansion/survival of immune cell subsets, I limited the analysis to the pairwise comparison of the abundance of the 20 S-clusters, with the proliferation of the 40 MNB and T clusters (Figure 26), analysing 800 unique pairwise comparisons.

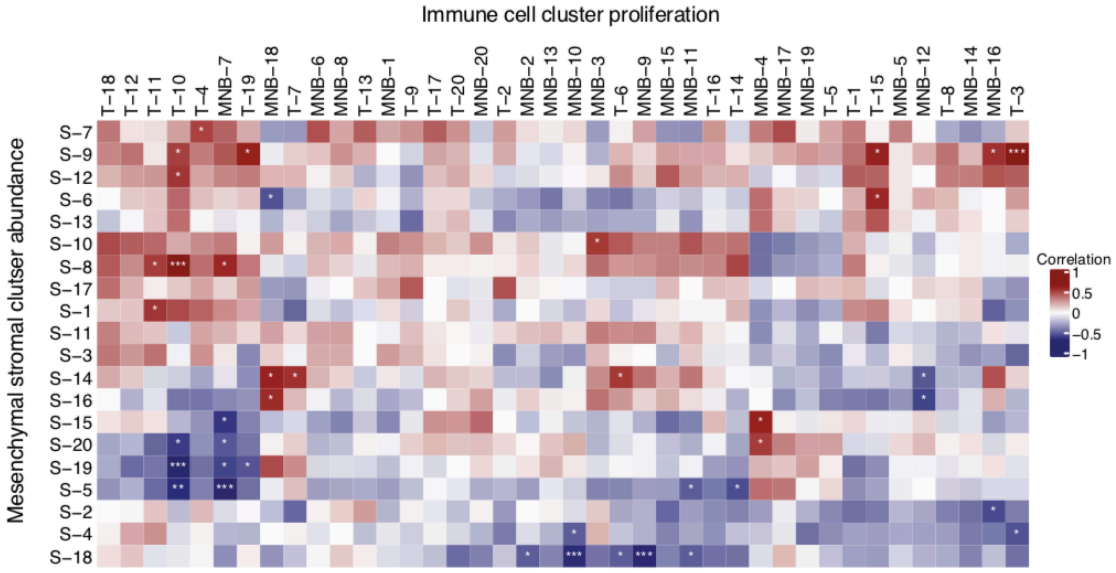

Figure 26. Associations between mesenchymal subset abundance and immune cell proliferative rates in pancreatic tumours

Correlation matrix displaying Spearman correlation coefficients of all pairwise comparisons between mesenchymal stromal subset abundance and immune cell subset proliferation rates. *p<0.05, **p<0.01, ***p<0.001.

Most pairwise comparisons showed no evidence of association between mesenchymal subset abundance and immune cell proliferation. However, the abundance of some specific mesenchymal stromal clusters was positively and negatively associated with the proliferation of several MNB and T clusters, which may suggest a cell-cell interaction/dependency *in vivo* (model in Figure 27). For example, the increased abundance of CD105+αSMA+ (MyCAF-like) cluster S-19, shows a strong association with both the reduced proliferation of the CD8+ T cell cluster T-10 (Figure 28). This mesenchymal cluster is also associated with the reduced proliferation of CD103+CD4+ T cell cluster T-19. When PDA tumours are separated into those with a high and low frequencies of cluster S-19, there is significantly less proliferation of clusters T-10 and T-19 in the tumours with high frequencies of S-19 (analysis for T-10 shown in Figure 28).

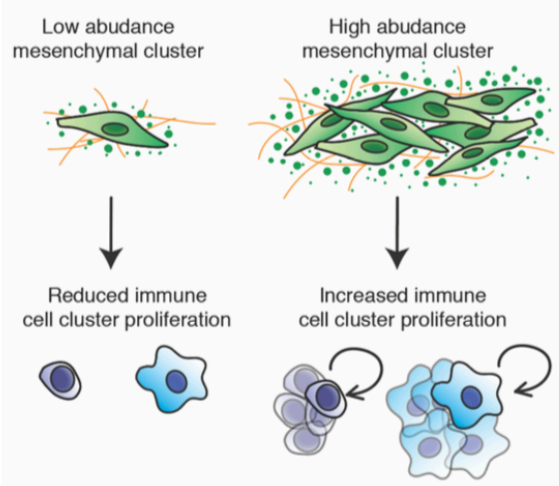

Figure 27. Stromal association model
Model depicting a hypothetical mesenchymal abundance and immune cell proliferation association that would generate positive correlations across different tumour samples

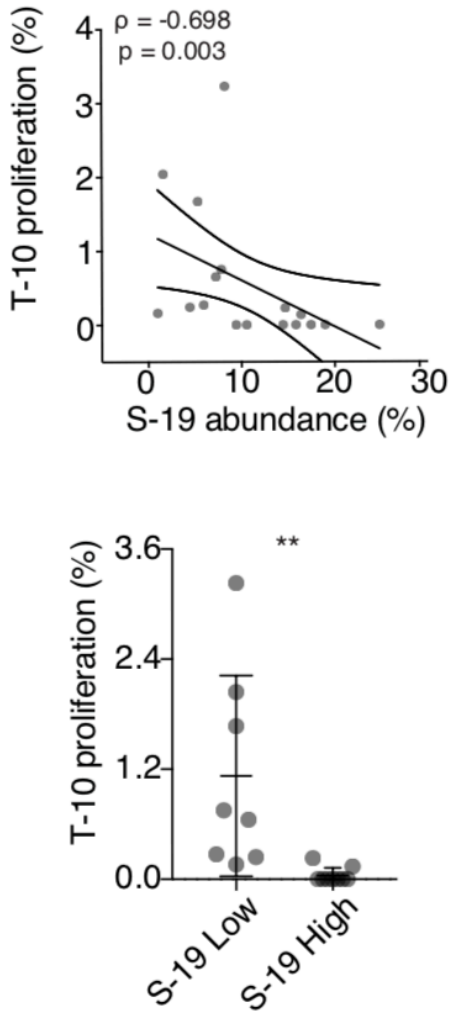

Figure 28. Association between subset S-19 and T-10

Spearman correlation analysis of the association between the abundance of mesenchymal subset S-19 and the proliferative fraction of T cell subset, T-10 (top) and analysis of T-10 proliferation in tumours with high and low levels of S-19 (bottom). ρ=Spearman correlation coefficient, 90% confidence intervals displayed. Data displayed as mean+/-standard deviation (SD). *p<0.05, **p<0.01, ***p<0.001.

The mesenchymal stromal cell type with the highest number of positive associations was S-9. In total, this mesenchymal subset had 5 positive associations with the proliferation of immune clusters. S-9 is a CD105- fibroblast cluster with the highest median expression of MHCII and CD74 of all mesenchymal cell clusters. Across all PDA samples, the strongest association of S-9 abundance with immune cluster proliferation (based on Spearman coefficient), was with the proliferation of cluster T-3. This is the CD8+ T cell cluster with tumour-specific, early exhausted, cytotoxic phenotype, described in the previous chapter. When the PDA tumours were separated into those with a high and low frequencies of cluster S-9, there is significantly more proliferation of cluster T-3 in the tumours with high frequencies of S-9 (Figure 29). It is notable that the abundance of no other stromal cluster was associated with the proliferation of this tumour specific CD8+ T cell cluster. The abundance of S-9 was also positively associated with the proliferation of several other T cell clusters, including the CD8+ T cell cluster T10, the CD103+CD4+ T cell cluster T-19 and CD103+ γδ T cell cluster T-15 (Figure 26). Example significant associations between mesenchymal cell abundance and immune cell proliferation are depicted in Figure 30.

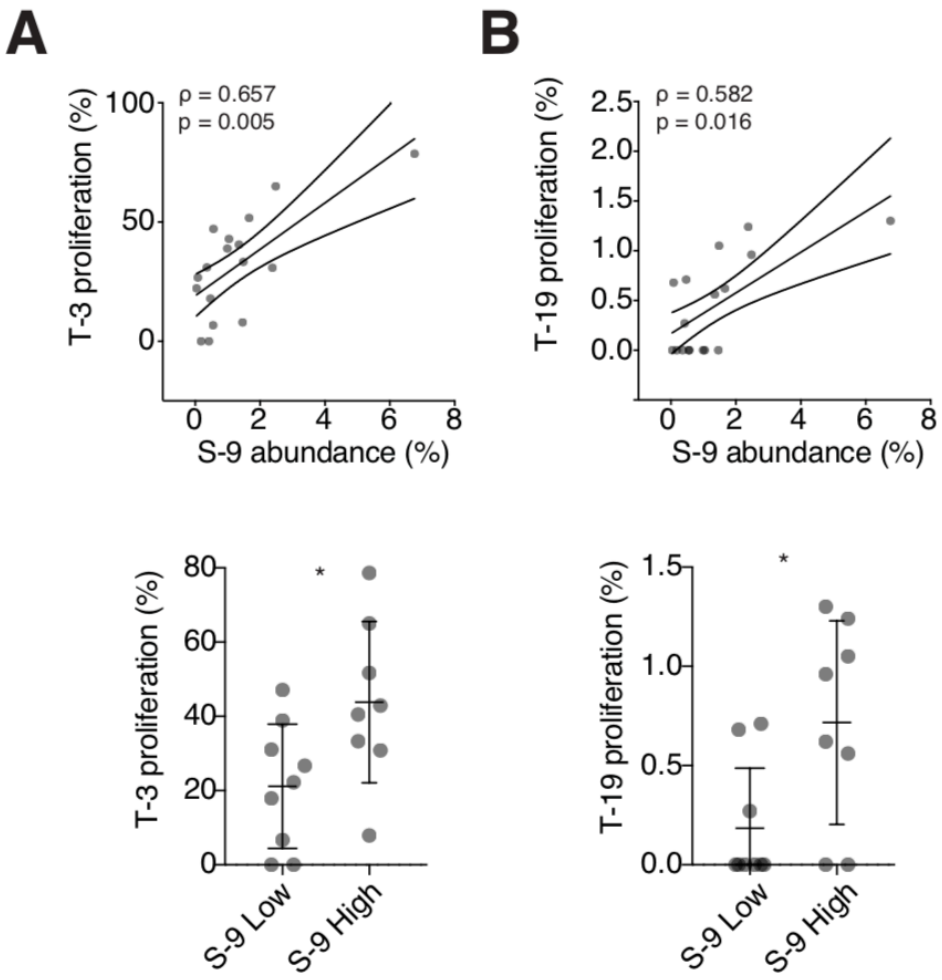

Figure 29. Association between subset S-9 and T-3 and T-19

Spearman correlation analysis of the association between the abundance of mesenchymal subset S-9 and the proliferative fraction of T cell subsets, T-3 (A, top) and T-19 *B, top) Analysis of T-3 (A, bottom) and T-19 (B, bottom) proliferation in tumours with high and low levels of S-9. ρ=Spearman correlation coefficient, 90% confidence intervals displayed. Data displayed as mean+/-standard deviation. *p<0.05, **p<0.01, ***p<0.001.

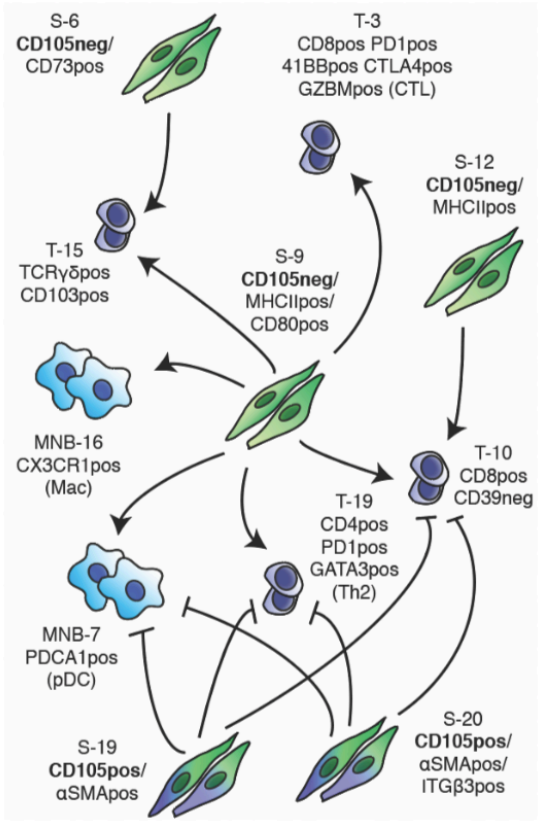

Figure 30. Putative associations in the pancreatic cancer microenvironment
Schematic illustrating selected significant associations between mesenchymal stromal subset abundance and immune cell proliferation

5.2 - Summary

In this chapter, I used the mass cytometry data detailed in the previous chapter to conduct a cross-correlation analysis that maps patterns of cellular interactions. The underlying hypothesis was that cross-correlation analysis will identify putative relationships between distinct groups of cells in the PDA TME. Such relationships may subsequently form the starting point for future mechanistic work. The methodology has several limitations (see below) but because it identifies known cell-cell relationships (e.g. between BECs/pericytes and cDCs/NK cells), it may be a feasible way to identify novel, and perhaps non-intuitive cell to cell relationships. The analysis particularly focussed on associations of immune cell subset proliferation with the abundance of mesenchymal stromal cell populations.

5.3 - Discussion

Unlike in tissue infection, wound regeneration or other largely reversible tissue processes, during tumour progression there is no resolution phase back to the healthy, steady state condition. The tumour and its environment evolve and progress over time, possibly through distinct phases characterised by changing evolutionary pressures. This is observed here to some degree, in that there is reduced abundance of BECs in larger PDA tumours, which matches the known progressive hypovascular nature of late stage PDA (Rhim et al., 2012). How tumour evolutionary pressures influence the fibroblast compartment specifically and vice-versa, are largely unknown. The data here provides insight into the cellular dynamics occurring in late stage KPC PDA tumours and the cross-correlation analysis suggests putative cell-cell interactions that may be driving ongoing changes in the microenvironment.

Data from three mass cytometry datasets (S, MNB and T) was compared by cross-correlation analysis. Such a method has been conducted by others, using mass cytometry data to infer cellular networks and cell-cell associations (Chevrier et al., 2017; Rapsomaniki et al., 2018; Spitzer et al., 2017). Previously, such analysis has only been conducted using relative abundance (i.e. cell fraction) data and this is the first analysis, to my knowledge, that incorporates proliferation and apoptosis rates into the associations. This method provides a more complete picture of the dynamic nature of the TME; many of the populations that showed minimal associations with the abundance of other cell clusters, showed associations with the proliferation or apoptosis of other clusters. This is important because typically researchers are only able to analyse tumours at a single time point. Thus, the proliferation/apoptotic rates of clusters give some idea on the 'direction' the TME is 'going in', at the time the sample was collected. The life cycle of murine GEMM tumours is greatly accelerated relative to human tumours: the period of initiation to symptomatic, end stage disease is of the order of months in GEMMs, compared with many years in human (Yachida et al., 2010). Indeed, most GEMM tumours are studied close to or at humane end point (as here). However, it is not known what stage of a GEMM tumour best represents the human disease. Such detail would be incredibly useful when trying to design preclinical therapy studies to be as representative as possible. Indeed, one way to better explore and quantify this, may be to compare proliferation/apoptosis rates of various cellular components between murine and human tumours.

Most other studies into cell-cell interactions in the TME are hypothesis driven: usually some prior information about a cell or pair of cells is directly tested. Whilst the cross-correlation analysis is somewhat hypothesis free (see below), it is highly likely that some of the correlations we observe within the cross-correlation analysis here are false positives or technical artefacts, especially because we analyse so many pairwise comparisons. However, the statistical significance of the Spearman correlation method used is estimated by permutation testing, which factors in the total number of comparisons. In addition, if many of the correlations were generated randomly, and only observed due to the number of comparisons tested, we would expect to see more negative correlations in all datasets (random associations would not be expected to have a bias for positive or negative correlation). Instead, negative correlations are very rare across all forms of the analysis, which gives some confidence that many of the significant correlations are some kind of co-regulated behaviour. Despite its limitations, the cross-correlation analysis presented here is one of the only ways in which novel or non-obvious interactions in the TME could be discovered in largely un-biased manner. Some level of prior bias is introduced during the selection of which markers included in the mass cytometry panels, although most of the markers (especially in the immune panels) are widely accepted, robust markers of cell types/phenotypes. Clearly, correlation does not equal causation and any putative relationships identified by the cross-correlation analysis need to be verified in follow up experiments, ideally within the *in vivo* context of similar KPC PDA tumours. I have some level of confidence in the cross-correlation method, because it identifies know associations in an unsupervised manner. For example, the reciprocal proliferative interaction between endothelial cells and pericytes (Sweeney and Foldes, 2018) and between cDC1s and NK/ILC cells (Barry et al., 2018; Bottcher et al., 2018; Cabeza-Cabrerizo et al., 2019).

Generally, the cross-correlation analysis suggests that the abundance, proliferation and apoptosis of the majority of cell clusters is not linked to other cell clusters. This may be for several reasons including:

- For some cell types, their growth/survival may be dependent on specific factors (e.g. a growth factor) or processes (e.g. epithelial cell contact) that are not required for the proliferation of other populations of cells. An example of this would be FLT3,

which would mostly be expected to drive proliferation of DCs independently to any other cell types.

- The mass cytometry panels may not have the markers needed to correctly separate out and annotate distinct clusters of cells that are functionally distinct, therefore associations of cells within these clusters with other cell types will likely be masked. A better understanding of cellular heterogeneity in tumours will improve this.
- Some processes may not occur in every tumour and thus will not show correlations across the whole cohort. Separating tumours into distinct cohorts may improve this.
- Some cell-cell associations *in vivo* may be so complex or multifactorial that a simple 1 v 1 correlation will not able to detect co-regulated behaviour, even if relationships exist. In such cases, hypothesis-driven studies and mechanistic work will be key to revealing relationships.
- I disaggregate the tumour and lose all spatial information – a pair of cells may show very highly co-regulated behaviour when they are in close proximity to each other in local niches but may not have global co-regulated behaviour when looking across the whole tumour. An example of this would be tertiary lymphoid structures (TLSs), in which immune aggregates of many cell types come together in a local niche and potently influence each other's behaviour. However, the cells in these structures contribute only a small fraction of each cell type across the whole tissue/tumour. Imaging methods would be needed to better understand the cell-cell phenotypes in rare niches.
- *In vivo* data from spontaneous GEMM tumours is complex and we may not have enough samples to detect subtle associations.

The low number of associations is particularly obvious in the apoptosis dataset and this may be an indicator that the programmed cell-death process in tumours are largely stochastic. For example, cell death may occur in a non-cell type specific manner because chaotic tumour growth causes vascular occlusion that results in large areas of poorly vascularised, hypoxic, nutrient poor regions.

A minority of cell cluster pairs in the PDA TME do show evidence that their abundance, proliferation and apoptosis is coordinated. Within this analysis, most associations between pairs of cells tend to occur between phenotypically similar cells (e.g. fibroblast to fibroblast co-regulation or T cell to T cell co-regulation). This is particularly frequent in

the proliferation analysis, which suggests that upstream regulators of proliferation are shared between similar cell types but not between cell-types of different ontogenies e.g. the factors that make CD8+ T cells proliferate cannot make pericytes proliferate. In addition, the proliferation analysis shows very few negative correlations i.e. the increased proliferation of one cell cluster tends not to be associated with the reduced proliferation of another cluster. This may indicate that regulators of proliferation (e.g. growth factors, cytokines or cell-cell contacts), can only act in a positive manner and a single factor/ligand that causes one cell subset to proliferate, is not capable of directly reducing proliferation of another cell subset. This is consistent with the idea that a specific factor can only initiate a restricted signalling response in a target cell and that some cells will or won't be responsive to the stimulus.

Whilst measurements of abundance, proliferation and apoptosis are clearly intricately linked, it is perhaps not surprising that one pair of cell clusters that have highly correlated proliferation, may not necessarily have highly correlated abundances. A major contributor of cell abundance is the net difference between proliferation and apoptosis, but other process such as cell migration into/out of the tumour can increase/decrease cell numbers without proliferation (important for immune cell accumulation during inflammation) and other cell death processes can occur that remove cells, such as necrosis, phagocyte engulfment or NK cell killing of 'stressed' cells. Indeed, phagocyte removal of myofibroblasts has been shown to be a feature of fibrosis resolution (Wernig et al., 2017). In particular, such cell death mechanisms are challenging to quantify with cytometry-based methods. Thus, exhaustive measurements of all factors influencing cell abundance may simply not be possible. In addition, relatively slow proliferating but large clusters are likely to remain dominant for an extended period of time, even in the presence of rapidly proliferating minor clusters. This is known to be particularly important for cell subsets that have lows rates of cellular diffusion through a tumour (Waclaw et al., 2015). Lastly, these tumours were all collected in mice that were at or near symptomatic stage of disease. Thus, the cellular abundance and proliferation and apoptosis rates measured here are likely reflective of very advanced disease and measuring these aspects throughout the entire period of adenocarcinoma development may be more reflective of the processes occurring in human tumours at clinically actionable stage.

Occasionally associations are observed between pairs of cell clusters from completely different compartments. In this regard, the strong correlation between the abundance of cluster S-9 (the distinctive CD105- fibroblast cluster with high expression of MHCII and CD74) and the proliferation of cluster T-3 (the tumour-specific CD8+ T cell cluster with a wide range of proliferative states), is particularly notable. Although a minor cluster, this T cell phenotype (PD1intCD39intTim3loTBEThiCD27hiGZMBhi) has been shown to play a central role in T cell-mediated control of tumour growth in other settings (either spontaneously or under immunotherapy) (van der Leun et al., 2020; Wei et al., 2017; Yost et al., 2019). Hence, the analysis here suggests that fibroblasts can exist in distinct phenotypes and some of these phenotypes are associated with the proliferation of important T cell subsets. Potentially this suggests that different fibroblast populations may have divergent effects on T cell phenotypes and anti-tumour immunity. Some studies have shown fibroblasts have the ability to modulate CD8+ T cell function but most reports suggest that fibroblasts have a net suppressive effect CD8+ T cell function (see introduction chapter). Many of these studies use *in vitro* fibroblast/T cell co-cultures that may not fully capture *in vivo* function. For example, 2D *in vitro* culture is known to profoundly alter fibroblast gene expression and phenotype (Calvo et al., 2013; Ohlund et al., 2017). Indeed, studies using PDA GEMMs and sophisticated genetic of pharmacological methods of fibroblast manipulation, suggest that fibroblasts have a net tumour suppressive function *in vivo* and is associated with vastly remodelled immune infiltrate (Lee et al., 2014a; Ozdemir et al., 2014; Rhim et al., 2014).

CD105+ and CD105- fibroblasts show distinct phenotypes across the large numbers of PDA tumours analysed. For example, CD105+ fibroblasts are typically more abundant and CD105- fibroblasts have higher expression of MHCII, CD74, CD73 and ITGα6 and higher proliferation (see previous chapter). In the cross-correlation analysis, CD105+ and CD105- fibroblast clusters also show associations with distinct immune cell phenotypes. For example, the abundance of the CD105- fibroblast cluster, S-9, was associated with increased proliferation of T cell clusters T-3, T-10, T-15 and T-19 and the abundance of the CD105+ fibroblast cluster, S-19 was negatively associated with the proliferation of two of these T cell clusters. As mentioned above, whilst a potentially useful starting point, these cell-cell associations need to be verified with orthogonal methods to avoid over interpretation of the data. For example, TGFβ has been shown to drive the αSMA+ phenotype seen in cluster S-19. As TGFβ also has cytostatic effects

on T cells, variable levels of TGFβ in each of the PDA tumours may explain the negative correlation observed. Whatever the mechanism for the observed associations, the difference in surface marker expression between CD105+ and CD105- fibroblasts, and the fact they have many different pair-wise associations with immune cells clusters, suggests potential functional differences between CD105+ and CD105- fibroblasts which I aimed to explore further.

Chapter 6 – Results – *Ex vivo* analysis of CD105+ and CD105- pancreatic fibroblasts

6.1 – Results

6.1.1 – CD105+ and CD105- fibroblasts show distinct frequencies and phenotypes in PDA tumours

The mass cytometry results described in the previous two chapters provide a detailed picture of the KPC PDA TME. One of the most striking observations was the presence of two clear and distinct groups of fibroblast clusters, one group consisting of CD105+ fibroblast clusters and the other consisting of CD105- fibroblast clusters. These two groups of clusters showed some similar gradients of marker expression indicative of different phenotypic states (e.g. high αSMA or high PDGFRα fractions) but also some phenotypes that were unique to the CD105- clusters (e.g. high expression MHCII antigen presentation proteins and specific integrin sub units). All 19 PDA tumours tested contained both CD105+ and CD105- fibroblasts, although the relative frequencies of each varied widely. CD105- fibroblasts, despite typically being less frequent that CD105+ fibroblast clusters, consistently showed higher proliferation rates at the time the tumours were collected (late stage). Lastly, cross-correlation analysis suggested that the abundance of CD105+/- fibroblasts in PDA tumours is each associated with the increased or reduced proliferation of different immune cell phenotypes, with minimal overlap in the specific immune subsets they were associated with. Because of such evidence of distinct behaviour, I hypothesised that CD105+ and CD105- fibroblasts represent functionally distinct populations in KPC PDA TME and I sought to better characterise these fibroblast populations.

I revisited the mesenchymal stroma mass cytometry data and separated the CD31-PDPN+CD90+ fibroblasts into CD105+ and CD105- fractions using traditional biaxial gating (as opposed to the high dimensional FlowSOM/UMAP workflow described previously). Determining the gating was straight forward as all protein expression (including that of CD105), was clearly bimodal. Comparing the populations as bulk CD105+/- groups demonstrated that, as expected, on average CD105+ fibroblasts contribute more of the total fibroblast population in PDA tumours (67.3±14.8% of all

fibroblasts) (Figure 31). This value varies widely though, with CD105+ fibroblasts ranging from as low as 38.7% to as high as 88.6% of all PDA fibroblasts, with 3/19 (16%) of PDA tumours actually containing more CD105- fibroblasts than CD105+ fibroblasts. There was no difference in the average CD105+:CD105- fibroblast ratio between the tumours from female and male mice (Figure 32).

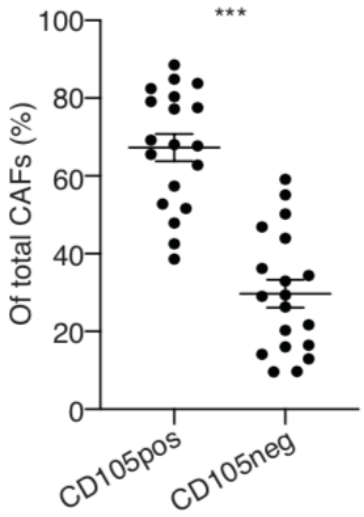

Figure 31. Fraction of CD105+ and CD105- pancreatic cancer fibroblasts within total fibroblasts
Data compared using unpaired t-test. Data displayed as mean+/-standard deviation. *p<0.05, **p<0.01, ***p<0.001.

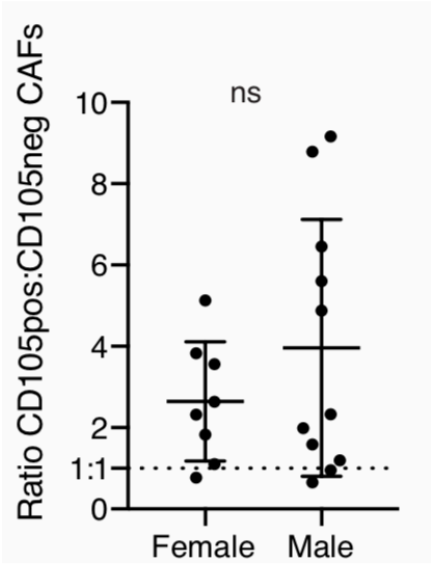

Figure 32. Ratio of CD105+:CD105- pancreatic cancer fibroblasts in female and male mice
Data compared using unpaired t-test. Data displayed as mean+/-standard deviation.

αSMA is the most frequently used marker of a myofibroblast-like phenotype, associated with increased stress fibre formation, contraction and ECM deposition. Comparing the fraction of αSMA+ cells in CD105+ and CD105- fibroblasts showed no difference (CD105+ mean = 65.1±15.7% v CD105- mean = 61.2±18.7%) (Figure 33). Despite there being no difference in average αSMA+ fraction between CD105+/- fibroblasts, this analysis revealed two striking findings. The first was that the fraction of αSMA+ cells varies very widely across PDA samples, over an almost three-fold range, from as low as 31.4% αSMA+ cells to as high as 92.8% αSMA+ cells. Because all samples are barcoded, pooled and stained for intracellular markers as a single sample, this is unlikely to be due to a technical issue with staining and likely represents true protein levels in these cells. The second striking observation is that CD105+ and CD105- fibroblasts from the same sample have remarkably coordinated fractions of αSMA+ cells ($p<0.001$). This suggests that even though all tumours contain various ratios of CD105+ and CD105- fibroblasts, the amount of these cells that are in a myofibroblast-like state appears to be globally regulated across the tumour, such that strikingly, almost exactly equal proportions of αSMA+ fractions are present in the CD105+ and CD105- fibroblast populations.

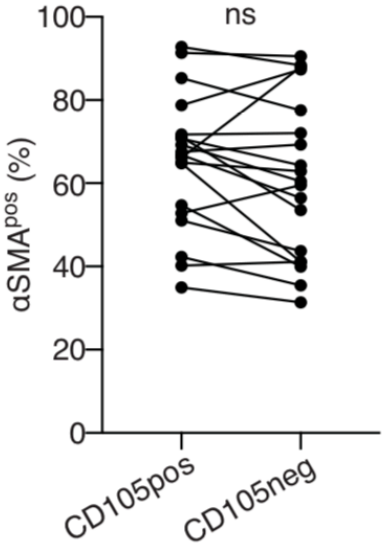

Figure 33. Myofibroblast distribution across pancreatic tumours
Fraction of αSMA+ myofibroblast-like CD105+ and CD105- fibroblasts in pancreatic tumours. CD105+ and CD105- data from the same tumours are linked. Data compared using paired t-test.

In agreement with the clustering-based analysis presented in previous chapters, analysis of the Ki67+IdU+ fractions within the bulk CD105+ and CD105- groups of fibroblasts

showed that on average, CD105- fibroblasts had more than double the fraction of cells in S-phase (3.3±1.8%) compared to CD105+ fibroblasts (1.4±0.8%), at the time these tumours were collected (Figure 34). In all samples apart from one, the actual value of the S-phase fraction was higher for CD105- fibroblasts. Proliferation rates showed high variation, particularly for CD105- fibroblasts (S-phase fraction range = 0.9% - 7.4%). Interestingly, as for the αSMA+ fractions, proliferative fractions showed coordination between CD105+ and CD105- fibroblasts within each tumour sample, such that tumours that had high proliferation rates in one fibroblast population, showed high proliferation in the other fibroblast population (p=0.03). Again, this suggests global regulation of the fibroblast proliferation that exerts itself on both CD105+ and CD105- populations, with potentially additional factors present in the tumours at this late stage contributing to higher CD105- fibroblast proliferation. Levels of apoptosis, as measured by CC3+ fraction, were not different between CD105+ and CD105- fibroblasts (Figure 34). The distinct pattern of proliferation was not a feature of all fibroblast phenotype comparisons: if all fibroblasts in these tumours were separated into myofibroblast-like (αSMAhiPDGFRαlo) and iCAF-like (αSMAloPDGFRαhi) phenotypes, no difference in proliferative fractions was observed (Figure 34)

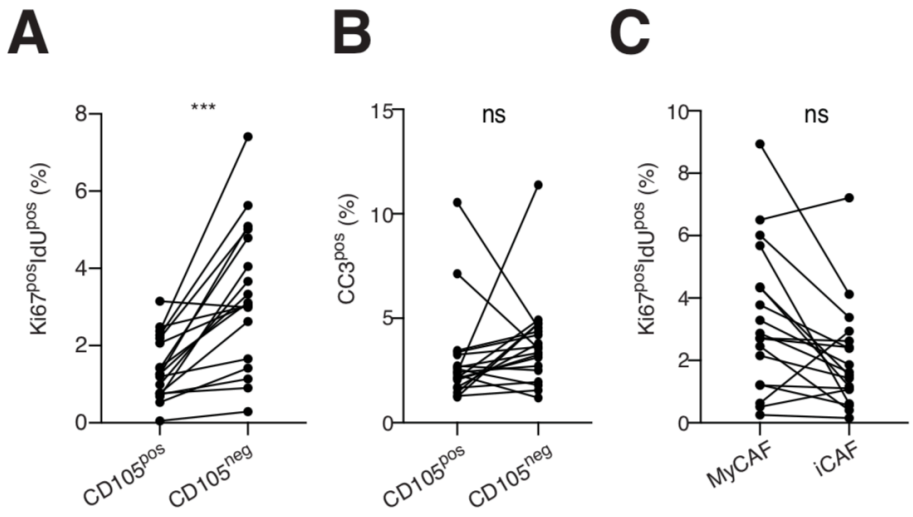

Figure 34. Proliferative and apoptotic phenotypes of fibroblast subsets
(A) The fraction of proliferative CD105+ and CD105- fibroblasts in pancreatic tumours. (B) The fraction of apoptotic CD105+ and CD105- fibroblasts in pancreatic tumours. (C) The proliferative fraction of MyCAF- and iCAF-like fibroblasts in pancreatic tumours. Data compared using paired t-test. *p<0.05, **p<0.01, ***p<0.001.

When taken as a single bulk population, CD105- fibroblasts had significantly higher fractions of cells positive for MHCII and CD74 than CD105+ fibroblasts (Figure 35), in

agreement with the analysis in previous chapters. The MHCII+CD74+ phenotype was relatively rare: only in a minority of the tumours (11%) did more than a third of all CD105- fibroblasts exist in this MHCII+ state. At the other end of MHCII expression, 6/19 (32%) PDA tumours showed <5% of all CD105- in this MHCII+ state. The reasons why only CD105- fibroblasts show this MHCII+CD74+ phenotype and CD105+ fibroblasts do not, and why such high variability exists across tumours is not clear (see discussion).

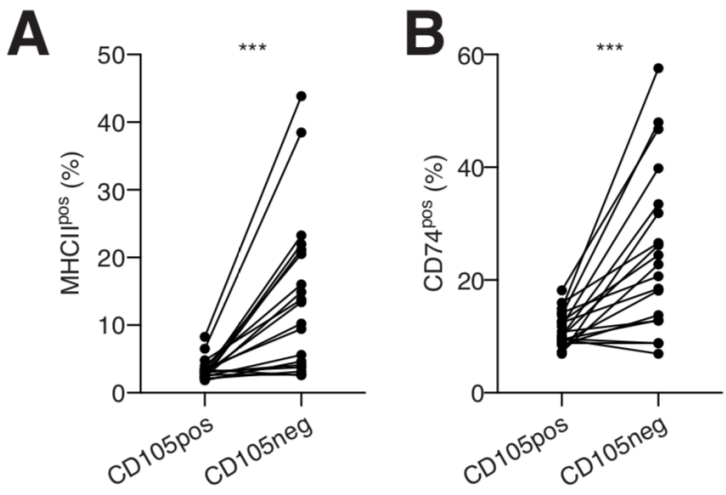

Figure 35. Expression of MHCII antigen presentation molecules in CD105+ and CD105- fibroblasts in pancreatic tumours
(A) Fraction of MHCII+ CD105+ and CD105- fibroblasts in pancreatic tumours.
(B) Fraction of CD74+ CD105+ and cD105- fibroblasts in pancreatic tumours.
Data compared using paired t-test. *p<0.05, **p<0.01, ***p<0.001.

6.1.2 – CD105+ and CD105- fibroblasts are present in human PDA tumours and show regional distribution

The data presented so far strongly suggested that CD105+ and CD105- fibroblasts have distinct phenotypes in KPC PDA tumours. However, before conducting functional experiments, I was keen to establish if these cell populations exist in human PDA, or if the observation was simply a mouse-specific phenomenon. Fresh human PDA samples are difficult to obtain, partly because, unfortunately, most PDA patients are not eligible for surgery due to advanced locally-invasive or metastatic disease. To query the fibroblast infiltrate in human PDA, I instead utilised a collection of archival FFPE human PDA samples. An optimised Tyramide Signal Amplification (TSA) staining protocol was used to simultaneously mark the presence of pan-cytokeratin (PCK) (predominantly expressed on PDA cancer cells), PDPN (a pan-fibroblast marker) and CD105. A representative image from the analysis is shown in Figure 36.

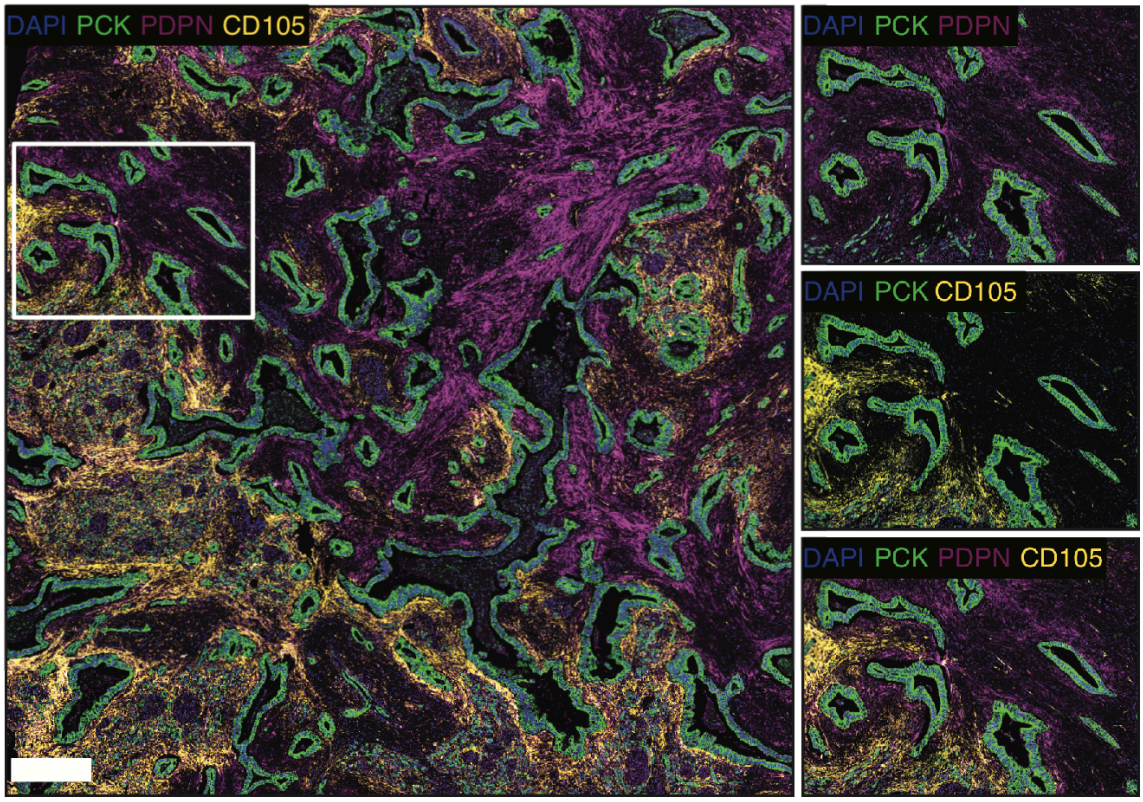

Figure 36. Immunohistochemistry analysis of human pancreatic ductal adenocarcinoma tumour
Tumour section is stained with antibodies targeting pan-cytokeratin (green), podoplanin (PDPN (purple) and CD105 (yellow). Nuclei stained with DAPI. Insert is expanded. Scale bar = 500 µm.

PDA cancer ducts are clearly marked by high PCK expression (green) and surrounded by a PCKlow stroma, rich in densely packed PDPN+ fibroblasts (purple). Because PDPN is also expressed by lymphatic endothelial cells, I cannot exclude the possibility that some of these cells are from lymphatic vessels. However, typically, lymphatic endothelial cells are rare in the TME and expected to make minimal contribution to the stroma. Within the PDPN+ stroma there are clear areas of CD105 positivity (yellow) and negativity (purple) suggesting CD105+ and CD105- fibroblasts are indeed present in human PDA tumours. CD105 is highly expressed on endothelial cells (blood and lymphatic) and thus the CD105+ vessels that can be seen within the regions of CD105- stroma, acts as a useful internal control, demonstrating that CD105 staining is effective in these regions and that there is a genuine lack of CD105 expression on the fibroblasts in these areas. Interestingly, the CD105+ and CD105- staining is regional, with large areas that contain either CD105+ or CD105- fibroblasts but not both at the same time. Indeed, some PDA cancer ducts can be seen to be surrounded on one side by CD105+ fibroblasts and on the other CD105- fibroblasts (insert).

6.1.3 – CD105+ and CD105- fibroblasts from PDA tumours can be separated by FACS and have distinct gene expression patterns

The staining patterns seen in the human FFPE PDA samples made me confident that differential expression of CD105 demarked two distinct populations of fibroblasts in murine and human PDA tumours. To begin to characterise these two populations, I aimed to isolate pure samples of CD105+ and CD105- fibroblasts directly *ex vivo* from mouse PDA tumours and measure their gene expression profiles. Mass cytometry is an antibody-based technique and the sample staining workflow is very similar to that used with flow cytometry-based techniques. Thus, I was able to derive a relatively simple FACS gating strategy and use the same antibody clones that I know had worked effectively in the mass cytometry experiment, but use the fluorescent conjugated versions for FACS. For this experiment, I also used tumour samples from the KPC GEMM, as for the mass cytometry experiments above. A total of 6 PDA tumour samples were analysed. CD105+ and CD105- fibroblast populations were successfully FACS isolated from all tumours. The FACS plots for each tumour are given in Figure 37. All tumours contained CD105+ and CD105- fibroblasts but to vastly different degrees, as excepted.

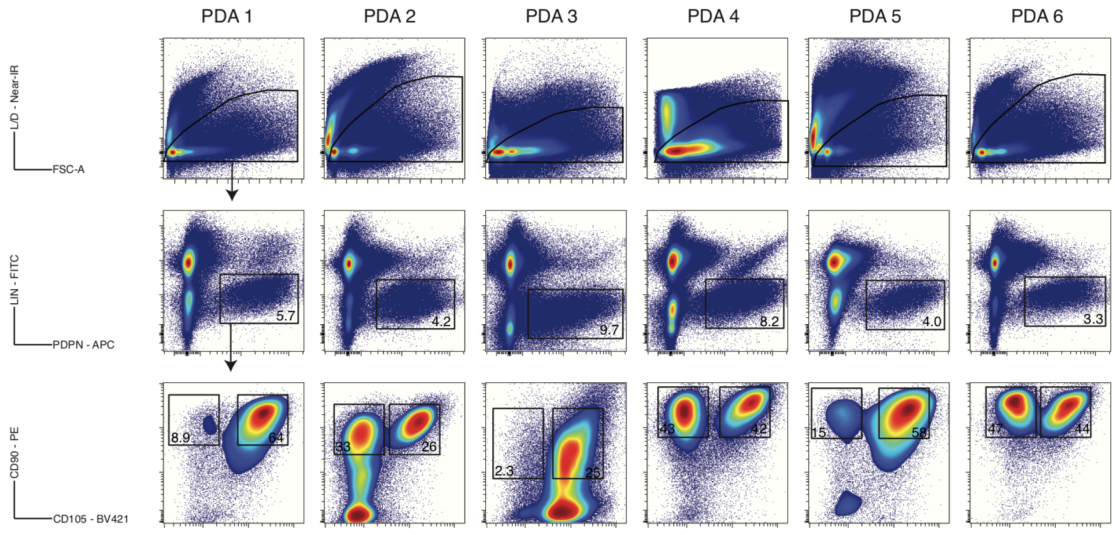

Figure 37. Isolation of CD105+ and CD105- fibroblasts from pancreatic tumours
FACS gating strategy to isolate pure fractions of CD105+ and CD105- fibroblasts form pancreatic tumours. The first two gates selecting single cells by scatter properties are not shown. LD = live/dead. LIN = lineage (EpCAM, CD45 and CD31). Frequency of each population as percentage is given within each gate.

For the CD105+ and CD105- fibroblasts that were collected by FACS, 5% of the sample was removed to expand the cells *in vitro* to confirm pure fibroblast morphology 24 h later (Figure 38) and for the remaining 95% of the sample, the RNA was isolated. The whole process of generating single cell suspensions from the tumours, collecting the cells and then isolating the RNA was done as quickly as possible (typically ~3 h), to limit gene expression changes induced by the process. RNA was sequenced to give the gene expression profiles of n=6 CD105+ PDA fibroblast samples and n=6 CD105- PDA fibroblast samples. CD105+ and CD105- PDA fibroblasts had significantly differential expression of *Eng*, the gene that encodes CD105, indicating that the FACS separation was successful. Both populations had equally high expression of *Col1a1*, *Col1a2*, *Vim*, *Pdp*n, and *Dcn*, all genes that are indicative of fibroblast identity (Figure 39). In addition, both populations have equal expression of MyCAF- and iCAF associated genes (Figure 40).

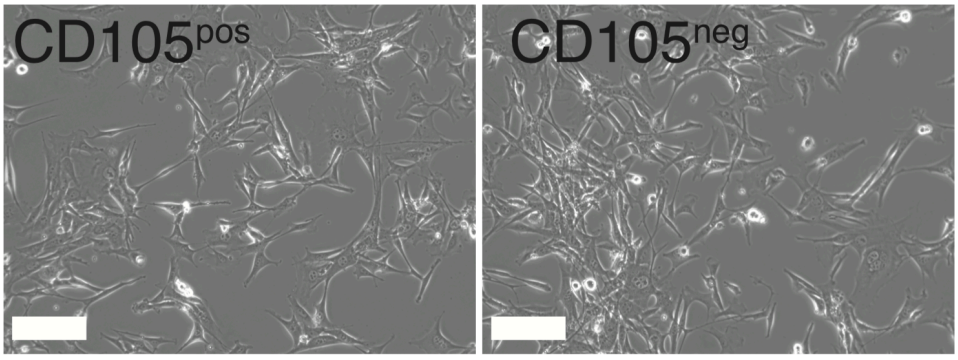

Figure 38. Morphology of FACS-isolated and cultured fibroblasts from pancreatic tumours
Fibroblasts were FACS isolated from pancreatic tumours and plated *in vitro* to assess mesenchymal morphology. Scale bar = 150 µm.

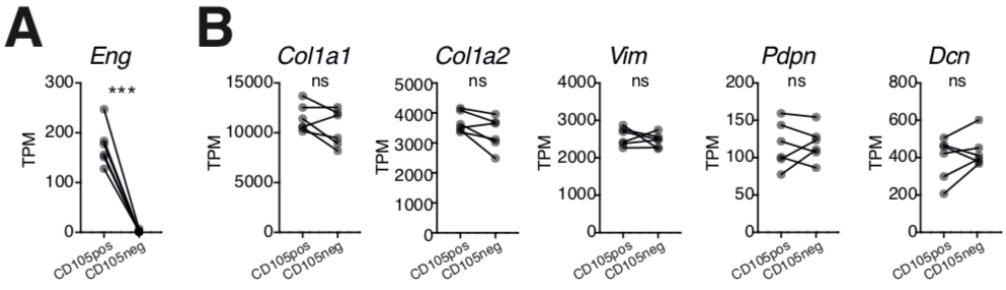

Figure 39. Gene expression of pancreatic cancer fibroblasts
(A) mRNA expression of *Eng*, the gene that encodes CD105, in CD105+ and CD105- fibroblasts.
(B) mRNA expression of canonical fibroblast genes in CD105+ and CD105- fibroblasts.
Expression values displayed as Transcripts per Kilobase Million (TPM). Data compared using paired t-test.
ns = not significant. $p<0.05$, $^{**}p<0.01$, $^{***}p<0.001$.

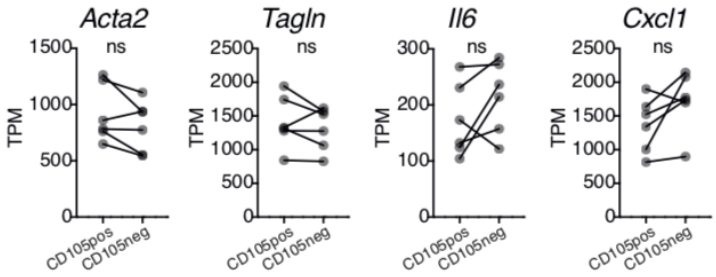

Figure 40. MyCAF and iCAF gene expression in pancreatic cancer fibroblasts
Displaying example MyCAF- (*Acta2* and *Tagln*) and iCAF- (*Il6* and *Cxcl1*) associated genes. Expression values displayed as Transcripts per Kilobase Million (TPM). Data compared using paired t-test. ns = not significant.

CD105+/- PDA fibroblasts had no difference in expression of *S100a4* (FSP1), *Dlk1*, *En1*, *Dpp4, Lrrc15, C5ar2, Mme, Sfrp1 and Ccl12* (Figure 41). These have all been suggested in other studies as marking distinct fibroblast subpopulations in tissues and tumours (including PDA) (see Introduction and Discussion sections). Interestingly, *Fap*, a previously reported fibroblast subpopulation gene, shows higher expression in CD105+ fibroblasts, although both populations have some expression of this gene.

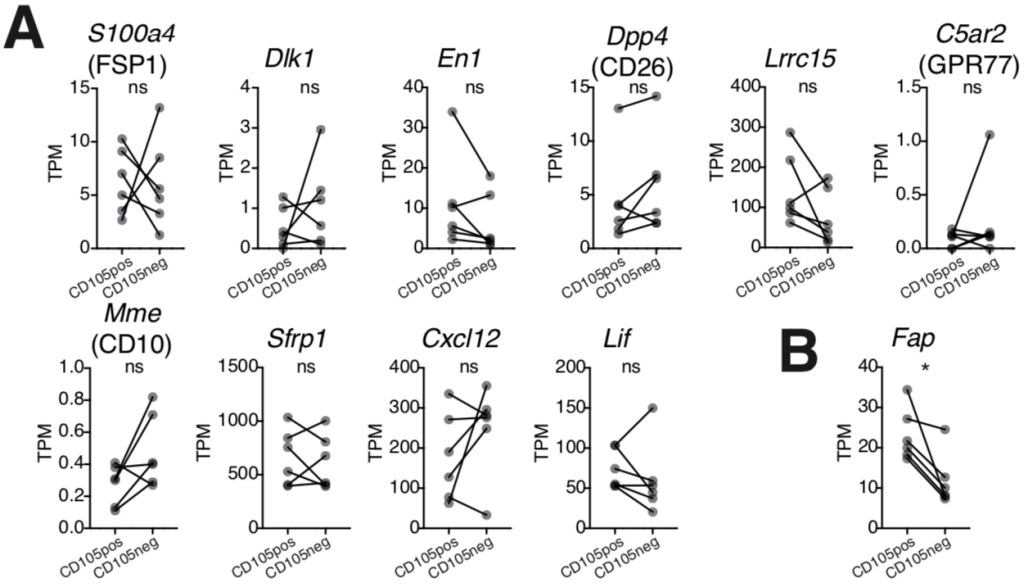

Figure 41. Expression of literature-reported fibroblast subset genes in pancreatic cancer fibroblasts
(A) Expression of genes previously reported in the literature to identify fibroblast subpopulations, in CD105+ and CD105- fibroblasts from pancreatic tumours. (B) Expression of *Fap* mRNA in CD105+ and CD105- fibroblasts from pancreatic tumours. Expression values displayed as Transcripts per Kilobase Million (TPM). Data compared using paired t-test. ns = not significant. p<0.05, **p<0.01, ***p<0.001.

Differential gene expression analysis identified 422 genes significantly more highly expressed in CD105+ PDA fibroblasts and 585 genes significantly more highly expressed in CD105- PDA fibroblasts (>two-fold, B.H.padj<0.05). A PCA plot showing

the variance in these differentially expressed genes (DEGs) for CD105+ (yellow) and CD105- (purple) is shown in Figure 42. Interestingly, the first principle component (PC1) which accounts for 27% of the total variance in differential gene expression, separates CD105+ and CD105- fibroblasts across every sample. This indicates the CD105 status of the fibroblasts is the major determinant of differential gene expression across the total 12 samples. PC2, accounts for 18% of the total variance and interestingly separates the paired samples from which tumour the fibroblasts came from. This could be due to technical reasons (e.g. the same delay in cell isolation during FACS for each sample) or be indicative of tumour-wide regulation of fibroblast gene-expression, regardless of CD105+/- status, and which varies widely between different spontaneous PDA tumours. In either regard, this analysis indicates that the variation due to CD105+ or CD105- status was dominant other sources of gene expression variation. 55% of the total variance was not explained by the first two PCs, suggesting additional drivers of differential fibroblast gene expression occurs in these spontaneous tumours.

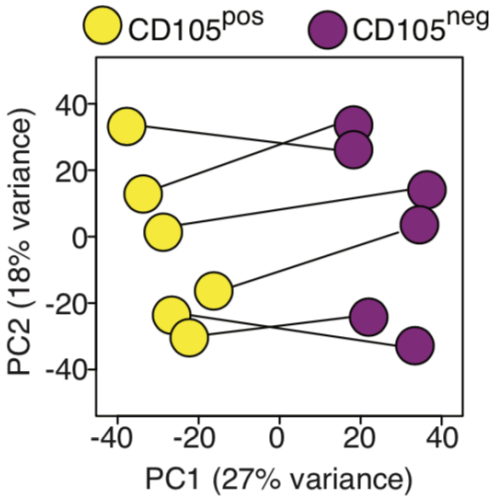

Figure 42. Principle component (PC) analysis of pancreatic cancer fibroblast gene expression
Plot displaying the first two PCs of variation across CD105+ and CD105- fibroblast differentially expressed genes (DEGs). Samples from the same tumour are linked.

Gene set enrichment analysis of the transcriptomic dataset indicated that CD105+ fibroblasts show enrichment of gene programs associated with epithelial to mesenchymal transition (consistent with mesenchymal identity of fibroblasts), as well as angiogenesis and coagulation (Figure 43). CD105- fibroblasts are enriched for genes associated with TNFα/NFkB and mTORC1 signalling. Consistent with the increased proliferative phenotype of CD105- PDA fibroblasts, seen in the prior mass cytometry analysis, several of the CD105- fibroblast enriched gene sets were associated with

proliferation: E2F targets, G2M checkpoint, mitotic spindle, and MYC targets. Interestingly, differences in metabolic processes between CD105+ and CD105- fibroblasts were also observed: genes associated with oxidative phosphorylation were enriched in the CD105+ PDA fibroblasts and those involved in glycolysis and hypoxia were enriched in the CD105- PDA fibroblasts. The enrichment plots for each of these enriched pathways are shown in Figure 44.

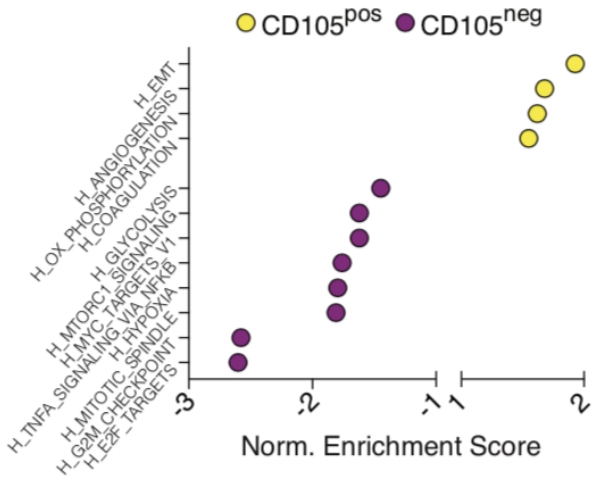

Figure 43. Enriched gene sets in pancreatic cancer fibroblasts
Plot displaying the Normalised Enrichment Score for selected significantly enriched gene sets between CD105+ (n=6) and CD105- (n=6) PDA fibroblast gene expression data. Analysis uses the Hallmark dataset. A positive score equates to enriched expression in CD105+ PDA fibroblasts and negative score equates to enriched expression in CD105- PDA fibroblasts.

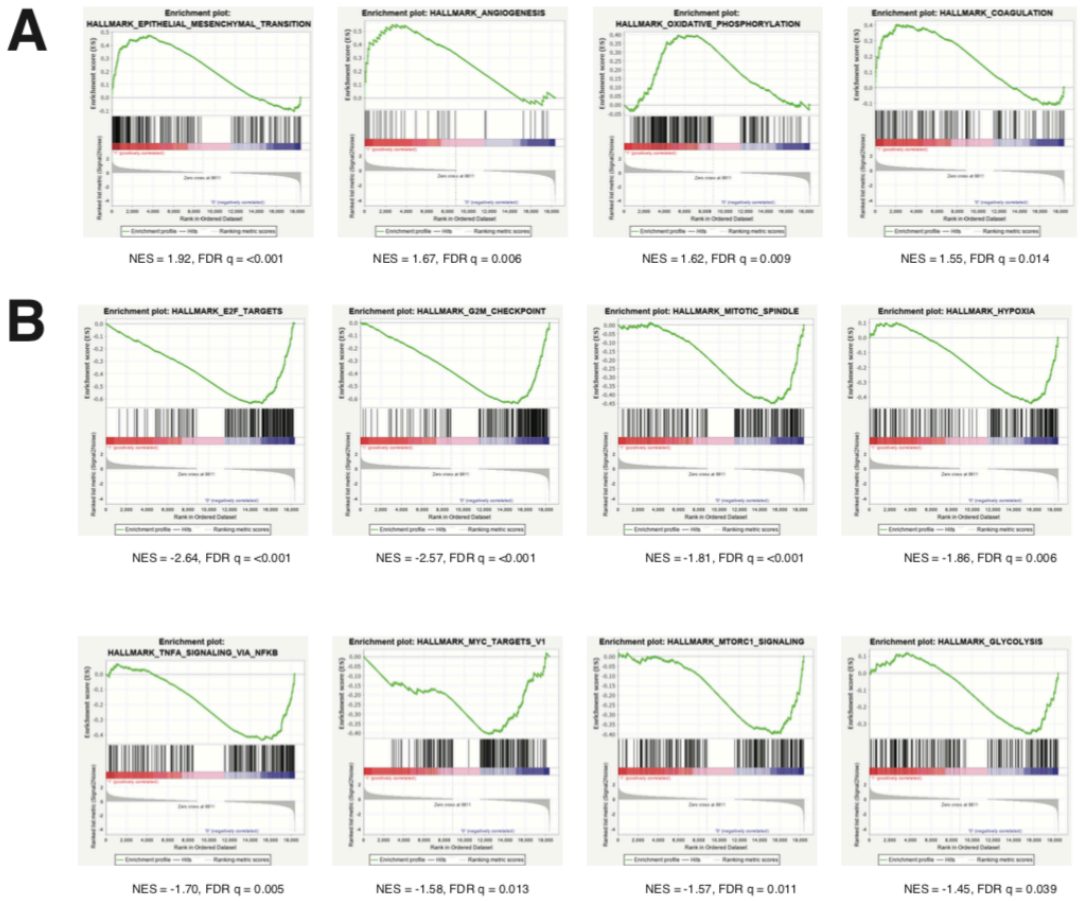

Figure 44. Enriched gene sets in pancreatic cancer fibroblasts
Plots displaying peak Enrichment Scores (ES) for ranked gene expression lists (top of plot), leading edge subsets (middle) and ranking metric (bottom) of genes within each specified Hallmark gene set when comparing gene expression profiles of CD105+ (n=6) and CD105- (n=6) PDA fibroblasts. (A) Hallmark gene sets enriched in CD105+ PDA fibroblasts. (B) Hallmark gene sets enriched in CD105- PDA fibroblasts. Normalised ES (NES) are given below each plot. False Discovery Rate (FDR) estimated by permutating gene sets as per software guidelines.

A notable feature of the CD105+/- fibroblast differentially expressed genes (DEGs) was the high number of genes encoding secreted factors, enzymes that generate secreted molecules or cell surface receptors, all of which could potentially engage in cell-cell communication in the PDA TME. All 1007 DEGs are plotted in a heatmap in Figure 45, with selected examples of differentially expressed secreted factors, enzymes or receptors highlighted. Several of these differentially expressed signalling factors have known roles relevant to cancer biology, for example CXCL2, GCSF (*Csf3*), IL10, CCL19, CXCL9 and CXCL13 are major immune cell chemo-attractants and modulators (Nagarsheth et al., 2017). Interestingly, several pairs of gene paralogs or pairs of genes with similar or redundant functions are differential expressed between CD105+/- fibroblasts. For example, CD105+ PDA fibroblasts express *Col8a1*, *Sema5b* and *Nos1* and CD105- fibroblasts express *Col24a1*, *Sema3a* and *Nos2*.

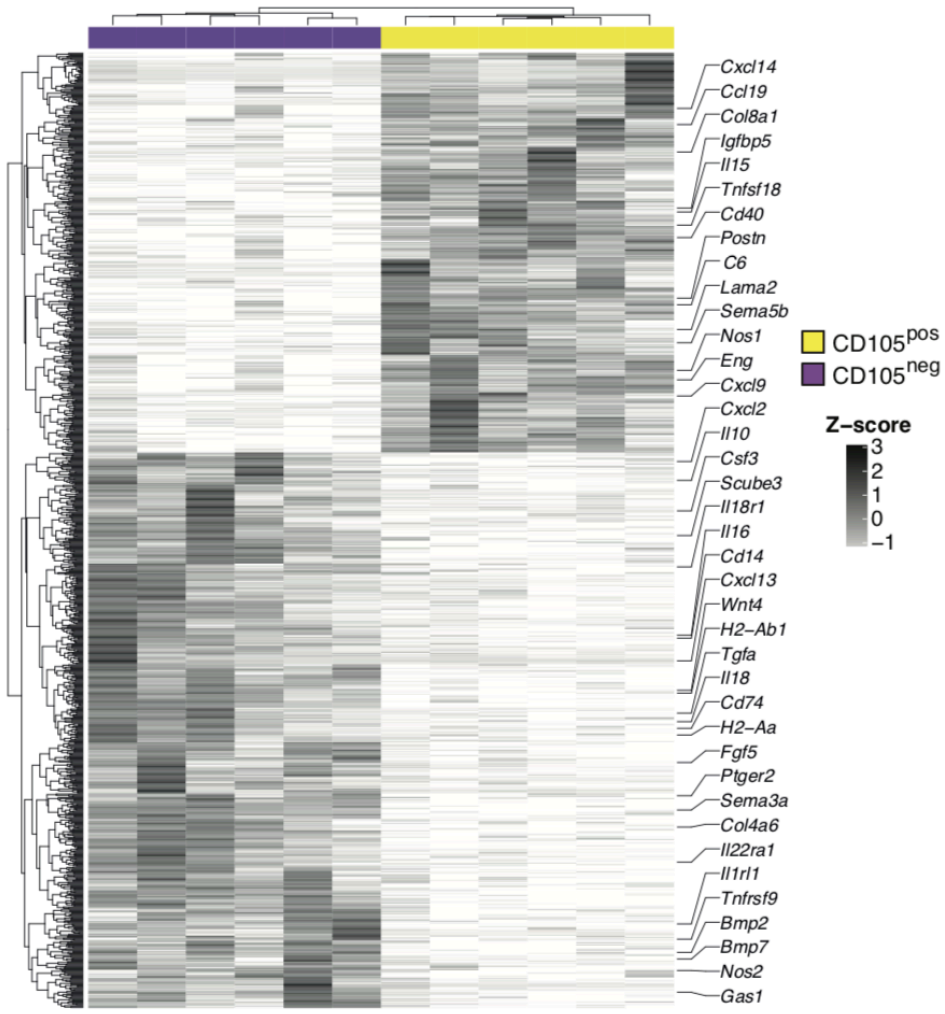

Figure 45. Differentially expressed genes (DEGs) in pancreatic cancer fibroblasts
Heatmap of expression levels of all 1007 CD105+ (n=6) and CD105- (n=6) PDA fibroblast DEGs, displayed as row normalized Z-scores. Example DEGs are highlighted that encode secreted and cell surface molecules or intracellular enzymes that produce secreted molecules.

Importantly, despite CD105+/- PDA fibroblasts having a total of 1007 DEGs, within the top 100 most highly expressed genes from CD105+/- PDA fibroblasts (by mean read counts), 93/100 genes are expressed by both populations across the PDA samples. These shared, highly expressed genes include many associated with classical fibroblast functions, such *Col1a1, Sparc, Fn1, Tnc, Lox, Timp3, Mmp2 and Myh9*. This is supportive of the fact that the CD105+ and CD105- cells isolated in this analysis (and observed in the earlier mass cytometry analysis) are *bona fide,* pure fibroblasts and one or the other population is unlikely to be another contaminating, un-related cell-type. The most highly expressed genes across CD105+ and CD105- fibroblasts are remarkably similar and therefore it is conceivable that major cell functions are highly similar between

the two populations, with some less highly expressed genes contributing to any divergent functional properties.

6.1.4 – CD105+ and CD105- fibroblasts are present in healthy/non-tumour bearing pancreas and demonstrate stable differential CD105 expression

The previously described data has outlined the existence of CD105+ and CD105- fibroblasts in murine and human PDA tumours, with consistently different gene expression patterns. I was curious to explore the possibility that these fibroblasts may be present in the healthy, non-tumour bearing pancreas. I thus sought to map the surface proteome of primary pancreatic fibroblasts in detail using the same mesenchymal stromal mass cytometry panel described in the previous chapters. I disaggregated the healthy pancreas from young adult (8-week-old) B6 mice and expanded the primary cells in culture. Fibroblast-like cells with mesenchymal morphology are able to adhere and proliferate rapidly under these culture conditions, whereas the majority of other cell-types do not adhere well (epithelial cells and lymphocytes) or do not proliferate (endothelial cells and myeloid cells) and quickly die or are overgrown by fibroblast-like cells. In addition to studying the surface proteome at baseline, I leveraged the fact that mass cytometry can analyse many samples in parallel and in addition included several stimulations/activating conditions. These included 16 different recombinant protein stimulations of known and putative fibroblast activating ligands and a condition in which RFP+ KPC PDA cancer cells were added to generate a direct cell co-culture with the fibroblasts (see Table 14 for recombinant protein details). The primary pancreatic fibroblasts were expanded from the healthy pancreas for 7 d, then stimulated with recombinant proteins/co-cultured with PDA cells for a further 3 d to allow sufficient time for alteration of the surface proteome and analysed by mass cytometry. KPC PDA cells were excluded from the analysis of the co-culture condition by selecting RFP- cells only. After 10 d of culture (7 d expansion, 3 d activation), the majority of the mono-culture samples were PCKloEpCAM-CD45-CD31PDPN+ fibroblast-like cells. In every condition, there are clearly two populations of fibroblasts with differential, bimodal expression of CD105. Remarkably all stimulations tested have minimal impact on the expression level of CD105 and its clear, bimodal distribution. On average CD105- fibroblasts make up 78.2±5.2% of all fibroblasts in the samples but the relative amounts of CD105+:CD105- varied in some stimulation conditions (Figure 46).

For example, TGFβ1 activation increases the relative frequency of CD105+ fibroblasts and TNFα or IFNγ activation increases the relative frequency of CD105- fibroblasts. Whilst bimodal CD105 expression was maintained across all conditions, many of the other markers show highly variable expression dependant on the activating stimulus, suggesting they are dynamically regulated by external factors. The surface proteome changes under activating conditions are similar for both CD105+ and CD105- fibroblasts, with some notable differences (Figure 46).

Table 14. Recombinant protein details for surface marker analysis

Primary pancreatic fibroblast stimulation for surface marker analysis at 3 d			
Recombinant protein	**Source**	**Identifier**	**Final concentration used (ng/mL)**
Recombinant mouse TGFB1	RnD Systems	7666-MB-005	2
Recombinant rat PDGF-BB	RnD Systems	520-BB-050	60
Recombinant mouse FGF2	RnD Systems	3139-FB-025	20
Recombinant human/mouse Activin-A	RnD Systems	338-AC-010	20
Recombinant mouse BMP2	RnD Systems	355-BM-010	20
Recombinant mouse BMP4	RnD Systems	5020-BP-010	20
Recombinant mouse BMP9	RnD Systems	5566-BP-010	20
Recombinant mouse MIF	Biolegend	599504	200
Recombinant mouse IFNg	PeproTech	315-05	20
Recombinant mouse TNFa	Peprotech	315-01A	15
Recombinant mouse IL1a	RnD Systems	400-ML-005	10
Recombinant mouse IL1b	PeproTech	211-11B	10
Recombinant mouse IL4	PeproTech	AF-214-14	20
Recombinant mouse IL13	RnD Systems	413-ML-005	20
Recombinant mouse IL22	RnD Systems	582-ML-010	20
Recombinant mouse LIF	PeproTech	250-02	5

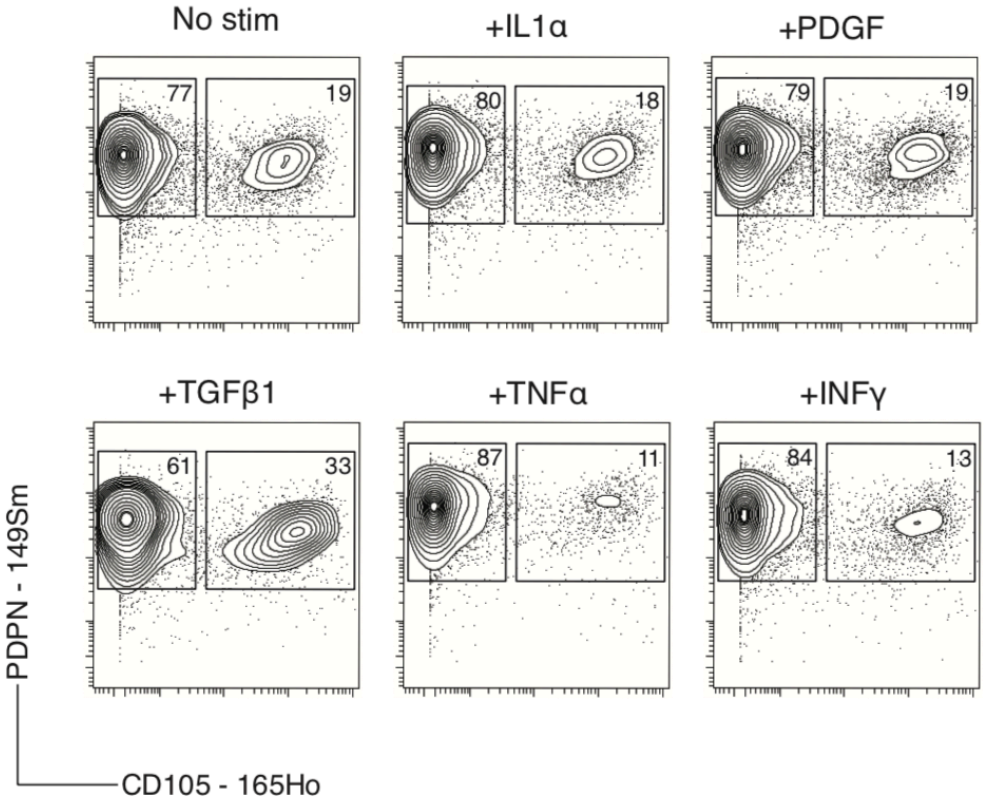

Figure 46. Relative frequency of pancreatic fibroblasts after stimulation
Representative biaxial mass cytometry plots showing relative frequencies of CD105+ and CD105- fibroblasts after 3 d of continuous stimulation with listed activating ligands. The frequency of CD105 and CD105- did not change for some conditions (IL1α and PDGF shown) but some factors altered the balance of CD105+ and CD105- fibroblasts. Population frequencies are displayed as percentages within each gate.

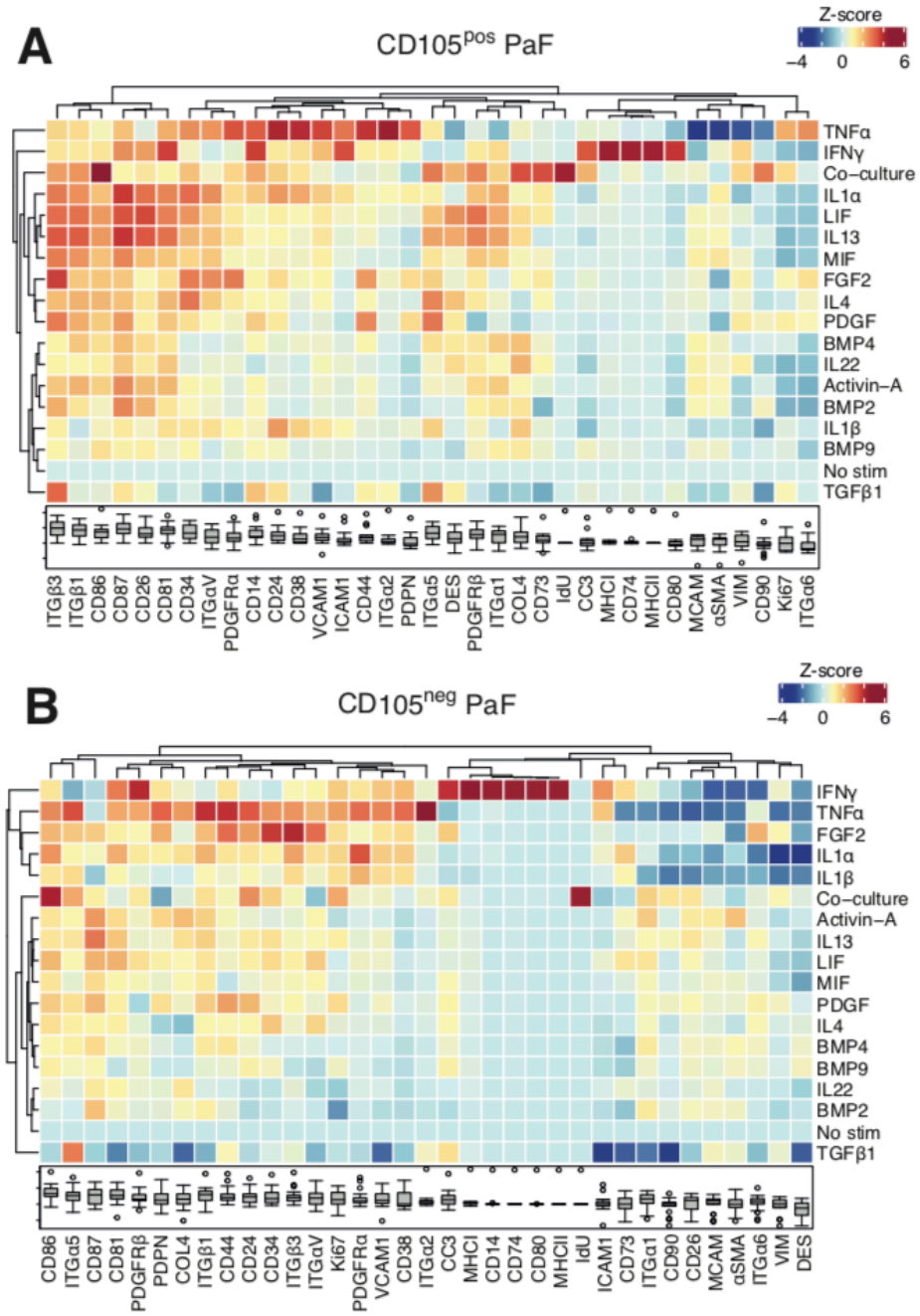

Figure 47. Phenotypic plasticity of pancreatic fibroblasts
Heatmap of median marker intensity (MMI) for each phenotypic marker on CD105+ (A) and CD105neg (B) PaFs, after either no stimulation or 3 days of continuous stimulation with listed fibroblast activating factors. Data is displayed as column normalized Z-scores.

Interestingly, both CD105+ and CD105- fibroblasts respond to IFNγ by upregulation of MHCI/II, CD74, CD80, ICAM1 and CC3. Upregulation of CD14 under this condition is unique to the CD105- fibroblasts. In response to TNFα, both CD105+/- fibroblasts show reduced expression of known MyCAF-associated proteins, including reduced αSMA and MCAM, as well as reduced CD90 expression. IL1α stimulation increases expression of many proteins in the CD105+ fibroblasts (such as CD87, CD26 and CD34) but has a

less marked impact on CD105- fibroblasts (less proteins increased and the PDGFRα increase is unique to CD105- fibroblasts). Interestingly, the related ligands, IL1α and IL1β have different effects on CD105+ fibroblasts and the conditions cluster separately, whereas IL1α and IL1β induce largely the same marker changes in CD105- fibroblasts and the conditions cluster together. TGFβ1 stimulation clusters separately to all other conditions for both CD105+/- fibroblasts. TGFβ1 stimulation induces expression of ITGα5 and ITGβ3 in CD105+ fibroblasts but only ITGα5 in CD105- fibroblasts. In CD105- fibroblasts, TGFβ1 downregulates expression of several surface molecules such as ICAM1, CD73, ITGα1 and CD90, which are minimally affected in TGFβ1 stimulation of CD105+ fibroblasts. FGF2 has similar effects on both CD105+/- fibroblasts (increased CD34, ITGβ3, ITGαV). The known fibroblast activators, PDGF and LIF both have stronger effects on the surface proteome of CD105+ fibroblasts than on CD105- fibroblasts. For example, LIF increased PDGFRβ expression in CD105+ fibroblasts but only minimally in CD105- fibroblasts. Co-culture also showed some similarities and differences: in both CD105+/- PAFs, direct PDA co-culture induced higher levels of CD86 expression, as well as increased proliferation, as seen by IdU staining. CD90 and ITGα1 expression were more highly upregulated by PDA direct co-culture in CD105+ fibroblasts. In conclusion, CD105+ and CD105- primary pancreatic fibroblasts show some similarities and some differences of their surface proteome changes after incubation with activating factors but notably, differential surface CD105 protein expression does not change in any condition.

6.1.5 – Generation of fibroblast cell lines demonstrates that CD105+/- expression is stable

CD105 was unique across all the surface markers tested in that its expression remained bimodal across all 18 conditions tested. I hypothesised that CD105+ and CD105- may represent distinct, stable lineages of fibroblasts in the murine pancreas that are not able to interconvert. I re-isolated primary pancreatic fibroblasts from the pancreas of an adult B6 mice and FACS separated them into pure CD105+ and CD105- populations (Figure 48) and generated immortalised cell lines of each population to enable extended *in vitro* expansion.

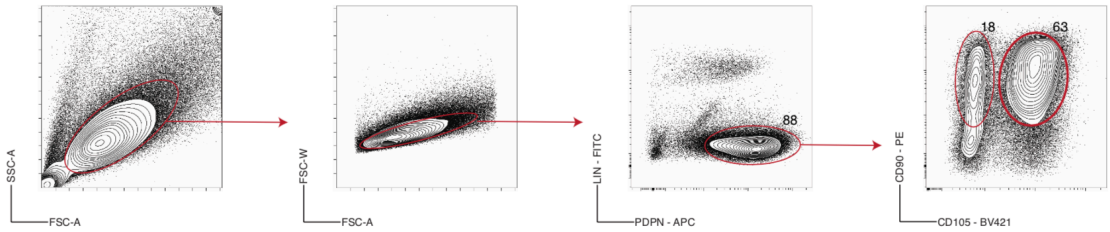

Figure 48. Flow cytometry plot of the gating used to isolate fibroblasts for cell line generation
Representative FACS gating strategy to isolate $CD105^{pos}$ and $CD105^{neg}$ pancreatic fibroblasts after 7 days of *in vitro* expansion from healthy murine pancreas. LIN = lineage (EpCAM, CD45 and CD31). Frequencies for gated populations given as percentages.

After various intervals of prolonged *in vitro* expansion, I tested CD105 expression by flow cytometry. After 7 weeks of continuous *in vitro* culture, CD105+ fibroblasts remained CD105+ and CD105- fibroblasts remained CD105- (Figure 49A), demonstrating highly stable differential expression of CD105. qPCR analysis of the CD105+ and CD105- fibroblasts showed the expected differential expression of *Eng* mRNA (Figure 49B) and this expression pattern was not altered by stimulation with KPC PDA conditioned media (Figure 49B) or altered at the protein level by direct co-culture with KPC PDA cells (Figure 49C). Thus, the CD105+ and CD105- pancreatic fibroblast cell lines appear to represent stable fibroblast lineages and could be used for further studies to better characterise functional differences between these fibroblast populations (see next chapter).

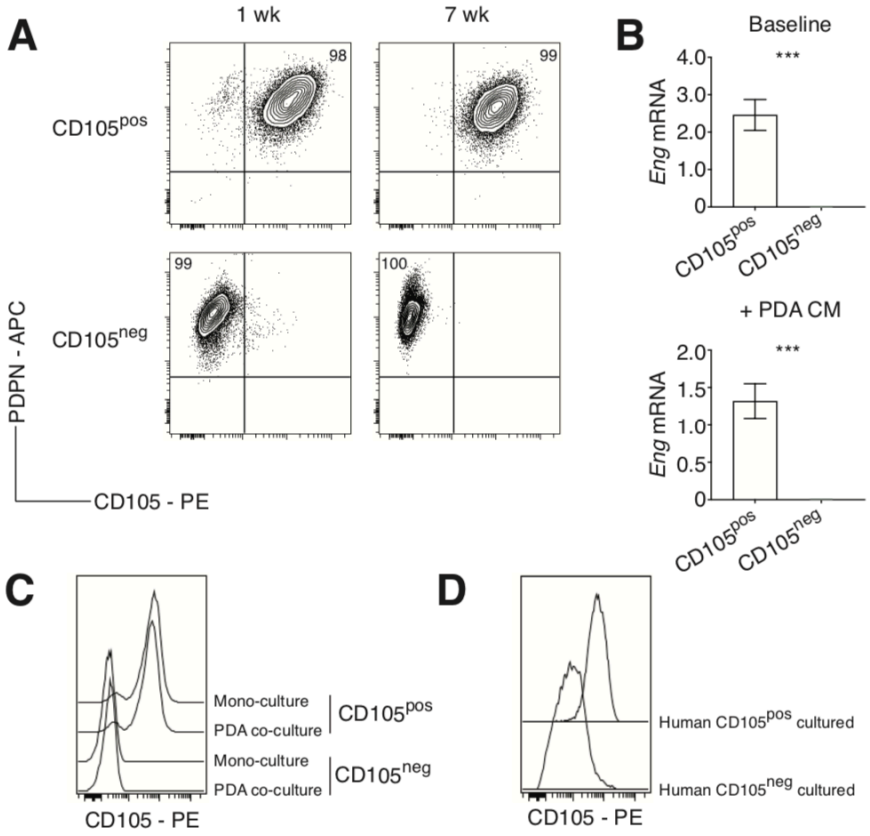

Figure 49. Stability of differential surface CD105 in pancreatic fibroblasts

(A) Flow cytometry analysis of PDPN and CD105 on FACS isolated and *in vitro* cultured CD105+ and CD105- pancreatic fibroblasts (PaFs) at 1 and 7 weeks of continuous *in vitro* culture. Plots are representative of n=4 experiments. Displaying relative frequency of relevant quadrants. (B) *Eng* mRNA expression of FACS isolated CD105+ (n=4) and CD105- PaFs (n=4) with no stimulation (top) and with addition of KPC PDA 3-day conditioned media (bottom). Gene expression measured by qPCR and normalized to the geometric mean of 4 housekeeping genes (HKGs) (*Gapdh, Tbp, Tubb4a, Ppia*). Data displayed as mean+/-standard deviation. (C) Representative flow cytometry analysis (n=4) of surface CD105 stability on GFP+CD105+ and GFP+CD105- PaFs in mono-culture or after direct co-culture with RFP+ KPC PDA tumor cells. (D) Representative flow cytometry analysis (n=3) of surface CD105 stability on FACS isolated CD105+ and CD105- human PaFs after >3 weeks of *in vitro* culture.

Low passage isolates of commercially available primary human pancreatic fibroblasts also revealed CD105+ and CD105- populations, that when FACS isolated and immortalised, also retained differential CD105 expression after extended *in vitro* culture (Figure 49D). IHC of the PDA FFPE samples used previously, revealed some PDA tumour samples that had areas of adjacent 'normal' pancreas tissue that showed signs of inflammation (probably from the tumour itself) and fibroblast expansion but no infiltrating, dysplastic cancer cell infiltration. PDPN and CD105 staining of these samples indicated that CD105+ fibroblasts in the human pancreas appear to be enriched in the intra-acinar areas of the human pancreas and CD105- fibroblasts appear to be enriched in the inter-acinar areas (Figure 50).

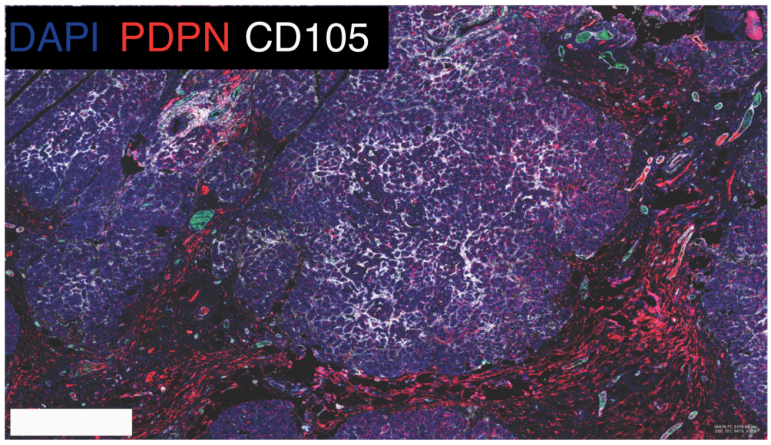

Figure 50. CD105+ and CD105- fibroblast localisation in inflamed human pancreas, adjacent to pancreatic tumour

Representative immunohistochemistry (IHC) analysis of normal but inflamed human pancreas tissue, adjacent to PDA tumours. Stained with DAPI (blue) and with antibodies targeting podoplanin (PDPN) (red) and CD105 (white). Scale bar = 750 µm.

6.2 – Summary

In this chapter, I describe the *ex vivo* analysis of KPC PDA CD105+ and CD105- fibroblasts and the initial *in vitro* characterisation of primary pancreatic CD105+ and CD105- fibroblasts. The hypothesis of this section was that CD105 expression demarks two distinct fibroblast populations in pancreatic tumours and in the normal pancreas. The data presented here, supports this hypothesis. CD105+ and CD105- fibroblasts are present in both murine and human normal pancreas and pancreatic tumours, have distinct gene expression profiles and respond differently to stimulating factors. Remarkably, positive and negative CD105 expression was highly stable under prolonged *in vitro* culture and activating conditions. Thus, CD105+/- fibroblasts may represent distinct, non-interchangeable fibroblast lineages, with distinct phenotypic behaviours.

6.3 – Discussion

CD105 is notable among all the proteins tested because its differential expression in fibroblasts remains incredibly consistent across a huge variety of *in vitro* and *in vivo* states. CD105 is widely used as a lineage marker of endothelial cells and pericytes because of its consistent and high expression on these cell types (Armulik et al., 2011; Bautch, 2017). It would be interesting to further explore the epigenetic factors that dictate the lineage specific expression of CD105 in endothelial cells and pericytes and whether

regulation of the same epigenetic factors may explain the strong CD105 expression in CD105+ fibroblasts or lack of factors explain the lack of expression in CD105- fibroblasts.

On average, CD105+ fibroblasts are more abundant in PDA tumours than CD105- fibroblasts. Interestingly, when primary fibroblasts from the murine pancreas are expanded by *in vitro* culture, by day 4-5 the cultures contain more CD105+ fibroblasts and then by day 10 the cultures are progressively dominated by increasing levels of CD105- fibroblasts. The reason for the apparent bias/selection for CD105+ fibroblasts in tumours and bias/selection for CD105- fibroblasts after extended *in vitro* culture, is not clear. It is possible that in tumours and *in vitro* culture, different responses to cytokines and growth factors (in the TME and in fetal bovine serum respectively) may selectively favour CD105+ or CD105- fibroblasts. Indeed, one of the enriched gene sets for CD105- PDA fibroblasts was TNFα signalling via NFkB. In addition, TNFα favoured expansion of CD105- fibroblasts over CD105+ fibroblasts *in vitro.* Inflammatory conditions in PDA tumours intensify as the tumour progresses (Collins et al., 2012) and this possibly includes increased levels of TNFα, which may explain the increased proliferation of CD105- fibroblasts in advanced tumours (despite them being less abundant than CD105+ fibroblasts). Another potential reason for different levels of proliferation between the CD105+ and CD105- fibroblast populations *in vivo*, may be due to differences in their S-phase durations, although this seems unlikely because current evidence suggests cells from the same species typically have similar S-phase durations (Behbehani, 2018, 2019; Behbehani et al., 2012). In addition, CD105+ and CD105- fibroblasts also show evidence of distinct levels of the more general proliferation-related protein Ki67. Further work would be needed to understand the key factors that dictate CD105+ and CD105- fibroblast abundance and proliferation *in vivo*.

The evidence presented here suggests that CD105+ and CD105- fibroblasts are not interchangeable populations. The fact that CD105+ fibroblasts are the dominant population in PDA tumours and that CD105- fibroblasts are preferably expanded from the pancreas by extended *in vitro* culture, may complicate the interpretation of many prior studies that have inferred *in vivo* fibroblast function from *in vitro* functional assays on fibroblasts expanded from normal pancreas. It is possible that in these *in vitro* assays there are very few, if any CD105+ fibroblasts and therefore the results may not represent the actual function of the major fibroblast population in PDA tumours *in vivo*. The data

here suggests that at least checking the CD105 status of fibroblast isolates would enable more accurate interpretation of the experimental results, particularly once any functional differences between CD105+ and CD105- fibroblasts are better defined. A recent publication has shown areas of prostate tumour stroma that are enriched for CD105 expression (Kato et al., 2019). The authors suggest that fibroblasts from prostate tumours are CD105hi when first isolated in culture and lose CD105 expression with passaging, although unfortunately the raw data to support this is not included in the publication. The data from the pancreatic fibroblasts presented here, suggests that differential CD105 expression is highly stable (as it is for endothelial cells and pericytes) and that mixed cultures show variation in CD105+:CD105- fibroblast ratios over time that needs to be accounted for when culturing and using primary fibroblasts.

For functional interrogation of differences between CD105+/- fibroblasts, I anticipated it would be more informative to study naïve pancreatic fibroblasts, that have not experienced prior activation in tumours. Evidence suggests that activation of fibroblasts in tumours generates epigenetic changes that are retained even when fibroblasts are removed from tumours (Albrengues et al., 2015). In addition, the data from the KPC tumours presented in chapter 4 shows that the phenotype of CD105+/- fibroblasts is highly variable in PDA tumours. I would not be able to control for this variability and would not know if any functional differences observed in subsequent studies using these fibroblasts were due to fundamental, consistent differences in the two populations or just due to different activation events that the populations had experienced previously in the tumour. Isolating CD105+/- fibroblasts from the same healthy pancreas would remove this potential confounding factor and homogenise the ‘activation history’ of the fibroblast cell lines. Importantly, it would make any future findings more reproducible as other researchers could easily isolate these fibroblast populations from other murine pancreas samples. Indeed, fibroblasts isolated from healthy tissues from inbred strains would be expected to be far less variable than fibroblasts isolated from different PDA tumours. Studying naïve fibroblasts that had not ‘seen’ cancer cells before, would also allow me to better study the process of fibroblasts ’activating’ towards a specific phenotype. Lastly, the KPC mice used in these studies are maintained on a mixed genetic background. Thus, I would not be able to transplant isolated PDA fibroblasts into any pure inbred hosts with intact adaptive immune systems, due to confounding alloimmunity. This would greatly limit the ability of the system to understand the interactions of fibroblasts with

tumour immunity and inflammation, for which data presented in the previous chapter suggests there are abundant interactions.

Both CD105+ and CD105- fibroblasts are clearly regulated to some degree in a similar manner. Much of the changes to the surface proteome were similar between the two populations across a range of PDA tumours and a range of *in vitro* stimulations. The *in vivo* co-ordinated expression of αSMA between CD105+/- fibroblasts in the same tumours was particularly remarkable and also supports the concept that CD105+ and CD105- fibroblasts have similar responses to many stimuli. The factors that regulate such a consistent αSMA levels between CD105+ and CD105- fibroblasts in the same PDA tumours are not clear. However, tumour stiffness is a known key upstream regulator of αSMA expression (Calvo et al., 2013) and is highly variable across PDA tumours (experiments conducted within our lab, Below et al. in press). Such contractile forces and altered stiffness are effective over macroscopic regions of fibrotic lesions (Liu et al., 2020) and may be a potential way in which αSMA expression is regulated equally in CD105+ and CD105- fibroblasts. TGFβ1 is another known regulator of αSMA expression and it is possible that CD105+ and CD105- fibroblasts in the same tumour receive similar TGFβ1 signals from clonal cancer cells. In the *in vitro* experiments presented here, TGFβ1 stimulation had only a minor impact on αSMA protein levels. This may be due to the fact the cells were grown *in vitro* on stiff plastic and in FBS, both known to activate fibroblasts towards a myofibroblast phenotype, with high levels of αSMA expression (Baranyi et al., 2019; Ohlund et al., 2017). It may not be possible to increase αSMA protein levels much further with TGFβ1 stimulation *in vitro*. Typically, when different cells are being tested for response to *in vitro* recombinant protein stimulations, most workflows stimulate target cells in separate flasks and this may miss important features of cell communication seen *in vivo*. One of the strengths of the *in vitro* stimulation experiment here was that CD105+ and CD105- primary pancreatic fibroblasts were present in the same flask and therefore experienced the exact same stimulation strength and duration, the same processing and staining and are therefore highly comparable. Hence, any differences in observed protein expression are unlikely due to technical aspects (e.g. slightly different volumes of stimulation media or different antibody staining concentrations) or population-specific aspects (e.g. differences in the doubling rate of one population changing cell numbers in the flask), that can introduce imprecise response measurements when cells are tested *in vitro* in separate flasks. Because the

cells are present in direct mixtures, it is also possible that some of the differences observed are due to ongoing direct cell-cell communication between the CD105+ and CD105- fibroblasts populations, an incredibly interesting aspect that I did not follow up on

Within the DEGs for CD105+ and CD105- fibroblasts, there was a large number of secreted factors, enzymes that generate secreted factors or cell surface receptors. The surface proteome and secreted proteome have been shown to increase in complexity as metazoans have evolved to more complex multicellular organisms, a pattern not shared with the intracellular proteome (Ramilowski et al., 2015). This has been hypothesized to reflect the increasing demand for effective cell-cell communication with increasing cellular specialisation. Thus, the differing expression of secreted factors and cell surface receptors observed here between CD105+ and CD105- fibroblasts in PDA tumours, may reflect distinct cell-cell communication properties, with a potential functional impact on tumour progression and/or response to therapy.

Interestingly. there were several examples where CD105+/- fibroblasts each expressed one of a pair of evolutionary/functionally related genes, for example *Nos1/Nos2* and *Sema3a/Sema5b*. Whether this differential expression or related genes has any convergent or divergent functional consequences is unknown and it may possibly reflect functional redundancy between different fibroblast lineages.

The similar phenotypic response of CD105+ and CD105- fibroblasts to IFNγ is particularly notable. In PDA tumours, only CD105- fibroblasts express high levels of MHCII, CD74 and CD80, yet when the CD105+ and CD105- fibroblasts are stimulated *in vitro* with IFNγ, both show increased expression of MHCII, CD74 and CD80 (and other proteins). This suggests that the different expression pattern seen *in vivo* is not due to an inherently different, lineage-restricted potential to respond to IFNγ. For example, CD105+ and CD105- fibroblasts may occupy different niches with different local levels of IFNγ. A study of the murine pancreas has indicated that a MHCII+CD74+ phenotype defines mesothelial cells but data presented here shows that IFNγ is able to induce expression of these proteins in all fibroblast pancreatic populations and care should be taken in using these proteins to define mesothelial cells in tissues, especially under pathogenic conditions (Dominguez et al., 2020).

CD90 is highly expressed on all fibroblasts in PDA tumours (indeed it can be used as a positive marker for selection by FACS). However, CD90 expression is seen to be variable in the *in vitro* fibroblast stimulations. Populations of CD90+ and CD90- fibroblasts are observed in rheumatoid arthritis and this CD90 expression has recently been shown to be regulated by notch signalling (Croft et al., 2019; Wei et al., 2020). Direct *in vitro* co-culture of primary pancreatic fibroblasts with PDA cells induced a similar increase in CD90 expression. This suggests CD90 in these conditions may be driven by cancer cell contact-induced notch signalling. Related to this, it is interesting to note that fibroblast expression of the two T cell co-stimulatory proteins CD80 and CD86, appears to be regulated by entirely different processes: CD80 is increased by IFNγ and CD86 is increased by heterotypic cell-cell contact with PDA cells. Whether these proteins on PDA fibroblasts are functionally important is not clear but considering their central importance during T cell priming and activation, their differential regulation is interesting.

Many of the surface markers that show variable expression under different stimulating conditions here, have been reported as markers of distinct fibroblast populations in other studies of fibroblasts in tissues and tumours (e.g. CD34, ICAM1, CD90) (Feig et al., 2013; Musso et al., 1999; Wei et al., 2020). Their variability here suggests these proteins likely mark distinct phenotypic/activation states *in vivo* but are dynamically regualted. In contrast, CD105 appears to identify distinct and non-exchangeable fibroblast populations, within which the expression of many of these markers shows high variability. Extended *in vitro* culture and a variety of stimulations were unable to induce CD105+ and CD105- fibroblasts to alter their CD105 expression. Because I have found no evidence that these populations interchanging and no evidence that a transitionary population exists, with intermediate expression of CD105 *in vivo* or *in vitro*, I refer to CD105+ and CD105- fibroblasts as distinct lineages. Whilst CD105 expression could be regulated, such as under extreme conditions, I have found no evidence that physiologically relevant conditions could cause exchange in either direction. Collectively, this data suggests that it important to define designated fibroblast populations as either:

1) permanent, non-exchangeable lineages or
2) as temporary, exchangeable activation/polarization states

There is an incomplete understanding of how fibroblast phenotypic and functional heterogeneity is conserved/regulated between mice and humans. With regards to CD105 expression, I have provided preliminary data to demonstrate that CD105+ and CD105- fibroblast populations are present in both mouse and human PDA tumours and normal pancreas, and that in both species the surface CD105 expression pattern is stable. Further detailed side by side comparisons would be needed to determine if functional differences are conserved across species.

Lastly, it is not known whether the fibroblasts in PDA tumours (or indeed in many other tumour types) derive from the local expansion of tissue-resident fibroblast populations or are recruited from distal sites. For example, bone marrow-derived mesenchymal stem cells are a reported as a source of fibroblasts in some tumours (Arina et al., 2016; Kurashige et al., 2018) (see Summary discussion). The data presented here indicates that fibroblasts in murine and human PDA have phenotypic equivalents (i.e. CD105+/-) in the non-tumour bearing organ,. Thus, this is suggestive of local expansion of fibroblasts as being the major source of fibroblasts in tumours. Formal lineage tracing models would be needed to determine this definitively. However, useful, selective lineage tracing for fibroblasts (subpopulations in tumours) is lacking (see Summary discussion). In this regard, the variety of DEGs detected between CD105+ and CD105- PDA fibroblasts in this study may provide a useful list of genes/gene promoters that could act to selectively trace or manipulate these fibroblast lineages *in vivo.* Interestingly, several human FFPE PDA tumour samples had inflamed 'normal' adjacent pancreatic tissue included in the sample. These normal tissue areas were more ordered than the tumours and appear to show CD105+ and CD105- fibroblasts in different locations, with CD105+ pancreatic fibroblasts present in the intra-acinar areas and the CD105- fibroblast in the inter-acinar areas. Interestingly, a publication in 2016 has highlighted that CD105+ stroma is observed in the intralobular areas of normal human mammary tissue and CD105- stroma in the interlobular areas (Morsing et al., 2016). This suggests that CD105+ and CD105- fibroblasts may be a common feature across different mammalian organs and that their distinct spatial distributions may also be conserved across tissues.

Chapter 7 – Results – Characterisation of *in vitro* functions of CD105+ and CD105- pancreatic fibroblasts

7.1 – Results

The hypothesis of this chapter and the next, is that CD105+ and CD105- pancreatic fibroblasts are functionally distinct. In particular, the aim of the experiments described in this chapter, was to interrogate whether there are *in vitro* functional differences between CD105+ and CD105- fibroblasts. The next chapter will explore *in vivo* functional differences. As *in vitro* fibroblast function is loosely defined concept, I specifically focussed on the now well-established ability of the pancreatic fibroblasts to undergo 'activation', a process in which a stimulus promotes a transition towards a new polarisation or activation state, including the recently characterised MyCAF- and iCAF-like polarizations.

7.1.1 – Gene expression analysis of CD105+ and CD105- pancreatic fibroblasts shows a shared potential for MyCAF- and iCAF-like phenotypic transitions

Fibroblast polarisation from a so-called quiescent state to an activated state is a widely accepted hallmark of fibroblast behaviour *in vivo*. One of the biggest advances in the understanding of pancreatic fibroblast activation has been the description of the MyCAF/iCAF paradigm (Biffi et al., 2019; Biffi and Tuveson, 2020; Elyada et al., 2019; Ohlund et al., 2014; Ohlund et al., 2017; Sahai et al., 2020; Somerville et al., 2020). Multiple studies have now provided compelling evidence that PDA fibroblasts have the potential to occupy two broadly distinct phenotypic states, the so called myofibroblast (MyCAF) state and the so called inflammatory (iCAF) state. The MyCAF state has historically been defined by high αSMA expression and stress fibre formation, although expression of many other MyCAF signature genes are now used, such *Ctgf*, *Tagln* and various collagen genes. iCAF cells are typically defined by reduced αSMA protein (or *Acta2* gene expression) and increased expression of several known inflammatory mediators, including *Il6*, *Cxcl1* and *Ccl2*. Unfortunately, different studies use different ways to define and classify MyCAF/iCAF-like fibroblast states (Biffi et al., 2019; Dominguez et al., 2020). A more accurate understanding of robust signature genes,

ideally linked to key cell functions, would likely improve the comparability between different studies.

In the previous chapters, both CD105+ and CD105- fibroblasts in PDA tumours *in vivo* are indeed seen to be present in both αSMA+ or αSMA- fractions, suggesting they both have capacity to undergo the MyCAF phenotypic switch. I sought to explore this further and better define the MyCAF/iCAF polarization dynamics in CD105+ and CD105- fibroblasts. The first experiment studied the potential of CD105+ and CD105- fibroblasts to express classical MyCAF/iCAF signature genes over long-term incubation/polarization with TGFβ1 (the ligand most often used to induce a MyCAF-like state) and IL1α (the ligand most often used to induce an iCAF-like state) (Ohlund et al., 2017). CD105+ and CD105- pancreatic fibroblasts were subjected to 3 d of continuous ligand stimulation and gene expression assessed by qPCR (see Table 15 for recombinant protein details and Figure 51 for data analysis).

Table 15. Recombinant protein details for 3-day stimulation

Pancreatic fibroblast stimulation for qPCR analysis at 3 d			
Recombinant protein	**Source**	**Identifier**	**Final concentration used (ng/mL)**
Recombinant mouse TGFB1	RnD Systems	7666-MB-005	2
Recombinant mouse IL1a	RnD Systems	400-ML-005	10

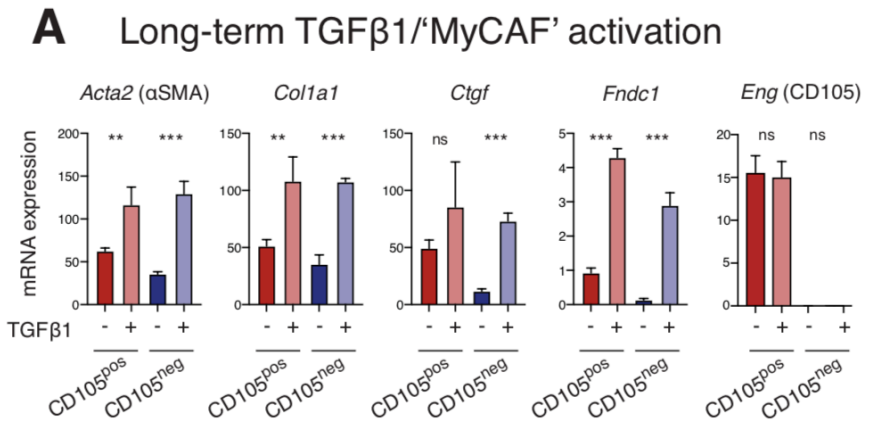

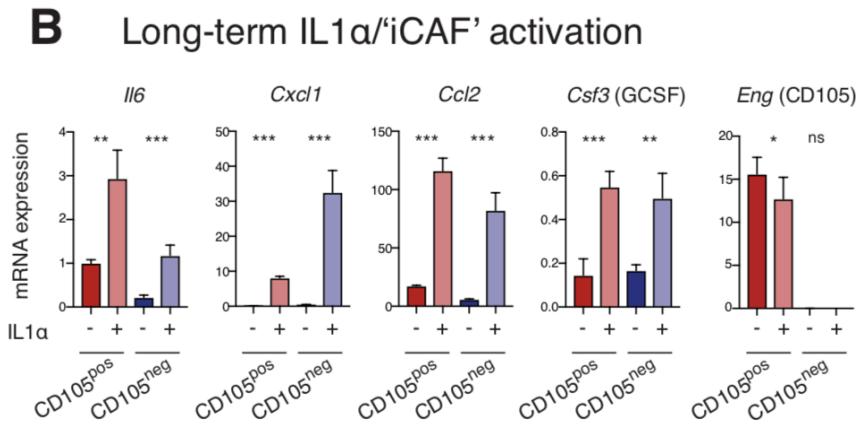

Figure 51. MyCAF and iCAF gene expression in pancreatic fibroblasts (PaFs) after extended stimulation

mRNA expression levels of MyCAF (A) and iCAF (B) associated genes from *in vitro* CD105+ and CD105- PaFs, at baseline or stimulated with recombinant mouse (rm) TGFβ1 or rmIL1α for 72 h. *Eng* expression is also displayed. Measured by qPCR and normalized to the geometric mean of 4 housekeeping genes (HKGs) (*Gapdh*, *Tbp*, *Tubb4a*, *Ppia*). n=4 samples per condition. Data displayed as mean+/-standard deviation. Samples are compared using unpaired t-test. *p<0.05, **p<0.01, ***p<0.001.

The pattern of gene expression changes for the TGFβ1/MyCAF polarization and IL1α/iCAF polarisation are found to be largely the same for both CD105+ and CD105- fibroblasts: expression of *Acta2*, *Col1a1* and *Fndc1* increase with TGFβ1 stimulation in both and *Il6*, *Cxcl1*, *Ccl2* and *Csf3* increase with IL1α stimulation in both. There is trend for increased *Ctgf* expression on TGFβ1 stimulation for CD105+ fibroblasts but this does not reach significance, possibly because the baseline (no stimulation) *Ctgf* mRNA in CD105+ fibroblasts is high. Indeed, for many of the genes, whilst the baseline level is different between CD105+ and CD105- fibroblasts, the stimulation has the effect of increasing gene expression, such that CD105+ and CD105- fibroblasts broadly have the same expression levels after stimulation (e.g. *Acta2*, *Col1a1*, *Ctgf*, *Fndc1*, *Ccl2*, *Csf3*). *Il6* and *Cxcl1* expression with IL1α stimulation follow slightly different behaviour, in that the final expression level is >2-fold different between the CD105+ and CD105- fibroblasts. Notably, *Eng* expression clearly stays distinct between CD105+ and CD105- samples, although interestingly IL1α stimulation reduces transcript levels in an incremental but significant manner in CD105+ cells. In summary, with long-term stimulation and high levels of ligand, both CD105+ and CD105- have the potential to adopt MyCAF- and iCAF-like states, as defined by literature-derived signature genes.

7.1.2 – Genome wide gene expression analysis highlights distinct sensitivity of CD105+/- pancreatic fibroblasts to activating ligands

The previous experiment demonstrated that CD105+ and CD105- fibroblasts both have the potential to express signature genes of the MyCAF- and iCAF-like phenotype, after continuous stimulation with polarising ligands for 3 days. This experiment set up is relatively artificial in that incubation with excess recombinant protein for long periods of time may not recapitulate the situation in complex, dynamic tissues like tumours. Receptor competition from other cell types can limit ligand availability and receptor-mediated endocytosis can actively remove ligand from the intracellular space (Zhou et al., 2018). Spatial separation of cells in the TME and restricted molecule diffusion, may also create strong ligand gradients and greatly reduce ligand availability to some cells (Farin et al., 2016; Ohlund et al., 2017). Accounting for these factors *in vitro* is challenging but I was keen to try and better understand the sensitivity of CD105+ and CD105- fibroblasts to MyCAF and iCAF polarising ligands. To do so, I aimed to activate cells and measure their gene expression profiles at a much earlier time point (6 h) (see Table 16 for recombinant protein stimulation). At this time point any difference in how quickly an activating signal was able to induce gene expression changes would likely be more apparent and would give an approximate measure of the sensitivity to the stimulus. In addition, because the genes-associated with the MyCAF and iCAF-like polarisation are not well defined, especially at an early time point, I opted to analyse genome wide gene expression by RNAseq. This would avoid confounding issues of not selecting appropriate target genes for qPCR and would allow me to accurately compare the number of response genes expressed, as well as the identity of the gene. CD105+ and CD105- fibroblasts were stimulated with TGFβ1 and IL1α for 6 h and cells were lysed and RNA extracted. An 'early DEG' was defined as any gene in CD105+ or CD105- fibroblasts that showed significantly altered expression compared to the no stimulation, baseline condition for that population, with a Benjamini-Hochberg adjusted p value <0.05. The results for this measurement of TGFβ1 and IL1α sensitivity were notably different to the results from the previous long-term stimulation experiment (Figure 51). After 6 h of TGFβ1 stimulation, CD105+ fibroblasts showed 151 early DEGs over baseline, whereas CD105- fibroblasts showed just 8 early DEGs at this early time point. All 8 of these CD105- fibroblast DEGs were also DEGs for CD105+ fibroblasts, with no DEG being unique to CD105- fibroblasts. The majority of these early DEGs shared

between CD105+ and CD105- fibroblasts, are not typically associated with the MyCAF phenotype in the current literature but the proteins they encode have established roles in cell communication and signal transduction, including a phosphatidylinositol-binding protein (*Sdcbp2*), cellular stress kinase (*Sgk1*), transcription factor (*Id2*) and Wnt ligand (*Wnt5a*). Many of the CD105+ fibroblast specific DEGs were genes encoding ECM modifying proteins (*Col27a1*, *Col8a2* and *Lox*) or known regulators of TGFβ signalling (*Ltbp2* and *Smad7*). Interestingly, with TGFβ1 stimulation at this early time point, the canonical MyCAF gene *Acta2* (αSMA) is not differentially expressed, suggesting its increased expression after TGFβ1 stimulation may be delayed or secondary effect.

Table 16. Recombinant protein details for 6 h fibroblast stimulation

Pancreatic fibroblast stimulation for RNAseq analysis at 6 h			
Recombinant protein	**Source**	**Identifier**	**Final concentration used (ng/mL)**
Recombinant mouse TGFB1	RnD Systems	7666-MB-005	2
Recombinant mouse IL1a	RnD Systems	400-ML-005	10
Recombinant mouse IFNg	PeproTech	315-05	20

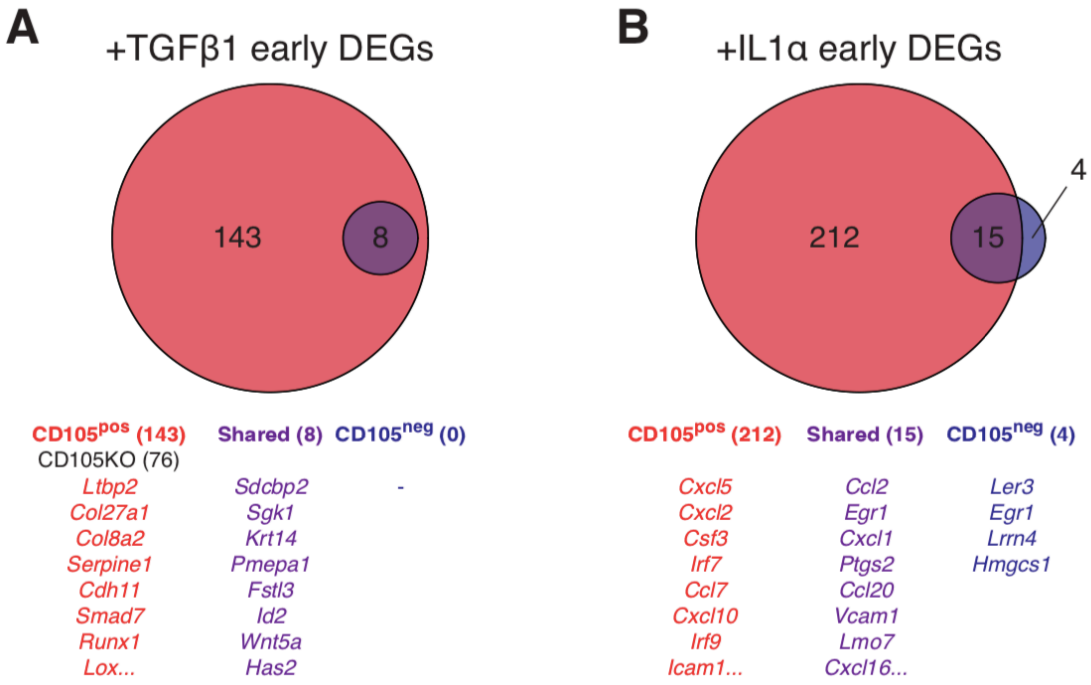

Figure 52. Differentially expressed genes in pancreatic fibroblasts after 6 h TGFβ1 and IL1α stimulation

Differential gene expression analysis of *in vitro* CD105^{pos} and CD105^{neg} PaFs after 6 h of stimulation with recombinant mouse (rm) TGFβ1 (A) and rmIL1α (B) (D). Differentially expressed genes (DEGs) are determined by comparing the stimulation condition with the relevant unstimulated cells. n=3 samples per condition. DEGs determined using DEseq2 with a Benjamini and Hochberg adjusted $p<0.05$. Data is displayed as Venn diagrams (top), with example genes listed (below). DEGs unique to CD105^{pos} PaFs are in in red, DEGs unique to CD105^{neg} PaFs are in blue and common/shared DEGs are in purple. The number of significant early DEGs for each, is displayed in parenthesis.

Why CD105+ and CD105- fibroblasts have distinct sensitives to TGFβ1 stimulation is not immediately obvious: between them there is no difference in expression of the type I TGFβ-family receptor, *Tgfbr1*, or type II TGFβ-family receptor, *Tgfbr2* (Figure 53), or the downstream TGFβ-signalling mediator *Smad2*. There is 1.6-fold higher *Smad3* expression in CD105+ fibroblasts, which may contribute to some of the increased sensitivity of CD105+ fibroblasts to TGFβ1 stimulation.

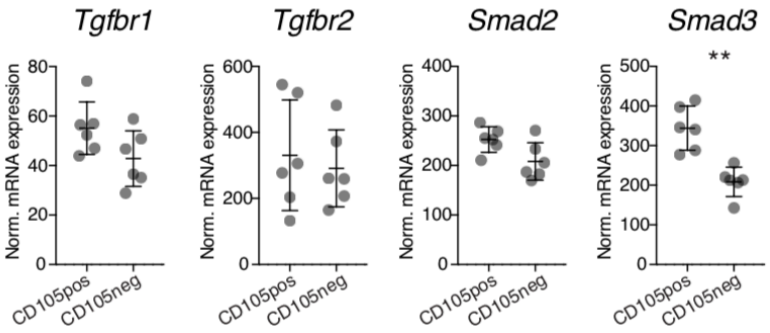

Figure 53. Expression of genes associated with TGFβ signal transduction in pancreatic fibroblasts
mRNA expression of genes associated with TGFβ signal transduction (*Tgfrb1*, *Tgfbr2*, *Smad2* and *Smad3*) in CD105+ (n=6) and CD105- (n=6) pancreatic fibroblasts. Gene expression measured by RNA sequencing and quantified as DEseq2 median ratio normalized expression values. Displaying expression values as mean+/-standard deviation. Samples are compared using unpaired t-test. *p<0.05, **p<0.01, ***p<0.001.

Despite no difference in expression of the TGFβ receptors, *Tgfbr1* and *Tgfbr2*, or the key TGFβ signalling mediator, *Smad2*, CD105+ fibroblasts have almost 20x more early DEGs induced by TGFβ1 stimulation, than CD105- fibroblasts. In endothelial cells, the CD105 protein itself has a known role in TGFβ signalling (Banerjee et al., 2012; Lebrin et al., 2004) and additional work in fibroblasts has shown similar signalling cascades present (Paauwe et al., 2018). It has been demonstrate (mainly in endothelial cells) that the CD105 protein has no signalling capacity on its own but plays a role in modulating the affinity of TGFβ-family ligands to the TGFβR1/2 signalling complex (Barbara et al., 1999). To interrogate whether the CD105 protein itself contributed to any of the TGFβ1-induced signalling in this assay, I sought to genetically delete *Eng* (the gene that encodes CD105) in CD105+ fibroblasts using multi-guideRNA (gRNA) CRISPR/Cas-9 gene editing. Loss of CD105 surface protein was confirmed by flow cytometry (Figure 54). 6 h TGFβ1 stimulation of these cells results in only 84 early DEGs over baseline (compared to 151 Early DEGs in the parental CD105+ cells), suggesting that the CD105 protein itself is responsible for about half of the early transcriptional response and sensitivity to TGFβ1 stimulation in CD105+ fibroblasts.

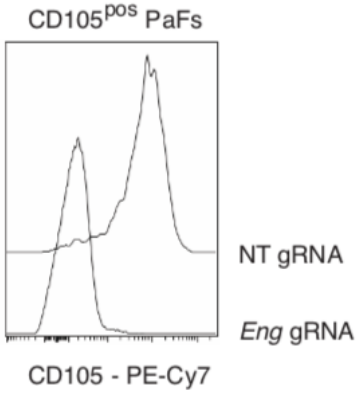

Figure 54. Validation of Eng gene editing in CD105+ pancreatic fibroblasts

Early response genes to IL1α stimulation followed a similar pattern, in that CD105+ fibroblasts have a greater number of early DEGs at 6 h, suggestive of higher sensitivity to this ligand. CD105+ fibroblasts have 227 early DEGs. 15 of these DEGs are shared with CD105- fibroblasts and CD105- fibroblasts had only 4 additional unique DEGs (to give a total of 19 early DEGs induced by IL1α in CD105- fibroblasts). In accordance with the literature, several of the shared IL1α early response genes seen here have been previously used to define the iCAF phenotype (e.g. *Ccl2* ,*Cxcl1, Vcam1*) (Ohlund et al., 2017). Interestingly, the IL1α sensitive CD105+ fibroblasts have higher expression of the canonical IL1 receptors, *Il1r1* and *Il1rap*, as well as higher expression of the major IL1 signalling mediator, *Myd88,* compared to CD105- fibroblasts, which may explain the increased sensitivity of CD105+ fibroblasts for IL1α (Figure 55).

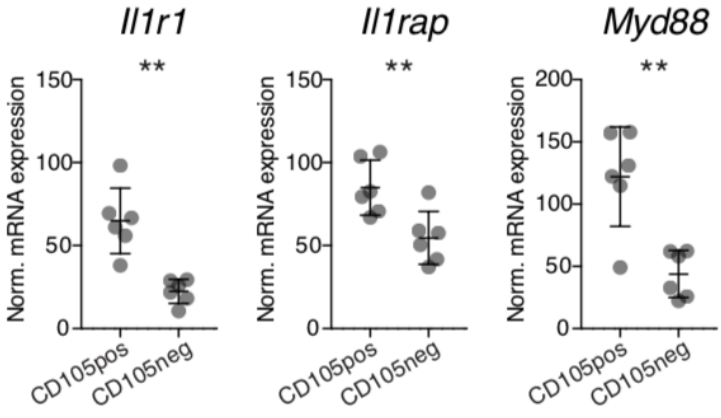

Figure 55. Expression of genes associated with IL1 signal transduction in pancreatic fibroblasts
mRNA expression of genes associated with IL1 signal transduction (*Il1r1*, *Il1rap* and *Myd88)* in CD105+ (n=6) and CD105- (n=6) pancreatic fibroblasts. Gene expression measured by RNA sequencing and quantified as DEseq2 median ratio normalized expression values. Displaying expression values as mean+/-standard deviation. Samples are compared using unpaired t-test. *p<0.05, **p<0.01, ***p<0.001.

Many of the CD105+ fibroblast-specific DEGs encoded additional cytokines/growth factors with known immune modulatory properties (e.g. *Cxl5*, *Cxcl2*, *Csf3*, *Ccl7*, *Cxcl10*) or functions in immune cell adhesion (e.g. *Icam1*), as well as transcription factors known to regulate inflammatory gene programs (*Irf7* and *Irf9*). It is possible that these transcription factors may go on to establish a delayed/secondary gene expression response. Indeed, in the literature the most widely used gene to define the iCAF phenotype is *Il6* but, interestingly, *Il6* is not a DEG for either CD105+ or CD105- fibroblasts at this early, 6 h time point. The qPCR data in the previous analysis clearly shows that with enough ligand and enough time (3 d), both CD105+ and CD105- fibroblasts can upregulate *Il6* expression in response to IL1α. Thus, expression of the major iCAF signature gene, *Il6,* may be part of a secondary/delayed response to IL1α stimulation.

Both TGFβ1 and IL1α stimulation show much higher numbers of DEGs in CD105+ fibroblasts than in CD105- fibroblasts. I was keen to asses if CD105+ fibroblasts are just generally more sensitive to all activating factors. Data presented in previous chapters, shows that *in vitro*, CD105+ and CD105- both respond to IFNγ with similar protein changes after 3 d (increased MHCI, MHCII, CD74 etc). Thus, I also measured the genome wide transcriptomic response of CD105+/- fibroblasts after 6 h of IFNγ stimulation. Gene expression measurement at 6 h after stimulation confirmed that both populations have a strong transcriptional response to IFNγ, suggesting that the relative lack of sensitivity of CD105- fibroblasts to TGFβ1 and IL1α was unlikely due to a general insensitivity to activation or a technical artefact specific to *in vitro or this* assay format. The majority of IFNγ early DEGs (234 genes) were shared between the two populations and included well established IFNγ response genes such as the transcription factor, *Irf1* and the MHCI-complex component, *H2-D1* (Figure 56). Interestingly, both CD105+ and CD105- populations had a number of unique early DEGs, not shared with the other population, suggestive of a largely similar 'core' IFNγ response, with some CD105+/- fibroblast population-specific differences.

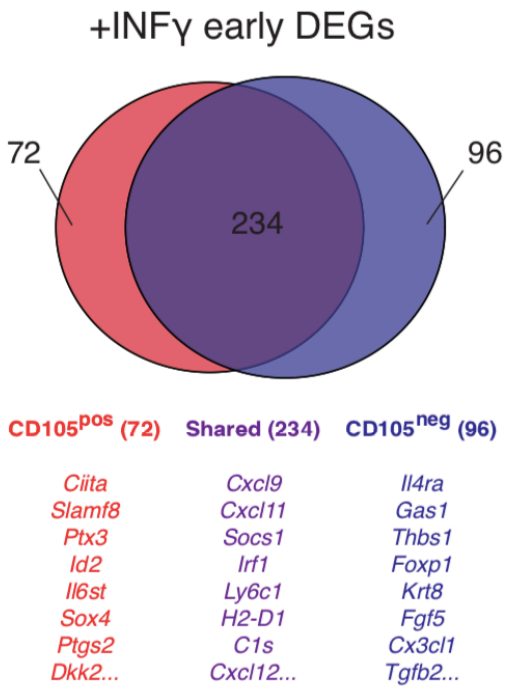

Figure 56. Differentially expressed genes in pancreatic fibroblasts after 6 h IFNγ stimulation
Differential gene expression analysis of *in vitro* CD105^{pos} and CD105^{neg} PaFs after 6 h of stimulation with recombinant mouse (rm) IFNγ. Differentially expressed genes (DEGs) are determined by comparing the stimulation condition with the relevant unstimulated cells. n=3 samples per condition. DEGs determined using DEseq2 software with a Benjamini and Hochberg adjusted p<0.05. Data is displayed as a Venn diagram (top), with example genes listed (below). DEGs unique to CD105^{pos} PaFs are in in red, DEGs unique to CD105^{neg} PaFs are in blue and common/shared DEGs are in purple. The number of significant early DEGs for each, is displayed in parenthesis.

7.1.3 – Mapping the phospho-proteome of CD105+/- fibroblast activation by mass cytometry

The results above suggest that whilst CD105+ and CD105- fibroblasts have the potential to undergo MyCAF- and iCAF-like transitions, CD105+ fibroblasts appear to be more sensitive to the respective activating ligands. Both CD105+ and CD105- fibroblasts are equally sensitive to IFNγ stimulation. Whilst TGFβ1 and IL1α activation of fibroblasts has received much attention since the description of the MyCAF and iCAF phenotypes, the signalling networks that transmit these extracellular signals specifically in fibroblasts have not been characterised in detail. In addition, the signalling networks engaged by other known but less studied fibroblast activating ligands (e.g. LIF), are poorly characterised. I hypothesised that some of the different transcriptomic responses of CD105+ and CD105- fibroblasts to stimulation, may be due to differential activation of phosphorylation networks within in each population. Thus, as part of characterising

CD105+ and CD105- fibroblasts *in vitro*, I aimed to better understand signalling node phosphorylation responses during activation. I generated RFP labelled CD105+ fibroblasts and GFP labelled CD105- fibroblasts by lentiviral transduction. Equal numbers of each population were mixed at a 1:1 ratio and plated overnight in multiple flasks in low serum media. Flasks containing the mixed cells were stimulated with recombinant proteins in low-serum media for exactly 5 min and then fixed to preserve signalling nodes, lifted, permeabilised, barcoded for mass cytometry, pooled and stained with a cell signalling mass cytometry panel (see Table 17 in this section for recombinant proteins and Table 5 in the Materials and Methods section for antibody details). This signalling mass cytometry panel contained a large number of highly validated antibodies targeting major phosphorylation sites, or other proteins known to play key roles in cell signalling, and would give a broad picture of the phosphorylation nodes and other post-translational modifications (PTMs) activated 5 min after recombinant protein stimulation. Anti-RFP and anti-GFP antibodies were included to allow easy identification of CD105+ and CD105- fibroblasts from each condition, respectively.

Table 17. Recombinant protein stimulation to study fibroblast signalling responses

Pancreatic fibroblast stimulation for phospho mass cytometry analysis at 5 min			
Recombinant protein	**Source**	**Identifier**	**Final concentration used (ng/mL)**
Recombinant mouse TGFB1	RnD Systems	7666-MB-005	2
Recombinant rat PDGF-BB	RnD Systems	520-BB-050	60
Recombinant mouse FGF2	RnD Systems	3139-FB-025	20
Recombinant human/mouse Activin-A	RnD Systems	338-AC-010	20
Recombinant mouse BMP2	RnD Systems	355-BM-010	20
Recombinant mouse BMP4	RnD Systems	5020-BP-010	20
Recombinant mouse BMP7	RnD Systems	5666-BP-010	20
Recombinant mouse BMP9	RnD Systems	5566-BP-010	20
Recombinant mouse BMP10	RnD Systems	6038-BP-025	20
Recombinant mouse IFNg	PeproTech	315-05	20
Recombinant mouse TNFa	Peprotech	315-01A	15
Recombinant mouse IL1a	RnD Systems	400-ML-005	10
Recombinant mouse IL1b	PeproTech	211-11B	10
Recombinant mouse IL6	PeproTech	216-16	5
Recombinant mouse LIF	PeproTech	250-02	5
Recombinant mouse MIF	Biolegend	599504	200
Recombinant mouse IL13	RnD Systems	413-ML-005	20
Recombinant mouse IL22	RnD Systems	582-ML-010	20

The median signal intensity for each protein phosphorylation site for CD105+ and CD105- fibroblasts is displayed at a heatmap in Figure 57. The baseline, no stimulation control condition has very low levels of signal in almost all of the signalling nodes measured, consistent with reduced signalling in the minimal (0.5%) dialysed FBS-containing media. Even at this baseline state though there are some minor differences between active signalling networks in CD105+ and CD105-fibroblasts, which may be due

to slightly different responses to the proteins contained in the 0.5% dFBS media (which is the minimal media required to keep the cells alive after being seeded). Whilst several stimulations activated known canonical pathways of the respective activating factors (e.g. IFNγ induced strong pSTAT1[Y701]), I found the most striking result was how promiscuous most of the activating factors were in terms of the breadth of signalling nodes they engaged outside of widely accepted canonical downstream nodes. The specific combination of nodes they activated and the extent of phosphorylation varied widely and was also clearly different for some factors between CD105+ and CD105- fibroblasts. This resulted in a unique signalling 'fingerprint' in CD105+ and CD105- fibroblasts across different stimulating conditions, some more or less divergent than others.

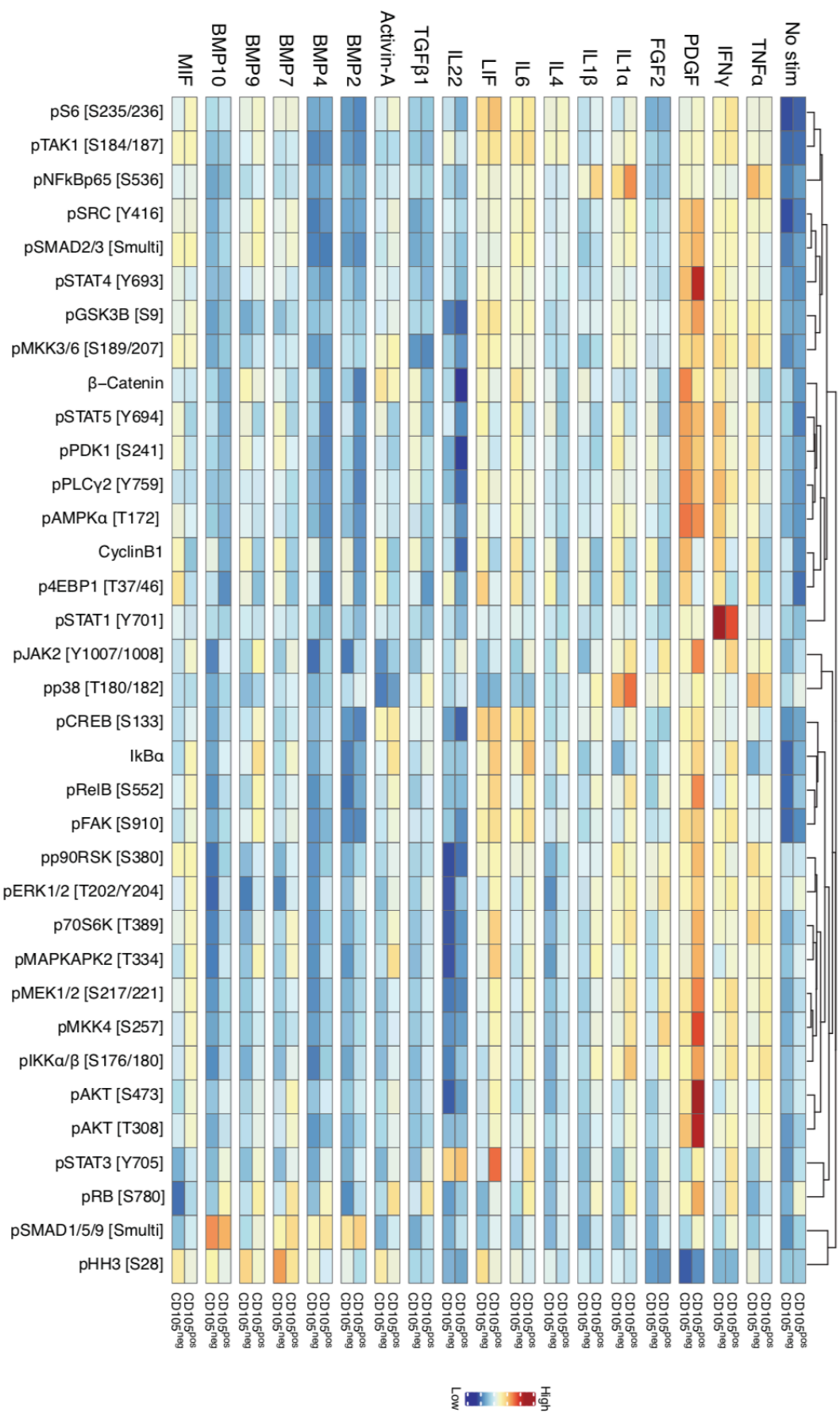
No stim
TNFα
IFNγ
PDGF
FGF2
IL1α
IL1β
IL4
IL6
LIF
IL22
TGFβ1
Activin-A
BMP2
BMP4
BMP7
BMP9
BMP10
MIF
pS6 [S235/236]
pTAK1 [S184/187]
pNFkBp65 [S536]
pSRC [Y416]
pSMAD2/3 [Smulti]
pSTAT4 [Y693]
pGSK3B [S9]
pMKK3/6 [S189/207]
β–Catenin
pSTAT5 [Y694]
pPDK1 [S241]
pPLCγ2 [Y759]
pAMPKα [T172]
CyclinB1
p4EBP1 [T37/46]
pSTAT1 [Y701]
pJAK2 [Y1007/1008]
pp38 [T180/182]
pCREB [S133]
IkBα
pRelB [S552]
pFAK [S910]
pp90RSK [S380]
pERK1/2 [T202/Y204]
p70S6K [T389]
pMAPKAPK2 [T334]
pMEK1/2 [S217/221]
pMKK4 [S257]
pIKKα/β [S176/180]
pAKT [S473]
pAKT [T308]
pSTAT3 [Y705]
pRB [S780]
pSMAD1/5/9 [Smulti]
pHH3 [S28]
CD105neg CD105pos
Low
High

Figure 57. Cell signalling responses of pancreatic fibroblasts
Mass cytometry (MC) analysis mapping cell signaling responses of CD105+ and CD105- pancreatic fibroblasts (PaFs) to selected soluble signals. RFP+CD105+ and GFP+CD105- PaFs are plated in the same flask to ensure identical stimulation and processing, and identified by the inclusion of antibodies targeting the respective fluorescent proteins. Cells were serum-starved for 16 h, stimulated and fixed after 5 min to preserve and capture early cell signaling events. Data is displayed as median mass intensities (MMI) and as column normalized Z-scores. For phosphorylation signaling node measurements the specific phospho site is described in brackets.

TGFβ1 stimulation showed a relatively minor response in both CD105+ and CD105- fibroblasts. This is likely because SMAD2/3 phosphorylation, the canonical TGFβ1 signalling mediator, is known to be a relatively slow signalling process, normally measured at 30-60 min after stimulation (van Caam et al., 2017). This analysis was conducted at 5 min to capture the majority of other signalling nodes, which have rapid responses (typically 30 s – 10 min). Despite this, TGFβ1 stimulation is still seen to cause increased levels of pp38 and pRB in CD105+ fibroblasts. TGFβ1 stimulation causes increases in B-catenin, pSTAT5, pPDK1 and pPLCγ2 levels in CD105- fibroblasts, pathways not typically associated with TGFβ1 signalling. Differential activation of these nodes between CD105+ and CD105- fibroblasts is also seen to some degree at baseline suggesting similar signalling activation even in low serum media, potentially from autocrine TGFβ1 signalling or TGFβ-family proteins in the dFBS.

Both CD105+ and CD105- fibroblasts respond to IL1α stimulation through increased levels of pp38, pNFκBp65 and pIKKα/β, and to a lesser extent, at other nodes including pRelB and pERK1/2. CD105+ fibroblasts had stronger phosphorylation responses than CD105- fibroblasts at almost every IL1α-induced node. This is consistent with the increased transcriptomic response of CD105+ fibroblasts to IL1α stimulation seen in the RNAseq study described above. Interestingly, the 'fingerprint' of response to IL1β was very similar to IL1α but more muted, even though the same concentration of each ligand was used.

The response to IFNγ was very broad and, remarkably, caused some level of change to almost all signalling nodes measured. IFNγ has a well characterised role in various immune cell processes but this data highlights the broad and complex action of the cytokine on non-immune cells too. Here, as expected, IFNγ induced the highest levels of pSTAT1 of any stimulation in both fibroblast populations, although the response was stronger in CD105- fibroblasts. In general, CD105- fibroblasts showed more nodes strongly activated by IFNγ, including pSTAT5, pPDK1, and pPLCγ2 again (as for

TGFβ1), as well as pAMPKα and p4EBP1. The degradation product of NFkB signalling, IkBa was higher in CD105+ fibroblasts, consistent with lower NFkB signalling in CD105+ fibroblasts under IFNγ stimulation.

The response to TNFα was notable in that whilst inducing a broad array of phosphorylation changes, the response in CD105- fibroblasts was stronger than that for CD105+ fibroblasts. For example, pNFkBp65, pp38 and p70S6K all increased after TNFα stimulation in both populations but to higher degree in CD105- fibroblasts. This is consistent with the *ex vivo* gene set enrichment analysis of KPC CD105+ and CD105- PDA fibroblasts (presented in chapter 6), in which the 'TNFα signalling via NFkB' gene set was enriched in CD105- PDA fibroblasts. In addition, TNFα is seen to enhance CD105- pancreatic fibroblast growth *in vitro* (Chapter 6). Again, as for several other stimulations, TNFα induced pSTAT5, pPDK1, pPLCγ2, pAMPKα specifically within the CD105- fibroblasts. It is unclear why this set of nodes is activated in CD105- fibroblasts across several stimulations.

The signalling response to PDGF was particularly striking in terms of the large number of nodes activated, how strongly the nodes changed and also with how different the response was between CD105+ and CD105- fibroblasts. In CD105+ fibroblasts, PDGF caused the strongest signalling response in several nodes, of all the stimulations tested. This included, pAKT at both the S473 and T308 sites, pIKKα/β, pMKK4, pMEK1/2, pJAK2 and pSTAT4. Whilst several of these nodes were also activated in CD105- fibroblasts, the extent was lower. CD105- fibroblasts again showed strong responses in B-catenin, pSTAT5, pPDK1, pPLCγ2 and p4EBP1, highlighting these as commonly utilised pathways in CD105- fibroblasts across several activating conditions. These pathways are not typically associated with PDGF signalling and demonstrate the networked nature of intracellular signalling. It is unlikely that activation of these pathways is due to secondary responses (e.g. autocrine secretion in response to the primary PDGF signal) because these measurements are taken 5 min after stimulations, but I cannot completely rule out the possibility. Some of the breadth and complexity of the PDGF response may due to the fact that the specific dimeric PDGF ligand used is PDGF-BB, one of five possible dimers from four PDGF monomer isoforms. PDGF-BB is the only PDGF dimer known to bind and activate all three PDGF receptor combinations. It would

be interesting to use this assay to compare the signalling differences between the five known PDGF dimer pairs.

LIF has been recently described as an important activating ligand of fibroblasts in human and murine PDA tumours, that can act in an autocrine manner to drive fibroblast functions which go on to impact cancer cell surivvial (Shi et al., 2019). Here LIF generated a broad response in both CD105+ and CD105- fibroblasts, quite distinct to other stimulating factors. Increases in pTAK1, pGSK3B and pCREB are seen in both CD105+ and CD105- fibroblasts to largely the same degree. LIF was the strongest inducer of pSTAT3 of all the activating ligands tested. This is consistent with pSTAT3 signalling being a key downstream pathway for LIF (Shi et al., 2019). Interestingly, LIF raised pSTAT3 levels only in CD105+ fibroblasts and had minimal impact on pSTAT3 levels in CD105- fibroblasts. LIF also induced increased levels pMAPKAPK2, p70S6K, pFAK, and pS6, more so in CD105+ fibroblasts than CD105- fibroblasts.

The other stimulations induced less dramatic changes to signalling networks. Of these the BMP-family ligands are notable for their induction of pSMAD1/5/9, the canonical BMP-family signalling mediator. The relatively understudied BMP10 was the strongest inducer. IL6 is the canonical secreted ligand of the iCAF phenotype and has previously been studied as a paracrine signal *from* fibroblasts (Flint et al., 2016; Ohlund et al., 2017). Here there is evidence that it can induce broad signalling changes in fibroblasts and thus may have some autocrine signalling properties in IL6-secreting fibroblasts. IL22 is notable for its relative lack of activation of almost all signalling nodes apart from its induction of pSTAT3, to largely the same degree in both CD105+ and CD105- fibroblasts.

7.2 – Summary

Experiments described in the previous chapters demonstrate the existence of non-interchangeable CD105+ and CD105- fibroblasts in the pancreas and in pancreatic tumours of humans and mice. The hypothesis of this section was that CD105+ and CD105- have distinct functions *in vitro*, particularly with respect to fibroblast activation. Collectively the experiments presented in this chapter have demonstrated that CD105+ and CD105- fibroblasts both share the capacity to undergo similar phenotypic/polarisation changes under activating conditions but do so with distinct

sensitivities. This was measured at the level of early and late gene transcription, as well as cell signalling networks of protein phosphorylation. Approximately half of the sensitivity of CD105+ fibroblasts to TGFβ1, is contributed by the CD105 protein itself. The sensitivity of CD105+ fibroblasts to IL1α may be due to the higher expression of the relevant IL1α receptors (*Il1r1* and *Il1rap*) and signalling mediators (*Myd88*). Analysis of fibroblast phospho-site changes after activating factor stimulation, highlights the complexity of cellular signalling and the divergent signalling responses between CD105+ and CD105- fibroblasts. Collectively these results demonstrate CD105+ and CD105- fibroblasts have distinct activation potential, that may act as starting points for mechanistic experiments to explore what factors regulate lineage-specific aspects, such as what dictates the CD105+:CD105- fibroblast ratio in PDA tumours and if differential activation may account for any phenotypic or functional differences between CD105+ and CD105- fibroblasts *in vivo*.

7.3 – Discussion

The recently characterised MyCAF and iCAF paradigm has greatly enhanced understanding of cancer-associated fibroblasts, particularly in PDA. Here, I show that both CD105+ and CD105- pancreatic fibroblasts have the ability, under extended activating conditions, to polarise into these two states, as defined by gene expression changes. Indeed, αSMAhi and αSMAlo fractions of both CD105+ and CD105- fibroblasts are frequently seen in the same PDA tumour (chapter 4). The fact that both CD105+ and CD105- fibroblasts are capable of undergoing MyCAF/iCAF phenotypic polarisation, suggests this 'MyCAF/iCAF switch' may be generalisable feature of fibroblasts and may even be a defining characteristic of this cell type. Indeed, defining unique fibroblast-specific features, separate from other mesenchymal cells, would improve our understanding of this, at times, ambiguously defined cell type. Pancreatic fibroblast MyCAF and iCAF switches are now well documented but several important aspects remain unknown. For example, the vast majority of characterisation has been conducted with mouse cells *in vitro*, with minor validation in human cells. In addition, the extent to which fibroblasts from other organs and tumour types, can undergo similar or related phenotypic switches is not well understood, although expression of αSMA is reported in a wide range of fibrosis-associated pathologies and often only within a fraction of the fibroblasts present (Hinz and Lagares, 2020). The results presented here suggest that

an additional line for future investigation will be to better understand the MyCAF/iCAF polarisation in the context of distinct fibroblast lineages, for example in CD105+ and CD105- fibroblasts. A recent scRNAseq of the murine pancreas and murine PDA has identified variable expression of *Eng* (the gene that encodes CD105) in fibroblast-like clusters, and the authors suggest that *Eng* expressing fibroblasts are the source of MyCAF fibroblasts in PDA tumours and fibroblasts not expressing *Eng* are the source of iCAF fibroblasts in PDA tumours, based on similar expression of some a selected list of genes (Dominguez et al., 2020). The results presented in this chapter and in Chapter 4 demonstrate that under *in vitro* stimulation and in PDA tumours, both CD105+ and CD105- fibroblasts have the capacity to undergo MyCAF-like and iCAF-like transitions. The difference between their findings and those presented here is not fully clear but may derive from the fact that CD105+ fibroblasts have a stronger response to TGFβ1 than CD105- fibroblasts (partly due to CD105 itself) and thus may appear more 'MyCAF-like' when comparing curated gene lists. Thus, in a head to head comparison CD105+ fibroblasts may appear to express higher levels of some selected MyCAF genes. In addition, those studies were conducted using a different PDA GEMM (*Pdx1-Cre; Kras$^{LSL-G12D/+}$; p16/p19$^{fl/fl}$*). Further work is needed to know if CD105+ and CD105- fibroblast lineages are a feature of all PDA GEMMs.

Whilst the MyCAF/iCAF paradigm is a highly reproducible phenotypic program in PDA fibroblasts, the understanding of its functional implications is notably lacking. For example, it is not clear if one or the other has a net tumour promoting effect or a net tumour restrictive effect. Some efforts have been attempted to address this but unfortunately are far from conclusive. TGFβ1 has been shown to induce some features the MyCAF-phenotype. In an attempt to understand the function of MyCAF fibroblasts in PDA, Biffi et al. treated KPC mice with a TGFβR inhibitor, which showed no net change in tumour growth (Biffi et al., 2019). TGFβ signalling in the TME is extremely complex and inhibition of TGFβR2 can have a broad spectrum of effects on many cells, for example TGFβR inhibition can directly enhance epithelial cancer cell growth but also improve immune-mediated control of tumours. Additionally, several mechanisms other than TGFβ stimulation are known to induce the MyCAF-like phenotype (e.g. microenvironment stiffness) and thus inhibiting TGFβ signalling doesn't necessarily equate to inhibition of MyCAF polarisation and function. Features of the iCAF phenotype have been shown to be induced by IL1α via JAK-STAT signalling, which is supported by

data presented in this chapter. KPC mice treated with a JAK inhibitor show smaller tumours at a single, fixed time point (Biffi et al., 2019). The interpretation of these results is that the iCAF polarisation is tumour promoting but such interpretation is challenging, mainly because in such experiments JAK/STAT signalling will be inhibited in many cell types in the PDA TME and not just in fibroblasts. Indeed, inhibiting a known potent inflammatory signalling pathway, would be expected to reduce tumour inflammation and reduce leukocyte infiltration generally. This could potentially account for the reduced tumour volume observed in that study, without actually equating to any change in tumour cell number or tumour progression. Indeed, no survival analysis was conducted in either study, so it is not clear that these smaller tumours are any less advanced/deadly than those in the control cohorts. Lastly, whilst IL1α-JAK/STAT signalling may contribute to some of the features of the iCAF phenotype, data presented here and in chapter 6, demonstrates that several other factors other than IL1α, such as TNFα, can induce iCAF-like changes in pancreatic fibroblasts. Thus, functional analysis of the consequences of the iCAF phenotype need to consider the fact that a single ligand/receptor/pathway may not be solely responsible for driving the phenotype.

In the context of the results presented in this chapter, any studies that seek to accurately understand the functional implications of the MyCAF and iCAF-polarised fibroblasts in tumours, will likely be confounded by the presence of various levels of CD105+ and CD105- fibroblasts, which themselves have divergent behaviour. One can envisage that within a single tumour at a single time point, there are at least four distinct fibroblast states: CD105+ fibroblasts in MyCAF- and iCAF-like states and CD105- fibroblasts in a MyCAF- and iCAF-like states, with the CD105+/- states being non-interchangeable and the MyCAF/iCAF states to some extent being dynamic (see below). Such complexity and heterogeneity of the fibroblast compartment may be one of the reasons for the extensive conflicting and contradictory results in the literature regarding fibroblast functions in tumours and may also be one of the contributing factors to why specific and effective fibroblast-targeting therapies have not been found. The data presented here suggests that future experiments trying to understand the MyCAF- and iCAF-like phenotypes could be made more accurate, by focussing the analysis on either isolated CD105+ or CD105- fibroblasts but not trying to understand the MyCAF/iCAF phenotypes in both at the same time.

The MyCAF and iCAF paradigm is an exciting development in fibroblast research and has led to a much-improved understanding of fibroblast plasticity during pathological/inflammatory conditions. Yet, many questions remain:

- Is the phenotypic switch *in vivo* well modelled by *in vitro* systems?
- What are the signalling and transcriptional regulators of these phenotypes and can they be blocked for therapeutic benefit in cancer or other pathologies?
- Can fibroblasts move/cycle between the two states indefinitely? Some existing data does support the idea that an activated pancreatic fibroblast can, to some extent, move between the two activation states *in vitro* but this was not explored in detail (Ohlund et al., 2017).
- Do strong or sustained polarising conditions generate more permanent states?
- Are the two states in direct competition with each other or can the same cell exhibit features of both? Is one state dominating or the 'default' state over the other? In this regard, TGFβ1 has been shown to have the capacity to interrupt IL1α/JAK/STAT signalling *in vitro* and LIF, produced in the iCAF state, can act in autocrine manner and block MyCAF-like differentiation (Biffi et al., 2019; Nguyen et al., 2017).
- Do activating stimuli need to be sustained or is an initiating signal sufficient? If the initiating stimulus is removed do fibroblasts revert to the naïve state or are the actively removed from the tissue, for example by undergoing apoptosis or signalling to phagocytes for removal?
- Do different polarisations have the same half-life/persistence *in vivo*?

With regards to the final question, CD105+ and CD105- fibroblasts in PDA tumours have different proliferation rates *in vivo* in late stage tumours, but MyCAF and iCAF fractions showed no significant proliferation difference. This suggests that proliferation of activated fibroblasts may be independent of the phenotypic state they are in. Thus, some fibroblast activating factors may only act to dictate MyCAF/iCAF polarisation (TGFβ1 and IL1α) and others may only regulate proliferation, survival etc. Related to this, data shown in this chapter demonstrates that PDGF stimulation strongly activates a wide variety of mitogenic and survival signalling pathways in both CD105+ and CD105- fibroblasts, including MAPK, AKT and STAT pathways but has minimal impact on expression of MyCAF/iCAF signature proteins in either population (Chapter 6).

A binary phenotypic MyCAF/iCAF switch is an attractive concept for its simplicity but is also likely to be an over simplification of fibroblast phenotype complexity. Similar terminology describing a two state activation phenotype of the so called classically activated M1 and alternatively activated M2 macrophages, has been widely adopted but has been demonstrated to be an oversimplification of macrophage differentiation and its usefulness has been challenged recently (Aras and Zaidi, 2017). Indeed, several lines of evidence presented here already suggest a MyCAF/iCAF binary switch may be an oversimplification. For example, we observe a fraction of iCAF-like CD105- fibroblasts in an MHCII+ state in PDA tumours (Chapter 6). scRNAseq results in similar PDA GEMMs have also noted a small fraction of cells with increased expression of antigen presentation machinery (Elyada et al., 2019). In addition, recent data in rheumatoid arthritis provides compelling evidence that Notch signalling in fibroblasts can drive a unique phenotype not seen in tumours (Wei et al., 2020). Hence a complex spectrum of fibroblast phenotypic states may be possible, each of which may contribute unique functions in developmental, homeostatic and pathological processes.

The MyCAF/myofibroblast terminology was originally based on the increased expression of αSMA and formation of αSMA stress fibres (Sandbo and Dulin, 2011). More recently the terminology has included increased expression of ECM and ECM-modifying genes. Likewise, the so called iCAF phenotype is named so because of the reproducible and defining increase in gene expression of several inflammatory cytokines. Increasingly the three iCAF signature genes used are *Il6*, *Cxc1* and *Ccl2* (Ohlund et al., 2017). With the genome-wide analysis conducted here, it is notable how distinct the gene expression programs between the MyCAF-like state and iCAF-like state are. Of the 151 early DEGs observed in CD105+ and/or CD105- fibroblasts stimulated with TGFβ1, there is not a single C-X-C or C-C motif chemokine gene that shows upregulated expression. Likewise, for the 234 DEGs observed in CD105+ and/or CD105- fibroblasts stimulated with IL1α, there is not a single collagen or MMP gene that shows upregulated expression at this early time point. Whilst the situation *in vivo* is likely more complex, it does appear that *in vitro* at least, the early MyCAF and iCAF gene expression programs initiated by TGFβ1 and IL1α respectively, align with ECM-modifying and inflammatory properties respectively, largely matching their 'MyCAF' and 'iCAF' nomenclature well. Despite these clear differences early in activation, delayed inflammatory-related genes that are part of the MyCAF gene expression program may contribute to fibroblast function *in vivo* and

delayed ECM-related genes that are part of the iCAF gene expression program may also contribute to fibroblast function *in vivo*. Indeed, a potential caveat with the analysis presented here, is the assumption that TGFβ1-stimulation is a good approximation for the MyCAF-phenotype, when other factors are known to induce the myofibroblast phenotype, such as tissue stiffening (Calvo et al., 2013). Regardless of the exact requirements of the initiating stimulus, it is apparent that at least two distinct states of fibroblasts with ECM-/inflammatory-enriched programs exist. Why these programs have evolved in the context of tissue development, homeostasis and pathological/repair processed, is not known but is an exciting area of future research.

The genome-wide transcriptomic analysis described in this chapter indicates that CD105+ are more sensitive than CD105- fibroblasts (based on early DEGs at 6h), to both TGFβ1 and IL1α stimulation and that both populations are equally responsive to IFNγ. Approximately half of the sensitivity to TGFβ1-stimualtion (76/151 DEGs) is due to CD105 itself, which has an established role in TGFβ1-signalling in endothelial cells. What dictates the remaining sensitivity (75/151 DEGs) is not clear, but CD105+ fibroblasts show higher levels of the TGFβ1-signalling mediator *Smad3*, although whether this is rate-limiting to signal flux is not clear. The different sensitivity to IL1α may be directly due to higher expression of the relevant receptors (*Il1r1* and *Il1rap*) and signalling mediators (*Myd88*) in CD105+ fibroblasts. A potential caveat here is that mRNA expression is only loosely correlated with protein expression generally (Liu et al., 2016) and using mRNA levels to infer the levels of membrane receptors is particularly challenging, as they are subject to extensive post-translation modifications (PTMs) and membrane trafficking regulation. Additionally, different levels of less-characterised co-receptors, signalling adapters/transducers and transcription factors, could all contribute to differential sensitivity to activation. Whether this difference in ligand sensitivity of CD105+ and CD105- pancreatic fibroblasts is important *in vivo* is not clear and requires further study. Notably, the results from the short-term stimulation (6 h) analysis presented here, contrast with those from the long-term stimulation (3 d), which indicates that both CD105+ and CD105- fibroblasts have the capacity to adopt similar MyCAF-like and iCAF-like gene expression levels if given enough time and ligand exposure. Which *in vitro* assay is more relevant to the *in vivo* setting is not clear, although they are not mutually exclusive models. *Ex vivo* analysis of fibroblasts in PDA tumours (Chapter 4) does show that CD105+ and CD105- fibroblasts are present in both MyCAF- and iCAF-

like states *in vivo* but this is based on just αSMA and PDGFRα/ICAM1 expression, which may not fully capture the complexity or extent of the MyCAF and iCAF phenotypes.

Data presented in the previous chapter demonstrates that IFNγ can increase the expression of proteins involved in MHCII-restricted antigen presentation (MHCII and CD74) equally well in both CD105+ and CD105- fibroblasts and the data presented in this chapter also shows that both fibroblast populations are equally sensitive to IFNγ. Yet *in vivo,* only CD105- fibroblasts show expression of these proteins. Thus, factors specific to *in vivo* tumours likely drive differential MHCII and CD74 expression. For example, IFNγ may be getting produced locally by T or NK cells in contact with CD105- fibroblasts but, for some yet unexplained reason, these cells are not in contact with CD105+ fibroblasts. Analysis of the spatial distribution of both CD105-MHCII+CD74+ fibroblasts and IFNγ-producing lymphocytes in PDA tumours, using new highly-multiplexed imaging technologies such as CODEX, would allow for interrogation of this hypothesis (see Summary discussion). IFNγ acting on *Pdgfrb* expressing stromal cells has been demonstrated as a key driver for inducing tumour ischaemia and regression of large tumours and thus understanding the effects of this powerful cytokine on stromal cells will possibly reveal key processes relevant to anti-tumour immunity and tumour control (Kammertoens et al., 2017).

Because of the limited tools to study fibroblast function in tumours *in vivo*, much of the functional and mechanistic understanding of cancer-associated fibroblasts is inferred from *in vitro* model systems. How appropriate this is and how well *in vitro* systems model *in vivo* fibroblast function is not well understood (see Summary discussion). It is known for example, that simple *in vitro* expansion of fibroblasts, from many different tissues, progressively activates them towards a myofibroblast state, which is partly attributed to the mechano-sensing properties of fibroblasts (Ohlund et al., 2017). For example, the healthy pancreas is a relatively soft environment (typically 1 kPa, as measured by atomic force microscopy) and during PDA development a highly stiffened environment develops (typical reported average 4-6 kPa, typical range 2-50 kPa) (Itoh et al., 2016; Rubiano et al., 2018). Yet the plastic used for *in vitro* culture flasks is far stiffer even than this (100-1000 kPa) (Swift et al., 2013). Stiffness-dependant, feed-forward activation loops have also been shown to be responsible for keeping fibroblasts in an activated state, even when an initiating activating stimulus has been removed, and stiffness appears to play

an important role in sustaining many fibrotic disorders (Bonnans et al., 2014; Calvo et al., 2013; Laklai et al., 2016; Tschumperlin et al., 2018). Thus, the sensitivity of fibroblasts to mechano-activation as they move from a soft (~1 kPa) environment to a plastic flask (100 kPa+), may greatly hinder the interpretation of 2D *in vitro* fibroblast experiments, particularly when trying to preserve the so called 'quiescent' phenotype of fibroblasts isolated from non-tumour bearing organs and study subsequent activation/polarisation. It may be impossible to have an 'non-activated' fibroblast in standard 2D cultures. One method of addressing this, may be to use Matrigel-based 3D cultures, as Matrigel has a low stiffness of <1 kPa. It is not clear if such 3D systems are any better at representing *in vivo* fibroblast biology, or indeed if fibroblasts can even be sustained and expanded in such conditions.

In this chapter, I conducted multiple recombinant protein stimulations and measured signalling network responses through protein phosphorylation changes. Whilst the data produced is intriguing, these *in vitro* studies need to be interpreted with caution. For example, the signalling node response to TGFβ1 at 5 min was relatively weak, even though this concentration of ligand induces wide-spread gene expression changes after 6 h. A later time point may have been more revealing because SMAD phosphorylation is known to be a relatively slow signalling process, but such a late time point would likely have been inappropriate for many of the other stimulations. Thus, conducting time course experiments with the cell signalling and gene expression assays, may reveal important information about fibroblast activation dynamics missed by single time point experiments. For example, without such a time course analysis, peak-, delayed- and secondary/autocrine-responses may be completely missed or misinterpreted.

Even though the mass cytometry experiment described in this chapter maps just a fraction of all possible signalling nodes during fibroblast activation, it gives some insight into the complexity of cellular signalling processes to simple, single recombinant protein stimulations. *In vivo*, complex and changing mixtures of activating ligands contribute to defining cell differentiation, phenotypes and function. Thus, studying combinations of stimulating ligands may better model the complex activating conditions occurring *in vivo* and reveal synergies or dominant/conflicting interactions between different activating factors. How signalling networks interact with combinations of activating factors is starting to become more studied and better quantified and novel methods to measure

cell signalling at single cell resolution, such as mass cytometry, have the potential to make a major contribution to this area (Bodenmiller et al., 2012; Krishnaswamy et al., 2014).

When trying to model *in vivo* behaviour with *in vitro* assays, the concentration of activating ligands needs to be carefully considered. The concentrations of the ligands used in these studies were chosen by either selecting 10-fold the suppliers reported cell activity EC50, with the aim of saturating receptors, or by aligning the protein concentration to that used in the most cited papers in the literature to improve comparability (these values were typically also close to 10x cell activity EC50 anyway) (Ohlund et al., 2017). Clearly this could be improved by basing *in vitro* stimulation concentrations on the concentration of the ligands actually observed *in vivo* but there is a lack of systematic measurements of growth factors and cytokines across different tissues and tumours. Unfortunately, such information may not even be that informative: there is often unequal distribution of ligands in tissues and even soluble signalling mediators, such as PDGF and CSF1, show a dependence on secreting-cell and target-cell physical contact (Farin et al., 2016; Zhou et al., 2018). Thus, high local concentrations or cell-cell contact, may drive important phenotypes even when total concentration across a tissue is low. Another consideration that will likely impact the accuracy of *in vitro* activation assays is that large quantities of ligands can be actively removed from culture media, even within hours of recombinant protein dosing, by processes such as ligand-mediated endocytosis or neutralising binding-partners (Zhou et al., 2018). Interestingly, this constant ligand removal is required to set up stable cell-cell communication circuits, so may be an important feature *in vivo*, but can introduce problems when studying phenotypic changes after long term *in vitro* stimulations (Zhou et al., 2018). For example, the initiating ligand may possibly only be present during the first few hours of the experiment and may not be present at later time points when a phenotype/function is actually measured. Thus, care needs to be taken with interpretation of such *in vitro* stimulation results, because secondary responses, such as autocrine signalling initiated by the first signal, may be dominant by the time actual measurements are taken. Titrating the concentration of activating ligands and conducting time course experiments would likely greatly improve the insight generated by stimulation experiments but would require complex experimental designs and suffer from reduced throughput.

Chapter 8 – Results – Characterisation of *in vivo* functions of CD105+ and CD105- pancreatic fibroblasts

8.1 – Results

8.1.1 – A subcutaneous syngeneic co-transplant model indicates CD105+ are tumour permissive and CD105- fibroblasts are highly tumour suppressive *in vivo*

The characterisation studies presented in the previous chapter highlight many similarities and differences between CD105+ and CD105- fibroblasts with respect to the process of *in vitro* fibroblast activation. Fibroblasts have been implicated in several pro-tumourigenic functions, such as the ability to directly influence cancer cell proliferation and survival via paracrine signals and cancer cell invasion by direct cell contact, as well as altering tumour angiogenesis and inflammation (Sahai et al., 2020). Considering this complex array of potential functions, I was keen to study the *in vivo* functions of CD105+ and CD105- fibroblasts in PDA tumours, in an empirical manner. My aim was to try to identify the key functional differences this way (top-down approach), as opposed to selecting a specific *in vitro* phenotypic difference and trying to understand it's *in vivo* implications (bottom-up approach). I hoped this methodology would select for the strongest/dominant differences between CD105+ and CD105- fibroblasts and avoid the potential for spending time studying an interesting *in vitro* phenotypic difference, that has minimal functional relevance to PDA tumour biology *in vivo*. Because CD105+ and CD105- PDA fibroblasts have shown different associations with immune cell phenotypes in PDA tumours (Chapter 5), I was also keen to analyse the function of CD105+ and CD105- fibroblasts in syngeneic models with fully intact immune systems. This was made possible because I derived the CD105+ and CD105- pancreatic fibroblasts from the pancreas of inbred B6 mice and the KPC PDA cell line to be used was from a fully B6 backcrossed KPC mouse. Therefore, all cell types could be transplanted into B6 hosts without confounding issues of alloimmunity, for example to antigens within the MHC loci or other highly polymorphic loci.

I opted to use a subcutaneous co-transplant model. The main advantage of this model is the level of control over the cells that are transplanted. In addition, subcutaneous models are also higher throughput and more straightforward to monitor than orthotopic

tumours. Whilst it is possible that some dermal fibroblasts would infiltrate the growing subcutaneous tumours, IHC of growing tumours did not show obvious dermal fibroblast accumulation (see later). Thus the majority of the fibroblasts in the early, growing tumours would derive from those implanted along with the cancer cells. I also opted implant a 1:1 ratio of $1x10^5$ PDA cancer cells to $1x10^5$ fibroblasts. Histology of PDA tumours suggests that typically, fibroblasts outnumber cancer cells, so a 1:1 ratio likely represents an under-approximation of that seen in spontaneous tumours (importantly the actual *in situ* cancer cell:fibroblast ratio in PDA tumours has not been accurately quantified in any study to date). Despite this, I thought it was important not to inject large numbers of fibroblasts in the co-transplant conditions, as this may induce nutrient deprivation or cancer cell/fibroblast competition artefacts, that would not be present in the PDA mono-transplant condition and may confound comparisons between the mono-transplant and co-transplant conditions.

An important aspect of his experiment was to confirm CD105+ and CD105- fibroblast retention in the growing subcutaneous co-transplants. If fibroblasts were not retained in the growing tumour, no valid conclusions could be drawn regarding the functional impact of the CD105+ and CD105- fibroblasts on *in vivo* tumour growth. In addition, if no injected fibroblasts were retained, it would also suggest that many of the injected fibroblasts had died, which may itself act as an inflammatory stimulus which could also alter tumour growth. To test this, I labelled both CD105+ and CD105- fibroblasts with GFP, which could then be detected histologically with an anti-GFP antibody in FFPE samples. When PDA cells and fibroblasts are co-transplanted subcutaneously in PBS, after 7 days there are no GFP+ fibroblasts present in the growing mass of tumour cells (Figure 58). I think this may be due the large area over which PBS-injected cells spread after subcutaneous injection and hypothesised that injection in Matrigel (a basement membrane extract from murine sarcoma tumours that polymerises at >4 °C) may retain the cancer cells and fibroblasts in close proximity, as the early tumour establishes and grows. Indeed, large numbers of viable, GFP+ fibroblasts are observed in the co-transplant plugs of both CD105+ and CD105- fibroblasts at day 7 when injected in Matrigel. Healthy GFP+ fibroblasts are well represented in both the CD105+ and CD105- fibroblast co-transplant conditions and are seen embedded within the remaining Matrigel and in close contact with GFP- cancer cells and infiltrating immune and vascular cells (Figure 58). By day 30, at which most tumours were close to or had past threshold tumour volumes, no GFP+

fibroblasts were retained in the final tumours of any co-transplant conditions (Figure 58B). This suggests that the co-transplanted fibroblasts are only retained for a portion of the experiment, possibly outcompeted by the rapidly growing PDA cell line. A full time course would be needed to better understand the dynamics of fibroblast retention in this model. Thus, this Matrigel method appeared to be a useful approach for studying fibroblasts in growing tumours *in vivo*. It is interesting to note that multiple studies in the literature co-transplant cancer cells and fibroblasts in PBS (McDonald et al., 2015; Paauwe et al., 2018). These studies typically do not check for fibroblast retention and the results presented here suggest that PBS co-transplants will not retain fibroblasts in such settings (even at early time points) and may not be effective way to study cancer cell-fibroblast interactions *in vivo*.

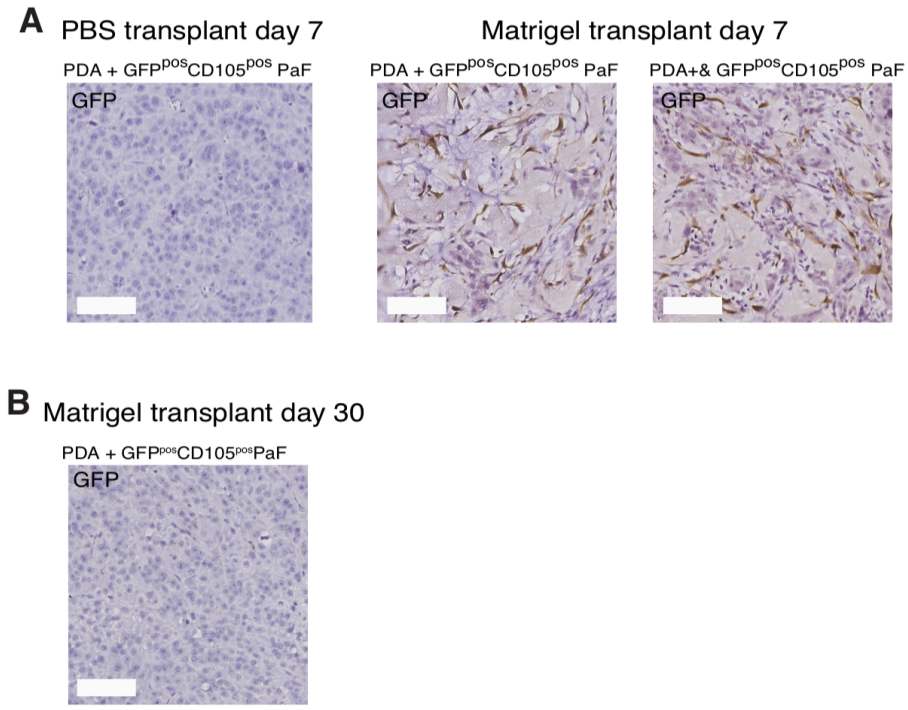

Figure 58. Development of a subcutaneous cancer cell and fibroblast co-transplant model
(A) Immunohistochemistry (IHC) of subcutaneous tumours from co-transplanted KPC PDA tumour cells and GFP+ pancreatic fibroblasts (PaFs) into syngeneic B6 mice. Stained with a GFP targeting antibody and Haematoxylin. No GFP+ fibroblasts are observed in the growing tumours after 7 days when the cells are injected in PBS but are highly abundant in growing tumours in which cells are injected in Matrigel. Scale bar = 80 μm. (B) No GFP+ fibroblasts are retained 30 days after KPC PDA tumour cells and GFP+ PaFs are co-transplanted.

When the KPC PDA cells were transplanted into B6 syngeneic hosts, steady growth is observed such that by day 20, tumour volume is 209±73 mm^3 (mean±standard error of the mean) (Figure 59). Co-transplant with a 1:1 ratio of CD105+ pancreatic fibroblasts

shows a trend for increasing tumour growth such that at day 20, tumour volume = 383±49 mm^3, although this does not reach statistical significance compared to the mono-transplant tumour volume. The most striking result was that with co-transplants containing KPC PDA cancer cells and CD105- pancreatic fibroblasts, a strong suppression of growth is observed, such that by day 20 the average tumour volume is just 57±18 mm^3. Remarkably, 2/5 mice from this condition showed no signs of residual tumour cells by the end of the experiment (day 34), macroscopically or histologically. Interestingly, a fourth condition, in which a 1:1 mixture of CD105+:CD105- fibroblasts was used (such that the total number of fibroblasts transplanted was the same as for the other co-transplant conditions), phenocopied the growth curve for the pure CD105- fibroblast co-transplant condition. This suggests that in 1:1 mixtures of fibroblasts, the growth suppressive phenotype of CD105- fibroblasts is dominant over the permissive effect of CD105+ fibroblasts. Notably, for this mixed transplant condition, all 5/5 mice had small but measurable tumours by the end of the study with no full tumour regressions. This permissive/suppressive phenotype was highly reproducible: by comparing the time it takes to reach a tumour volume of >400 mm^3, I was able to directly compare this study with three repeated studies in a Kaplan-Meir analysis (even though they had tumour volumes measured on different days). Across all four separate studies, there was a strong tumour suppressive effect seen when CD105- fibroblasts were co-transplanted with the cancer cells. Repeating the experiment with a second KPC PDA cell line (isolated independently, from a different KPC tumour), showed a similar pattern in that CD105+ fibroblast co-transplants were permissive to normal tumour growth (day 21 tumour volume = 323±32 mm^3) and CD105- fibroblast co-transplants were highly tumour suppressive (day 21 tumour volume = 83±22 mm^3). For this cell line, all 5/5 CD105- co-transplants had some minor evidence of residual tumour cells at the end of the study (day 30), albeit many conditions still showed extensive tumour control even at this late stage. The effect of the combined fibroblast co-transplant with this PDA cell line again showed a suppressive phenotype. Thus, in growing subcutaneous tumours from two different PDA cell lines, CD105+ pancreatic fibroblasts are tumour permissive and CD105-pancreatic fibroblasts are highly tumour suppressive, even when diluted by 50% with permissive CD105+ pancreatic fibroblasts.

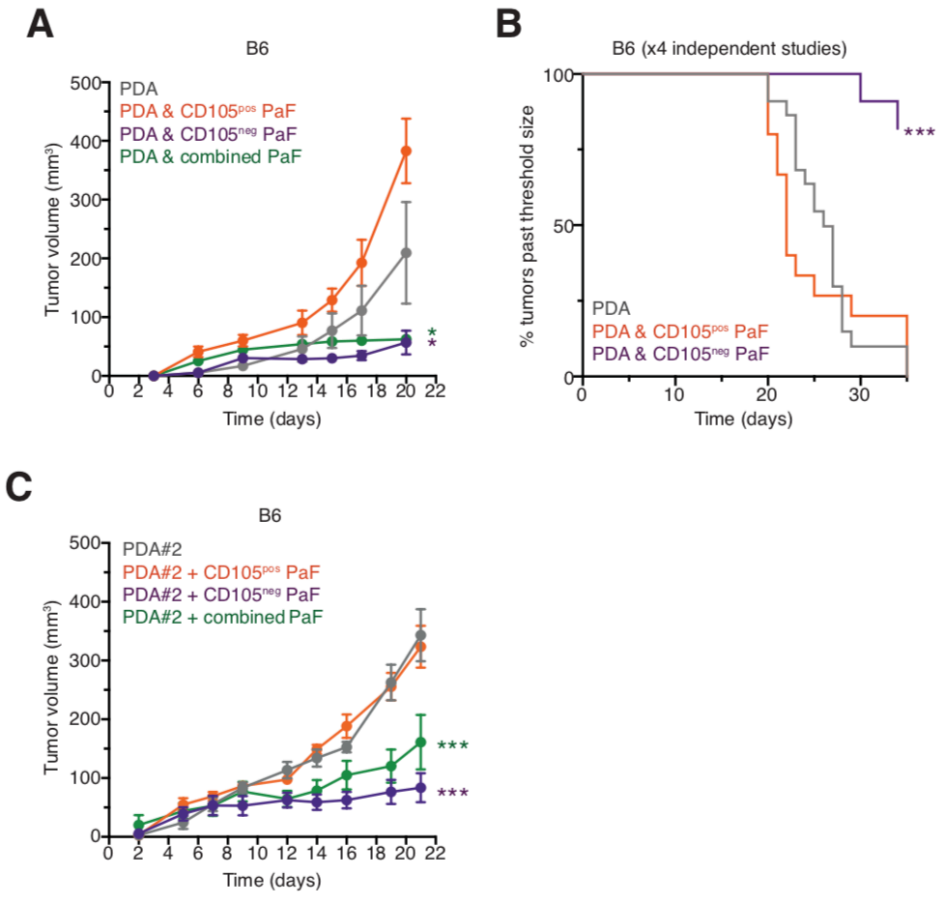

Figure 59. Fibroblast regulation of tumour growth in syngeneic hosts

A) Tumor growth of KPC PDA cells following subcutaneous transplantation of 10^5 PDA tumor cells or co-transplantation of 10^5 PDA tumors cells with 10^5 CD105+ or CD105- pancreatic fibroblasts (PaFs), into syngeneic B6 mice. n=5 mice per condition. Data is representative of n=4 separate experiments. For the combined condition a 1:1 mixture of CD105+:CD105- PaFs was used, such that the total number of co-transplanted PaFs remained constant. Data is displayed as mean tumor volumes+/-standard error of the mean. (B) Kaplan Meier analysis of the combined fraction of B6 mice from (A) and three other separate studies, exceeding a threshold tumor volume of 400 mm^3 (n=4 independent studies). (C) As for Figure (A) but using an alternative KPC PDA cell line, also derived from a fully B6 backcrossed mouse. Conditions are compared using 2-way ANOVA (A and C) and log rank test (B). *p<0.05, **p<0.01, ***p<0.001.

8.1.2 – Differential functions of CD105+ and CD105- pancreatic fibroblasts *in vivo* are dependent on adaptive immunity but not fibroblast MHCII antigen presentation

Experiments outlined in Chapter 6 and in this chapter had shown that CD105+ and CD105- PDA and pancreatic fibroblasts had differential expression of many genes and proteins known modulate immune cell function. In addition, the cross-correlation analysis of the KPC PDA TME (Chapter 5) had shown associations between the abundance of CD105+ or CD105- PDA fibroblasts and the abundance and phenotypes of several immune cell types, particularly those of CD4+ and CD8+ T cells. Therefore, I sought to

determine whether the striking difference of growth of CD105+ and CD105- co-transplants was due to differential interactions with the immune system. I thus repeated the previously described co-transplant experiment in 'NSG' mice. The inbred NOD background of these mice results in reduced functioning of the complement system, as well as reduced dendritic cell and macrophage function. The *Prkdc*^{scid} mutation results in defective non-homologous end joining (NHEJ) during V(D)J recombination, and therefore this model lacks mature T cells and B cell. Lastly, the homologous mutation in the common interleukin 2 receptor gamma chain, results in loss of signalling capacity of IL-2, IL-4, IL-7, IL-9 and IL-15, with a wide range of effects, most importantly blockade of NK cell development. Thus, NSG mice are highly immunodeficient (to the degree that human cells can be successfully grafted). Repeating the subcutaneous co-transplant experiment in NSG mice showed that the differential permissive/suppressive effect seen in the immunocompetent B6 hosts is completely lost in hosts with major defects in innate and adaptive immunity, such that all conditions grow at the same rate with no significant difference at any time point (Figure 60).

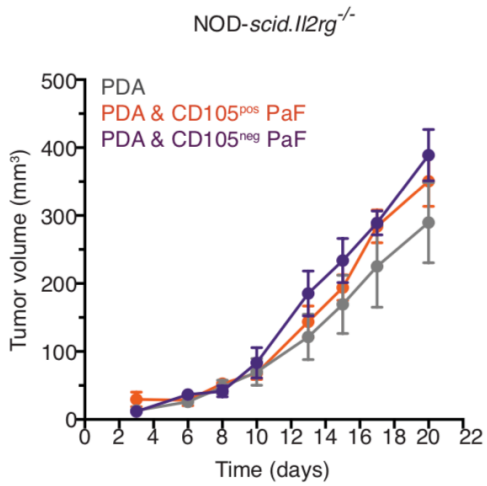

Figure 60. Fibroblast regulation of tumour growth in NSG mice
Tumor growth of KPC PDA cells following subcutaneous transplantation of 10^5 PDA tumor cells or co-transplantation of 10^5 PDA tumors cells with 10^5 CD105+ or CD105- pancreatic fibroblasts (PaFs), into NOD-scid.Il2rg-/- mice (n=4 to 5 per condition). Data is displayed as mean tumor volumes+/-standard error of the mean. Conditions are compared using 2-way ANOVA. *p<0.05, **p<0.01, ***p<0.001.

NSG mice have a large number of defects in myeloid and lymphocyte compartments and I sought to narrow down what aspect of tumour immunity and/or inflammation was being modulated to result in the permissive/suppressive phenotype seen in B6 hosts. To achieve this, I first repeated the subcutaneous co-transplant experiment in B6.*Rag1*$^{-/-}$ hosts (Mombaerts et al., 1992). These mice also have defective V(D)J recombination of

T cell receptor and immunoglobulin genes and lack mature T and B cells but have no direct defects in myeloid or NK cell development and function. In *Rag*$^{-/-}$ hosts, all conditions grew at the same rate (Figure 61), suggesting that the difference in the permissive and suppressive effects of CD105+ and CD105- fibroblasts, is mediated enitrely by adaptive immunity (that is T or B cell-mediated immunity). Interestingly, across all conditions, growth in *Rag1*$^{-/-}$ mice showed a more exponential character than in NSG mice, potentially suggesting that some aspects of innate immunity, that are defective in NSG mice, contribute to increased tumour growth in *Rag1*$^{-/-}$ mice.

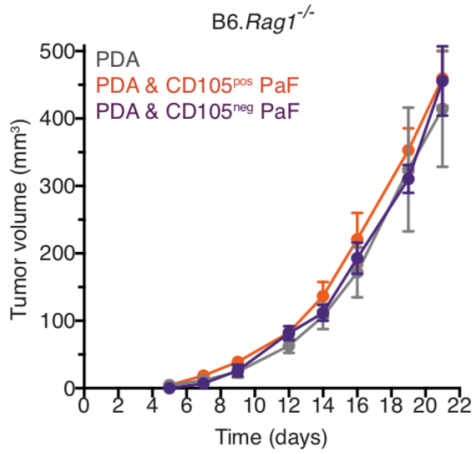

Figure 61. Fibroblast regulation of tumour growth in Rag1 mice
Tumor growth of KPC PDA cells following subcutaneous transplantation of 10^5 PDA tumor cells or co-transplantation of 10^5 PDA tumors cells with 10^5 CD105+ or CD105- pancreatic fibroblasts (PaFs), into B6.Rag1-/- mice (n=6 per condition). Data is displayed as mean tumor volumes+/-standard error of the mean. Conditions are compared using 2-way ANOVA. *p<0.05, **p<0.01, ***p<0.001.

B6.*Batf3-/-* mice lack the transcription factor BATF3 (Hildner et al., 2008) and have defective development of cDC1s, a DC subset of transcriptionally- and functionally-related CD8a+ DCs in lymphoid organs and CD103+ DCs in tissues, which can eb collectively identified by the chemokine receptor XCR1. cDC1s are a relatively rare cell type but are highly specialised in cross-presentation, a unique process in which MHCI-restricted antigens collected from cell corpses are delivered to DC endosomes, via the C-type lectin DNGR-1, and presented to naïve CD8+ T cells. Loss of cDC1s in *Batf3-/-* mice results in a greatly reduced ability to prime *de novo* CD8+ T cell responses to non-self microbial or cancer antigens. Repeating the co-transplant experiment in *Batf3-/-* hosts showed that the majority of the suppressive effect and long-term tumour control seen in the CD105- fibroblast co-transplant conditions, was lost when cDC1s were absent and CD8+ T cell priming was limited (Figure 62). Interestingly, despite loss of

tumour control, there was still a minor but statistically significant reduction in tumour growth in the CD105- fibroblast co-transplant condition compared to the mono-transplant condition. Thus, CD8+ T cell-mediated priming is required for the full anti-tumour effect of CD105- fibroblasts, however additional mechanisms of adaptive immune control may also be occurring in B6 hosts, for example CD4+ T cell-mediated immunity. In this context, there are caveats with the *Batf3-/-* model that need to be considered (see discussion).

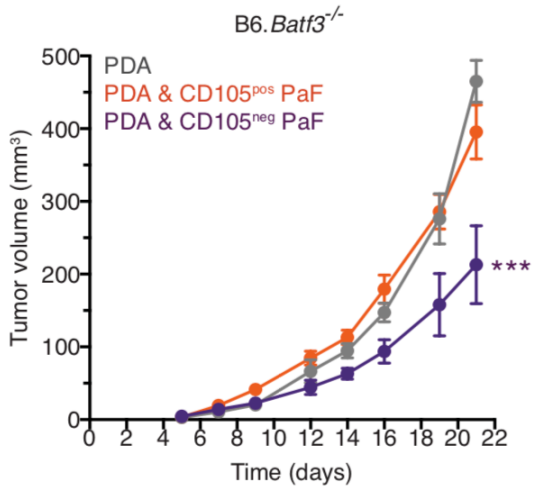

Figure 62. Fibroblast regulation of tumour growth in Batf3 mice
Tumor growth of KPC PDA cells following subcutaneous transplantation of 10^5 PDA tumor cells or co-transplantation of 10^5 PDA tumors cells with 10^5 CD105+ or CD105- pancreatic fibroblasts (PaFs), into B6.Batf3-/- mice (n=8-9 per condition). Data is displayed as mean tumor volumes+/-standard error of the mean. Conditions are compared using 2-way ANOVA. *p<0.05, **p<0.01, ***p<0.001.

The fibroblasts used in this experiment are GFP+ (which allows confirmation of their presence in tumours) and it is possible that this contributes to immunogenicity of these co-transplanted cells. I repeated the experiment (with PDA cell line #2) and parental GFP- fibroblasts cells and the same permissive/suppressive phenotype is observed. Thus, GFP antigens do not contribute to the distinct permissive and suppressive effects of CD105+ and CD105- fibroblasts.

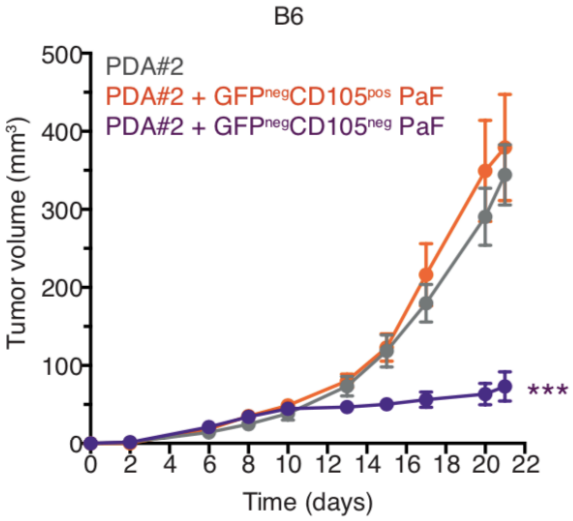

Figure 63. Fibroblast regulation of tumour growth, with no fibroblast GFP expression
Tumour growth of KPC PDA cells following subcutaneous transplantation of 10^5 PDA tumour cell lines or co-transplantation of 10^5 PDA tumour cells with 10^5 CD105+ or CD105- pancreatic fibroblasts (PaFs) lacking GFP expression, into syngeneic B6 mice. n=5 mice per condition. Data is displayed as mean tumor volumes+/-standard error of the mean. Conditions are compared using 2-way ANOVA. *p<0.05, **p<0.01, ***p<0.001.

CD105 expression is obviously one of the defining features of CD105+ and CD105- fibroblasts and the CD105 protein itself contributes to approximately half of the early sensitivity to TGFβ1 (chapter 7). Because TGFβ1 is a key fibroblast activator and I see such a striking *in vivo* phenotype in CD105- fibroblasts, I was keen to test whether the divergent phenotypes of CD105+ and CD105- fibroblasts in the subcutaneous co-transplant model are dependent on the presence or absence of CD105 expression itself, respectively. CD105+ parental fibroblasts in which CD105 was knocked out using CRISPR/Cas-9 (previous chapter) were used. The same parental line, transfected with Cas-9 and a pair of non-targeting (NT) gRNAs as control cells were used for the control condition. These cells were each co-transplanted with PDA cancer cells following the same subcutaneous method as before, into immune competent B6 hosts. As can be seen in Figure 64, the two co-transplant conditions grow at the same rate with no significant difference in tumour volume at any time point. Therefore, CD105+ fibroblasts cannot be made to become tumour suppressive by loss of CD105. Thus, CD105 protein serves as a very useful marker of different fibroblast lineages in PDA tumours (and the healthy pancreas) and increases sensitivity to TGFβ1 signalling *in vitro* but it is not centrally important to the permissive/suppressive phenotype observed *in vivo*.

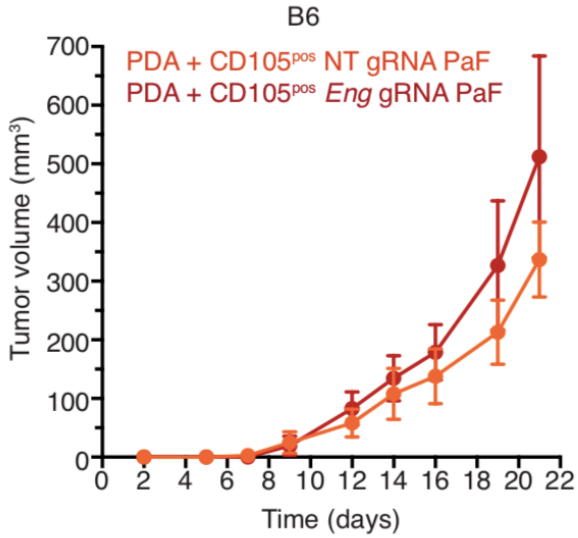

Figure 64. Fibroblast regulation of tumour growth, with no fibroblast GFP expression
Tumour growth of KPC PDA cells following subcutaneous co-transplantation of 10^5 PDA tumour cells with 10^5 CD105+ pancreatic fibroblasts (PaFs) into syngeneic B6 mice. CD105+ PaFs with *Eng* gene disrupted by CRISPR/Cas-9 gene editing are compared to CD105+ PaFs transfected with non-targeting (NT) gRNAs. n=5 mice per condition. Data is displayed as mean tumor volumes+/-standard error of the mean. Conditions are compared using 2-way ANOVA. *p<0.05, **p<0.01, ***p<0.001.

A consistent observation seen in PDA tumours was the high expression of proteins involved in MHCII antigen presentation specifically within CD105- PDA fibroblasts, with very little expression seen in CD105+ PDA fibroblasts. This was despite the fact that *in vitro* both populations have the capacity to express these proteins (Chapter 6). Because the suppressive effect seen in the subcutaneous co-transplant model was dependant on adaptive immunity and MHCII-restricted antigen presentation is centrally important to effective functioning of adaptive immunity, I aimed to test whether the suppressive effect seen in the CD105- fibroblast co-transplants was dependant on MHCII-restricted antigen presentation. I used CRISPR/Cas-9 to delete *H2Ab1* (the beta chain gene of the MHCII loci of B6 strain) and *Cd74* (the invariant chain required for MHCII protein stabilisation and transport) in CD105- fibroblasts to determine if they play a role in the highly suppressive effect seen in immunocompetent hosts. CD105- fibroblasts trasnfected with a pair of NT gRNAs was used as the control. Neither MHCII or CD74 are expressed in these cells under steady-state *in vitro* culture conditions, so I performed knockout validation of extracellular MHCII and intracellular CD74 protein by stimulating a culture of these cells with IFNγ. Gene editing was successful for both (Figure 65). Importantly, the CRISPR/Cas-9 method used was based on a triple gRNA system that favours large (>50bp) genomic deletions rather than small indels, resulting in high knockout effectivity

(typically >95%) without selection. The lack of selection requirement here is important because I would not have been able to FACS isolate knock out cells without prior IFNγ stimulation, an activating process which would likely change their properties regardless of successful gene editing. The large genomic deletions caused by this method, typically stop all gene transcription/translation but even if a gene is still able to be transcribed/translated, it will be in the form of a largely truncated and likely dysfunctional protein. Indeed, the fact that robust anti-MHCII and anti-CD74 antibodies fail to detect these protein products suggests either successful gene deletion or a largely altered protein. Collectively this made me confident that these targets had been sufficiently knocked out.

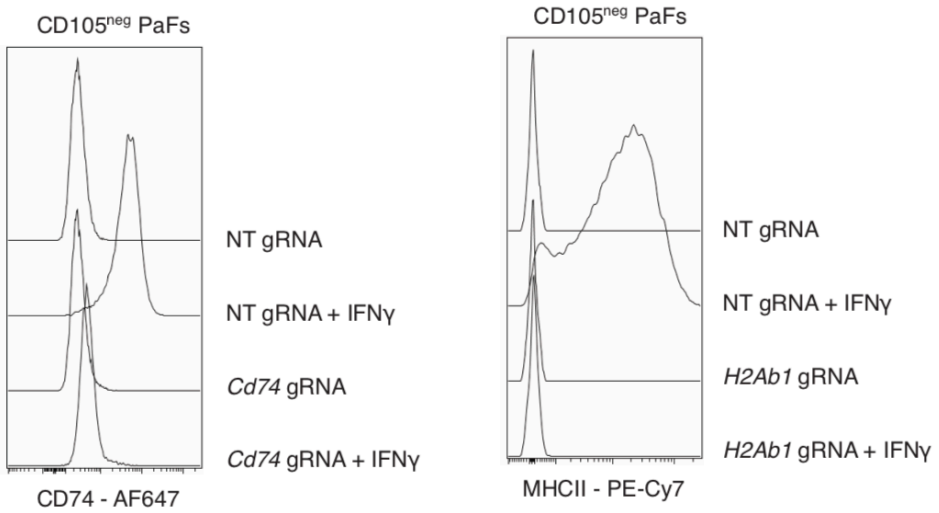

Figure 65. Validation of gene knockouts in CD105- pancreatic fibroblasts (PaFs) by CRISPR/Cas-9 gene editing

Flow cytometry validation of CD74 (left) and MHCII (right) knock out in CD105- PaFs by CRISPR/Cas-9 gene editing. Protein expression was induced by 3 day treatment with IFNγ. Intracellular CD74 and surface MHCII measured.

Repeating the co-transplant experiment in B6 hosts demonstrated that all co-transplants with CD105- fibroblasts still showed an equally suppressive phenotype, regardless if *H2Ab1* or *Cd74* had been deleted (Figure 66). Thus, this data suggests that fibroblast MHCII-mediated antigen presentation plays no role in the suppressive phenotype of CD105- fibroblasts *in vivo*.

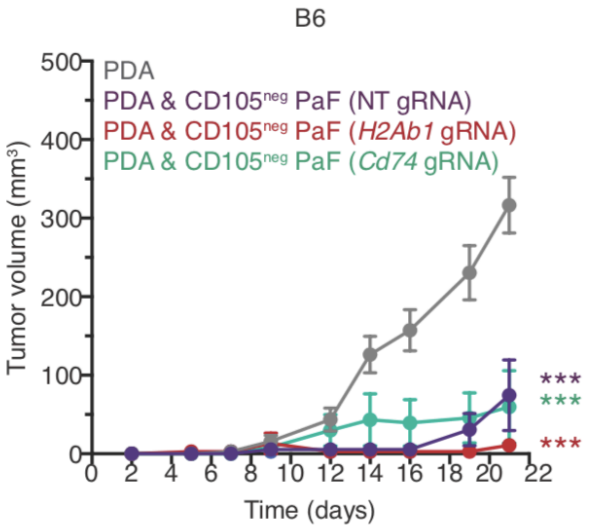

Figure 66. Fibroblast regulation of tumour growth with loss of fibroblast MHCII antigen presentation

Tumour growth of KPC PDA cells following subcutaneous co-transplantation of 10^5 PDA tumour cells with 10^5 CD105- pancreatic fibroblasts (PaFs) into syngeneic B6 mice. CD105- PaFs with *H2Ab1* and *Cd74* gene disrupted by CRISPR/Cas-9 gene editing are compared to CD105- PaFs transfected with non-targeting (NT) gRNAs. n=5 mice per condition. Data is displayed as mean tumor volumes+/-standard error of the mean. Conditions are compared using 2-way ANOVA. *p<0.05, **p<0.01, ***p<0.001.

8.2 – Summary

In a syngeneic subcutaneous co-transplant model, CD105+ pancreatic fibroblasts are fully permissive to tumour growth whereas CD105- pancreatic fibroblasts are highly tumour restrictive in a manner entirely dependent on adaptive immunity. This enhancement of anti-tumour immunity and tumour control with CD105- fibroblasts is independent of fibroblast MHCII-restricted antigen presentation and independent of CD105 status.

8.3– Discussion

The results presented in this chapter demonstrate that in a syngeneic host, subcutaneous co-transplants of CD105+ and CD105- fibroblasts show distinct functions: CD105+ pancreatic fibroblasts are fully tumour permissive and do not alter tumour growth in this setting, CD105- pancreatic fibroblasts are highly tumour suppressive, to the point that complete tumour regressions are observed and 1:1 mixtures of both fibroblasts have a net tumour suppressive effect. The differential permissive/suppressive effect is entirely dependent on adaptive immunity with a major contribution from CD8+ T

cell-mediated immunity. Recent scRNAseq analysis of KPC tumours has suggested extensive transcriptional fibroblast heterogeneity in murine PDA tumours (Dominguez et al., 2020; Elyada et al., 2019). Notably, these studies do not isolate different fibroblast populations to assess the stability of these differences and to define lineage vs phenotype differences. Importantly, whilst such studies give an incredibly detailed snapshot of the transcriptomic heterogeneity present in fibroblasts in tumours they do not define key functional differences between fibroblast populations, for which live cell isolation is required. Thus, in the absence of methods for *in vivo* fibroblast manipulation (see Summary discussion), isolating distinct fibroblast populations is an important way to better understand fibroblast function.

A key result presented here, is that of the equal growth rates seen in *Rag1-/-* hosts. This result suggests that when no adaptive immunity is present, there is no growth advantage or disadvantage to these KPC PDA tumour cells from either pancreatic fibroblast population. Many non-immunogenic fibroblast functions are reported to play a pro-tumourigenic role in fibroblast-mediated regulation of tumour growth, such as altered paracrine signalling, altered angiogenesis, or altered cancer cell migration (Erdogan et al., 2017; Kalluri, 2016; Sahai et al., 2020; Shi et al., 2019; Tape et al., 2016). Most of these studies report a pro-tumourigenic impact on cancer cells, yet the equal growth in the *Rag1*$^{-/-}$ hosts presented here demonstrates that in the absence of adaptive immunity, both fibroblast populations minimally contribute to tumour growth. It may be that fibroblasts need more time to be 'educated' by tumour cells to become 'cancer-associated fibroblasts' or pro-tumourigenic features have to be selected by evolution of the microenvironment over long periods of time. However, it is notable that many of the studies that suggest fibroblasts have pro-tumourigenic properties are conducted *in vitro* or *in vivo* in immune-deficient hosts (Somerville et al., 2020). The results presented here suggest that interactions between PDA fibroblasts and adaptive immunity are dominant over other other non-immunogenic interactions and thus *in vitro* and immune incompetent *in vivo* model systems will not capture these important effects. Indeed, in support of this, seminal research using transgenic mouse models of PDA, in which PDA fibroblasts are depleted *in situ*, show that fibroblast depletion actually results in accelerated tumour progression and that PDA fibroblasts have a net tumour-suppressive effect (Lee et al., 2014a; Ozdemir et al., 2014; Rhim et al., 2014). The results in those studies closely align with the findings presented in this thesis. Interestingly, two of these

studies also report a greatly altered immune infiltrate in the fibroblast-depleted tumours, which also aligns with the data presented in this thesis, that suggests fibroblasts have the potential to directly regulate immune cell abundance and phenotype. Further work studying the detailed mechanisms of fibroblast-immune cell interactions will likely lead to a more complete appreciation of the key factors that dictate whether a fibroblast is tumour-promoting or tumour-restrictive in a fully immune competent host. In conclusion, the regulation of inflammation and immunity by distinct fibroblast lineages should to be considered when making judgments about the relative pro- and anti-tumour effects of fibroblasts and syngeneic models used where possible.

The differential permissive/suppressive result described here is very striking but raises two important questions:

1) Do the subcutaneous co-transplant model described here, recapitulate what occurs in spontaneous mouse PDA tumours?
2) Do the fibroblast-mediated processes in the tumours of various murine models of PDA (subcutaneous or spontaneous), recapitulate what actually occurs in human PDA?

The second question will be covered in more detail in the Summary Discussion chapter. With respect to the first question, this subcutaneous model is certainly a very artificial system, as are most subcutaneous tumour transplants. One of the limitations of such co-transplant tumour models for studying fibroblasts generally, is that fibroblasts tend to be lost from the growing tumour and therefore the time they have to exert an influence over the microenvironment is limited. Importantly, during optimisation GFP+ CD105+ and CD105- fibroblasts are both found retained in the Matrigel plugs to a similar extent by day 7. Thus, differences in CD105+ and CD105- fibroblast survival during the cell preparation and transplant likely do not account for the differential effect on tumour growth. Fibroblasts are retained in the transplants for at least 7 days but are not present in the end stage tumours at day 30. A full time course would be needed to better characterise the duration of retention for each fibroblast population. Therefore, it appears that the majority of the effect of the fibroblast populations occurs within the initial period of the study and the later time point measurements are most likely ‘outgrowth’ of changes that occur in these early stages. Finding conditions that enable longer fibroblast retention may allow for a better understanding of fibroblast function in more advanced tumours.

For example, CD105+ fibroblasts in these studies show a neutral net effect on tumour growth: they neither promote or restrict tumour growth, even in fully immune competent mice. Yet they may have an important phenotype in late stage tumours which cannot be accurately modelled with subcutaneous co-transplants. This may be particularly relevant to this study because the fibroblasts used are derived from a naïve, non-tumour bearing pancreas and may need extended contact with (or 'education' by) PDA cancer cells to induce phenotypes more relevant to those seen in spontaneous PDA tumours, which develop over a period of months.

Why cancer cells outgrow fibroblasts in co-transplant models, yet do not do so in spontaneous tumours is not clear. One possible reason is that the KPC PDA cell lines used here are highly aggressive. The cells have been extensively passaged *in vitro*, which would have resulted in rapidly growing clones being selected over a long period of time. Such 2D *in vitro* expanded KPC cell lines are able to effectively form rapidly growing subcutaneous tumours, even when very low numbers of cells are injected: injections of 100 cells can form tumours. Interestingly, this highly aggressive phenotype and lack of dependence on survival signals from the microenvironment, is not a property typically shared with freshly isolated human PDA cells, which can often be challenging to expand as homogenous 2D *in vitro* cultures (Baker et al., 2016). If the KPC PDA cells have become largely independent of survival factors supplied by the microenvironment, the aggressive nature of these murine PDA cells may be masking any pro-tumourigenic functions of fibroblasts that may be important in spontaneous tumours. In other words, KPC PDA cells appear to grow extremely efficiently on their own, so it is unlikely we will see an additional growth advantage from pro-tumourigenic fibroblast functions. In addition, KPC cell lines grown *in vitro* are typically more mesenchymal than tumour cells observed in human PDA and may be less dependent on paracrine factors from the microenvironment required to sustain epithelial growth. Mesenchymal cancer cells are also more invasive than epithelial cells and so these cell lines may be less dependent on 'collective invasion' that has been described for cancer cells and fibroblasts (Brabletz et al., 2018; Labernadie et al., 2017). Using murine PDA cells that more closely recapitulate human PDA cells, will be an important improvement to the model. In this regard, tumour organoids have been proposed to preserve more features of the original tumour (including genetic heterogeneity), better mimic the *in vivo* growth patterns of PDA tumours and induce a less altered phenotype with extended passaging (Baker et al.,

2016; Baker et al., 2019; Tiriac et al., 2019; Tuveson and Clevers, 2019). An important difference between 2D and 3D organoid cell lines is that 3D organoid cell lines are passaged in Matrigel, which avoids cells contacting the stiff surface of plastic, which can alter cancer cells through similar mechano-sensing pathways as in fibroblasts (e.g. high levels of Hippo- and FAK-pathway signalling) (Calvo et al., 2013; Sulzmaier et al., 2014). Thus, co-transplanting syngeneic mouse PDA organoids and fibroblasts, may preserve the ability to study the system in the context of a full immune system but better mimic spontaneous PDA growth rates, extend cancer cell/fibroblast interactions in the transplants and more accurately model fibroblast pro- and anti-tumourigenic functions.

There are other potential issues with the subcutaneous model to consider, particularly because the phenotype observed is related to activation of the immune system. In this model, the cells have to be injected in Matrigel to retain cancer cells and fibroblasts together. Matrigel is a complex extract from Engelbreth-Holm-Swarm (EHS) mouse sacroma tumours and contains predominantly basement membrane proteins, such as laminins, collagen IV, fibronectin and hepran sulfate proetoglycans but also many other less characterised proteins (Hughes et al., 2010). It is widely used for a variety of *in vitro* culture experiments, as well as implanting cells into immune-deficient and immune-competent murine hosts (Benton et al., 2011; Ogura et al., 2017). The growth factor-reduced version of Matrigel is used in the subcutaneous model to limit the introduction of activating factors into the transplants. Whilst Matrigel is of mouse origin, the spontaneous tumour cells used to generate the protein mix, are on a ST/Eh background (Hayashi et al., 2004). Thus, when implanted into B6 mice it is possible that some of the Matrigel components will elicit a humoral or cell-based immune reaction. Clearly, this would be the same for all conditions, so it is hard to envisage how this would contribute to the differential subcutaneous growth observed but may, for example, introduce unrealistic levels of inflammation. Indeed, recognition of dead cell debris or damage-associated molecular patterns (DAMPs) may explain the large influx of macrophages that are known to occur within Matrigel plugs *in vivo* (Ogura et al., 2017). Another issue with Matrigel is that its composition is poorly defined and variable, such that there is known lot to lot variation in properties (Serban and Prestwich, 2008). In this regard, during optimisation of these studies two different Matrigel lots were used, that had no appreciable differences in *in vivo* growth patterns. An alternative to Matrigel could be to use synthetic matrices. Such matrix technology has improved greatly in recent years and

may offer a better alternative to Matrigel (Jenkins and Little, 2019; Silva and Mooney, 2004). Synthetic matrix components do not need to be generated in living mice and will reduce animal usage in line with the 3Rs ethical framework (The 3Rs, 2020). Also, synthetic components can be selected to have minimal immunogenicity and can be better defined for consistency across batches. Lastly, the matrix composition can be chemically tuned for desired properties that may support prolonged fibroblast growth and extend cancer cell-fibroblast interactions, such as altered stiffness or the inclusion of specific peptide sequences for improved adhesion or degradative properties.

Another potential confounding issue with the subcutaneous co-transplant model is that the fibroblasts used in these studies are immortalised to generate stably growing cell lines. Primary fibroblasts begin to senescence after relatively few passages *in vitro* and show distinct phases of growth and quiescence, that makes them incompatible with large studies where phenotypic consistency is important. Primary fibroblasts also tend to survive poorly with repeated standard manipulations, such as cell culture splitting and cryogenic storage and often show altered growth patterns after such stresses. Thus, immortalisation is required to enable FACS purification and expansion of fibroblast populations to sufficient numbers for comparative functional experiments. In addition, immortalization improves cell viability, an important consideration for *in vivo* co-transplant experiments: implanting variable mixtures of live/dead cells would likely generate an immunogenic phenotype not specifically related to any fibroblast function. To immortalize the fibroblasts used in these studies, I used retroviral transduction to induce stable expression of the S40 large T antigen (SV40LT), a hexamer protein that perturbs RB and P53 protein functions, favouring cell cycle progression and enhancing cell survival (Ahuja et al., 2005; DeCaprio et al., 1988). Both CD105+ and CD105- fibroblasts were isolated from the same B6 pancreas, immortalized with the same retroviral-containing supernatant, for the same transduction duration and selected and passaged in exactly the same way. Thus, it is difficult to conceive why immortalized CD105- fibroblasts would be immunogenic *in vivo* because of immortalization, whereas CD105+ fibroblasts are not. Both populations express MHC class I to the same level (Chapter 6) and thus would be expected to present any SV40LT MHCI-restricted epitopes to a similar extent. I initially thought expression of SV40LT antigens, combined with the increased expression of MHCII we observe on CD105- fibroblasts (Chapter 4), was one possible reason for different *in vivo* behaviour but fibroblast MCHII was later

shown not to contribute to any of the suppressive phenotype of CD105- fibroblasts (this chapter). Generation of fibroblast cell lines using a different immortalisation method (e.g. E6/E7 immortalisation) and applying them in the same co-transplant experiment, would give additional confidence that epitopes of the SV40LT antigen are not contributing to any immunogenicity of CD105- fibroblasts, although this would be introducing other potential viral epitopes to the cells. The only way to fully remove confounding issues of working with primary cells or having to use immortalisation methods, would be to work with endogenous fibroblasts, ideally *in situ* manipulations thorough genetic methods. Appropriate transgenic models to effectively manipulate fibroblasts in tumours with sufficient precision are not currently available (see Summary discussion).

Related to the potential immunogenicity of SV40LT, differential expression of a GFP antigen could potentially induce immunogenicity *in vivo*. This again was unlikely: both CD105+ and CD105- fibroblasts were transduced with the same lentiviral-containing supernatant and express the same levels of GFP protein, as measured by flow cytometry. The recently developed GFP-targeting 'JEDI' TCR CD8+ T cell system does indeed demonstrate that GFP epitopes can be targeted by T cells, but the known epitope is H2Kd-restricted and there are no known H2Kb-restricted GFP epitopes which would be relevant to the B6 mice-derived cells used here. Consistent with this, co-transplantation of CD105+ and CD105- fibroblasts with no GFP expression, into B6 hosts, shows the same growth permissive and suppressive phenotype respectively, as the GFP-expressing versions, formally excluding GFP as the driving immunogenic factor.

The artificial nature of the subcutaneous co-transplant model is also one of the strengths of the system. Firstly, it removes confounding issues of infiltration of other pancreatic fibroblasts into the growing tumour that would likely occur with orthotopic transplants to the pancreas. Whilst I cannot exclude a contribution from dermal fibroblast infiltration, IHC analysis of the tumours shows no obvious GFP- fibroblasts present at early or late time points (day 30 tumours are mostly tumour cells). The model also allowed me to make methodical changes to the system and explore their impact, for example co-transplanting pure populations of fibroblasts (CD105+ or CD105-), defined ratios of mixed fibroblasts, or using fibroblasts with specific genes deleted. In addition, the experiment is easily repeated in a variety of different transgenic hosts that for example, lack certain components of the immune system. This versatility could be further exploited

to better understand the mechanisms of immune regulation in the future. Unfortunately, such controlled fibroblast manipulation is simply not possible with current spontaneous tumour models. In a general sense, the subcutaneous co-transplant model effectively allows for the mixing of cancer cells and populations of fibroblasts, encourage close interactions, including cell-cell contact and measure what happens when this system is exposed to the demands of a growing tumour *in vivo*, such as requirements for blood vessel formation, invasive front contact with the host and interactions with an intact immune system.

Two separate PDA cancer cell lines were used in the subcutaneous co-transplant model. The permissive and suppressive effect of co-transplanted CD015+ and CD105- fibroblasts, respectively, was observed with both PDA cell lines. Notably, the extent of CD105- fibroblast-mediated suppression was greater for PDA cell line #1, which had more sustained growth suppression and 2/5 mice showing full rejections, compared to PDA cell line #2 which had no full rejections. In addition, the 1:1 mixture of CD105+:CD105- fibroblast condition with PDA cell line #1 showed a fully suppressive phenotype where the same condition with PDA cancer cell line #2 showed a more intermediate phenotype with increased growth. Thus, the permissive/suppressive phenotype is not simply specific to PDA cell line #1 but the strength of suppressive effect is dependent on the identity of the cancer cell line. The reasons why the two PDA cancer cell lines behave slightly differently is not clear. One potential reason is that the two cell lines may have different levels of antigenicity for adaptive immunity to act on. An interesting future experiment would be to repeat the co-transplants experiment with a wide range of PDA cancer cell lines. Indeed, finding groups of cell lines with either high or low levels of suppression due to co-transplanted CD105- fibroblasts, may provide clues as to the specific mechanism driving the suppressive phenotype.

The cases of full tumour rejections with the CD105- fibroblast co-transplants in B6 hosts, are quite remarkable, particularly consider the aggressive growth behaviour of the PDA cancer cells used and that large numbers of PDA cancer cells (10^5) that are injected into the mice. It is possible that a minority of cancer cells survive in these mice (and that with enough time tumours would have grown out), but macroscopic dissection and histologic analysis of the injection site shows no evidence of residual cancer cells. Full immune-mediated rejection is suggestive of immunological memory and it would be interesting to

test if this was occurring by re-challenging the tumour-free mice with a bolus of the same cancer cells.

The loss of the CD105- fibroblast suppressive phenotype in *Rag1-/-* hosts demonstrates the mechanism is entirely dependent on adaptive immunity, which could include contributions from T or B lymphocytes. Whilst the majority of the phenotype is lost in *Batf3-/-* mice (which suggests that the sustained tumour suppression of CD105- fibroblasts is CD8+ T cell dependant), there is still some growth suppression observed. Therefore, these experiments do not fully exclude the possibility of contributions from mature CD4+ T cells or even B cells. Repeating the co-transplant experiments in B6 mice treated with depleting antibodies targeting CD4+ and CD8+ T cells would formally test the dependence of the mechanism on each T cell compartment and also formally rule out a role of B cells.

As mentioned, the fully suppressive phenotype of CD105- fibroblasts is lost in *Batf3-/-* mice but some tumour suppression is still observed, which results in the CD105- fibroblast co-transplant condition growing slower than the mono-transplant and CD105+ fibroblast co-transplant condition. This implies that adaptive immune mechanisms outside of CD8+ T cell-mediated tumour control are contributing. However, the *Batf3-/-* model is not a perfect model for cDC1 deletion: inflammatory conditions (such as IL12 expression) can cause expression of *Batf* and *Batf2* in DC progenitors, which compensates for the loss of *Batf3* and allows for cDC1 formation and *de novo* CD8+ T cell priming (Grajales-Reyes et al., 2015; Hildner et al., 2008). Thus, an ongoing inflammatory reaction in the cell/Matrigel transplants may allow for cDC1 formation and some level of CD8+ T cell priming, which would suppress growth just as for the B6 hosts. A new model of cDC1 depletion, which removes an IRF8 enhancer sequence, is resistant to such genetic compensation (Durai et al., 2019) and would allow for formal proof of the requirement for cDC1 cross-presentation in the tumour suppressive phenotype of CD105- fibroblasts.

Whilst the 1:1 CD105+:CD105- fibroblast co-transplant condition recapitulated the suppressive effect seen with the pure CD105- fibroblast co-transplant conditions, no full tumour rejections were observed, indicating that adding CD105+ fibroblasts dilutes the suppressive phenotype of CD105- fibroblasts to some extent. In tumours the ratio of

CD105+:CD105- fibroblasts varies widely (e.g. Chapter 4) and it would be informative to see what the impact is of varying the CD105+:CD105- fibroblast ratio in the co-transplant model.

For the co-transplant models, I also used a 1:1 mixture of cancer cells:fibroblasts. PDA tumours appear to have a higher abundance of fibroblast-like cells to epithelial cancer cells by histological methods and it may be revealing to test different ratios of cancer cells and fibroblasts in the co-transplant model, to see if new phenotypes emerge. The histological analysis of cancer cell:fibroblast ratios in PDA tumours is complicated by the different morphologies and cell sizes of these cell types and the presence and absence of cancer cells that have undergone EMT. Thus, there is little consensus on what the 'average' cancer cell:fibroblast ratio is in human PDA tumours, or indeed what range of ratios is typically observed. In addition, there may be a limit to how many fibroblasts can be co-transplanted in this model before confounding issues of nutrient competition with cancer cells occur.

CD105+ fibroblasts with CD105 genetically deleted by CRISPR/Cas-9 technology, show the same *in vivo* growth characteristic as CD105+ fibroblasts. Thus, CD105 is not required for the permissive fibroblast state of CD105+ fibroblasts. This also suggests that the tumour suppressive phenotype of CD105- fibroblasts is not driven by their lack of CD105 expression. Forced expression of CD105 in CD105- fibroblasts and observation of the same *in vivo* suppressive phenotype, would prove this. Thus, CD105 appears to be a useful marker to sperate functionally distinct fibroblast lineages in the mammalian pancreas and in pancreatic tumours, but the CD105 protein itself does not appear to drive the key functional difference seen here.

It is not clear how the MyCAF and iCAF-like fibroblast polarisations of CD105+ and CD105- fibroblasts contribute to the *in vivo* permissive and suppressive phenotypes observed in these experiments. As described in the previous chapter, very little is known about the functional consequences of the MyCAF and iCAF states generally, let alone in the context of different fibroblast lineages. Also mentioned previously, *in vitro* culture is thought to promote a myofibroblast phenotype, thus the injected fibroblasts are likely in a state more aligned with that of myofibroblast differentiation. However, it is not known how this phenotype might change when the cells are injected in Matrigel, which is far

softer than plastic. To address the contribution of the MyCAF- and iCAF-like states to the *in vivo* properties observed in these co-transplant studies, it may be feasible to pre-treat the fibroblasts with activating factors such as TGFβ1, IL1α, TNFα and IFNγ before injection into the mice. A limitation of this will be that stimulation can only be done prior to the *in vivo* injections and thus the activated state may not be maintained for sufficiently long *in vivo* to observe a discernible phenotype. Indeed, the pre-formed state may be rapidly overridden by new activating factors in the Matrigel plug, such as direct cancer cell contact. In addition, several of these cytokines/growth factors have cytostatic or cytotoxic functions (e.g. TNFα and IFNγ) and this may introduce confounding issues caused by injecting senescing, dead or dying fibroblasts. Alternatively, as a better understanding of the transcription factors required for induction of the MyCAF- and iCAF-like states emerges, it may be possible to delete these genes in each fibroblast population, effectively 'locking' them out of either the MyCAF- or iCAF-like states. These cells could then be implanted in the same manner and *in vivo* growth monitored. This would reveal the dependency of the permissive and suppressive growth phenotypes on the MyCAF- or iCAF-like states. In this regard, the transcriptomic and phosphorylation analysis of MyCAF and iCAF-inducing stimulations may be particularly informative for picking the key downstream regulators of the MyCAF- and iCAF-like states to target.

In PDA tumours, CD105- fibroblasts express high levels of MHCII, with minimal expression seen on CD105+ fibroblasts. Because CD105- fibroblasts are suppressive to tumour growth in the co-transplant model, in a mechanism dependant on adaptive immunity, a logical question to ask is does MHCII-mediated antigen presentation play a role in the tumour suppressive properties of CD105- fibroblasts? Applying MHCIIKO and CD74KO CD105- fibroblasts, generated by CRISPR/Cas-9 gene editing, to the syngeneic subcutaneous co-transplant model, indicates that the suppressive phenotype of CD105- fibroblasts is completely independent fibroblast MHCII-antigen presentation and must be acting through other mechanisms. Recent scRNAseq studies of PDA GEMM tumours has also noted MHCII expression on a minor cluster of fibroblasts (Elyada et al., 2019). These cells have been designated as 'antigen-presenting CAFs' or apCAFs, a terminology that has now been widely used within the CAF research field in general (Kieffer et al., 2020). The concept of antigen presentation by fibroblasts was suggested >30 years ago, although unequivocal proof fibroblasts in tumours actively process and present exogenous tumour antigens *in vivo* and that this antigen

presentation plays any functional role in tumour biology is still lacking (Umetsu et al., 1986). Thus, it is likely that this apCAF nomenclature is misleading and not conductive to improved understanding of fibroblast functions. For example, it is possible that these MHCII+ fibroblasts simply occupy a distinct microenvironmental niche, potentially in areas of increased IFNγ, and that MHCII-expression is downstream of other functionally more important aspects of these cells. For example, MHCII expression in CD105- fibroblasts could simply be downstream of cell-cell interactions with specific IFNγ-expressing T cell subsets. It has been suggested that more accurate classification of the mononuclear phagocyte lineage has come from linking nomenclature primarily to ontogeny and secondarily to location, function and phenotype, (Guilliams et al., 2014). Such a system for classifying fibroblasts, and mesenchymal cells more generally, would likely be an improved and more robust system, and would lay a framework for a more systematic understanding of fibroblast functions. In this regard, distinct CD105+ and CD105- fibroblast lineages may form separate, non-interchangeable 'branches' of such a 'fibroblast ontogeny map'.

Chapter 9 – Results – Mapping CD105+ and CD105- fibroblasts across different tissues, tumour types and species

9.1 – Results

9.1.1 – CD105+ and CD105- fibroblasts are present in low-passage primary cultures from major mouse organs

Collectively the previous chapters have described functionally distinct CD105+ and CD105- fibroblast lineages in murine healthy pancreas and spontaneous murine pancreatic tumours. These stable populations are also observed in primary human fibroblast isolations from non-tumour bearing pancreas and in human pancreatic tumours. Published data from dermal fibroblast research and scRNAseq studies in other tissues and tumours, has demonstrated that many other organs and tumours show evidence of fibroblast heterogeneity (Driskell and Watt, 2015; Puram et al., 2017). Therefore, I hypothesised that distinct CD105+ and CD105- fibroblasts may be a feature of other tissues and tumour types and this may contribute to fibroblast heterogeneity. In addition, many organs and GEMM tumour types, have not previously had their fibroblast heterogeneity characterised. To address this, I first aimed to measure the surface proteome of fibroblasts from 18 mouse organs, from a broad range of anatomical locations and functions. Fibroblasts are typically a minor cell population in most healthy tissues and are notoriously challenging to release from their strong cell-cell and cell-ECM contacts. Thus, analysis of fibroblasts from healthy organs directly *ex vivo*, typically requires highly optimised, tissue-specific disaggregation protocols. Instead, I chose to leverage the fact that, as for the pancreas, fibroblasts from other organs are able to grow and expand with standard *in vitro* culture techniques relatively quickly compared to other cells types, yielding cultures where the majority of surviving cells are low passage primary fibroblasts (or fibroblast-like) (Ichim et al., 2018; Sahai et al., 2020). In addition, I was keen to analyse the cells in this way because this ‘outgrowth’ method is routinely how primary fibroblasts are isolated for functional studies. Thus, using similar methods to expand fibroblasts as those used by others, would give insight into the fibroblast composition that these widely used protocols generate.

I disaggregated 18 different mouse organs and expanded primary fibroblasts from each by *in vitro* culture, as had been done for the pancreatic fibroblasts previously. Adherent, fibroblast-like cells grew out of th pancreas, as expected, and for all of the other 17 organs tested. However, the different tissues showed a wide variation in how long it takes before sufficient cell numbers were obtained for analysis (organs are listed in Table 7). For example, whilst fibroblast isolations from a single murine pancreas typically take ~5-7 d to generate sufficient cells for analysis, fibroblasts expanded from a single mouse prostate take >3 weeks. Such extended lengths of *in vitro* passaging is likely to favour fast growing fibroblast lineages or phenotypes. Thus, analysis at late time points is more likely to underestimate the heterogeneity of fibroblasts present in the initial organs. To address this, for organs that showed low initial numbers of expanding fibroblasts (prostate, bladder, bone marrow and thymus), I used multiple starting organs which enabled analysis of fibroblast composition to be conducted more quickly after disaggregation. For example, by combining 5 different mouse prostates, the fibroblasts could be analysed after 6 d of *in vitro* expansion. The number of organs used, the chosen disaggregation method, whether Dispase was or wasn't used and how many days of culture elapsed before the analysis, are all listed in Table 7 in the Materials and Methods section. Early passage mouse embryonic fibroblasts (MEFs) were also included in the analysis.

For analysis of fibroblast composition, I stained the cells with the mesenchymal stroma mass cytometry panel, as used previous experiments (Chapters 4 and 6). The panel includes a range of markers to identify a general population of fibroblast-like cells away from the rare remaining epithelial cells, endothelial cells and pericytes in the cultures. Notably, the fibroblast-like cells, that made up the majority of cells from each sample expressed high levels of mesenchymal proteins (VIM, αSMA etc), as well as uniformly high expression of PDPN. Positive PDPN expression across all fibroblasts was also observed with the *ex vivo* KPC pancreatic analysis and the *in vitro* pancreatic fibroblast stimulation analysis presented in previous chapters. Thus, PDPN appears to be a useful, broad marker of murine fibroblasts, regardless of the tissue the fibroblasts come from. Within this fibroblast fraction, I investigated the expression levels of CD105 in each sample. There are clear CD105+ and CD105- fractions of cells within the fibroblast-like cells from the pancreas (as described in previous chapters) and, remarkably, there was evidence of fractions of fibroblasts with differential expression of CD105 across the

isolations from 11/17 of the other tissues (Figure 67). The tissues with clear CD105+ and CD105- fibroblasts are: the colon, small intestine, mammary tissue, skin, prostate, stomach, adipose tissue, bone marrow, spleen, thymus and MEFs.

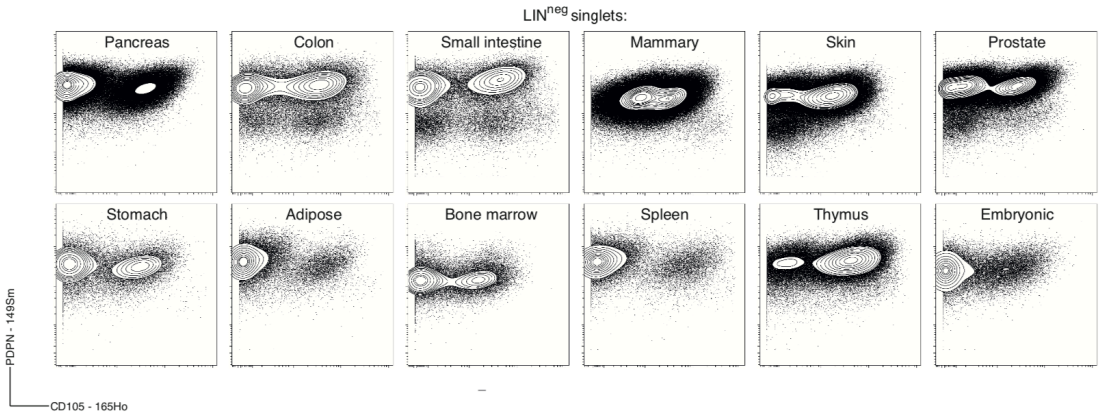

Figure 67. CD105+ and CD105- fibroblast are present in many normal murine tissues
Mass cytometry (MC) analysis of in vitro expanded, low passage, primary fibroblast isolations from a range of mouse organs. Cells expressing canonical markers of epithelial, immune, endothelial and perivascular cells are excluded from the analysis and live, singlets are displayed in plots showing PDPN and CD105 levels.

The difference in the levels of CD105 expression between the CD105high/low fractions varied widely, in that whilst the absolute level of CD105 (i.e. the median signal intensity) in the CD105+ fraction was very similar across each tissue isolation, the cells with lower CD105 expression either has no CD105 expression or had low but detectable levels of expression (i.e. CD105intermediate). An unusual staining pattern is particularly noticeable in the mammary tissue fibroblasts, which shows evidence of two populations separated by CD105 expression but with only slightly different levels of expression, appearing as if CD105hi and CD105lo populations are 'compressed' (a similar observation is seen in the cells isolated from the skin and the thymus). In addition, whilst some isolations have clear bimodal signal of CD105 (pancreas, adipose, spleen), others have 'smears' of staining. This may represent evidence of some populations with intermediate levels of CD105 expression (bone marrow and MEFs are the clearest examples) or may be due to overstaining during the antibody labelling step. It is not clear if this is genuine CD105 protein levels: if it is a staining issue, better resolution could be achieved with optimised staining and washing steps. Another notable feature is the presence of cells with reduced but non-zero expression of PDPN in the colon and small intestine-derived samples only. These fibroblasts have not previously been observed in any of the pancreatic fibroblast isolations I have conducted. It is not clear if these are fibroblasts or some other cell type that has or has gained PDPN expression and

fibroblast-like features. For example, epithelial cells, endothelial cells and pericytes can all undergo mesenchymal transitions, a process in which PDPN expression is reported to increase (Puram et al., 2017; Renart et al., 2015). Why these cells appear in samples specifically from the colon and small intestine (and kidney and liver - see later), is not clear.

Isolations from 4 other organs (lung, bladder, oesophagus and heart) showed relatively homogenous CD105 expression, in that all fibroblasts in the isolations were CD105+ (Figure 68). The liver sample was notable in that it was almost entirely formed from this intermediate PDPN population, with very few PDPNhi cells. In a similar manner, a large fraction of the kidney fibroblast-like cells showed intermediate PDPN staining too, and the remaining cells were CD105-.

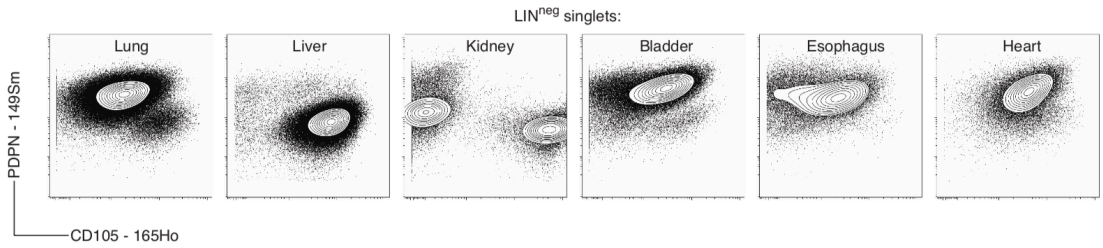

Figure 68. In vitro expanded fibroblasts from several mouse organs appear homogenous
Mass cytometry (MC) analysis of *in vitro* expanded, low passage, primary fibroblast isolations from the remaining mouse organs not displayed in the previous figure. Cells expressing canonical markers of epithelial, immune, endothelial and perivascular cells are excluded from the analysis and live, singlets are displayed in plots showing PDPN and CD105 levels.

Both the liver and lung isolations appeared to be relatively homogenous at the time point analysed (15 and 10 days, respectively). Both these organs are highly relevant to pancreatic cancer, as the major and minor sites of metastatic colonisation, respectively (Yachida et al., 2010). Thus, I was keen to analyse the fibroblast isolations from these organs at an earlier time point, in case the extended *in vitro* expansion had lost some of the fibroblast heterogeneity present in the tissue. I re-analysed new fibroblast isolations from both tissues, at 7 days using flow cytometry (which requires a lower cell input than mass cytometry) (Figure 69). At this earlier time point, the majority of cells from both the liver and the lung were fibroblast-like cells with a PDPN+CD105+ phenotype (consistent with the previous experiment) but also contained minor populations of PDPN+CD105- cells, that are presumably lost or outgrown at later time points. Thus, CD105+ and CD105- fibroblasts are a feature of many healthy mammalian organs which are present

to varying amounts in *in vitro* cultures of primary fibroblasts and some fibroblast populations are lost after even minimal *in vitro* culture..

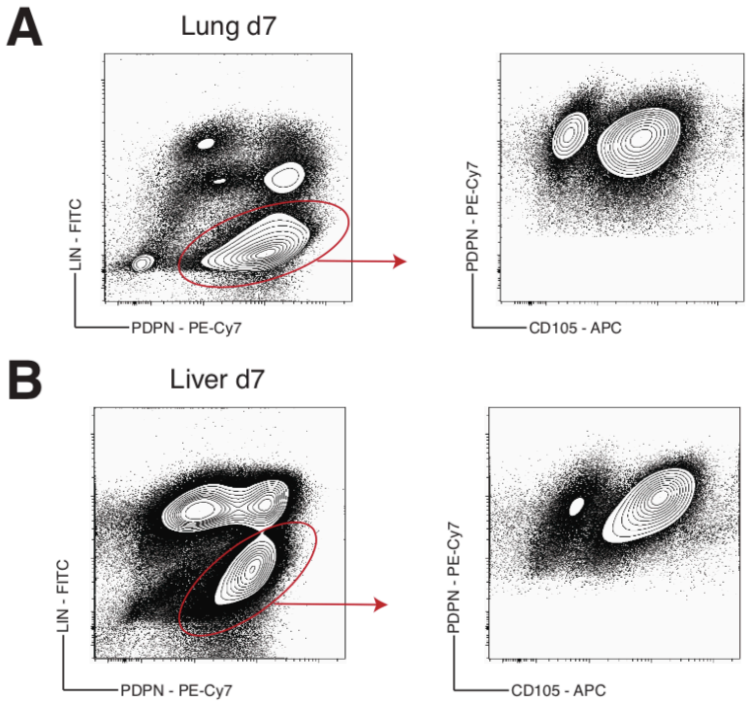

Figure 69. Earlier analysis of low passage fibroblasts reveals fibroblast heterogeneity in murine lung and liver

Flow cytometry analysis of EpCAM-CD45-CD31- (LIN-) and PDPN+ lung (A) and liver (B) fibroblasts from day 7 primary cell isolations, an earlier time-point than the analysis of these isolations by MC in the previous figure.

9.1.2 – CD105+ and CD105- fibroblasts are present in the tumours of different spontaneous GEMMs and human cancers with relative abundance regulated in a tissue-specific manner

The previous analysis revealed that fibroblast isolations from a wide range of different mouse organs show evidence of CD105+ and CD105- fibroblast fractions, suggesting such fibroblast populations are a common feature across different tissues. I sought to understand if CD105+ and CD105- fibroblasts were also present in different tumour-types. Because cancer cell transplantation methods rarely develop the strong fibrotic response seen in spontaneous human cancers, I opted to study fibroblast heterogeneity (with a focus on CD105+/- populations), across multiple different GEMMs of spontaneous murine cancer. For this analysis, I used the KPC pancreatic model as before, as well as spontaneous models of four other tumours types:

- KPN mice, which develop spontaneous colorectal and intestinal tumours that model progression and morphology of poorly differentiated, metastatic CSM4-like human colorectal cancer (Jackstadt et al., 2019).
- KP mice, which develop multi-focal, spontaneous lung adenocarcinomas that model human non-small cell lung cancer (NSCLC) (Meuwissen et al., 2001).
- MMTV-PyMT mice, which develop spontaneous mammary tumours that model luminal/ductal, ER-negative, metastatic human breast tumours driven by hyper-activated kinase signalling (Guy et al., 1992).
- BRAFV600E mice, which develop multi-focal, spontaneous skin tumours that model UV-initiated human melanoma (Dhomen et al., 2009).

Notably, the KPC pancreatic, KPN colorectal and KP lung models are all driven by oncogenic *Kras* mutations and loss of function *Trp53* mutations. This would, to some extent allow comparison of the fibroblast composition of tumours in which cancer cell growth and survival is driven by very similar oncogenic mechanisms. The BRAFV600E melanoma model also has hyperactivated MEK/ERK signalling (but via an oncogenic *Braf* mutation). MMTV-PyMT cancer cells are driven by the viral polyomavirus middle T-antigen, which has pleotropic functions including hyper activation of SRC, PI3K and PLCγ signalling (Shanzer et al., 2015).These GEMMs model several major human cancers and capture:

- a range of oncogenic drivers, with some overlapping features
- epithelial (KPC, KPN, KP and MMTV-PyMT) and non-epithelial (BRAFV600E) tumour-types
- different anatomical locations

KPC pancreatic (n=4), KPN colorectal (n=5), MMTV-PyMT mammary (n=4), KP lung (n=4) and BRAFV600E melanoma (n=3) tumours were disaggregated and analysed using the mesenchymal stroma mass cytometry panel. In a similar manner for the KPC pancreatic (n=19) study described in Chapter 4, high dimensional analysis and clustering was run for all live, single cells from each sample separately. This allowed annotation of all major cell types using canonical markers. To focus the analysis on fibroblasts specifically, all clusters lacking expression of epithelial, endothelial, pericyte and immune cell markers and having high expression of common fibroblast markers (e.g. VIM,

PDPN), were extracted from each sample for downstream analysis. As for the previous KPC pancreatic analysis and the *in vitro* primary multi-organ fibroblast analysis, PDPN was a very useful broad fibroblast marker. The pure fibroblast clusters from each tumour sample (depleted of cancer cells, immune cells, endothelial cells and pericytes), were combined and the 20 tumour samples analysed as a group. The resulting UMAP projection, with the FlowSOM generated clusters overlaid, is shown in Figure 70, along with stacked bar graphs showing the contribution of each cluster to the total fibroblasts. Such analysis reveals a high degree of fibroblast heterogeneity between samples from different tumour-types, between samples from the same tumour type and even between fibroblasts within the same sample. MMTV-PyMT mammary, KP lung and BRAFV600E melanoma tumours all contain heterogenous populations of fibroblasts and interestingly, each of these cluster away from the others in a tissue-specific manner, such that all fibroblast clusters from mammary tumours are together, all from lung tumours are together and all from melanoma tumours are together. The most striking observation with this analysis is that the fibroblast clusters from the KPC pancreatic and KPN colorectal tumours, show distinct clusters within each sample, but the clusters show a high degree of overlap between pancreatic and colorectal tumours. This is quite notable because even with >30 fibroblast-specific markers measured, the clusters from pancreatic and colorectal tumours cannot be distinguished from each other by the FlowSOM algorithm. For example, every KPC pancreatic (n=4) and KPN colorectal (n=5) sample contains fibroblasts in both the GEMM CAF 12 (GCAF-12) cluster and the GCAF-19 cluster. Considering the high parameter nature of this analysis, this alignment between pancreatic and colorectal tumour fibroblasts is quite remarkable.

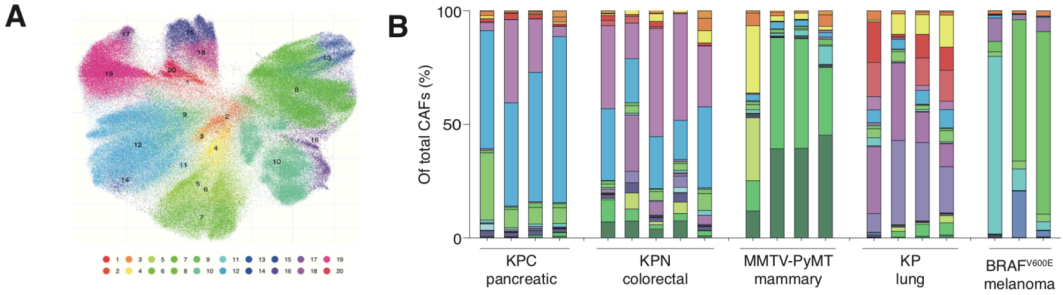

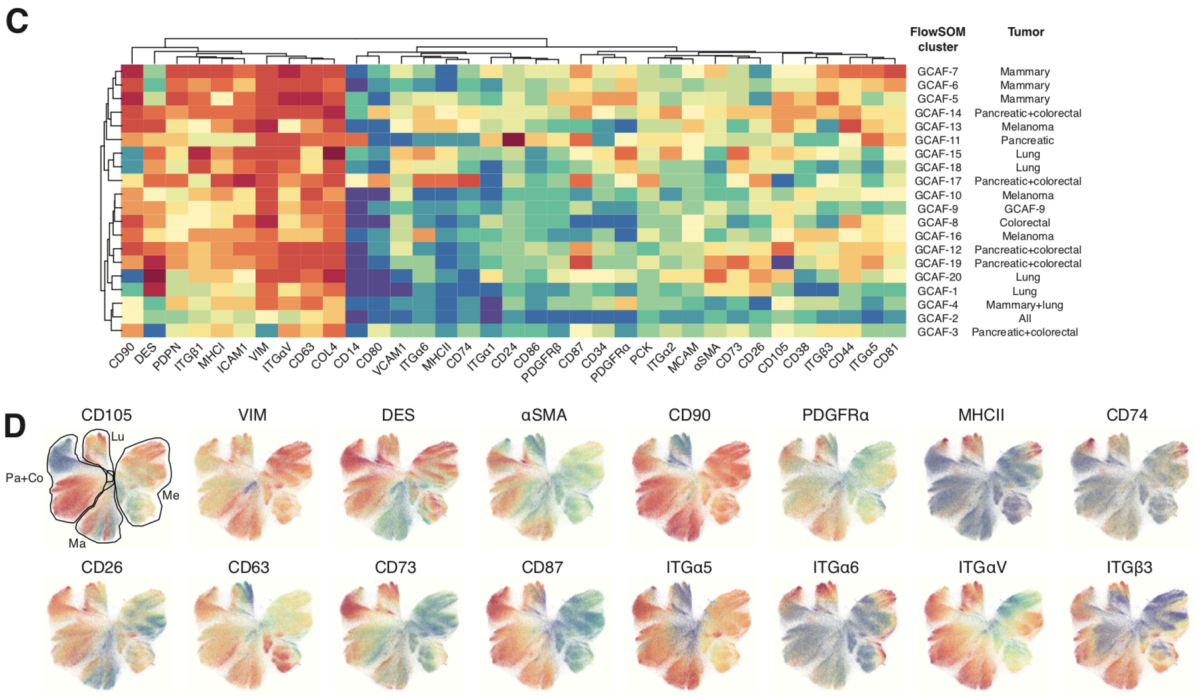

Figure 70. Heterogenous fibroblast populations across different tumour types
(A) UMAP projection of fibroblasts from autochthonous murine tumours (n=20 tumour samples in total). Genetically engineered mouse models (GEMMs) used are the KPC pancreatic (n=4), KPN colorectal (n=5), MMTV-PyMT mammary (n=4), KP lung (n=4) and BRAFV600E melanoma (n=3) GEMMs. FlowSOM clusters are color-coded. (B) Stacked bar graphs displaying each FlowSOM GEMM CAF (GCAF) cluster as a fraction within total CAFs. FlowSOM colours based on (A). (C) Heatmap displaying marker median mass intensities (MMIs) for each FlowSOM GCAF cluster. Phenotypic markers and GCAF clusters are grouped using unsupervised hierarchical clustering based on marker MMIs. Tumour-type/s that the GCAF clusters predominantly arise from are listed. (D) UMAP projection from (A) displaying overlaid signal intensity of example phenotypic markers. The tumour-type of origin are highlighted on the CD105 plot. Pa = pancreatic, Co = colorectal, Ma = mammary, Lu = lung and Me = melanoma.

The mammary, lung and melanoma tumour fibroblasts separated away from each other and from the shared pancreatic and colorectal tumour fibroblast clusters, in a tissue specific manner. This was driven by tissue-specific combinations of surface protein expression, that appeared in a ‘patchwork’ of expression patterns consistent across different tumours from the same tissue. For example, mammary tumour fibroblasts separated away from all other fibroblast clusters due to low DES expression and specifically clustered away from melanoma clusters because of uniformly high CD87 expression, away from most pancreatic and colorectal clusters because of expression of high PDGFRα and PDGFRβ and away from lung fibroblasts because of CD90 and ITGα5 expression. This potentially suggests tissue-specific regulation of these widely used fibroblast markers. Indeed, the staining for CD90 is particularly distinct. CD90, is found to be expressed on all KPC pancreatic and KPN colorectal fibroblasts, all MMTV-PyMT mammary fibroblasts and all BRAFV600E melanoma fibroblasts, yet almost all KP lung fibroblasts lack CD90 expression (GCAF-1, -15, -18 and -20). These lung fibroblasts

show features typical of fibroblasts in tumours (VIM, PDPN, αSMA etc) and are unlikely to be another cell type.

The fibroblast cluster identified in KPC pancreatic fibroblasts, with a unique MHCII+CD74+ phenotype (Chapter 4), was also present in this data set (GCAF-17). Interestingly, this cluster that was found in both KPC pancreatic and KPN colorectal samples, again highlighting the remarkable similarity between fibroblasts from these two tumour types. A minor melanoma CAF cluster (GCAF13) also shows this MCHII+CD74+ phenotype and the two major lung CAF clusters (GCAF-15 and -18) show elevated levels of MHCII only.

The analysis indicates that all samples contain shared but rare clusters, GCAF-2, 3 and 4. These clusters were present in every sample from every tumour type. Whilst its possible these cells may represent a common fibroblast state, or even a common undifferentiated phenotype, it is also possible they represent fibroblasts that lack expression of most markers in the panel, either coincidently or due to under-staining during the experimental protocol. Further work would be needed to understand if this observation is a technical artefact or whether these cells really do represent a common fibroblast phenotype seen across all 5 different tumour types.

The previous chapters have described how CD105 is a useful marker of functionally distinct fibroblasts in the murine pancreas. CD105 again showed interesting staining patterns in the fibroblasts from the 5 different tumour types. The expression of CD105 is shown for each tumour-type, with all samples from each tumour type plotted separately (n=3-5 for each tumour type) (Figure 71).

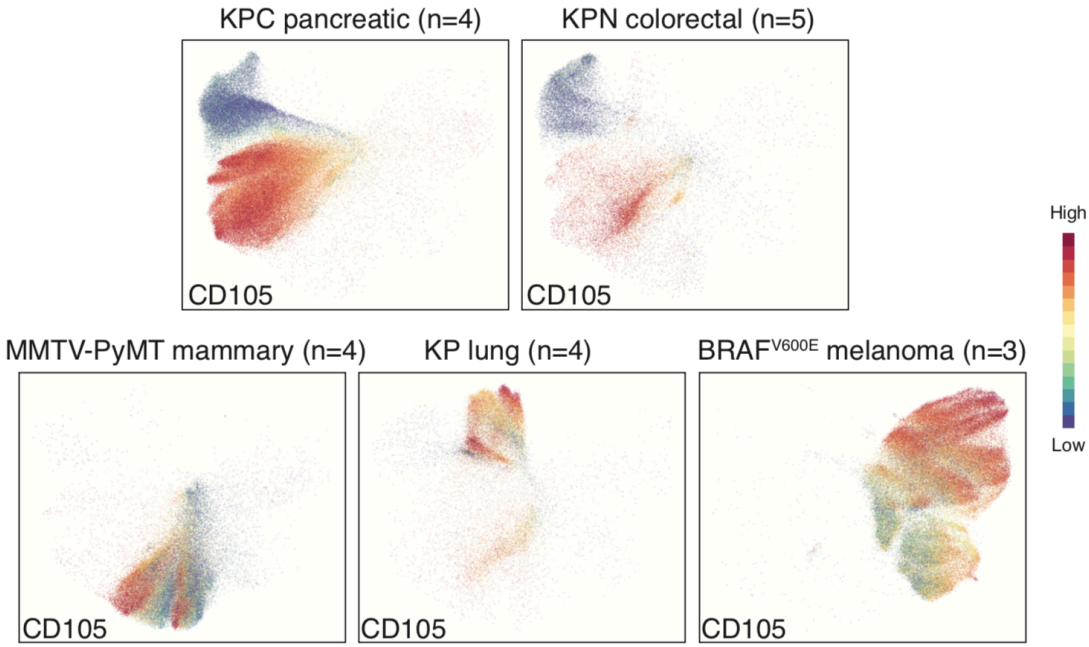

Figure 71. CD105 expression in fibroblasts across different tumour types
UMAP projection from displaying overlaid signal intensity of CD105 and separated into different tumor-types.

Again, the most striking observation here is that CD105+ and CD105- fibroblasts are clearly present in both pancreatic and colorectal tumours. Indeed, the main driver of separation between the two major pancreatic and colorectal shared fibroblast clusters (GCAF-12 and GCAF-14) is differential CD105 expression. The ratio of CD105:CD105- varies across the tumour types (see below). Mammary tumours also contain CD105+ and CD105- fibroblast populations but the difference in CD105 expression appears to be highly compressed. Interestingly, this was also seen in the *in vitro* expanded, healthy mammary tissue fibroblasts, suggesting differential CD105 protein expression regulation is distinct in fibroblasts from this tissue. The majority of fibroblasts from the lung and melanoma tumours are positive for CD105 expression, with very few CD105- fibroblasts. The minor CD105- cells that are present in lung and melanoma tumour samples, do not show clear bimodal staining and have a more graduated reduction of CD105 expression, although this is typically >10-fold lower levels of CD105 expression than CD105+ fibroblasts. This 'smear' or graduated expression is also seen in the *in vitro* primary cell isolations from these organs.

The ratio of CD105+:CD105- fibroblasts identified in the 5 different tumour types varied widely (Figure 72). For this analysis, data from the additional 19 KPC pancreatic tumours

analysed in Chapter 4 were added to more accurately report the KPC pancreatic fibroblast CD105+:CD105- ratio. The analysis shows that the relative abundance of CD105+ fibroblasts is highest in KP lung and BRAFV600E melanoma tumours (>6-fold more CD105+ fibroblasts than CD105- fibroblasts) but show a range of ratios, for example some KP lung tumours show >10-fold more CD105+ fibroblasts than CD105- fibroblasts with one KP lung sample actually containing more CD105- fibroblasts. KPN colorectal and MMTV-PyMT mammary tumour fibroblasts are notable in that they have approximately equivalent CD105+ and CD105- fibroblast frequencies. As reported in Chapter 4, KPC pancreatic tumours show a wide range of ratios of CD105+:CD105- fibroblasts and on average there are 3-fold more CD105+ than CD105- fibroblasts.

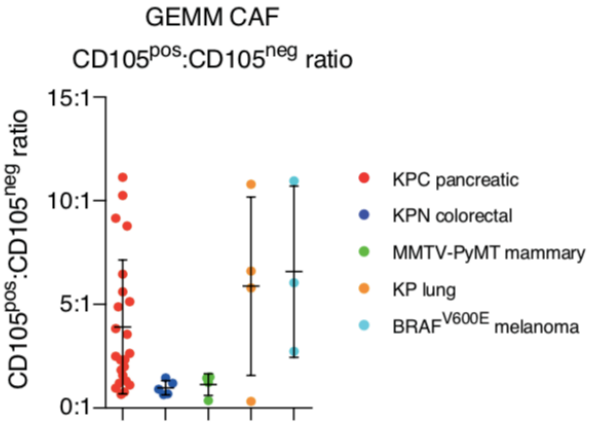

Figure 72. CD105+:CD105- fibroblast ratio analysis across different tumour types
MC analysis of the ratio of CD105pos:CD105neg CAFs in tumours from genetically engineered mouse models (GEMMs) of pancreatic (KPC) (n=24), colorectal (KPN) (n=5), mammary (MMTV-PyMT) (n=4), lung (KP) (n=4) and melanoma ($BRAF^{v600E}$) (n=3) cancer. Data from the n=19 PDA tumour samples analysed in section 4 were added to increase the accuracy of the ratio measured for the pancreatic GEMM tumours. Displayed as mean+/-standard deviation.

These mice were not dosed with IdU. However, fibroblast proliferation in these samples can instead be measured just from the fraction of cells positive for Ki67. Proliferation analysis of CD105+ and CD105- fractions across each tumour showed that KPC pancreatic, KPN colorectal and MMTV-PyMT mammary tumour fibroblasts had approximately similar Ki67+ fractions, with >10% of both CD105+ and CD105- CAFs showing Ki67 positivity (Figure 73). Notably KP lung fibroblasts had the lowest proliferation and BRAFV600E melanoma fibroblasts had intermediate levels of proliferation. This broadly matches the total abundance of fibroblasts generally observed in these tumours (i.e. KPC pancreatic and KPN colorectal tumours have large numbers of fibroblasts and BRAFV600E melanoma and KP lung tumours have few). As noted in

previous chapters, at this collection time point, CD105- fibroblasts in KPC pancreatic tumours had higher proliferation rates than CD105+ fibroblasts. Interestingly this differential proliferation in late stage tumours, was not seen in any of the other tumour types, which each showed the same proliferation in CD105+ and CD105- fibroblasts. Accurate comparisons of proliferation rates of fibroblasts between different GEMMs may be confounded because the tumours all have different latencies and growth durations and are also are collected at time points that correspond to different 'clinical' times. For example, KPC pancreatic and KPN colorectal tumours are collected at late stage when the mouse is starting to show signs of systematic disease and the KP lung tumours are taken at a fixed time point after tumour initiation in mice that are otherwise healthy and in which tumour collection could have been delayed by several weeks.

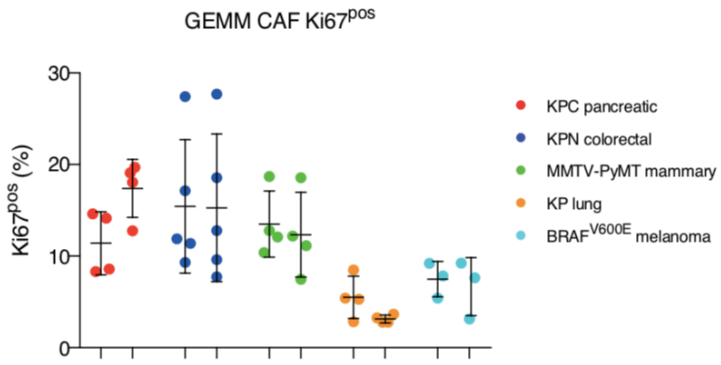

Figure 73. Proliferation rates of fibroblasts across different tumour types
MC analysis of proliferation rates of CD105+ and CD105- fibroblasts from genetically engineered mouse models (GEMMs) of pancreatic (KPC) (n=24), colorectal (KPN) (n=5), mammary (MMTV-PyMT) (n=4), lung (KP) (n=4) and melanoma ($BRAF^{v600E}$) (n=3) cancer. Displayed as mean+/-standard deviation.

Collectively, these results support the hypothesis that heterogenous fibroblasts are present in most murine tissues and tumours and that CD105 can be useful marker to separate fibroblast populations. In particular, abundant CD105+ and CD105- fibroblasts can be found in spontaneous murine pancreatic, colorectal and mammary tumours and CD105+ fibroblasts are more frequent than CD105- fibroblasts in spontaneous murine lung and melanoma tumours. To explore whether these findings are relevant to human tumours, I again utilized immunofluorescent imaging analysis of FFPE tumours from human advanced colorectal adenocarcinomas, triple negative breast adenocarcinomas and non-small cell lung adenocarcinomas. A representative image of x5 FFPE samples of each tumour type are shown in Figure 74. PCK staining in green identifies cancerous epithelium and CD105 staining is shown in red. CD105 staining of the vasculature can

be clearly seen because of the distinct morphology of collapsed blood vessels and acts as a positive control that CD105 staining has worked successfully throughout the stroma. For the human colorectal tumours, large areas of stroma are observed, containing cells with fibroblast morphology and a large number of CD105+ endothelial cells are also observed. Across, the human colorectal tumours tested, there is notable lack of CD105+ fibroblasts in the samples and CD105- fibroblasts dominant the stroma around the cancer cells. In the breast cancer samples, the stroma of the samples is again dominated by CD105- fibroblasts but local regions with large numbers of CD105+ fibroblast-like cells can be observed. In the human non-small cell lung cancer tumours, the stroma surrounding the PCK+ cancer cells contain many fibroblast-like cells but this time they are almost entirely CD105+. Thus, the majority of fibroblasts in human colorectal tumours appear to have CD105- phenotype, human breast tumours contain mixtures of CD105+ and CD105- fibroblasts and the stroma of human non-small cell lung tumours is dominated, almost exclusively (based on imaging methods) by CD105+ fibroblasts. Detailed imaging analysis of larger cohorts of tumours from each tumour type would verify these observations and provide more accurate quantification of CD105+/- fibroblast abundance *in situ* in human tumours.

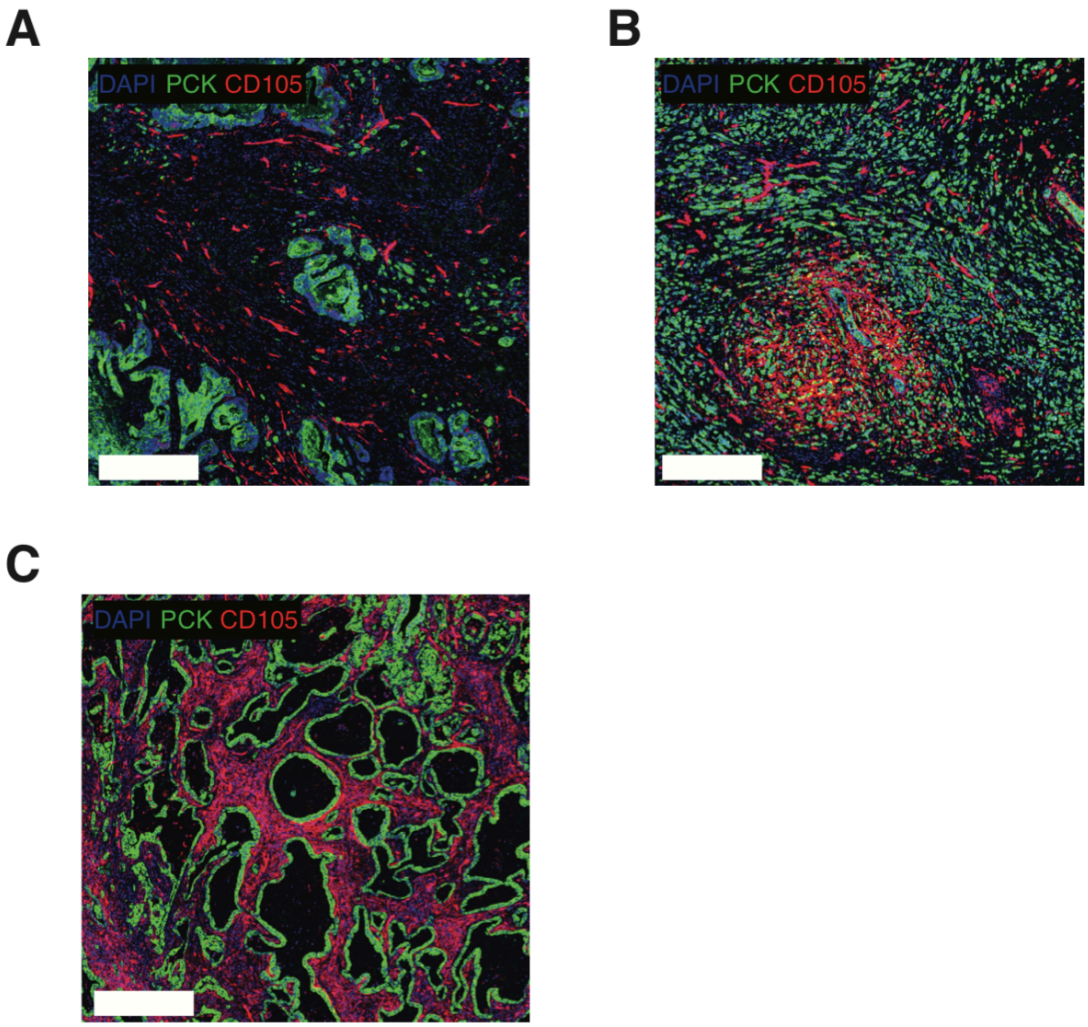

Figure 74. Immunohistochemistry analysis of human tumours
Representative immunohistochemistry (IHC) analysis of human colorectal adenocarcinoma, mammary invasive ductal carcinoma and lung adenocarcinoma tumor samples stained with DAPI (blue) and with antibodies targeting pan-cytokeratin (PCK) (green) and CD105 (red). CD105+ endothelial cells with classical blood vessel morphology are distributed throughout the tumors and act as an internal control for robust CD105 antibody staining. Scale bar = 500 µm.

9.2 – Summary

In this chapter, I outline the analysis of fibroblast heterogeneity across primary, low-passage fibroblasts isolated from 18 healthy murine organs, as well as fibroblasts isolated directly *ex vivo* from tumours of 5 distinct GEMMs of spontaneous cancer. The hypothesis of this section was that analysing a high number of different tissues/tumours simultaneously would reveal patterns of convergent and divergent fibroblast phenotypes. In this regard, both CD105+ and CD105- fibroblast populations were observed in the majority of healthy and tumour bearing samples, although to widely varying frequencies.

Pancreatic and colorectal tumours showed a remarkably high similarity in the phenotype of the fibroblasts present, including identical phenotypes of CD105+ and CD105- fibroblast populations and a minor PDPN+CD105-MHCIII+CD74+ fraction.

9.3 – Discussion

The data presented in this chapter supports the concept that fibroblast heterogeneity is a common feature of healthy organs and tumours and that CD105 demarks at least two populations of fibroblasts in many tissues and tumours. An important next step would be to isolate CD105+ and CD105- fibroblasts from each of the tissues/tumours and asses firstly, whether differential CD105 expression is stable (as for pancreatic fibroblasts) and secondly, whether the functional properties of these CD105+/- fibroblasts are consistent with those of CD105+/- pancreatic fibroblasts. This could be done by looking at *in vitro* fibroblast activation (for example, the sensitivity to MyCAF and iCAF polarisation) and by studying *in vivo* function (for example, interactions with adaptive immunity in a subcutaneous co-transplant model). This may reveal a common lineage commitment of functionally distinct fibroblasts across multiple mammalian organs demarked by CD105. Additionally, an important step would be to determine whether CD105+ and CD105- fibroblasts present in human tissues and tumours are also phenotypically stable, which could be done by *in vitro* isolation and expansion (as was done for the human pancreatic fibroblasts in Chapter 6).

A central question that is important to the data presented in this section is, are the fibroblasts analysed in this chapter 'true' fibroblasts or simply mesenchymal cells present in each TME that have a fibroblast-like phenotype? This is a common problem encountered in fibroblast research of healthy organs but particularly so in pathologic tissues, in which inflammation and wound repair programs, can lead to new phenotypic states being accessed by a variety of tissue-resident and infiltrating cell types. Such extreme conditions can cause induction of phenotypic features of fibroblasts in non-fibroblast cells (e.g. epithelial to mesenchymal transition). The application of mass cytometry (and other high parameter technologies) addresses some of these issues in that by measuring a large number of markers (for example, compared to flow cytometry), the ability to discriminate between different cell types is enhanced. One way to be confident that the cells identified here are 'true' fibroblasts would be to isolate them and

investigate morphology, gene expression and function, but again here there are no standard/universally accepted functional assays to prove fibroblast identify. PDPN looks to be a particularly useful pan-marker of murine fibroblasts from many of the tissues/tumours analysed but caution must be used in seeking a general marker. Other cell types express PDPN, such as lymphatic endothelial cells and lung alveolar type 1 (AT1) epithelial cells. Fortunately, these cell types express other markers that discriminate them as non-fibroblasts, such as CD31 and cytokeratins, respectively. However, other PDPN+ cells may not have such clear expression of other lineage markers. In addition, markers that appear to be very useful general markers in one tissue/tumour are not broadly expressed by fibroblasts in other tissues/tumours. For example, CD90 was a comprehensive, pan-fibroblast marker for KPC pancreatic, KPN colorectal, MMTV-PYMT mammary and BRAFV600E melanoma fibroblasts but has almost no expression on KP lung fibroblasts. CD90- pancreatic fibroblasts are also observed from healthy tissue isolations (Chapter 6), indicating that the CD90+ phenotype is only a common fibroblast marker in PDA tumours and not necessarily useful in the healthy pancreas. Thus, care must be taken in deciding which markers do and don't identify fibroblasts. With the KPC pancreatic analysis in chapter 4, I became confident about the annotation of clusters. For example, being able to use a lineage tracing model greatly added to the confidence in the mass cytometry analysis workflow to be able to separate fibroblasts from mesenchymal cancer cells. Increased familiarity with the tissue/tumour of interest, the use of lineage tracing models and adding additional, tissue-specific markers when needed, will help better define fibroblasts and improve future analysis of other tissues/tumours. For example, melanoma occurs from malignant transformation of melanocytes, which during development derive from neural-crest cells and thus do not express many of the markers that were included in the panel to identify epithelial/adenocarcinoma cancer cells. Including antibodies that target melanocyte-specific markers, such as SOX10, would specifically improve annotation within that tumour type. As the composition of tissues and tumours becomes better defined, useful markers of other less well defined infiltrating cells will improve. For example, including markers of various cell types such as chondrocytes, different basal cells, neurons, Schwann cells, adipocytes and mesothelial cells, would reduce incorrect classification of these as being 'true' fibroblasts, based on a currently restricted list of markers. In this regard, the huge number of scRNAseq studies now being conducted may reveal useful makers of various different cell types that could be included in flow or mass cytometry

analysis. Indeed, running parallel mass cytometry and scRNAseq analysis on the same sample would likely complement each other (but would be associated with a high cost). Another caveat here is that some of these 'contaminating' cell types are established sources of fibroblasts, especially under pathological conditions and excluding them completely may exclude cells that are actively contributing to fibroblast populations and function in the tissue/tumour (see Summary discussion). There is no simple solution to the problem of fibroblast identification but increased understanding of fibroblast heterogeneity will likely improve the accuracy of fibroblast annotation in complex tissues.

A wide range of tissues were analysed in this study but a notable, fibroblast-rich tissue compartment that was not analysed was that of connective tissues. Fibroblasts have an established role in connective tissue formation, homeostasis and pathogenesis, for example fibroblast-mediated joint degradation is a hallmark feature of rheumatoid arthritis (Mizoguchi et al., 2018). I did not isolate fibroblasts from connective tissue because doing so requires specialised protocols and fibroblast isolation is potentially confounded by the abundance of other mesenchymal cell types present, such as chondrocytes. Because of the central role fibroblasts have in connective tissue pathologies and the fact that fibroblast heterogeneity has already been observed in these tissues, detailed analysis of fibroblast populations in connective tissue, would likely reveal interesting and clinically relevant findings, as well as providing a useful comparison to 'soft' tissue fibroblasts (Croft et al., 2019; Mizoguchi et al., 2018; Wei et al., 2020).

The *in vitro* analysis of low passage fibroblasts presented in this chapter, demonstrates extensive fibroblast heterogeneity in many tissues. Because each tissue yields different numbers of released fibroblasts, which take different lengths of time to grow to sufficient numbers for analysis, it is not possible to compare aspects such as fibroblast abundance and phenotype (e.g. αSMA expression), directly between *in vitro* expanded tissues. In addition, *in vitro* outgrowth method also likely underestimates fibroblast heterogeneity, as rare or slower growing fibroblast lineages or phenotypes, will be over grown by fibroblast populations that are more abundant or better suited to *in vitro* culture conditions. This can be observed in this study, where extended culture of liver and lung fibroblasts for >10 days suggests only CD105+ fibroblasts only are present in these tissues, yet earlier analysis of the cultures reveals minor CD105- fibroblast populations

present. It is also possible that *in vitro* culture may convert non-fibroblast cells to fibroblast-like cells via mesenchymal transitions. Additionally, *in vitro* growth alters fibroblast phenotypes, so understanding how observed phenotypes relate to *in vivo* phenotypes becomes challenging. Thus, an improvement on the method used, would be analyse healthy tissue fibroblasts directly *ex vivo* from the tissue of interest, as was done for the *ex vivo* GEMM tumour analysis. Fibroblasts are typically rare in most healthy tissues and because they have extensive cell-cell and cell-matrix contacts, and are therefore challenging to release during disaggregations and are normally underrepresented in single cell isolations. Protocols could be optimised for each healthy tissue, to release the maximum number of fibroblasts and analyse these directly *ex vivo*. This would require a large time commitment, as individual tissues typically require a tissue-specific disaggregation enzyme mixtures and protocols but would greatly improve the physiological relevance of the findings.

The fibroblasts from KPC pancreatic and KPN colorectal tumours show similar phenotypes, such that even when high dimensional analysis is conducted using >30 markers in the mass cytometry panel, clusters of CD105+ and CD105- fibroblasts from each tumour type overlap completely. Thus, for future experiments aimed at testing whether the functional differences between CD105+ and CD105- fibroblasts that are observed for pancreatic fibroblasts, can also occur in other organs, it would be sensible to start with a similar analysis of CD105+ and CD105- colorectal fibroblasts. Why the fibroblasts from these two tumours are so similar is not clear. The KPC and KPN models are both driven by oncogenic *Kras* and loss of function *Trp53* mutations. Whilst initiating mutations may play a role in the convergent fibroblast phenotype seen, the KP lung model is also driven by the same mutations, yet the KP lung fibroblast composition and phenotype are very different to the KPC and KPN tumours. For example, KP lung tumours contain very few CD105- fibroblasts and the fibroblasts do not express CD90, a pan-fibroblast marker in other tumours. Thus, tumour-specific similarities and differences may be more a product of differences in fibroblast phenotype and function already present in the tissue prior to tumour formation. The pancreas and colon both derive from the embryonic foregut, so fibroblasts in each organ may share some developmental similarities. Alternatively, the functional demands shared by tissues of the gastrointestinal tract, such as nutrient/metabolite levels or the constant presence of commensal bacteria, may have caused pancreatic and colorectal fibroblast phenotypes

and functions to converge or stay converged during evolution. A publication from 2018 noted colorectal tumours contain CD105+ fibroblasts (Paauwe et al., 2018). The study focussed on fibroblast invasion properties and unfortunately, the stability of CD105 expression in colorectal fibroblasts and the function of CD105- fibroblasts was not explored. However, this study supports the concept that CD105+/- fibroblasts may be a feature of multiple human tumour types. A better understanding of both fibroblast development and functional demands across different tissues, would likely reveal which tissue fibroblasts are most closely related in a more systematic and definitive manner. If tissue-specific factors dominant fibroblast function, this has major implications for how fibroblast-targeting therapies would be best developed and potentially impact their relevance to cancer therapy across different tumour types but also within the same tumour type in the metastatic setting (see Summary discussion).

It is interesting to note that whilst fibroblasts from pancreatic and colorectal tumours show remarkable similarity, fibroblast clusters from all other tumours separated distinctly in a tissue-specific manner. No single marker identified fibroblasts from one tissue completely. Typically, it was a combination of positive or negative expression of a series of already established markers, that identified the tissue specific nature of the fibroblast clusters, in particular, combinatorial expression of CD90, CD87, PDGFRα, PDGFRβ and ITGα5 is able to distinguish fibroblasts from different tissues. How stable these expression patterns are for each tissue type are not clear and what factors regulate the expression of these markers, in such a tissue-specific manner, is also unknown. For example, it is not known if tissue-specific fibroblast differences in tumours arise from signals coming directly from the tumour/parenchymal cells themselves or possibly some other microenvironmental cell type. The immune infiltrate of tumours is known to vary widely, so immune cell composition may also directly alter fibroblast phenotype in a tissue-specific manner (Allen et al., 2020). It may even be possible that some of these tissue-defining signals may come from more unusual sources, such as tissue-specific differences in stiffness, nutrient/oxygen availability or microbiome exposure.

CD105 expression across many of the tissues and tumours typically shows bimodal expression, that is CD105+ and CD105- populations could clearly be separated. A notable, exception to this was mammary tissue fibroblasts, that showed ‘compressed’ bimodal expression, such that two populations appeared to be present with different

CD105 expression, but the level of CD105 expression was more similar than that seen in other tissues/tumours. Interestingly, this was also seen in the *in vitro* expanded fibroblasts from healthy mammary tissues. This potentially supports the idea that mammary tissue-resident fibroblasts are the major source of fibroblasts in mammary tumours but this would need verifying. It also suggests that there is some altered regulation of CD105 protein expression that is specific to mammary tissue fibroblasts. An improved mechanistic understanding of the epigenetic regulation of CD105 protein in fibroblasts (and indeed epigenetic imprinting more generally in fibroblasts), will likely lead to improved understanding about what drives tissue-specific fibroblast phenotypes, including different levels of CD105 expression.

In the KPC pancreatic and KPN colorectal tumours, there is consistently a population of MHCII+CD74+ fibroblasts overserved, specifically within the CD105- fraction of fibroblasts. Even if fibroblast MHCII expression is not functionally important, it does suggest that these fibroblasts in both pancreatic and colorectal tumours are in unique environment/niche *in vivo*. It is thus very interesting to note that MHCII+ fibroblasts are also observed in melanoma and lung tumours but only on CD105+ fibroblasts. If MHCII expression in fibroblasts is downstream of specific cell-cell interactions, for example between fibroblasts and IFNγ-producing T cells, then this may suggest the fibroblast-leukocyte interactions in pancreatic and colorectal tumours are similar to each other and different to those occurring in melanoma and lung tumours, which again are similar to each other. Further work is needed to better understand what is driving MHCII expression specifically in CD105+ or CD105- fibroblasts in these tumours and what this can tell us about the different microenvironmental processes occurring.

The ratio of CD105+:CD105- fibroblasts varied widely across different murine and human tumour types. In a general sense it appears that (with the limited number of human samples measured) the CD105+:CD105- ratio observed in spontaneous murine tumours is similar to the ratio observed in the analogous human tumours. For example, CD105- fibroblasts are a common feature of murine and human pancreatic, colorectal and mammary tumours but are rare in murine and human lung tumours. Human melanoma tumours could not be assessed by IHC here because a robust melanoma cancer cell marker had not been optimised for staining (although melanoma-specific markers like SOX10 could be tested in the future). A greater number of human FFPE tumours would

also need to be analysed to draw a more conclusive comparison. What dictates the ratio of CD105+:CD105- fibroblast *in vivo* is not known. *Ex vivo* analysis of the healthy organs (as discussed above) would enable improved understanding of whether the CD105+:CD105- fibroblast ratio seen in tumours simply represents a proportional expansion of different CD105+:CD105- ratios already present in the healthy tissue or whether there is selective expansion of one fibroblast population over the other as each tumour-type develops. An experiment that may give some insight into any selective expansion, is to simultaneously measure the CD105+:CD105- fibroblast ratio in tumours and the levels of cytokines/growth factors (for example, by multiplexed ELISA). This would enable comparison between the CD105+:CD105- fibroblast ratio and the presence of known fibroblast activators/growth factors which may control the ratio.

Chapter 10 – Summary discussion and future directions

10.1 – General summary of research findings

Fibroblasts are a mesenchymal cell type found in the stromal regions of most mammalian tissues. They are a major source of extracellular matrix (ECM) and ECM-modifying components in development, health and disease, and have a number of other reported, non-ECM functions, such as modulation of epithelial cell functions via paracrine signalling. Fibroblasts are highly abundant in primary and metastatic pancreatic ductal adenocarcinoma (PDA) tumours and have been ascribed putative pro- and anti-tumourigenic functions. Notably, a consensus on how fibroblasts contribute to PDA tumour progression and therapeutic response is lacking. A major challenge to the accurate annotation of fibroblast functions in PDA tumours is the extensive heterogeneity of this cell type, as has now been observed across multiple single cell RNA sequencing studies. Such cellular heterogeneity can manifest itself as completely distinct and non-interchangeable 'lineages' or as the same parental population, in distinct but variable phenotypic 'states'. In this regard, PDA fibroblasts have a now well-documented capacity to move between at least two phenotypic polarisations, the so called myofibroblast- and inflammatory-like fibroblast states. This remarkable plasticity has likely further complicated annotation of fibroblast functions. In parallel, dermal fibroblast research has provided compelling evidence that irreversible lineage restriction of fibroblasts occurs during embryonic development. These distinct fibroblast lineages are retained throughout adulthood and have different, non-overlapping functions during tissue homeostasis and wound repair. Whether such fibroblast lineages exist in other mammalian organs or in tumours is not known.

Importantly, a detailed understanding of the functions of individual fibroblast populations in PDA tumours, has been hindered by a lack of robust cell surface markers for live cell isolation and characterisation. In addition, the key cell types that fibroblasts interact with in the PDA TME are also largely unknown. To address this, I have developed a single cell, mass cytometry workflow focussing on cell surface proteins, that has allowed detailed annotation of the microenvironment of tumours from a PDA genetically engineered mouse model (GEMM). The analysis reveals complex and highly variable cellular ecosystems within the PDA TME and suggests a number of novel fibroblast-

immune cell associations. A particularly notable feature across all PDA tumour samples was the presence of distinct fibroblast populations that could be separated by differential surface expression of CD105. The abundance of CD105+ and CD105- fibroblasts varies widely across PDA tumours and each has a distinct gene expression profile. CD105+ and CD105- fibroblasts are present in human PDA tumours, as well as healthy/non-tumour bearing murine and human pancreas. Moreover, differential CD105 expression is highly stable, suggesting CD105 demarks distinct, non-interchangeable fibroblast lineages. In addition, both populations have the potential to adopt myofibroblast and inflammatory gene expression patterns under extended stimulation with TGFβ1 and IL1α, respectively, but CD105+ fibroblasts show a higher sensitivity to undergoing polarisation to either state. Further gene expression and cell signalling analysis of CD105+ and CD105- fibroblasts, highlights the complexity of fibroblast activation and demonstrates differences in transcriptomic and signalling responses of CD105+ and CD105- fibroblasts that would likely confound analysis of bulk fibroblast isolations.

To better understand the *in vivo* functional properties of CD105+ and CD105- fibroblasts, in an unbiased empirical fashion, I developed a syngeneic subcutaneous co-transplant model. CD105+ fibroblasts are fully tumour permissive, in that they do not enhance or restrict PDA tumour growth, and CD105- fibroblasts are found to be highly tumour suppressive. The potent suppressive function of CD105 is entirely dependent on adaptive immunity, with a major contribution from cDC1-mediated cross-priming of CD8+ T cells, suggesting that fibroblast and immune cell interactions are a key feature of PDA tumour growth. CRISPR/Cas-9-mediated deletion of CD105 in CD105+ fibroblasts does not induce tumour suppressive potential, suggesting that whilst CD105 is a useful pancreatic fibroblast lineage marker, lack of CD105 expression does not drive the dominant in vivo function of CD105- fibroblasts. Whilst CD105- fibroblasts are frequently found to express proteins involved in MHCII antigen presentation *in vivo*, deletion of these genes does not impact the suppressive function of CD105- fibroblasts, suggesting alternative mechanisms are responsible for the enhancement of anti-tumour immunity.

Applying the single cell analysis workflow to primary fibroblasts from 18 other murine organs and tumours from 4 other spontaneous cancer GEMMs, indicates that CD105+ and CD105- fibroblasts are a feature of most tissues and are present to variable levels in other tumour types. Notably, populations of fibroblasts from colorectal tumours share

a high degree of phenotypic similarity to those from pancreatic tumours. Collectively, this data highlights potential conservation of CD105+ and CD105- fibroblast lineage restriction across different anatomical locations, that may have implications for a variety of normal and pathological fibroblast-driven processes.

10.2 – Expected outcomes from research findings

CD105 was originally included in the mesenchymal stromal mass cytometry panel because it is a reported marker of MSCs and is also robustly expressed on pericytes and endothelial cells (Barry et al., 1999; Dominici et al., 2006; Jin et al., 2017; Sugden et al., 2017). The results presented in this thesis demonstrate that at least two functionally distinct fibroblast populations exist in murine and human pancreas and PDA and that they can be separated based on stable, differential expression of CD105. Thus, an expected outcome from this work is that future studies of fibroblast function in the pancreas or in PDA, will improve the accuracy of their conclusions by first checking the CD105 status of the fibroblasts they are working with or ideally, separating fibroblast isolations into CD105+ and CD105- fractions and study their functions separately. For example, a simple isolation of primary fibroblasts from the pancreas contains a mixture of CD105+ and CD105- fibroblasts and the ratio changes during *in vitro* culture. At day 4 there is a higher fraction of CD105+ fibroblasts present than at day 10. Thus, analysis conducted on the bulk population at these two time points will likely show different results. The data presented here demonstrates CD105+ and CD105- fibroblasts have divergent behaviours and therefore, I expect that separation based on CD105 status, would greatly improve the consistency, accuracy and reproducibility of any results generated using pancreatic fibroblasts. CD105+ and CD105- fibroblasts are observed in many other mammalian organs and tumour types and it is possible that a similar approach of monitoring or isolating based on CD105 would be beneficial when studying fibroblasts from other tissues, tumours or pathologies. Importantly, more work is needed to determine whether the functional diversity of CD105+ and CD105- fibroblasts extends to other tissues and tumours.

A second expected outcome from this work is an appreciation that to fully understand fibroblast functions, a detailed understanding of interactions between fibroblasts and adaptive immunity will be required. Fibrosis and inflammation are already established as

highly intertwined biological processes and fibroblasts are well known to be activated by inflammatory factors (Biffi et al., 2019; Meng et al., 2014). The data presented in this PhD thesis suggests that, in addition, to being downstream of inflammatory signals, specific populations of fibroblasts can act directly upstream of important immune functions and can dictate anti-tumour immunity. The ability of fibroblasts to directly modulate immune cell behaviour is less well documented than other fibroblast functions, such as ECM modification. The data presented in this thesis suggests that understanding of how fibroblasts contribute to immune cell functions have probably been complicated by the heterogeneity of fibroblasts and that not all populations of fibroblasts interact with the immune system in the same way. Indeed, distinct lineages (e.g. CD105+ and CD105) and phenotypic states (e.g. MyCAF- and iCAF-like) are likely all present at the same time in a single tumour, highly complicating functional annotation of the general fibroblast population. The studies presented here that compare tumour growth in immune-competent and immune-deficient mice, indicate that the interaction between CD105- fibroblasts and adaptive immunity is the dominant functional phenotype *in vivo,* with little or minor contributions from more established fibroblast functions, such as paracrine cancer cell signalling, altered cancer migration/EMT and tumour angiogenesis. Thus, a more complete understanding of dominant fibroblast functions will require directly comparing fibroblast functions in immune-competent and immune-deficient models and interrogating fibroblast and immune cell interactions.

10.3 – Application of additional technologies to study fibroblast heterogeneity

A notable limitation of the mass cytometry approaches used in this PhD project, and indeed of other single cell technologies, such as scRNAseq and flow cytometry experiments, is that they require the target sample to be disaggregated into a single cell suspension and thus all spatial information is lost. Cell-cell contact of fibroblasts is a key driver on fibroblast-mediated functions and a key driver of inflammation and immune functions is the compartmentalisation of groups of immune cells together (Sautes-Fridman et al., 2019; Wei et al., 2020; Zhou et al., 2018). Thus, a key step in improved understanding of fibroblast phenotype and function in the future will to integrate high parameter novel single cell technologies with analysis that preserves spatial information of cell types and phenotypes in tissues. One such novel method is 'CODEX', an iterative imaging analysis platform that allows >40 markers to be measured on the same FFPE

tissue slice by immunofluorescence-based imaging methods (Goltsev et al., 2018). Such high parameter studies will enable the number of measured parameters required to simultaneously map fibroblast and immune cell heterogeneity, whilst preserving the spatial organising of these cell types in tumours. These methods will enable more information to be extracted from the huge number of archival FFPE tumour samples stored by clinical and biomedical research institutions and has potential to greatly improve understanding of fibroblast behaviour in human tumours. Another benefit of using such spatial distribution analysis is that the cellular architecture of murine and human FFPE tumours can be directly compared, which may help contribute to answering one of the most pressing outstanding questions in tumour fibroblast research: how well do mouse fibroblast systems model human fibroblast systems? (See section 10.4.3)

Novel technologies such as mass cytometry, scRNAseq and highly multiplexed imaging methods, all have the potential to make major contributions to improved understanding of fibroblast heterogeneity and functions in tumours and tissues. However, their selection for each specific analysis needs to be considered carefully. A detailed understanding of the advantages and disadvantages of each technology is needed to fairly evaluate which is the best tool for the desired purpose and how the technologies can be efficiently combined to provide complimentary and synergistic data.

10.4 – Outstanding research questions and future directions

10.4.1 – What are the most important functions of fibroblasts in tumours *in vivo*?

One of the most important areas for future PDA fibroblast research, will be to improve understanding of fibroblast functions in tumours *in vivo*, particularly with respect to the functions of specific subpopulations of fibroblasts. Indeed, before fibroblasts can be considered as potential therapeutic targets, a better understanding of their functional properties and the 'division of labour' between subpopulations is needed. For example, understanding of fibroblast heterogeneity and function in tumours, lags far behind the understanding of fibroblast function in mammalian skin (see Chapter 1). One of the reasons for this has been the successful application of *in vivo* lineage tracing models in dermal fibroblast research, that have revealed distinct fibroblast lineages, their

developmental hierarchies and their specific *in vivo* functional contributions to skin homeostasis and wound healing (Driskell et al., 2013). Such a detailed understanding of fibroblasts in PDA tumours is lacking and similar lineage tracing models would likely be huge step forward towards the development of effective stromal targeting therapies.

There are limited methods for studying fibroblast function in tumours *in situ* and until more robust models are developed, co-transplant models may be a useful tool for generating hypotheses to test in more representative spontaneous tumours models. The results described in this PhD project have outlined a dramatic tumour suppressive phenotype of CD105- fibroblast and PDA tumour cell co-transplants, that is entirely dependent on adaptive immunity. A key next step would be to understand the mechanism of this fibroblast-mediated enhancement of anti-tumour immunity. One approach to do this would be to compare the bulk gene expression between the growing PDA-only mono-transplant, the CD105+ fibroblast co-transplant and the CD105- fibroblast co-transplant conditions. This would reveal key gene expression changes between fibroblast-mediated permissive and suppressive growth states. A time course analysis would likely be needed because it is not known when during co-transplant growth, that the key interactions with adaptive immunity are occurring. If the gene expression profile is measured too late, the key gene expression changes may be missed completely or will appear as a generic immune response (e.g. IFN and cytotoxic signature). In addition, to gene expression measurements, analysis of the immune cell infiltrate (as measured by flow cytometry or mass cytometry) and cytokine/growth-factor abundance (as measured by multiplexed ELISA), would likely provide clues about the key immunological processes occurring during the permissive versus suppressive growth conditions. Again, measurements across a range of time points would give a more detailed understanding of the evolving adaptive immune reaction. The relative contributions of CD4+ or CD8+ T cells could be assessed by using appropriate depleting antibodies and the role of specific cytokines could be assessed using blocking antibodies (e.g. neutralising anti-TNFα antibodies) or transgenic mice lacking relevant ligands or receptors (e.g. *Ifng*$^{-/-}$ or *Infgr*$^{-/-}$). Lastly, detailed imaging analysis may reveal the spatial distribution of fibroblasts and immune cells that are key to generating the differential growth. Thus, the co-transplant model may provide a useful system to study the interactions between fibroblast and adaptive immunity in the context of a growing PDA tumour. Importantly though, any proposed mechanism will need to be validated, firstly in

spontaneous murine model (see next paragraph) and ultimately investigated in human tumours (see section 10.4.3).

As mentioned, there are currently very limited tools to study fibroblasts in tumours *in situ*. This is stark contrast to the field of tumour immunobiology, in which the huge variety of *in vivo* tools available for research has greatly accelerated understanding of specific immune cell functions in tumour and responses to immunotherapy (Hildner et al., 2008). For example, transgenic mouse models are readily available that constitutively lack specific aspects of the immune system (as for the NSG, *Rag1-/-* and *Batf3-/-* mice used in this PhD project) or in which specific cell types or genes can be modulated in a conditional manner (e.g. through Cre-recombinase, DTR expression or tetracycline-controlled systems). Indeed, a variety of immune cell types can be effectively depleted in wild-type hosts and methods for generating bone marrow chimeras add a further flexible tool for explorative science. Analogous methods for deleting fibroblast subpopulations or modulating fibroblast gene expression/functions in specific fibroblast populations in tumours *in situ* are lacking. As such, the majority of fibroblast functional studies in tumours are reductionist, using *in vitro* model systems or *in vivo* transplants of isolated fibroblasts, as have been used in this PhD project. *In vitro* models and *in vivo* transplant models likely do not fully capture the impact fibroblasts have on tumour progression, maintenance and therapeutic resistance. For example, when fibroblasts are co-transplanted with cancer cells, the cancer cells typically overtake stromal cells rapidly which does not happen in spontaneous tumours. In addition, *in vitro* expansion risks irreversibly altering fibroblast function, through artificial isolation methods and manipulations. Thus, understanding of fibroblast function in tumours would be greatly advanced by the development of mouse models, in which fibroblast function can be modulated in specific subpopulations of fibroblasts, as has analogously been achieved in the study of tumour immunology.

Strains of mice have been developed that utilize Cre-recombinase technology and fibroblast-associated genes such as *Col1a1, Pdgfrα, Fap and Acta2* for lineage tracing and have been successfully used to track and isolate general fibroblast populations. The usefulness of such systems to directly modulate fibroblast gene expression *in vivo* (e.g. by crossing to LSL-deletor strains) or similar methods to deplete fibroblasts in tumours (e.g. using DTR or HSV-TK expression systems) is limited though. Firstly, these genes

are known to be highly expressed by other non-fibroblast mesenchymal cells, such a pericytes and smooth muscle cells. Therefore, if used to alter gene expression or deplete cells, these systems will modulate other important mesenchymal compartments, such as the vasculature. In addition, these genes are known to be expressed by fibroblasts in many different organs. Thus, using these systems to manipulate fibroblast gene function will likely induce complex systemic effects which may confound findings. For example, depletion of FAP+ stromal cell causes systemic cachexia and anaemia (Roberts et al., 2013). Lastly and importantly, several of the genes used to drive these models are also broadly expressed by most fibroblasts, so genetic manipulation or deletion cannot be restricted to specific lineages or phenotypes of fibroblasts. Thus, selection of more specific gene promoters will an essential step towards *in situ* manipulation of specific populations of fibroblasts in tumours. Distinct lineages of fibroblasts have been traced in the skin by leveraging fibroblast lineage-restricted expression of *Dlk1* or *En1* (Driskell et al., 2013; Rinkevich et al., 2015). It would be particularly interesting to see if these lineage tracing models are able to delineate CD105+ and CD105- fibroblasts in the pancreas. In a similar manner, a detailed understanding of fibroblast lineage restricted gene expression programs in tumours, will be key to *in vivo* modulation of fibroblast functions in cancer.

As mentioned above, orthotopically transplanted PDA tumour cell lines rarely develop a fibrotic reaction and thus do not model human PDA accurately. This has meant the 'gold-standard' model in the field has become the spontaneous KPC model. But herein lies another confounding issue to studying fibroblasts *in situ*: the KPC (as for most other spontaneous models of cancer) uses the Cre-recombinase system to initiate tumourigenesis and thus the Cre-recombinase system cannot simultaneously be used to modulate fibroblast function. There are three possible approaches that may circumvent this issue to improve future experiments for *in situ* modulation of fibroblast function.

The first would be to combine Cre-recombinase systems for cancer initiation, with flippase-based systems for stromal cell manipulation (or vice versa). These models have been demonstrated to be compatible and allow complex, simultaneous gene manipulation (Schonhuber et al., 2014). Thus, spontaneous tumours would develop in the context of genetically modified fibroblasts. Again, an important step here would be to

identify appropriate gene protomers to target specific fibroblast populations. Thus, a comprehensive understanding of gene expression patterns in fibroblasts will be key. In this regard, differential expression of collagens seen in this study may be particularly useful. During this PhD project, several genes are consistently found to be expressed selectively by either CD105+ or CD105- fibroblasts, for example, *Col8a1* and *Col4a6,* respectively. This could potentially be used to drive fibroblast lineage-restricted gene manipulation or fibroblast subpopulation depletion via expressed DTR/HSV-TK systems. In addition, heterogenous populations of fibroblasts in the lung have been shown to differentially express *Col13a1* and *Col14a1*, suggesting these genes may also be useful for tracing or manipulating specific lung fibroblast populations (Xie et al., 2018). Indeed, a similar method may have already inadvertently been proven experimentally: two models of colitis-induced carcinoma show opposite effects on tumour progression when stromal *Ikkb* is deleted under control of either the *Col1a2* or *Col5a1* gene promoter, suggesting these genes may not only be expressed in different stromal compartments, but that these stromal compartments have opposing roles in inflammation-driven tumourigenesis (Koliaraki et al., 2015; Pallangyo et al., 2015). Whether such specific collagen genes are restricted to fibroblasts only, have sufficient subpopulation selectivity or are expressed to sufficient levels for highly penetrant recombination, will require further detailed studies. In addition, the range of commercially available Flippase-based models is limited and such models are typically custom generated, which can be expensive and time consuming.

A second approach would be to delete fibroblast activating factors that exclusively derive from tumour cells by crossing the KPC to other Cre-deletor models. This has already been successfully demonstrated in arguably the most sophisticated PDA *in situ* fibroblast-altered model to date, in which the KPC model was crossed with a $Shh^{fl/fl}$, model (Rhim et al., 2014). KPC tumours develop in which the cancer cells are unable to activate adjacent fibroblasts via SHH secretion. Such deletion is obviously only relevant to fibroblast-activating factors that derive directly from cancer cells and could not be used to study factors that derive from other cells of the TME. In such cases, pharmacological blockade of fibroblast-activating factors may be useful. However, this comes with the caveat that this method is not selective and will block the targeted pathway in other cell types.

A third option is to find transplantable systems that generate a robust fibrotic response and therefore more closely resemble human PDA. Transplants of 2D PDA cell lines, even when done orthotopically, induce far less fibrosis than that seen in spontaneous murine and human PDA tumours. If cell transplant systems could be found that recapitulate the fibrotic TME of human PDA, this would enable the broad range of existing and novel Cre-dependant models to be used as hosts and would greatly widen the scope for *in situ*-fibroblast modulation. Notably, improved fibrotic responses have been described with orthotopic implants of KPC PDA organoids into the murine pancreas (Boj et al., 2015) and work in our own lab has largely supported these findings. In addition, an orthotopic transplant model system would greatly improve the ease-of-use and throughput of PDA *in vivo* work: the KPC GEMM is logistically a challenging model to work with. The ability of organoid orthotopic transplants to recapitulate the TME of spontaneous murine and human tumours has been almost exclusively based on simple qualitative staining of αSMA by IHC (Boj et al., 2015). More detailed, quantitative comparisons between organoid-initiated and spontaneous murine and human PDA tumours are needed to better understand the relevance of this new and exciting model system.

As described in more detail in the next section, very little is known about the functions of different fibroblast populations in normal tissue development and homeostasis and the models described above, may also offer flexible tools to better understand fibroblast biology in non-tumour settings.

Fibroblasts are one of the major producers of ECM and ECM modifying components and manipulation of the ECM is a major way in which fibroblasts exert their functions (Kalluri, 2016). Thus, to fully characterise fibroblast functions in tumours, a better understanding of the functions of the ECM is needed. ECM production and remodelling are commonly assessed, but the functional consequence of these and how the modified ECM regulates the functions of other cells, are poorly understood. Studies that do focus on the ECM, have demonstrated ECM composition, fibre orientation and stiffness can all profoundly influence the functions of cancer cells, immune cells and blood vessels in the TME (Baker et al., 2013; Lebid et al., 2020; Saatci et al., 2020). Despite this, most analysis methods for studying cell behaviour in the TME, including those used in this thesis, measure cells after tissue disaggregation and complete degradation of the ECM. In

addition, 2D *in vitro* models are poorly suited to studying the roles of ECM on cell function. Thus, studying fibroblast-derived ECM in tumour samples *in situ*, or finding *in vitro* models that allow realistic ECM networks to be generated, will be needed to better understand how fibroblasts exert their various functions in tumours through ECM modulation.

In summary, improved understanding of how fibroblasts functionally influence tumours will require improved model systems that capture the broadest range of fibroblast functions possible (e.g. including immune cell interactions and ECM modulation). It is highly unlikely that any single model system will fully recapitulate fibroblast behaviour in human tissues or pathologies. Thus. the biggest improvements in the accuracy of fibroblast research, will likely come from the rational combination of multiple *in vitro* and *in vivo* model systems, in which the advantages and limitations of each are well defined. Whilst thorough characterisation of such models is time consuming and costly, the entire fibroblast-research community, across multiple research areas, will benefit from such critical analysis.

10.4.2 – Do fibroblasts in tumours come from expansion of local, tissue-resident fibroblasts or other sources? Why are there different fibroblast populations present in healthy tissues? What dictates their accumulation in tumours?

Another important area for future fibroblast research, is to determine the origin of fibroblasts and their subsets in tumours. Indeed, improved understanding of the cellular origin of fibroblasts in tumours, may in turn lead to better understanding of why different fibroblast populations have different functions. For example, is there a reason why in the normal pancreas, CD105- fibroblasts are present that are able to enhance adaptive immune function? Does this have some immunological function related to pathogen control? Do CD105- fibroblasts in the pancreas influence autoimmune pathologies, such as type-1 diabetes? Tumours are complex and chaotic places and may not be the best place to study the functions of different fibroblast populations. In this regard, better defining the origins of fibroblasts and understanding fibroblast behaviour in healthy organs may possibly be a more appropriate way to reveal key drivers of differential functions. For example, fibroblasts are typically studied during pathogenesis and are often cited as being ‘quiescent’ until ‘activated’, which suggests a baseline level of

inactivity. Yet fibroblasts have well established roles in normal tissue development and homeostasis throughout an organism's lifetime. For example, during the development and repair of the skin after wounding and supporting the intestinal epithelium via paracrine signalling (Driskell et al., 2013; Karpus et al., 2019). Thus, understanding of the roles of pancreatic fibroblasts in the healthy pancreas, may better reveal the reasons CD105+ and CD105- fibroblasts have evolved divergent functions.

Local fibroblasts and more distal sources, such as bone-marrow derived mesenchymal stem cells, have been suggested to be sources of fibroblasts in tumours. The contribution from the bone marrow in most models appears to be minimal (see introduction chapter). Indeed, the high degree of similarity between CD105+ and CD105- fibroblasts in the murine pancreas and in murine PDA tumours is supportive of local expansion of fibroblasts rather than distal recruitment. Epithelial cells, pericytes, endothelial cell, adipocytes and mesothelial cells have all been shown to undergo mesenchymal transitions and have the potential to adopt fibroblast-like morphologies and gene expression patterns. Whether fibroblasts in tumours that originally derive from such different cell types, behave in the same way once transitioned or are inherently different because of their ontogeny, is not clear. Indeed, how reversible each of these mesenchymal transitions is, is also not well understood, although reversal of fibroblasts to adipocytes has been reported (Plikus et al., 2017). Quantifying the contribution of different cell types to the fibroblast compartment of tumours will be challenging and application of robust lineage tracing models will be needed. Such lineage tracing models will need to be highly specific, which will require a detailed understanding of the gene expression profiles of fibroblasts and other putative fibroblast sources throughout development, as well as robust cytometry and imaging workflows to follow lineage tracers in pure fibroblast subpopulations. In this regard, the type of mass cytometry analysis described in this thesis, would be an ideal platform to track and follow mesenchymal transitions in heterogeneous fibroblast populations, using lineage marker expression.

The mass cytometry data presented in Chapter 4 demonstrates that whilst fibroblasts, pericytes and endothelial cells share common features with each other, they all form very distinct clusters with no overlap. No intermediate populations with mixed marker expression indicative of pericyte- or endothelial-to-fibroblast transition were observed in

any of the 19 PDA tumours tested. Thus, it seems unlikely these cell types are a source of any major fibroblast fraction in these tumours, although lineage-tracing models would be needed to test this fully. Interestingly, mesothelial cells are known to undergo mesenchymal transitions but are a relatively understudied source of tumour fibroblasts. The pancreas (as for many internal organs) is surrounded by a single-cell layer of mesothelial cells, that in other tissues is known to rapidly expand after tissue damage (Li et al., 2013). Indeed, some data in this thesis does support the concept that mesothelial cells may possibly be a source of fibroblasts in PDA tumours. For example, subpopulations of CD105- fibroblasts in PDA tumours have high expression of PDPN but show some level of expression of PCK. This unusual, mixed PDPN+PCK+ phenotype is a hallmark feature of mesothelial cells, although cells that have fully undergone mesenchymal transitions would be expected to lose expression of defining mesothelial proteins (such a cytokeratins) and express proteins typically associated with mesenchymal and fibroblasts identity (e.g. CD90, PDGFRα, αSMA) (Mutsaers et al., 2015). Gene expression analysis of fibroblasts from murine pancreas and PDA tumours, does indeed detect low levels of expression of known mesothelial genes (e.g. *Krt8/18*, *Wt1*, *Msln*, *Upk3b*, *Ezr*) in CD105- fibroblasts compared to CD105+ fibroblasts. However, it is possible these may simply be minor contaminating PDPN+ mesothelial cells falling within the fibroblast FACS gate. Several studies have demonstrated that mesothelial cells can be a source of fibroblast-like cells under pathological conditions. For example, mesothelial cells undergoing mesothelial to mesenchymal transition have been shown to be a major source of hepatic stellate cells and myofibroblasts after liver injury (Li et al., 2013) and mesothelial cells are a major contributor to fibrotic reactions to peritoneal dialysis (Lopez-Cabrera, 2014; Namvar et al., 2018). In addition, mesothelial cells are major contributors to fibrotic adhesions after internal organ surgery and they contribute to mesenchymal cell types during development of trunk organs (Koopmans and Rinkevich, 2018; Mutsaers et al., 2015). Mesothelial cell can also be a source of vascular mesenchymal cells during the development of the mammalian gut (Wilm et al., 2005). FSP1, a known marker of mesothelial cells, has been reported to be expressed on subpopulations of fibroblasts in tumours (Sugimoto et al., 2006). Notably, some evidence suggests mesothelial to mesenchymal transitions can be a source of fibroblasts in locally advanced human colorectal cancer (Gordillo et al., 2020). In such cases, the mesothelium is reached during invasive tumour growth, thus conversion of mesothelial cells to fibroblasts may be a feature of advanced/invasive tumours. Interestingly, the

mesothelium as source of immune-enhancing fibroblasts may fit with a role in limiting pathogen spread, directly from one internal organ to another. In addition, mesothelial cells may adopt fibroblast function when expanded *in vitro*, and therefore they may make a significant contribution to *in vitro* primary fibroblast cultures from the pancreas and other internal organs. Thus, studying tumour formation in the context of a robust mesothelial lineage tracing model (e.g. *Wt1-Cre* or *Msln-Cre)* will be key to revealing if this relatively understudied cell type can contribute to the fibroblast compartment of tumours. More generally, much further work is needed to better understand where fibroblasts in tumours come from and how their cell of origin influences their functions in tumours.

In addition to understanding fibroblast cell of origin, it will be interesting to determine what dictates the relative abundance of various fibroblast populations/lineages in tumours. For example, in KPC PDA tumours, a wide range of CD105+:CD105- fibroblast ratios are observed. However, the signals that dictate the relative abundance of each fibroblast lineage is not clear. The *in vitro* stimulation experiments presented in this thesis, suggest that at the level of signalling node activation, gene expression and protein expression, CD105+ and CD105- fibroblasts can have very different responses to activating factors. For example, CD105+ fibroblasts have stronger early transcriptional responses to TGFβ1 and IL1α and CD105- fibroblasts had stronger signalling responses to TNFα. Both populations respond in a similar manner to IFNγ and both CD105+ and CD105- fibroblasts have a strong response to PDGF, but the signalling pathways activated were very different. Thus, some of these soluble proteins may play a role in dictating the balance between CD105+ and CD105- fibroblasts in tumours. Whether the fibroblast factors that induce 'activation' are also the ones that induce population expansion, is largely unknown. For example, IL1α is a well-established, potent inducer of the iCAF phenotype, but does IL1α result in expansion of iCAFs *in vivo*? The wide variation in the CD105+:CD105- fibroblast ratio seen in KPC tumours may allow for correlations to be drawn: cytokine/GF levels and CD105+:CD105- fibroblasts ratios can be measured simultaneously and it might be possible to associate the levels of specific factors with the abundance of different fibroblast populations. Another method may be to use antibodies or transgenic mice to block/neutralise specific signalling ligands or receptors and assess the impact this has on the CD105+:CD105- ratio. Blocking fibroblast activating pathways to promote the accumulation of anti-tumourigenic

fibroblast phenotypes or lineages, may be one way to target the PDA stroma for therapeutic benefit.

10.4.3 – How well do murine fibroblasts model human fibroblasts? How can we improve translatability of murine fibroblast research?

One of the most important questions in fibroblast biology, and possibly one of the hardest to answer, is how similar are fibroblast functions between mice and humans, and by extension, how well do our mouse model systems recapitulate the fibroblast processes that occur in people? Answering this question will be key to the successful development of fibroblast-targeting therapies across a range of diseases. In this regard, understanding of fibroblast heterogeneity and fibroblast function may provide one of the most robust, meaningful and quantifiable features to compare fibroblasts between mice and humans and to begin to draw conclusions. A shared feature of mammalian fibroblasts, that has been known for a long time, is the ability of both mouse and human fibroblasts to adopt the so called myofibroblast (MyCAF-like) phenotype, broadly defined by high αSMA expression and stress fibre formation. As a more detailed understanding of the MyCAF-like and, more recently, the iCAF-like phenotype has evolved, gene expression comparisons can now be made between murine and human PDA fibroblasts and have revealed the MyCAF and iCAF-like phenotypes are largely conserved between the species (Dominguez et al., 2020; Elyada et al., 2019). The general agreement in gene expression profiles between major fibroblast phenotypes in murine and human PDA tumours provides some confidence that mice can be used to model these specific fibroblast phenotypes, although more detailed comparisons of actual fibroblast functions will be an important next step. At least two fibroblast lineages exist in murine skin, which can be identified by differential expression of *Dpp4 in vivo* (Driskell et al., 2013; Rinkevich et al., 2015). Two scRNAseq studies of human skin samples have revealed that differential expression of *Dpp4* is also able to define distinct fibroblast populations in human skin (Philippeos et al., 2018; Tabib et al., 2018). Similar studies comparing murine and human fibroblasts in other tissues, will broaden our understanding of how similar fibroblast composition is between the two species. The key comparison will then be whether the functions of fibroblast subpopulations are conserved between species.

As well as the similarity between MyCAF/iCAF-like states in murine and human PDA, the results in this thesis demonstrate that CD105+ and CD105- fibroblasts are also present in both murine and human PDA tumours. The analysis of human fibroblasts presented in this thesis is limited and further work is needed to compare the gene expression patterns and response to activating factors between murine and human CD105+ and CD105- fibroblasts. A key experiment will be to directly isolate CD105+ and CD105- fibroblasts from human PDA tumours and measure their gene expression profiles and compare this to the gene expression profiles of the respective murine populations. Another particularly interesting piece of follow up work would be to try to understand if CD105- fibroblasts promote anti-tumour immunity in humans, as observed here in mice. To do so will be challenging and effective comparisons will likely only be possible once the mechanism for CD105- fibroblast-mediated enhancement of anti-tumour immunity is better understood. For example, if the mechanism works through cell-cell interactions with a specific immune cell type and CD105- fibroblasts, such interactions could be investigated in human PDA tumour samples by imaging analysis.

Importantly, the difference in sample collection between mice and human tumour needs to be considered when comparing data from the species. For example, sampling differences may introduce large biases and limit the accuracy of mouse to human comparisons. Typically, mouse tumours are collected whole and disaggregated and therefore, the entire sample (core and invasive edge) is analysed. In contrast, most human tumour samples are taken as small core biopsies from within the larger tumour mass. Normally the centre of the tumour is targeted for sampling to increase the chances of collecting tumour cells (for example, for assessment by pathologists). This may mean that the majority of human biopsies do not measure processes at the tumour borders and invasive edge, which is where a lot of important tumour biology occurs. For example, the invasive front is often where the immune system interacts most directly with the tumour and where initial fibroblast activation and polarisation would be expected to take place. The increased use of ultrasound guided fine needle biopsies to sample tumours has increased the number of samples available for research use, but may exaggerate this sampling bias even more: ultrasound is used to accurately guide the collection needle to areas of high tumour density within the patient and a very small needle biopsy is taken, typically aiming for the tumour core/centre. Related to this sampling bias, is the fact that improved disaggregation methods will be needed to improve the study of

fibroblasts: fibroblasts are underrepresented in tumour analysis generally and more complete cell dissociation methods will release higher number of fibroblasts to study and may also be needed to release specific fibroblast phenotypes (e.g. those tightly bound to ECM networks).

Human tumours develop over much longer periods of time than spontaneous murine tumours, and this may be another important difference that contributes to species-specific differences in fibroblast composition. The most widely used GEMM of PDA is the KPC mouse, which only has macroscopic adenocarcinoma stage disease for ~1 month (Hingorani et al., 2005). Even though human PDA tumours are typically diagnosed late in disease progression, modelling of mutation rates has suggested they can develop over periods of time >10 years (Yachida et al., 2010). Thus, if different fibroblast lineages and phenotypes have different persistence over long periods of time, this may result in major differences between mice and humans. The longer duration of tumour progression that occurs in human PDA tumours, may also allow more time for the tumour to exert selective effects on the TME. A recent scRNAseq study has indicated that most fibroblasts in human PDA tumours are in the MyCAF-like state and that murine tumours have more iCAF-like fibroblasts that humans (Dominguez et al., 2020). Studies using more quantitative technologies than scRNAseq need to be conducted to accurately measure such species-specific composition differences (although again the sampling bias may have an impact here).

One possible way to better predict human fibroblast behaviour with mouse models, may be study fibroblast function across multiple mouse organs. Nine years ago, Friedman and colleagues proposed that because the patterning of mammalian organs occurred prior to the evolutionary divergence between the ancestors of mice and humans, common ‘core’ fibrosis pathways that are found in multiple mouse organs are more likely to be evolutionarily conserved in humans (Mehal et al., 2011). In addition, studying the same pathway in different murine organs is usually easier than trying to study the same pathway in the same organ but in a different species. Thus, conservation of a fibroblast behaviour across different murine organs would strongly suggest the pathway/phenotype predates speciation. One notable example would be robust proof of MyCAF/iCAF-like functions across fibroblasts from different organs, which would be suggestive of a high degree of conservation in human tissues. Focussing on such common pathways will

reduce the chance that novel fibroblast findings are relevant only to mice and hopefully improve the rate at which fibroblast-targeting therapies succeed in clinical trials. Such comparisons between tissues are feasible because fibroblasts are present in most mammalian organs and this may represent an important factor to leverage in fibroblast research, that is simply not feasible for other cell types. Notably, gene knockout mice or inhibitor studies can readily be adapted to study fibroblast function from one organ to another. Most studies focus on fibroblasts in one organ or tumour type and studies mapping fibroblast heterogeneity, phenotype and function across multiple different are less common. Such multi-organ studies will require more resources and expertise than projects focussed on a single organ and will likely require increased collaboration among research networks. However, broadening fibroblast studies across different organs may greatly enhance the therapeutic relevance of such research. In addition, publishing findings that are discordant between organs (and therefore likely less relevant to human biology), will be extremely useful for mapping tissue-specific or murine-specific aspects of fibroblast function. However, scientific research in general has a poor record of publishing negative data (Nature Career Column, 2019). Specifically related to fibroblast-targeting therapies in cancer, understanding of shared fibroblast functions across organs may also be particularly important in the metastatic setting and for developing therapies that are effective in targeting tumours that have spread to distant sites. Developing a fibroblast targeting therapy that is exquisitely effective in the primary tumour but ineffective (or even worse tumour-promoting) at metastatic sites will have limited utility in the majority of cancer patients. Indeed, demonstrating fibroblast targeting therapies can be broadly applicable across different tissues is more likely to encourage research investment from large pharmaceutical companies. Ultimately, the real test of the relevance of any mouse model system for studying fibroblast function, will be when fibroblast-targeting therapies that are active in mouse models, are moved forward and tested in human clinical trials.

10.5 – Concluding statement

PDA is a terrible disease that causes a huge amount of suffering to patients and their loved ones. Innovative and novel approaches need to be explored to improve patient outcomes. Targeting the PDA TME has been proposed as one such approach (Chen and Song, 2019; Hosein et al., 2020). However, the complicated and constantly evolving

cellular ecosystems of tumours pose a major challenge to the development of effective therapies. In particular, the variety of competing pro- and anti-tumourigenic functions, need to be better understood to ensure that TME-targeting therapies are developed and tested in a rational and informed manner. Without such understanding, it will be difficult to find treatments that maximise efficacy, whilst minimising unwanted effects. Fibroblasts are one of the most abundant cell types in the PDA TME, yet very little is known about their functional contributions to PDA tumour progression and therapeutic resistance *in vivo*. The results described in this thesis specifically highlight CD105+ and CD105- fibroblasts as distinct, non-overlapping fibroblast lineages in PDA tumours, with divergent functions dependant on interactions with adaptive immunity. These results may be a small step to an improved understanding of fibroblasts in the PDA TME. Much further work is required to better understand the specific functions of CD105+ and CD105- fibroblast populations, the mechanisms that drive divergent behaviours, the relevance of these findings to other murine organs and ultimately the clinical relevance of these findings to the human disease.

Chapter 11 – Appendix and references

11.1 – References

Abe, R., Donnelly, S.C., Peng, T., Bucala, R., and Metz, C.N. (2001). Peripheral blood fibrocytes: differentiation pathway and migration to wound sites. J Immunol *166*, 7556-7562.

Aboussekhra, A. (2011). Role of cancer-associated fibroblasts in breast cancer development and prognosis. Int J Dev Biol *55*, 841-849.

Aghajanian, H., Kimura, T., Rurik, J.G., Hancock, A.S., Leibowitz, M.S., Li, L., Scholler, J., Monslow, J., Lo, A., Han, W., et al. (2019). Targeting cardiac fibrosis with engineered T cells. Nature *573*, 430-433.

Agorku, D.J., Langhammer, A., Heider, U., Wild, S., Bosio, A., and Hardt, O. (2019). CD49b, CD87, and CD95 Are Markers for Activated Cancer-Associated Fibroblasts Whereas CD39 Marks Quiescent Normal Fibroblasts in Murine Tumor Models. Front Oncol *9*, 716.

Ahmed, K.A., Munegowda, M.A., Xie, Y., and Xiang, J. (2008). Intercellular trogocytosis plays an important role in modulation of immune responses. Cell Mol Immunol *5*, 261-269.

Ahuja, D., Saenz-Robles, M.T., and Pipas, J.M. (2005). SV40 large T antigen targets multiple cellular pathways to elicit cellular transformation. Oncogene *24*, 7729-7745.

Aiello, N.M., Bajor, D.L., Norgard, R.J., Sahmoud, A., Bhagwat, N., Pham, M.N., Cornish, T.C., Iacobuzio-Donahue, C.A., Vonderheide, R.H., and Stanger, B.Z. (2016). Metastatic progression is associated with dynamic changes in the local microenvironment. Nat Commun *7*, 12819.

Albrengues, J., Bertero, T., Grasset, E., Bonan, S., Maiel, M., Bourget, I., Philippe, C., Herraiz Serrano, C., Benamar, S., Croce, O., et al. (2015). Epigenetic switch drives the conversion of fibroblasts into proinvasive cancer-associated fibroblasts. Nat Commun *6*, 10204.

Alitalo, K., Kuismanen, E., Myllyla, R., Kiistala, U., Asko-Seljavaara, S., and Vaheri, A. (1982). Extracellular matrix proteins of human epidermal keratinocytes and feeder 3T3 cells. J Cell Biol *94*, 497-505.

Allen, B.M., Hiam, K.J., Burnett, C.E., Venida, A., DeBarge, R., Tenvooren, I., Marquez, D.M., Cho, N.W., Carmi, Y., and Spitzer, M.H. (2020). Systemic dysfunction and plasticity of the immune macroenvironment in cancer models. Nat Med.

American Cancer Society (2019). Cancer Facts and Figures 2019, https://www.cancer.org/research/cancer-facts-statistics/all-cancer-facts-figures/cancer-facts-figures-2019.html.

Andea, A., Sarkar, F., and Adsay, V.N. (2003). Clinicopathological correlates of pancreatic intraepithelial neoplasia: a comparative analysis of 82 cases with and 152 cases without pancreatic ductal adenocarcinoma. Mod Pathol *16*, 996-1006.

Anderson, G., Moore, N.C., Owen, J.J., and Jenkinson, E.J. (1996). Cellular interactions in thymocyte development. Annu Rev Immunol *14*, 73-99.

Annes, J.P., Munger, J.S., and Rifkin, D.B. (2003). Making sense of latent TGFbeta activation. J Cell Sci *116*, 217-224.

Aras, S., and Zaidi, M.R. (2017). TAMeless traitors: macrophages in cancer progression and metastasis. Br J Cancer *117*, 1583-1591.

Arina, A., Idel, C., Hyjek, E.M., Alegre, M.L., Wang, Y., Bindokas, V.P., Weichselbaum, R.R., and Schreiber, H. (2016). Tumor-associated fibroblasts predominantly come from local and not circulating precursors. Proc Natl Acad Sci U S A *113*, 7551-7556.

Armulik, A., Genove, G., and Betsholtz, C. (2011). Pericytes: developmental, physiological, and pathological perspectives, problems, and promises. Dev Cell *21*, 193-215.

Arwert, E.N., Milford, E.L., Rullan, A., Derzsi, S., Hooper, S., Kato, T., Mansfield, D., Melcher, A., Harrington, K.J., and Sahai, E. (2020). STING and IRF3 in stromal fibroblasts enable sensing of genomic stress in cancer cells to undermine oncolytic viral therapy. Nature Cell Biology.

Auciello, F.R., Bulusu, V., Oon, C., Tait-Mulder, J., Berry, M., Bhattacharyya, S., Tumanov, S., Allen-Petersen, B.L., Link, J., Kendsersky, N.D., et al. (2019). A Stromal Lysolipid-Autotaxin Signaling Axis Promotes Pancreatic Tumor Progression. Cancer Discov *9*, 617-627.

Augsten, M., Hagglof, C., Olsson, E., Stolz, C., Tsagozis, P., Levchenko, T., Frederick, M.J., Borg, A., Micke, P., Egevad, L., et al. (2009). CXCL14 is an autocrine growth factor for fibroblasts and acts as a multi-modal stimulator of prostate tumor growth. Proc Natl Acad Sci U S A *106*, 3414-3419.

Bailey, J.M., Swanson, B.J., Hamada, T., Eggers, J.P., Singh, P.K., Caffery, T., Ouellette, M.M., and Hollingsworth, M.A. (2008). Sonic hedgehog promotes desmoplasia in pancreatic cancer. Clin Cancer Res *14*, 5995-6004.

Bailey, P., Chang, D.K., Nones, K., Johns, A.L., Patch, A.M., Gingras, M.C., Miller, D.K., Christ, A.N., Bruxner, T.J., Quinn, M.C., et al. (2016). Genomic analyses identify molecular subtypes of pancreatic cancer. Nature *531*, 47-52.

Baker, A.M., Bird, D., Welti, J.C., Gourlaouen, M., Lang, G., Murray, G.I., Reynolds, A.R., Cox, T.R., and Erler, J.T. (2013). Lysyl oxidase plays a critical role in endothelial cell stimulation to drive tumor angiogenesis. Cancer Res *73*, 583-594.
Baker, L.A., Tiriac, H., Clevers, H., and Tuveson, D.A. (2016). Modeling pancreatic cancer with organoids. Trends Cancer *2*, 176-190.
Baker, L.A., Tiriac, H., and Tuveson, D.A. (2019). Generation and Culture of Human Pancreatic Ductal Adenocarcinoma Organoids from Resected Tumor Specimens. Methods Mol Biol *1882*, 97-115.
Banerjee, S., Dhara, S.K., and Bacanamwo, M. (2012). Endoglin is a novel endothelial cell specification gene. Stem Cell Res *8*, 85-96.
Bankhead, P., Loughrey, M.B., Fernandez, J.A., Dombrowski, Y., McArt, D.G., Dunne, P.D., McQuaid, S., Gray, R.T., Murray, L.J., Coleman, H.G., et al. (2017). QuPath: Open source software for digital pathology image analysis. Sci Rep *7*, 16878.
Baranyi, U., Winter, B., Gugerell, A., Hegedus, B., Brostjan, C., Laufer, G., and Messner, B. (2019). Primary Human Fibroblasts in Culture Switch to a Myofibroblast-Like Phenotype Independently of TGF Beta. Cells *8*.
Barbara, N.P., Wrana, J.L., and Letarte, M. (1999). Endoglin is an accessory protein that interacts with the signaling receptor complex of multiple members of the transforming growth factor-beta superfamily. J Biol Chem *274*, 584-594.
Barry, F.P., Boynton, R.E., Haynesworth, S., Murphy, J.M., and Zaia, J. (1999). The monoclonal antibody SH-2, raised against human mesenchymal stem cells, recognizes an epitope on endoglin (CD105). Biochem Biophys Res Commun *265*, 134-139.
Barry, K.C., Hsu, J., Broz, M.L., Cueto, F.J., Binnewies, M., Combes, A.J., Nelson, A.E., Loo, K., Kumar, R., Rosenblum, M.D., et al. (2018). A natural killer-dendritic cell axis defines checkpoint therapy-responsive tumor microenvironments. Nat Med *24*, 1178-1191.
Bartis, D., Mise, N., Mahida, R.Y., Eickelberg, O., and Thickett, D.R. (2014). Epithelial-mesenchymal transition in lung development and disease: does it exist and is it important? Thorax *69*, 760-765.
Bartoschek, M., Oskolkov, N., Bocci, M., Lovrot, J., Larsson, C., Sommarin, M., Madsen, C.D., Lindgren, D., Pekar, G., Karlsson, G., et al. (2018). Spatially and functionally distinct subclasses of breast cancer-associated fibroblasts revealed by single cell RNA sequencing. Nat Commun *9*, 5150.
Baryawno, N., Przybylski, D., Kowalczyk, M.S., Kfoury, Y., Severe, N., Gustafsson, K., Kokkaliaris, K.D., Mercier, F., Tabaka, M., Hofree, M., et al. (2019). A Cellular Taxonomy of the Bone Marrow Stroma in Homeostasis and Leukemia. Cell *177*, 1915-1932 e1916.
Bautch, V.L. (2017). Endoglin moves and shapes endothelial cells. Nat Cell Biol *19*, 593-595.
Bautista-Hernandez, L.A., Gomez-Olivares, J.L., Buentello-Volante, B., and Bautista-de Lucio, V.M. (2017). Fibroblasts: The Unknown Sentinels Eliciting Immune Responses Against Microorganisms. Eur J Microbiol Immunol (Bp) *7*, 151-157.
Bayne, L.J., Beatty, G.L., Jhala, N., Clark, C.E., Rhim, A.D., Stanger, B.Z., and Vonderheide, R.H. (2012). Tumor-derived granulocyte-macrophage colony-stimulating factor regulates myeloid inflammation and T cell immunity in pancreatic cancer. Cancer Cell *21*, 822-835.
Becht, E., McInnes, L., Healy, J., Dutertre, C.A., Kwok, I.W.H., Ng, L.G., Ginhoux, F., and Newell, E.W. (2018). Dimensionality reduction for visualizing single-cell data using UMAP. Nat Biotechnol.
Bechtel, W., McGoohan, S., Zeisberg, E.M., Muller, G.A., Kalbacher, H., Salant, D.J., Muller, C.A., Kalluri, R., and Zeisberg, M. (2010). Methylation determines fibroblast activation and fibrogenesis in the kidney. Nat Med *16*, 544-550.
Behbehani, G.K. (2018). Cell Cycle Analysis by Mass Cytometry. Methods Mol Biol *1686*, 105-124.
Behbehani, G.K. (2019). Mass Cytometric Cell Cycle Analysis. Methods Mol Biol *1989*, 193-215.
Behbehani, G.K., Bendall, S.C., Clutter, M.R., Fantl, W.J., and Nolan, G.P. (2012). Single-cell mass cytometry adapted to measurements of the cell cycle. Cytometry A *81*, 552-566.
Bendall, S.C., Nolan, G.P., Roederer, M., and Chattopadhyay, P.K. (2012). A deep profiler's guide to cytometry. Trends Immunol *33*, 323-332.
Benton, G., Kleinman, H.K., George, J., and Arnaoutova, I. (2011). Multiple uses of basement membrane-like matrix (BME/Matrigel) in vitro and in vivo with cancer cells. Int J Cancer *128*, 1751-1757.
Bergmann, C., and Distler, J.H. (2017). Epigenetic factors as drivers of fibrosis in systemic sclerosis. Epigenomics *9*, 463-477.
Bernard, V., Semaan, A., Huang, J., San Lucas, F.A., Mulu, F.C., Stephens, B.M., Guerrero, P.A., Huang, Y., Zhao, J., Kamyabi, N., et al. (2019). Single-Cell Transcriptomics of Pancreatic Cancer Precursors Demonstrates Epithelial and Microenvironmental Heterogeneity as an Early Event in Neoplastic Progression. Clin Cancer Res *25*, 2194-2205.
Bhattacharjee, V., Zhou, Y., and Yen, T.J. (2014). A synthetic lethal screen identifies the Vitamin D receptor as a novel gemcitabine sensitizer in pancreatic cancer cells. Cell Cycle *13*, 3839-3856.

Bhattacharyya, S., Midwood, K.S., Yin, H., and Varga, J. (2017). Toll-Like Receptor-4 Signaling Drives Persistent Fibroblast Activation and Prevents Fibrosis Resolution in Scleroderma. Adv Wound Care (New Rochelle) *6*, 356-369.
Bhattacharyya, S., Oon, C., Kothari, A., Horton, W., Link, J., Sears, R.C., and Sherman, M.H. (2020). Acidic fibroblast growth factor underlies microenvironmental regulation of MYC in pancreatic cancer. J Exp Med *217*.
Biffi, G., Oni, T.E., Spielman, B., Hao, Y., Elyada, E., Park, Y., Preall, J., and Tuveson, D.A. (2019). IL1-Induced JAK/STAT Signaling Is Antagonized by TGFbeta to Shape CAF Heterogeneity in Pancreatic Ductal Adenocarcinoma. Cancer Discov *9*, 282-301.
Biffi, G., and Tuveson, D.A. (2020). Diversity and Biology of Cancer-Associated Fibroblasts. Physiol Rev.
Bissell, M.J., and Hines, W.C. (2011). Why don't we get more cancer? A proposed role of the microenvironment in restraining cancer progression. Nat Med *17*, 320-329.
Bleul, C.C., Fuhlbrigge, R.C., Casasnovas, J.M., Aiuti, A., and Springer, T.A. (1996). A highly efficacious lymphocyte chemoattractant, stromal cell-derived factor 1 (SDF-1). J Exp Med *184*, 1101-1109.
Bocchino, M., Agnese, S., Fagone, E., Svegliati, S., Grieco, D., Vancheri, C., Gabrielli, A., Sanduzzi, A., and Avvedimento, E.V. (2010). Reactive oxygen species are required for maintenance and differentiation of primary lung fibroblasts in idiopathic pulmonary fibrosis. PLoS One *5*, e14003.
Bochet, L., Lehuede, C., Dauvillier, S., Wang, Y.Y., Dirat, B., Laurent, V., Dray, C., Guiet, R., Maridonneau-Parini, I., Le Gonidec, S., et al. (2013). Adipocyte-derived fibroblasts promote tumor progression and contribute to the desmoplastic reaction in breast cancer. Cancer Res *73*, 5657-5668.
Bodenmiller, B., Zunder, E.R., Finck, R., Chen, T.J., Savig, E.S., Bruggner, R.V., Simonds, E.F., Bendall, S.C., Sachs, K., Krutzik, P.O., et al. (2012). Multiplexed mass cytometry profiling of cellular states perturbed by small-molecule regulators. Nat Biotechnol *30*, 858-867.
Boj, S.F., Hwang, C.I., Baker, L.A., Chio, II, Engle, D.D., Corbo, V., Jager, M., Ponz-Sarvise, M., Tiriac, H., Spector, M.S., et al. (2015). Organoid models of human and mouse ductal pancreatic cancer. Cell *160*, 324-338.
Bonnans, C., Chou, J., and Werb, Z. (2014). Remodelling the extracellular matrix in development and disease. Nat Rev Mol Cell Biol *15*, 786-801.
Bordignon, P., Bottoni, G., Xu, X., Popescu, A.S., Truan, Z., Guenova, E., Kofler, L., Jafari, P., Ostano, P., Rocken, M., et al. (2019). Dualism of FGF and TGF-beta Signaling in Heterogeneous Cancer-Associated Fibroblast Activation with ETV1 as a Critical Determinant. Cell Rep *28*, 2358-2372 e2356.
Bottcher, J.P., Bonavita, E., Chakravarty, P., Blees, H., Cabeza-Cabrerizo, M., Sammicheli, S., Rogers, N.C., Sahai, E., Zelenay, S., and Reis, E.S.C. (2018). NK Cells Stimulate Recruitment of cDC1 into the Tumor Microenvironment Promoting Cancer Immune Control. Cell *172*, 1022-1037 e1014.
Bottcher, J.P., and Reis e Sousa, C. (2018). The Role of Type 1 Conventional Dendritic Cells in Cancer Immunity. Trends Cancer *4*, 784-792.
Brabletz, T., Kalluri, R., Nieto, M.A., and Weinberg, R.A. (2018). EMT in cancer. Nat Rev Cancer *18*, 128-134.
Brahmer, J.R., Tykodi, S.S., Chow, L.Q., Hwu, W.J., Topalian, S.L., Hwu, P., Drake, C.G., Camacho, L.H., Kauh, J., Odunsi, K., et al. (2012). Safety and activity of anti-PD-L1 antibody in patients with advanced cancer. N Engl J Med *366*, 2455-2465.
Brandt, D., and Hedrich, C.M. (2018). TCRalphabeta(+)CD3(+)CD4(-)CD8(-) (double negative) T cells in autoimmunity. Autoimmun Rev *17*, 422-430.
Bray, F., Ferlay, J., Soerjomataram, I., Siegel, R.L., Torre, L.A., and Jemal, A. (2018). Global cancer statistics 2018: GLOBOCAN estimates of incidence and mortality worldwide for 36 cancers in 185 countries. CA Cancer J Clin *68*, 394-424.
Bucala, R., Spiegel, L.A., Chesney, J., Hogan, M., and Cerami, A. (1994). Circulating fibrocytes define a new leukocyte subpopulation that mediates tissue repair. Mol Med *1*, 71-81.
Busek, P., Mateu, R., Zubal, M., Kotackova, L., and Sedo, A. (2018). Targeting fibroblast activation protein in cancer - Prospects and caveats. Front Biosci (Landmark Ed) *23*, 1933-1968.
Businesswire.com (2012). Infinity Pharmaceuticals Update, www.businesswire.com/news/home/20120127005146/en/Infinity-Reports-Update-Phase-2-Study-Saridegib#.UxAvFfRdVxV.
Cabeza-Cabrerizo, M., van Blijswijk, J., Wienert, S., Heim, D., Jenkins, R.P., Chakravarty, P., Rogers, N., Frederico, B., Acton, S., Beerling, E., et al. (2019). Tissue clonality of dendritic cell subsets and emergency DCpoiesis revealed by multicolor fate mapping of DC progenitors. Sci Immunol *4*.
Calon, A., Espinet, E., Palomo-Ponce, S., Tauriello, D.V., Iglesias, M., Cespedes, M.V., Sevillano, M., Nadal, C., Jung, P., Zhang, X.H., et al. (2012). Dependency of colorectal cancer on a TGF-beta-driven program in stromal cells for metastasis initiation. Cancer Cell *22*, 571-584.
Calvo, F., Ege, N., Grande-Garcia, A., Hooper, S., Jenkins, R.P., Chaudhry, S.I., Harrington, K., Williamson, P., Moeendarbary, E., Charras, G., et al. (2013). Mechanotransduction and YAP-dependent matrix

remodelling is required for the generation and maintenance of cancer-associated fibroblasts. Nat Cell Biol *15*, 637-646.
Cancer Genome Atlas Research Network (2017). Integrated Genomic Characterization of Pancreatic Ductal Adenocarcinoma. Cancer Cell *32*, 185-203 e113.
Cassetta, L., and Pollard, J.W. (2018). Targeting macrophages: therapeutic approaches in cancer. Nat Rev Drug Discov *17*, 887-904.
Chang, H.Y., Chi, J.T., Dudoit, S., Bondre, C., van de Rijn, M., Botstein, D., and Brown, P.O. (2002). Diversity, topographic differentiation, and positional memory in human fibroblasts. Proc Natl Acad Sci U S A *99*, 12877-12882.
Chen, L., and Flies, D.B. (2013). Molecular mechanisms of T cell co-stimulation and co-inhibition. Nat Rev Immunol *13*, 227-242.
Chen, X., and Song, E. (2019). Turning foes to friends: targeting cancer-associated fibroblasts. Nat Rev Drug Discov *18*, 99-115.
Chen, Y.T., Chang, F.C., Wu, C.F., Chou, Y.H., Hsu, H.L., Chiang, W.C., Shen, J., Chen, Y.M., Wu, K.D., Tsai, T.J., et al. (2011). Platelet-derived growth factor receptor signaling activates pericyte-myofibroblast transition in obstructive and post-ischemic kidney fibrosis. Kidney Int *80*, 1170-1181.
Cheung, P., Vallania, F., Warsinske, H.C., Donato, M., Schaffert, S., Chang, S.E., Dvorak, M., Dekker, C.L., Davis, M.M., Utz, P.J., et al. (2018). Single-Cell Chromatin Modification Profiling Reveals Increased Epigenetic Variations with Aging. Cell *173*, 1385-1397 e1314.
Chevrier, S., Levine, J.H., Zanotelli, V.R.T., Silina, K., Schulz, D., Bacac, M., Ries, C.H., Ailles, L., Jewett, M.A.S., Moch, H., et al. (2017). An Immune Atlas of Clear Cell Renal Cell Carcinoma. Cell *169*, 736-749 e718.
Clifford, R.L., Fishbane, N., Patel, J., MacIsaac, J.L., McEwen, L.M., Fisher, A.J., Brandsma, C.A., Nair, P., Kobor, M.S., Hackett, T.L., et al. (2018). Altered DNA methylation is associated with aberrant gene expression in parenchymal but not airway fibroblasts isolated from individuals with COPD. Clin Epigenetics *10*, 32.
Collins, M.A., Bednar, F., Zhang, Y., Brisset, J.C., Galban, S., Galban, C.J., Rakshit, S., Flannagan, K.S., Adsay, N.V., and Pasca di Magliano, M. (2012). Oncogenic Kras is required for both the initiation and maintenance of pancreatic cancer in mice. J Clin Invest *122*, 639-653.
Consortium, I.T.P.-C.A.o.W.G. (2020). Pan-cancer analysis of whole genomes. Nature *578*, 82-93.
Costa, A., Kieffer, Y., Scholer-Dahirel, A., Pelon, F., Bourachot, B., Cardon, M., Sirven, P., Magagna, I., Fuhrmann, L., Bernard, C., et al. (2018). Fibroblast Heterogeneity and Immunosuppressive Environment in Human Breast Cancer. Cancer Cell *33*, 463-479 e410.
Cox, T.R., Bird, D., Baker, A.M., Barker, H.E., Ho, M.W., Lang, G., and Erler, J.T. (2013). LOX-mediated collagen crosslinking is responsible for fibrosis-enhanced metastasis. Cancer Res *73*, 1721-1732.
Croft, A.P., Campos, J., Jansen, K., Turner, J.D., Marshall, J., Attar, M., Savary, L., Wehmeyer, C., Naylor, A.J., Kemble, S., et al. (2019). Distinct fibroblast subsets drive inflammation and damage in arthritis. Nature *570*, 246-251.
Dalin, S., Sullivan, M.R., Lau, A.N., Grauman-Boss, B., Mueller, H.S., Kreidl, E., Fenoglio, S., Luengo, A., Lees, J.A., Vander Heiden, M.G., et al. (2019). Deoxycytidine Release from Pancreatic Stellate Cells Promotes Gemcitabine Resistance. Cancer Res *79*, 5723-5733.
Davidson, S., Efremova, M., Riedel, A., Mahata, B., Pramanik, J., Huuhtanen, J., Kar, G., Vento-Tormo, R., Hagai, T., Chen, X., et al. (2020). Single-Cell RNA Sequencing Reveals a Dynamic Stromal Niche That Supports Tumor Growth. Cell Rep *31*, 107628.
DeCaprio, J.A., Ludlow, J.W., Figge, J., Shew, J.Y., Huang, C.M., Lee, W.H., Marsilio, E., Paucha, E., and Livingston, D.M. (1988). SV40 large tumor antigen forms a specific complex with the product of the retinoblastoma susceptibility gene. Cell *54*, 275-283.
Del Chiaro, M., Segersvard, R., Lohr, M., and Verbeke, C. (2014). Early detection and prevention of pancreatic cancer: is it really possible today? World J Gastroenterol *20*, 12118-12131.
DeNardo, D.G., and Ruffell, B. (2019). Macrophages as regulators of tumour immunity and immunotherapy. Nat Rev Immunol *19*, 369-382.
Dey, P., Li, J., Zhang, J., Chaurasiya, S., Strom, A., Wang, H., Liao, W.T., Cavallaro, F., Denz, P., Bernard, V., et al. (2020). Oncogenic KRAS-Driven Metabolic Reprogramming in Pancreatic Cancer Cells Utilizes Cytokines from the Tumor Microenvironment. Cancer Discov *10*, 608-625.
Dhomen, N., Reis-Filho, J.S., da Rocha Dias, S., Hayward, R., Savage, K., Delmas, V., Larue, L., Pritchard, C., and Marais, R. (2009). Oncogenic Braf induces melanocyte senescence and melanoma in mice. Cancer Cell *15*, 294-303.
Di Carlo, S.E., and Peduto, L. (2018). The perivascular origin of pathological fibroblasts. J Clin Invest *128*, 54-63.
Ding, N., Yu, R.T., Subramaniam, N., Sherman, M.H., Wilson, C., Rao, R., Leblanc, M., Coulter, S., He, M., Scott, C., et al. (2013). A vitamin D receptor/SMAD genomic circuit gates hepatic fibrotic response. Cell *153*, 601-613.

Dobie, R., Wilson-Kanamori, J.R., Henderson, B.E.P., Smith, J.R., Matchett, K.P., Portman, J.R., Wallenborg, K., Picelli, S., Zagorska, A., Pendem, S.V., et al. (2019). Single-Cell Transcriptomics Uncovers Zonation of Function in the Mesenchyme during Liver Fibrosis. Cell Rep *29*, 1832-1847 e1838.

Dolberg, D.S., Hollingsworth, R., Hertle, M., and Bissell, M.J. (1985). Wounding and its role in RSV-mediated tumor formation. Science *230*, 676-678.

Dominguez, C.X., Muller, S., Keerthivasan, S., Koeppen, H., Hung, J., Gierke, S., Breart, B., Foreman, O., Bainbridge, T.W., Castiglioni, A., et al. (2020). Single-Cell RNA Sequencing Reveals Stromal Evolution into LRRC15(+) Myofibroblasts as a Determinant of Patient Response to Cancer Immunotherapy. Cancer Discov *10*, 232-253.

Dominici, M., Le Blanc, K., Mueller, I., Slaper-Cortenbach, I., Marini, F., Krause, D., Deans, R., Keating, A., Prockop, D., and Horwitz, E. (2006). Minimal criteria for defining multipotent mesenchymal stromal cells. The International Society for Cellular Therapy position statement. Cytotherapy *8*, 315-317.

Donati, G., Proserpio, V., Lichtenberger, B.M., Natsuga, K., Sinclair, R., Fujiwara, H., and Watt, F.M. (2014). Epidermal Wnt/beta-catenin signaling regulates adipocyte differentiation via secretion of adipogenic factors. Proc Natl Acad Sci U S A *111*, E1501-1509.

Dong, A., Wodziak, D., and Lowe, A.W. (2015). Epidermal growth factor receptor (EGFR) signaling requires a specific endoplasmic reticulum thioredoxin for the post-translational control of receptor presentation to the cell surface. J Biol Chem *290*, 8016-8027.

Drilon, A., Laetsch, T.W., Kummar, S., DuBois, S.G., Lassen, U.N., Demetri, G.D., Nathenson, M., Doebele, R.C., Farago, A.F., Pappo, A.S., et al. (2018). Efficacy of Larotrectinib in TRK Fusion-Positive Cancers in Adults and Children. N Engl J Med *378*, 731-739.

Driskell, R.R., Lichtenberger, B.M., Hoste, E., Kretzschmar, K., Simons, B.D., Charalambous, M., Ferron, S.R., Herault, Y., Pavlovic, G., Ferguson-Smith, A.C., et al. (2013). Distinct fibroblast lineages determine dermal architecture in skin development and repair. Nature *504*, 277-281.

Driskell, R.R., and Watt, F.M. (2015). Understanding fibroblast heterogeneity in the skin. Trends Cell Biol *25*, 92-99.

Durai, V., Bagadia, P., Granja, J.M., Satpathy, A.T., Kulkarni, D.H., Davidson, J.T.t., Wu, R., Patel, S.J., Iwata, A., Liu, T.T., et al. (2019). Cryptic activation of an Irf8 enhancer governs cDC1 fate specification. Nat Immunol *20*, 1161-1173.

Dvorak, H.F. (2019). Tumors: Wounds That Do Not Heal-A Historical Perspective with a Focus on the Fundamental Roles of Increased Vascular Permeability and Clotting. Semin Thromb Hemost *45*, 576-592.

Egawa, G., Osawa, M., Uemura, A., Miyachi, Y., and Nishikawa, S. (2009). Transient expression of ephrin b2 in perinatal skin is required for maintenance of keratinocyte homeostasis. J Invest Dermatol *129*, 2386-2395.

El Agha, E., Moiseenko, A., Kheirollahi, V., De Langhe, S., Crnkovic, S., Kwapiszewska, G., Szibor, M., Kosanovic, D., Schwind, F., Schermuly, R.T., et al. (2017). Two-Way Conversion between Lipogenic and Myogenic Fibroblastic Phenotypes Marks the Progression and Resolution of Lung Fibrosis. Cell Stem Cell *20*, 571.

Elyada, E., Bolisetty, M., Laise, P., Flynn, W.F., Courtois, E.T., Burkhart, R.A., Teinor, J.A., Belleau, P., Biffi, G., Lucito, M.S., et al. (2019). Cross-Species Single-Cell Analysis of Pancreatic Ductal Adenocarcinoma Reveals Antigen-Presenting Cancer-Associated Fibroblasts. Cancer Discov *9*, 1102-1123.

Erdogan, B., Ao, M., White, L.M., Means, A.L., Brewer, B.M., Yang, L., Washington, M.K., Shi, C., Franco, O.E., Weaver, A.M., et al. (2017). Cancer-associated fibroblasts promote directional cancer cell migration by aligning fibronectin. J Cell Biol *216*, 3799-3816.

Erez, N., Truitt, M., Olson, P., Arron, S.T., and Hanahan, D. (2010). Cancer-Associated Fibroblasts Are Activated in Incipient Neoplasia to Orchestrate Tumor-Promoting Inflammation in an NF-kappaB-Dependent Manner. Cancer Cell *17*, 135-147.

Evrard, M., Kwok, I.W.H., Chong, S.Z., Teng, K.W.W., Becht, E., Chen, J., Sieow, J.L., Penny, H.L., Ching, G.C., Devi, S., et al. (2018). Developmental Analysis of Bone Marrow Neutrophils Reveals Populations Specialized in Expansion, Trafficking, and Effector Functions. Immunity *48*, 364-379 e368.

Farin, H.F., Jordens, I., Mosa, M.H., Basak, O., Korving, J., Tauriello, D.V., de Punder, K., Angers, S., Peters, P.J., Maurice, M.M., et al. (2016). Visualization of a short-range Wnt gradient in the intestinal stem-cell niche. Nature *530*, 340-343.

Feig, C., Jones, J.O., Kraman, M., Wells, R.J., Deonarine, A., Chan, D.S., Connell, C.M., Roberts, E.W., Zhao, Q., Caballero, O.L., et al. (2013). Targeting CXCL12 from FAP-expressing carcinoma-associated fibroblasts synergizes with anti-PD-L1 immunotherapy in pancreatic cancer. Proc Natl Acad Sci U S A *110*, 20212-20217.

Feldmann, G., Beaty, R., Hruban, R.H., and Maitra, A. (2007). Molecular genetics of pancreatic intraepithelial neoplasia. J Hepatobiliary Pancreat Surg *14*, 224-232.

Fendrich, V., Oh, E., Bang, S., Karikari, C., Ottenhof, N., Bisht, S., Lauth, M., Brossart, P., Katsanis, N., Maitra, A., et al. (2011). Ectopic overexpression of Sonic Hedgehog (Shh) induces stromal expansion and metaplasia in the adult murine pancreas. Neoplasia *13*, 923-930.

Ferland-McCollough, D., Slater, S., Richard, J., Reni, C., and Mangialardi, G. (2017). Pericytes, an overlooked player in vascular pathobiology. Pharmacol Ther *171*, 30-42.
Ferlay, J., Colombet, M., Soerjomataram, I., Mathers, C., Parkin, D.M., Pineros, M., Znaor, A., and Bray, F. (2019). Estimating the global cancer incidence and mortality in 2018: GLOBOCAN sources and methods. Int J Cancer *144*, 1941-1953.
Fernandes-Alnemri, T., Litwack, G., and Alnemri, E.S. (1994). CPP32, a novel human apoptotic protein with homology to Caenorhabditis elegans cell death protein Ced-3 and mammalian interleukin-1 beta-converting enzyme. J Biol Chem *269*, 30761-30764.
Ferrer-Font, L., Mayer, J.U., Old, S., Hermans, I.F., Irish, J., and Price, K.M. (2020). High-Dimensional Data Analysis Algorithms Yield Comparable Results for Mass Cytometry and Spectral Flow Cytometry Data. Cytometry A.
Festa, E., Fretz, J., Berry, R., Schmidt, B., Rodeheffer, M., Horowitz, M., and Horsley, V. (2011). Adipocyte lineage cells contribute to the skin stem cell niche to drive hair cycling. Cell *146*, 761-771.
Fletcher, A.L., Lukacs-Kornek, V., Reynoso, E.D., Pinner, S.E., Bellemare-Pelletier, A., Curry, M.S., Collier, A.R., Boyd, R.L., and Turley, S.J. (2010). Lymph node fibroblastic reticular cells directly present peripheral tissue antigen under steady-state and inflammatory conditions. J Exp Med *207*, 689-697.
Flint, T.R., Janowitz, T., Connell, C.M., Roberts, E.W., Denton, A.E., Coll, A.P., Jodrell, D.I., and Fearon, D.T. (2016). Tumor-Induced IL-6 Reprograms Host Metabolism to Suppress Anti-tumor Immunity. Cell Metab *24*, 672-684.
Frere, C., Bournet, B., Benzidia, I., Jamelot, M., Debourdeau, P., Hij, A., Rafii-Elayoubi, H., Buscail, L., Farge, D., and Groupe francophone thrombose et, c. (2018). [Venous thromboembolism and pancreatic cancer]. J Med Vasc *43*, 246-254.
Fujiwara, H., Ferreira, M., Donati, G., Marciano, D.K., Linton, J.M., Sato, Y., Hartner, A., Sekiguchi, K., Reichardt, L.F., and Watt, F.M. (2011). The basement membrane of hair follicle stem cells is a muscle cell niche. Cell *144*, 577-589.
Fukumura, D., Xavier, R., Sugiura, T., Chen, Y., Park, E.C., Lu, N., Selig, M., Nielsen, G., Taksir, T., Jain, R.K., et al. (1998). Tumor induction of VEGF promoter activity in stromal cells. Cell *94*, 715-725.
Furuya, S., and Furuya, K. (2007). Subepithelial fibroblasts in intestinal villi: roles in intercellular communication. Int Rev Cytol *264*, 165-223.
Gabrilovich, D.I., Ostrand-Rosenberg, S., and Bronte, V. (2012). Coordinated regulation of myeloid cells by tumours. Nat Rev Immunol *12*, 253-268.
Gaggioli, C., Hooper, S., Hidalgo-Carcedo, C., Grosse, R., Marshall, J.F., Harrington, K., and Sahai, E. (2007). Fibroblast-led collective invasion of carcinoma cells with differing roles for RhoGTPases in leading and following cells. Nat Cell Biol *9*, 1392-1400.
Galichon, P., Finianos, S., and Hertig, A. (2013). EMT-MET in renal disease: should we curb our enthusiasm? Cancer Lett *341*, 24-29.
Gaublomme, J.T., Li, B., McCabe, C., Knecht, A., Yang, Y., Drokhlyansky, E., Van Wittenberghe, N., Waldman, J., Dionne, D., Nguyen, L., et al. (2019). Nuclei multiplexing with barcoded antibodies for single-nucleus genomics. Nat Commun *10*, 2907.
Gengenbacher, N., Singhal, M., and Augustin, H.G. (2017). Preclinical mouse solid tumour models: status quo, challenges and perspectives. Nat Rev Cancer *17*, 751-765.
Gilbert, R.W.D., Vickaryous, M.K., and Viloria-Petit, A.M. (2016). Signalling by Transforming Growth Factor Beta Isoforms in Wound Healing and Tissue Regeneration. J Dev Biol *4*.
Golan, T., Hammel, P., Reni, M., Van Cutsem, E., Macarulla, T., Hall, M.J., Park, J.O., Hochhauser, D., Arnold, D., Oh, D.Y., et al. (2019). Maintenance Olaparib for Germline BRCA-Mutated Metastatic Pancreatic Cancer. N Engl J Med *381*, 317-327.
Goldstein, D., El-Maraghi, R.H., Hammel, P., Heinemann, V., Kunzmann, V., Sastre, J., Scheithauer, W., Siena, S., Tabernero, J., Teixeira, L., et al. (2015). nab-Paclitaxel plus gemcitabine for metastatic pancreatic cancer: long-term survival from a phase III trial. J Natl Cancer Inst *107*.
Goltsev, Y., Samusik, N., Kennedy-Darling, J., Bhate, S., Hale, M., Vazquez, G., Black, S., and Nolan, G.P. (2018). Deep Profiling of Mouse Splenic Architecture with CODEX Multiplexed Imaging. Cell *174*, 968-981 e915.
Gong, Y., Scott, E., Lu, R., Xu, Y., Oh, W.K., and Yu, Q. (2013). TIMP-1 promotes accumulation of cancer associated fibroblasts and cancer progression. PLoS One *8*, e77366.
Gopinathan, A., Morton, J.P., Jodrell, D.I., and Sansom, O.J. (2015). GEMMs as preclinical models for testing pancreatic cancer therapies. Dis Model Mech *8*, 1185-1200.
Gordillo, C.H., Sandoval, P., Munoz-Hernandez, P., Pascual-Anton, L., Lopez-Cabrera, M., and Jimenez-Heffernan, J.A. (2020). Mesothelial-to-Mesenchymal Transition Contributes to the Generation of Carcinoma-Associated Fibroblasts in Locally Advanced Primary Colorectal Carcinomas. Cancers (Basel) *12*.

Grajales-Reyes, G.E., Iwata, A., Albring, J., Wu, X., Tussiwand, R., Kc, W., Kretzer, N.M., Briseno, C.G., Durai, V., Bagadia, P., et al. (2015). Batf3 maintains autoactivation of Irf8 for commitment of a CD8alpha(+) conventional DC clonogenic progenitor. Nat Immunol *16*, 708-717.

Grande, M.T., Sanchez-Laorden, B., Lopez-Blau, C., De Frutos, C.A., Boutet, A., Arevalo, M., Rowe, R.G., Weiss, S.J., Lopez-Novoa, J.M., and Nieto, M.A. (2015). Snail1-induced partial epithelial-to-mesenchymal transition drives renal fibrosis in mice and can be targeted to reverse established disease. Nat Med *21*, 989-997.

Greter, M., Helft, J., Chow, A., Hashimoto, D., Mortha, A., Agudo-Cantero, J., Bogunovic, M., Gautier, E.L., Miller, J., Leboeuf, M., et al. (2012). GM-CSF controls nonlymphoid tissue dendritic cell homeostasis but is dispensable for the differentiation of inflammatory dendritic cells. Immunity *36*, 1031-1046.

Groom, J.R., and Luster, A.D. (2011). CXCR3 in T cell function. Exp Cell Res *317*, 620-631.

Guido, C., Whitaker-Menezes, D., Capparelli, C., Balliet, R., Lin, Z., Pestell, R.G., Howell, A., Aquila, S., Ando, S., Martinez-Outschoorn, U., et al. (2012). Metabolic reprogramming of cancer-associated fibroblasts by TGF-beta drives tumor growth: connecting TGF-beta signaling with "Warburg-like" cancer metabolism and L-lactate production. Cell Cycle *11*, 3019-3035.

Guilliams, M., Ginhoux, F., Jakubzick, C., Naik, S.H., Onai, N., Schraml, B.U., Segura, E., Tussiwand, R., and Yona, S. (2014). Dendritic cells, monocytes and macrophages: a unified nomenclature based on ontogeny. Nat Rev Immunol *14*, 571-578.

Guy, C.T., Cardiff, R.D., and Muller, W.J. (1992). Induction of mammary tumors by expression of polyomavirus middle T oncogene: a transgenic mouse model for metastatic disease. Mol Cell Biol *12*, 954-961.

Hahne, F., LeMeur, N., Brinkman, R.R., Ellis, B., Haaland, P., Sarkar, D., Spidlen, J., Strain, E., and Gentleman, R. (2009). flowCore: a Bioconductor package for high throughput flow cytometry. BMC Bioinformatics *10*, 106.

Han, G., Spitzer, M.H., Bendall, S.C., Fantl, W.J., and Nolan, G.P. (2018). Metal-isotope-tagged monoclonal antibodies for high-dimensional mass cytometry. Nat Protoc *13*, 2121-2148.

Harris, W.J., Huang, X., Lynch, J.T., Spencer, G.J., Hitchin, J.R., Li, Y., Ciceri, F., Blaser, J.G., Greystoke, B.F., Jordan, A.M., et al. (2012). The histone demethylase KDM1A sustains the oncogenic potential of MLL-AF9 leukemia stem cells. Cancer Cell *21*, 473-487.

Hartmann, F.J., Mrdjen, D., McCaffrey, E., Glass, D.R., Greenwald, N.F., Bharadwaj, A., Khair, Z., Baranski, A., Baskar, R., Angelo, M., et al. (2020). Multiplexed Single-cell Metabolic Profiles Organize the Spectrum of Cytotoxic Human T Cells. bioRxiv, 2020.2001.2017.909796.

Hartmann, N., Giese, N.A., Giese, T., Poschke, I., Offringa, R., Werner, J., and Ryschich, E. (2014). Prevailing role of contact guidance in intrastromal T-cell trapping in human pancreatic cancer. Clin Cancer Res *20*, 3422-3433.

Hashimoto, N., Jin, H., Liu, T., Chensue, S.W., and Phan, S.H. (2004). Bone marrow-derived progenitor cells in pulmonary fibrosis. J Clin Invest *113*, 243-252.

Hausmann, C., Zoschke, C., Wolff, C., Darvin, M.E., Sochorova, M., Kovacik, A., Wanjiku, B., Schumacher, F., Tigges, J., Kleuser, B., et al. (2019). Fibroblast origin shapes tissue homeostasis, epidermal differentiation, and drug uptake. Sci Rep *9*, 2913.

Haviv, I., Polyak, K., Qiu, W., Hu, M., and Campbell, I. (2009). Origin of carcinoma associated fibroblasts. Cell Cycle *8*, 589-595.

Hay, E.D. (2005). The mesenchymal cell, its role in the embryo, and the remarkable signaling mechanisms that create it. Dev Dyn *233*, 706-720.

Hayashi, Y., Emoto, T., Futaki, S., and Sekiguchi, K. (2004). Establishment and characterization of a parietal endoderm-like cell line derived from Engelbreth-Holm-Swarm tumor (EHSPEL), a possible resource for an engineered basement membrane matrix. Matrix Biol *23*, 47-62.

Hegde, S., Krisnawan, V.E., Herzog, B.H., Zuo, C., Breden, M.A., Knolhoff, B.L., Hogg, G.D., Tang, J.P., Baer, J.M., Mpoy, C., et al. (2020). Dendritic Cell Paucity Leads to Dysfunctional Immune Surveillance in Pancreatic Cancer. Cancer Cell *37*, 289-307 e289.

Heinzelmann, K., Lehmann, M., Gerckens, M., Noskovicova, N., Frankenberger, M., Lindner, M., Hatz, R., Behr, J., Hilgendorff, A., Konigshoff, M., et al. (2018). Cell-surface phenotyping identifies CD36 and CD97 as novel markers of fibroblast quiescence in lung fibrosis. Am J Physiol Lung Cell Mol Physiol *315*, L682-L696.

Henriksen, A., Dyhl-Polk, A., Chen, I., and Nielsen, D. (2019). Checkpoint inhibitors in pancreatic cancer. Cancer Treat Rev *78*, 17-30.

Hildner, K., Edelson, B.T., Purtha, W.E., Diamond, M., Matsushita, H., Kohyama, M., Calderon, B., Schraml, B.U., Unanue, E.R., Diamond, M.S., et al. (2008). Batf3 deficiency reveals a critical role for CD8alpha+ dendritic cells in cytotoxic T cell immunity. Science *322*, 1097-1100.

Hingorani, S.R., Petricoin, E.F., Maitra, A., Rajapakse, V., King, C., Jacobetz, M.A., Ross, S., Conrads, T.P., Veenstra, T.D., Hitt, B.A., et al. (2003). Preinvasive and invasive ductal pancreatic cancer and its early detection in the mouse. Cancer Cell *4*, 437-450.

Hingorani, S.R., Wang, L., Multani, A.S., Combs, C., Deramaudt, T.B., Hruban, R.H., Rustgi, A.K., Chang, S., and Tuveson, D.A. (2005). Trp53R172H and KrasG12D cooperate to promote chromosomal instability and widely metastatic pancreatic ductal adenocarcinoma in mice. Cancer Cell *7*, 469-483.
Hinz, B., and Lagares, D. (2020). Evasion of apoptosis by myofibroblasts: a hallmark of fibrotic diseases. Nat Rev Rheumatol *16*, 11-31.
Ho, W.J., Jaffee, E.M., and Zheng, L. (2020). The tumour microenvironment in pancreatic cancer - clinical challenges and opportunities. Nat Rev Clin Oncol.
Hong, S.M., Goggins, M., Wolfgang, C.L., Schulick, R.D., Edil, B.H., Cameron, J.L., Handra-Luca, A., Herman, J.M., and Hruban, R.H. (2012). Vascular invasion in infiltrating ductal adenocarcinoma of the pancreas can mimic pancreatic intraepithelial neoplasia: a histopathologic study of 209 cases. Am J Surg Pathol *36*, 235-241.
Hosein, A.N., Brekken, R.A., and Maitra, A. (2020). Pancreatic cancer stroma: an update on therapeutic targeting strategies. Nat Rev Gastroenterol Hepatol.
Hosein, A.N., Huang, H., Wang, Z., Parmar, K., Du, W., Huang, J., Maitra, A., Olson, E., Verma, U., and Brekken, R.A. (2019). Cellular heterogeneity during mouse pancreatic ductal adenocarcinoma progression at single-cell resolution. JCI Insight *5*.
Hruban, R.H., Adsay, N.V., Albores-Saavedra, J., Compton, C., Garrett, E.S., Goodman, S.N., Kern, S.E., Klimstra, D.S., Kloppel, G., Longnecker, D.S., et al. (2001). Pancreatic intraepithelial neoplasia: a new nomenclature and classification system for pancreatic duct lesions. Am J Surg Pathol *25*, 579-586.
Hruban, R.H., Maitra, A., and Goggins, M. (2008). Update on pancreatic intraepithelial neoplasia. Int J Clin Exp Pathol *1*, 306-316.
Huang, S., and Susztak, K. (2016). Epithelial Plasticity versus EMT in Kidney Fibrosis. Trends Mol Med *22*, 4-6.
Hughes, C.S., Postovit, L.M., and Lajoie, G.A. (2010). Matrigel: a complex protein mixture required for optimal growth of cell culture. Proteomics *10*, 1886-1890.
Humphries, J.D., Byron, A., and Humphries, M.J. (2006). Integrin ligands at a glance. J Cell Sci *119*, 3901-3903.
Ichim, T.E., O'Heeron, P., and Kesari, S. (2018). Fibroblasts as a practical alternative to mesenchymal stem cells. J Transl Med *16*, 212.
Ireson, C.R., Alavijeh, M.S., Palmer, A.M., Fowler, E.R., and Jones, H.J. (2019). The role of mouse tumour models in the discovery and development of anticancer drugs. Br J Cancer *121*, 101-108.
Itoh, Y., Takehara, Y., Kawase, T., Terashima, K., Ohkawa, Y., Hirose, Y., Koda, A., Hyodo, N., Ushio, T., Hirai, Y., et al. (2016). Feasibility of magnetic resonance elastography for the pancreas at 3T. J Magn Reson Imaging *43*, 384-390.
Ivanov, N.A., Tao, R., Chenoweth, J.G., Brandtjen, A., Mighdoll, M.I., Genova, J.D., McKay, R.D., Jia, Y., Weinberger, D.R., Kleinman, J.E., et al. (2016). Strong Components of Epigenetic Memory in Cultured Human Fibroblasts Related to Site of Origin and Donor Age. PLoS Genet *12*, e1005819.
Jackson, E.L., Willis, N., Mercer, K., Bronson, R.T., Crowley, D., Montoya, R., Jacks, T., and Tuveson, D.A. (2001). Analysis of lung tumor initiation and progression using conditional expression of oncogenic K-ras. Genes Dev *15*, 3243-3248.
Jackstadt, R., van Hooff, S.R., Leach, J.D., Cortes-Lavaud, X., Lohuis, J.O., Ridgway, R.A., Wouters, V.M., Roper, J., Kendall, T.J., Roxburgh, C.S., et al. (2019). Epithelial NOTCH Signaling Rewires the Tumor Microenvironment of Colorectal Cancer to Drive Poor-Prognosis Subtypes and Metastasis. Cancer Cell *36*, 319-336 e317.
Jacobetz, M.A., Chan, D.S., Neesse, A., Bapiro, T.E., Cook, N., Frese, K.K., Feig, C., Nakagawa, T., Caldwell, M.E., Zecchini, H.I., et al. (2013). Hyaluronan impairs vascular function and drug delivery in a mouse model of pancreatic cancer. Gut *62*, 112-120.
Jenkins, T.L., and Little, D. (2019). Synthetic scaffolds for musculoskeletal tissue engineering: cellular responses to fiber parameters. NPJ Regen Med *4*, 15.
Jin, Y., Muhl, L., Burmakin, M., Wang, Y., Duchez, A.C., Betsholtz, C., Arthur, H.M., and Jakobsson, L. (2017). Endoglin prevents vascular malformation by regulating flow-induced cell migration and specification through VEGFR2 signalling. Nat Cell Biol *19*, 639-652.
Kakarla, S., Chow, K.K., Mata, M., Shaffer, D.R., Song, X.T., Wu, M.F., Liu, H., Wang, L.L., Rowley, D.R., Pfizenmaier, K., et al. (2013). Antitumor effects of chimeric receptor engineered human T cells directed to tumor stroma. Mol Ther *21*, 1611-1620.
Kalluri, R. (2003). Basement membranes: structure, assembly and role in tumour angiogenesis. Nat Rev Cancer *3*, 422-433.
Kalluri, R. (2016). The biology and function of fibroblasts in cancer. Nat Rev Cancer *16*, 582-598.
Kammertoens, T., Friese, C., Arina, A., Idel, C., Briesemeister, D., Rothe, M., Ivanov, A., Szymborska, A., Patone, G., Kunz, S., et al. (2017). Tumour ischaemia by interferon-gamma resembles physiological blood vessel regression. Nature *545*, 98-102.

Karacosta, L.G., Anchang, B., Ignatiadis, N., Kimmey, S.C., Benson, J.A., Shrager, J.B., Tibshirani, R., Bendall, S.C., and Plevritis, S.K. (2019). Mapping lung cancer epithelial-mesenchymal transition states and trajectories with single-cell resolution. Nat Commun *10*, 5587.

Karouzakis, E., Raza, K., Kolling, C., Buckley, C.D., Gay, S., Filer, A., and Ospelt, C. (2018). Analysis of early changes in DNA methylation in synovial fibroblasts of RA patients before diagnosis. Sci Rep *8*, 7370.

Karpus, O.N., Westendorp, B.F., Vermeulen, J.L.M., Meisner, S., Koster, J., Muncan, V., Wildenberg, M.E., and van den Brink, G.R. (2019). Colonic CD90+ Crypt Fibroblasts Secrete Semaphorins to Support Epithelial Growth. Cell Rep *26*, 3698-3708 e3695.

Kato, M., Placencio-Hickok, V.R., Madhav, A., Haldar, S., Tripathi, M., Billet, S., Mishra, R., Smith, B., Rohena-Rivera, K., Agarwal, P., et al. (2019). Heterogeneous cancer-associated fibroblast population potentiates neuroendocrine differentiation and castrate resistance in a CD105-dependent manner. Oncogene *38*, 716-730.

Khan, O., Giles, J.R., McDonald, S., Manne, S., Ngiow, S.F., Patel, K.P., Werner, M.T., Huang, A.C., Alexander, K.A., Wu, J.E., et al. (2019). TOX transcriptionally and epigenetically programs CD8(+) T cell exhaustion. Nature *571*, 211-218.

Kieffer, Y., Hocine, H.R., Gentric, G., Pelon, F., Bernard, C., Bourachot, B., Lameiras, S., Albergante, L., Bonneau, C., Guyard, A., et al. (2020). Single-cell analysis reveals fibroblast clusters linked to immunotherapy resistance in cancer. Cancer Discov.

King, I.A., and Pope, F.M. (1986). Synthesis of cellular and extracellular glycoproteins by cultured human keratinocytes and their response to retinoids. Biochim Biophys Acta *887*, 263-274.

Kobayashi, H., Enomoto, A., Woods, S.L., Burt, A.D., Takahashi, M., and Worthley, D.L. (2019). Cancer-associated fibroblasts in gastrointestinal cancer. Nat Rev Gastroenterol Hepatol *16*, 282-295.

Koliaraki, V., Pasparakis, M., and Kollias, G. (2015). IKKbeta in intestinal mesenchymal cells promotes initiation of colitis-associated cancer. J Exp Med *212*, 2235-2251.

Koopmans, T., and Rinkevich, Y. (2018). Mesothelial to mesenchyme transition as a major developmental and pathological player in trunk organs and their cavities. Commun Biol *1*, 170.

Kosyakova, N., Kao, D.D., Figetakis, M., Lopez-Giraldez, F., Spindler, S., Graham, M., James, K.J., Won Shin, J., Liu, X., Tietjen, G.T., et al. (2020). Differential functional roles of fibroblasts and pericytes in the formation of tissue-engineered microvascular networks in vitro. NPJ Regen Med *5*, 1.

Kozuka, S., Sassa, R., Taki, T., Masamoto, K., Nagasawa, S., Saga, S., Hasegawa, K., and Takeuchi, M. (1979). Relation of pancreatic duct hyperplasia to carcinoma. Cancer *43*, 1418-1428.

Kraman, M., Bambrough, P.J., Arnold, J.N., Roberts, E.W., Magiera, L., Jones, J.O., Gopinathan, A., Tuveson, D.A., and Fearon, D.T. (2010). Suppression of antitumor immunity by stromal cells expressing fibroblast activation protein-alpha. Science *330*, 827-830.

Krishnaswamy, S., Spitzer, M.H., Mingueneau, M., Bendall, S.C., Litvin, O., Stone, E., Pe'er, D., and Nolan, G.P. (2014). Systems biology. Conditional density-based analysis of T cell signaling in single-cell data. Science *346*, 1250689.

Kriz, W., Kaissling, B., and Le Hir, M. (2011). Epithelial-mesenchymal transition (EMT) in kidney fibrosis: fact or fantasy? J Clin Invest *121*, 468-474.

Kumar, S., Lun, X.K., Bodenmiller, B., Rodriguez Martinez, M., and Koeppl, H. (2020). Stabilized Reconstruction of Signaling Networks from Single-Cell Cue-Response Data. Sci Rep *10*, 1233.

Kuninty, P.R., Bansal, R., De Geus, S.W.L., Mardhian, D.F., Schnittert, J., van Baarlen, J., Storm, G., Bijlsma, M.F., van Laarhoven, H.W., Metselaar, J.M., et al. (2019). ITGA5 inhibition in pancreatic stellate cells attenuates desmoplasia and potentiates efficacy of chemotherapy in pancreatic cancer. Sci Adv *5*, eaax2770.

Kurashige, M., Kohara, M., Ohshima, K., Tahara, S., Hori, Y., Nojima, S., Wada, N., Ikeda, J.I., Miyamura, K., Ito, M., et al. (2018). Origin of cancer-associated fibroblasts and tumor-associated macrophages in humans after sex-mismatched bone marrow transplantation. Commun Biol *1*, 131.

Kuwana, M., Okazaki, Y., Kodama, H., Izumi, K., Yasuoka, H., Ogawa, Y., Kawakami, Y., and Ikeda, Y. (2003). Human circulating CD14+ monocytes as a source of progenitors that exhibit mesenchymal cell differentiation. J Leukoc Biol *74*, 833-845.

Labernadie, A., Kato, T., Brugues, A., Serra-Picamal, X., Derzsi, S., Arwert, E., Weston, A., Gonzalez-Tarrago, V., Elosegui-Artola, A., Albertazzi, L., et al. (2017). A mechanically active heterotypic E-cadherin/N-cadherin adhesion enables fibroblasts to drive cancer cell invasion. Nat Cell Biol *19*, 224-237.

Lakins, M.A., Ghorani, E., Munir, H., Martins, C.P., and Shields, J.D. (2018). Cancer-associated fibroblasts induce antigen-specific deletion of CD8 (+) T Cells to protect tumour cells. Nat Commun *9*, 948.

Laklai, H., Miroshnikova, Y.A., Pickup, M.W., Collisson, E.A., Kim, G.E., Barrett, A.S., Hill, R.C., Lakins, J.N., Schlaepfer, D.D., Mouw, J.K., et al. (2016). Genotype tunes pancreatic ductal adenocarcinoma tissue tension to induce matricellular fibrosis and tumor progression. Nat Med *22*, 497-505.

Lawson, K.A., Meneses, J.J., and Pedersen, R.A. (1991). Clonal analysis of epiblast fate during germ layer formation in the mouse embryo. Development *113*, 891-911.

Le, D.T., Durham, J.N., Smith, K.N., Wang, H., Bartlett, B.R., Aulakh, L.K., Lu, S., Kemberling, H., Wilt, C., Luber, B.S., et al. (2017). Mismatch repair deficiency predicts response of solid tumors to PD-1 blockade. Science *357*, 409-413.
Le, D.T., Uram, J.N., Wang, H., Bartlett, B.R., Kemberling, H., Eyring, A.D., Skora, A.D., Luber, B.S., Azad, N.S., Laheru, D., et al. (2015). PD-1 Blockade in Tumors with Mismatch-Repair Deficiency. N Engl J Med *372*, 2509-2520.
Lebid, A., Chung, L., Pardoll, D.M., and Pan, F. (2020). YAP Attenuates CD8 T Cell-Mediated Anti-tumor Response. Front Immunol *11*, 580.
LeBleu, V.S., Macdonald, B., and Kalluri, R. (2007). Structure and function of basement membranes. Exp Biol Med (Maywood) *232*, 1121-1129.
LeBleu, V.S., and Neilson, E.G. (2020). Origin and functional heterogeneity of fibroblasts. FASEB J *34*, 3519-3536.
LeBleu, V.S., Taduri, G., O'Connell, J., Teng, Y., Cooke, V.G., Woda, C., Sugimoto, H., and Kalluri, R. (2013). Origin and function of myofibroblasts in kidney fibrosis. Nat Med *19*, 1047-1053.
Lebrin, F., Goumans, M.J., Jonker, L., Carvalho, R.L., Valdimarsdottir, G., Thorikay, M., Mummery, C., Arthur, H.M., and ten Dijke, P. (2004). Endoglin promotes endothelial cell proliferation and TGF-beta/ALK1 signal transduction. EMBO J *23*, 4018-4028.
Lecomte, J., Masset, A., Blacher, S., Maertens, L., Gothot, A., Delgaudine, M., Bruyere, F., Carnet, O., Paupert, J., Illemann, M., et al. (2012). Bone marrow-derived myofibroblasts are the providers of pro-invasive matrix metalloproteinase 13 in primary tumor. Neoplasia *14*, 943-951.
Lee, J.J., Perera, R.M., Wang, H., Wu, D.C., Liu, X.S., Han, S., Fitamant, J., Jones, P.D., Ghanta, K.S., Kawano, S., et al. (2014a). Stromal response to Hedgehog signaling restrains pancreatic cancer progression. Proc Natl Acad Sci U S A *111*, E3091-3100.
Lee, S.J., Kim, K.H., and Park, K.K. (2014b). Mechanisms of fibrogenesis in liver cirrhosis: The molecular aspects of epithelial-mesenchymal transition. World J Hepatol *6*, 207-216.
Lemos, D.R., and Duffield, J.S. (2018). Tissue-resident mesenchymal stromal cells: Implications for tissue-specific antifibrotic therapies. Sci Transl Med *10*.
Li, J., He, Y., Hao, J., Ni, L., and Dong, C. (2018). High Levels of Eomes Promote Exhaustion of Anti-tumor CD8(+) T Cells. Front Immunol *9*, 2981.
Li, Y., Lua, I., French, S.W., and Asahina, K. (2016). Role of TGF-beta signaling in differentiation of mesothelial cells to vitamin A-poor hepatic stellate cells in liver fibrosis. Am J Physiol Gastrointest Liver Physiol *310*, G262-272.
Li, Y., Wang, J., and Asahina, K. (2013). Mesothelial cells give rise to hepatic stellate cells and myofibroblasts via mesothelial-mesenchymal transition in liver injury. Proc Natl Acad Sci U S A *110*, 2324-2329.
Liberzon, A., Birger, C., Thorvaldsdottir, H., Ghandi, M., Mesirov, J.P., and Tamayo, P. (2015). The Molecular Signatures Database (MSigDB) hallmark gene set collection. Cell Syst *1*, 417-425.
Liebau, S., Mahaddalkar, P.U., Kestler, H.A., Illing, A., Seufferlein, T., and Kleger, A. (2013). A hierarchy in reprogramming capacity in different tissue microenvironments: what we know and what we need to know. Stem Cells Dev *22*, 695-706.
Liu, L., Yu, H., Zhao, H., Wu, Z., Long, Y., Zhang, J., Yan, X., You, Z., Zhou, L., Xia, T., et al. (2020). Matrix-transmitted paratensile signaling enables myofibroblast-fibroblast cross talk in fibrosis expansion. Proc Natl Acad Sci U S A *117*, 10832-10838.
Liu, Y., Beyer, A., and Aebersold, R. (2016). On the Dependency of Cellular Protein Levels on mRNA Abundance. Cell *165*, 535-550.
Lopez-Cabrera, M. (2014). Mesenchymal Conversion of Mesothelial Cells Is a Key Event in the Pathophysiology of the Peritoneum during Peritoneal Dialysis. Adv Med *2014*, 473134.
Love, M.I., Huber, W., and Anders, S. (2014). Moderated estimation of fold change and dispersion for RNA-seq data with DESeq2. Genome Biol *15*, 550.
Lovisa, S., LeBleu, V.S., Tampe, B., Sugimoto, H., Vadnagara, K., Carstens, J.L., Wu, C.C., Hagos, Y., Burckhardt, B.C., Pentcheva-Hoang, T., et al. (2015). Epithelial-to-mesenchymal transition induces cell cycle arrest and parenchymal damage in renal fibrosis. Nat Med *21*, 998-1009.
Lu, J., and Shenoy, A.K. (2017). Epithelial-to-Pericyte Transition in Cancer. Cancers (Basel) *9*.
Luche, H., Weber, O., Nageswara Rao, T., Blum, C., and Fehling, H.J. (2007). Faithful activation of an extra-bright red fluorescent protein in "knock-in" Cre-reporter mice ideally suited for lineage tracing studies. Eur J Immunol *37*, 43-53.
Lun, X.K., Szklarczyk, D., Gabor, A., Dobberstein, N., Zanotelli, V.R.T., Saez-Rodriguez, J., von Mering, C., and Bodenmiller, B. (2019). Analysis of the Human Kinome and Phosphatome by Mass Cytometry Reveals Overexpression-Induced Effects on Cancer-Related Signaling. Mol Cell *74*, 1086-1102 e1085.
Lun, X.K., Zanotelli, V.R., Wade, J.D., Schapiro, D., Tognetti, M., Dobberstein, N., and Bodenmiller, B. (2017). Influence of node abundance on signaling network state and dynamics analyzed by mass cytometry. Nat Biotechnol *35*, 164-172.

Mace, T.A., Ameen, Z., Collins, A., Wojcik, S., Mair, M., Young, G.S., Fuchs, J.R., Eubank, T.D., Frankel, W.L., Bekaii-Saab, T., et al. (2013). Pancreatic cancer-associated stellate cells promote differentiation of myeloid-derived suppressor cells in a STAT3-dependent manner. Cancer Res *73*, 3007-3018.

Madsen, C.D., Pedersen, J.T., Venning, F.A., Singh, L.B., Moeendarbary, E., Charras, G., Cox, T.R., Sahai, E., and Erler, J.T. (2015). Hypoxia and loss of PHD2 inactivate stromal fibroblasts to decrease tumour stiffness and metastasis. EMBO Rep *16*, 1394-1408.

Maier, B., Leader, A.M., Chen, S.T., Tung, N., Chang, C., LeBerichel, J., Chudnovskiy, A., Maskey, S., Walker, L., Finnigan, J.P., et al. (2020). A conserved dendritic-cell regulatory program limits antitumour immunity. Nature *580*, 257-262.

Mak, K.M., and Mei, R. (2017). Basement Membrane Type IV Collagen and Laminin: An Overview of Their Biology and Value as Fibrosis Biomarkers of Liver Disease. Anat Rec (Hoboken) *300*, 1371-1390.

Marangoni, R.G., Korman, B.D., Wei, J., Wood, T.A., Graham, L.V., Whitfield, M.L., Scherer, P.E., Tourtellotte, W.G., and Varga, J. (2015). Myofibroblasts in murine cutaneous fibrosis originate from adiponectin-positive intradermal progenitors. Arthritis Rheumatol *67*, 1062-1073.

Marino, S., Vooijs, M., van Der Gulden, H., Jonkers, J., and Berns, A. (2000). Induction of medulloblastomas in p53-null mutant mice by somatic inactivation of Rb in the external granular layer cells of the cerebellum. Genes Dev *14*, 994-1004.

Maurer, C., Holmstrom, S.R., He, J., Laise, P., Su, T., Ahmed, A., Hibshoosh, H., Chabot, J.A., Oberstein, P.E., Sepulveda, A.R., et al. (2019). Experimental microdissection enables functional harmonisation of pancreatic cancer subtypes. Gut *68*, 1034-1043.

Mavropoulos, A., Allo, B., He, M., Park, E., Majonis, D., and Ornatsky, O. (2017). Simultaneous Detection of Protein and mRNA in Jurkat and KG-1a Cells by Mass Cytometry. Cytometry A *91*, 1200-1208.

McDonald, L.T., Russell, D.L., Kelly, R.R., Xiong, Y., Motamarry, A., Patel, R.K., Jones, J.A., Watson, P.M., Turner, D.P., Watson, D.K., et al. (2015). Hematopoietic stem cell-derived cancer-associated fibroblasts are novel contributors to the pro-tumorigenic microenvironment. Neoplasia *17*, 434-448.

McGinnis, C.S., Patterson, D.M., Winkler, J., Conrad, D.N., Hein, M.Y., Srivastava, V., Hu, J.L., Murrow, L.M., Weissman, J.S., Werb, Z., et al. (2019). MULTI-seq: sample multiplexing for single-cell RNA sequencing using lipid-tagged indices. Nat Methods *16*, 619-626.

Mehal, W.Z., Iredale, J., and Friedman, S.L. (2011). Scraping fibrosis: expressway to the core of fibrosis. Nat Med *17*, 552-553.

Meng, X.M., Nikolic-Paterson, D.J., and Lan, H.Y. (2014). Inflammatory processes in renal fibrosis. Nat Rev Nephrol *10*, 493-503.

Mercer, K., Giblett, S., Green, S., Lloyd, D., DaRocha Dias, S., Plumb, M., Marais, R., and Pritchard, C. (2005). Expression of endogenous oncogenic V600EB-raf induces proliferation and developmental defects in mice and transformation of primary fibroblasts. Cancer Res *65*, 11493-11500.

Meuwissen, R., Linn, S.C., van der Valk, M., Mooi, W.J., and Berns, A. (2001). Mouse model for lung tumorigenesis through Cre/lox controlled sporadic activation of the K-Ras oncogene. Oncogene *20*, 6551-6558.

Miller, B.C., Sen, D.R., Al Abosy, R., Bi, K., Virkud, Y.V., LaFleur, M.W., Yates, K.B., Lako, A., Felt, K., Naik, G.S., et al. (2019). Subsets of exhausted CD8(+) T cells differentially mediate tumor control and respond to checkpoint blockade. Nat Immunol *20*, 326-336.

Mimitou, E.P., Cheng, A., Montalbano, A., Hao, S., Stoeckius, M., Legut, M., Roush, T., Herrera, A., Papalexi, E., Ouyang, Z., et al. (2019). Multiplexed detection of proteins, transcriptomes, clonotypes and CRISPR perturbations in single cells. Nat Methods *16*, 409-412.

Mizoguchi, F., Slowikowski, K., Wei, K., Marshall, J.L., Rao, D.A., Chang, S.K., Nguyen, H.N., Noss, E.H., Turner, J.D., Earp, B.E., et al. (2018). Functionally distinct disease-associated fibroblast subsets in rheumatoid arthritis. Nat Commun *9*, 789.

Mombaerts, P., Iacomini, J., Johnson, R.S., Herrup, K., Tonegawa, S., and Papaioannou, V.E. (1992). RAG-1-deficient mice have no mature B and T lymphocytes. Cell *68*, 869-877.

Morsing, M., Klitgaard, M.C., Jafari, A., Villadsen, R., Kassem, M., Petersen, O.W., and Ronnov-Jessen, L. (2016). Evidence of two distinct functionally specialized fibroblast lineages in breast stroma. Breast Cancer Res *18*, 108.

Mueller, S., Engleitner, T., Maresch, R., Zukowska, M., Lange, S., Kaltenbacher, T., Konukiewitz, B., Ollinger, R., Zwiebel, M., Strong, A., et al. (2018). Evolutionary routes and KRAS dosage define pancreatic cancer phenotypes. Nature *554*, 62-68.

Musso, A., Condon, T.P., West, G.A., De La Motte, C., Strong, S.A., Levine, A.D., Bennett, C.F., and Fiocchi, C. (1999). Regulation of ICAM-1-mediated fibroblast-T cell reciprocal interaction: implications for modulation of gut inflammation. Gastroenterology *117*, 546-556.

Mutsaers, S.E., Birnie, K., Lansley, S., Herrick, S.E., Lim, C.B., and Prele, C.M. (2015). Mesothelial cells in tissue repair and fibrosis. Front Pharmacol *6*, 113.

Nagarsheth, N., Wicha, M.S., and Zou, W. (2017). Chemokines in the cancer microenvironment and their relevance in cancer immunotherapy. Nat Rev Immunol *17*, 559-572.

Namvar, S., Woolf, A.S., Zeef, L.A., Wilm, T., Wilm, B., and Herrick, S.E. (2018). Functional molecules in mesothelial-to-mesenchymal transition revealed by transcriptome analyses. J Pathol *245*, 491-501.
Nature Career Column (2019). Highlight negative results to improve science.
Nature Research TRACERx Collection (2020). TRACERx Collection.
Neesse, A., Michl, P., Frese, K.K., Feig, C., Cook, N., Jacobetz, M.A., Lolkema, M.P., Buchholz, M., Olive, K.P., Gress, T.M., et al. (2011). Stromal biology and therapy in pancreatic cancer. Gut *60*, 861-868.
Nguyen, H.N., Noss, E.H., Mizoguchi, F., Huppertz, C., Wei, K.S., Watts, G.F.M., and Brenner, M.B. (2017). Autocrine Loop Involving IL-6 Family Member LIF, LIF Receptor, and STAT4 Drives Sustained Fibroblast Production of Inflammatory Mediators. Immunity *46*, 220-232.
Nolan-Stevaux, O., Lau, J., Truitt, M.L., Chu, G.C., Hebrok, M., Fernandez-Zapico, M.E., and Hanahan, D. (2009). GLI1 is regulated through Smoothened-independent mechanisms in neoplastic pancreatic ducts and mediates PDAC cell survival and transformation. Genes Dev *23*, 24-36.
O'Connell, J.T., Sugimoto, H., Cooke, V.G., MacDonald, B.A., Mehta, A.I., LeBleu, V.S., Dewar, R., Rocha, R.M., Brentani, R.R., Resnick, M.B., et al. (2011). VEGF-A and Tenascin-C produced by S100A4+ stromal cells are important for metastatic colonization. Proc Natl Acad Sci U S A *108*, 16002-16007.
Ogura, M., Bridgeman, V.L., and Malanchi, I. (2017). Macrophages unlock progression of breast cancer cells experiencing matrigel-segregation in transplantation models. Sci Rep *7*, 11028.
Ohlund, D., Elyada, E., and Tuveson, D. (2014). Fibroblast heterogeneity in the cancer wound. J Exp Med *211*, 1503-1523.
Ohlund, D., Handly-Santana, A., Biffi, G., Elyada, E., Almeida, A.S., Ponz-Sarvise, M., Corbo, V., Oni, T.E., Hearn, S.A., Lee, E.J., et al. (2017). Distinct populations of inflammatory fibroblasts and myofibroblasts in pancreatic cancer. J Exp Med *214*, 579-596.
Olivares, O., Mayers, J.R., Gouirand, V., Torrence, M.E., Gicquel, T., Borge, L., Lac, S., Roques, J., Lavaut, M.N., Berthezene, P., et al. (2017). Collagen-derived proline promotes pancreatic ductal adenocarcinoma cell survival under nutrient limited conditions. Nat Commun *8*, 16031.
Olive, K.P., Jacobetz, M.A., Davidson, C.J., Gopinathan, A., McIntyre, D., Honess, D., Madhu, B., Goldgraben, M.A., Caldwell, M.E., Allard, D., et al. (2009). Inhibition of Hedgehog signaling enhances delivery of chemotherapy in a mouse model of pancreatic cancer. Science *324*, 1457-1461.
Ozdemir, B.C., Pentcheva-Hoang, T., Carstens, J.L., Zheng, X., Wu, C.C., Simpson, T.R., Laklai, H., Sugimoto, H., Kahlert, C., Novitskiy, S.V., et al. (2014). Depletion of carcinoma-associated fibroblasts and fibrosis induces immunosuppression and accelerates pancreas cancer with reduced survival. Cancer Cell *25*, 719-734.
Paauwe, M., Schoonderwoerd, M.J.A., Helderman, R., Harryvan, T.J., Groenewoud, A., van Pelt, G.W., Bor, R., Hemmer, D.M., Versteeg, H.H., Snaar-Jagalska, B.E., et al. (2018). Endoglin Expression on Cancer-Associated Fibroblasts Regulates Invasion and Stimulates Colorectal Cancer Metastasis. Clin Cancer Res *24*, 6331-6344.
Pallangyo, C.K., Ziegler, P.K., and Greten, F.R. (2015). IKKbeta acts as a tumor suppressor in cancer-associated fibroblasts during intestinal tumorigenesis. J Exp Med *212*, 2253-2266.
Paquet-Fifield, S., Schluter, H., Li, A., Aitken, T., Gangatirkar, P., Blashki, D., Koelmeyer, R., Pouliot, N., Palatsides, M., Ellis, S., et al. (2009). A role for pericytes as microenvironmental regulators of human skin tissue regeneration. J Clin Invest *119*, 2795-2806.
Park, J., Shrestha, R., Qiu, C., Kondo, A., Huang, S., Werth, M., Li, M., Barasch, J., and Susztak, K. (2018). Single-cell transcriptomics of the mouse kidney reveals potential cellular targets of kidney disease. Science *360*, 758-763.
Pear, W.S., Nolan, G.P., Scott, M.L., and Baltimore, D. (1993). Production of high-titer helper-free retroviruses by transient transfection. Proc Natl Acad Sci U S A *90*, 8392-8396.
Pechhold, K., Patterson, N.B., Craighead, N., Lee, K.P., June, C.H., and Harlan, D.M. (1997). Inflammatory cytokines IFN-gamma plus TNF-alpha induce regulated expression of CD80 (B7-1) but not CD86 (B7-2) on murine fibroblasts. J Immunol *158*, 4921-4929.
Peters, M.L.B., Eckel, A., Mueller, P.P., Tramontano, A.C., Weaver, D.T., Lietz, A., Hur, C., Kong, C.Y., and Pandharipande, P.V. (2018). Progression to pancreatic ductal adenocarcinoma from pancreatic intraepithelial neoplasia: Results of a simulation model. Pancreatology *18*, 928-934.
Philip, M., Fairchild, L., Sun, L., Horste, E.L., Camara, S., Shakiba, M., Scott, A.C., Viale, A., Lauer, P., Merghoub, T., et al. (2017). Chromatin states define tumour-specific T cell dysfunction and reprogramming. Nature *545*, 452-456.
Philippeos, C., Telerman, S.B., Oules, B., Pisco, A.O., Shaw, T.J., Elgueta, R., Lombardi, G., Driskell, R.R., Soldin, M., Lynch, M.D., et al. (2018). Spatial and Single-Cell Transcriptional Profiling Identifies Functionally Distinct Human Dermal Fibroblast Subpopulations. J Invest Dermatol *138*, 811-825.
Phillips, R.J., Burdick, M.D., Hong, K., Lutz, M.A., Murray, L.A., Xue, Y.Y., Belperio, J.A., Keane, M.P., and Strieter, R.M. (2004). Circulating fibrocytes traffic to the lungs in response to CXCL12 and mediate fibrosis. J Clin Invest *114*, 438-446.

Plikus, M.V., Guerrero-Juarez, C.F., Ito, M., Li, Y.R., Dedhia, P.H., Zheng, Y., Shao, M., Gay, D.L., Ramos, R., Hsi, T.C., et al. (2017). Regeneration of fat cells from myofibroblasts during wound healing. Science *355*, 748-752.
Pober, J.S., Merola, J., Liu, R., and Manes, T.D. (2017). Antigen Presentation by Vascular Cells. Front Immunol *8*, 1907.
Pols, M.S., and Klumperman, J. (2009). Trafficking and function of the tetraspanin CD63. Exp Cell Res *315*, 1584-1592.
Potenta, S., Zeisberg, E., and Kalluri, R. (2008). The role of endothelial-to-mesenchymal transition in cancer progression. Br J Cancer *99*, 1375-1379.
Powell, D.W., Pinchuk, I.V., Saada, J.I., Chen, X., and Mifflin, R.C. (2011). Mesenchymal cells of the intestinal lamina propria. Annu Rev Physiol *73*, 213-237.
Provenzano, P.P., Cuevas, C., Chang, A.E., Goel, V.K., Von Hoff, D.D., and Hingorani, S.R. (2012). Enzymatic targeting of the stroma ablates physical barriers to treatment of pancreatic ductal adenocarcinoma. Cancer Cell *21*, 418-429.
Provenzano, P.P., and Keely, P.J. (2011). Mechanical signaling through the cytoskeleton regulates cell proliferation by coordinated focal adhesion and Rho GTPase signaling. J Cell Sci *124*, 1195-1205.
Puram, S.V., Tirosh, I., Parikh, A.S., Patel, A.P., Yizhak, K., Gillespie, S., Rodman, C., Luo, C.L., Mroz, E.A., Emerick, K.S., et al. (2017). Single-Cell Transcriptomic Analysis of Primary and Metastatic Tumor Ecosystems in Head and Neck Cancer. Cell *171*, 1611-1624 e1624.
Raab, S., Klingenstein, M., Liebau, S., and Linta, L. (2014). A Comparative View on Human Somatic Cell Sources for iPSC Generation. Stem Cells Int *2014*, 768391.
Rahib, L., Smith, B.D., Aizenberg, R., Rosenzweig, A.B., Fleshman, J.M., and Matrisian, L.M. (2014). Projecting cancer incidence and deaths to 2030: the unexpected burden of thyroid, liver, and pancreas cancers in the United States. Cancer Res *74*, 2913-2921.
Ramilowski, J.A., Goldberg, T., Harshbarger, J., Kloppmann, E., Lizio, M., Satagopam, V.P., Itoh, M., Kawaji, H., Carninci, P., Rost, B., et al. (2015). A draft network of ligand-receptor-mediated multicellular signalling in human. Nat Commun *6*, 7866.
Rapsomaniki, M.A., Lun, X.K., Woerner, S., Laumanns, M., Bodenmiller, B., and Martinez, M.R. (2018). CellCycleTRACER accounts for cell cycle and volume in mass cytometry data. Nat Commun *9*, 632.
Redd, M.J., Cooper, L., Wood, W., Stramer, B., and Martin, P. (2004). Wound healing and inflammation: embryos reveal the way to perfect repair. Philos Trans R Soc Lond B Biol Sci *359*, 777-784.
Renart, J., Carrasco-Ramirez, P., Fernandez-Munoz, B., Martin-Villar, E., Montero, L., Yurrita, M.M., and Quintanilla, M. (2015). New insights into the role of podoplanin in epithelial-mesenchymal transition. Int Rev Cell Mol Biol *317*, 185-239.
Rhim, A.D., Mirek, E.T., Aiello, N.M., Maitra, A., Bailey, J.M., McAllister, F., Reichert, M., Beatty, G.L., Rustgi, A.K., Vonderheide, R.H., et al. (2012). EMT and dissemination precede pancreatic tumor formation. Cell *148*, 349-361.
Rhim, A.D., Oberstein, P.E., Thomas, D.H., Mirek, E.T., Palermo, C.F., Sastra, S.A., Dekleva, E.N., Saunders, T., Becerra, C.P., Tattersall, I.W., et al. (2014). Stromal elements act to restrain, rather than support, pancreatic ductal adenocarcinoma. Cancer Cell *25*, 735-747.
Rinkevich, Y., Walmsley, G.G., Hu, M.S., Maan, Z.N., Newman, A.M., Drukker, M., Januszyk, M., Krampitz, G.W., Gurtner, G.C., Lorenz, H.P., et al. (2015). Skin fibrosis. Identification and isolation of a dermal lineage with intrinsic fibrogenic potential. Science *348*, aaa2151.
Rinn, J.L., Bondre, C., Gladstone, H.B., Brown, P.O., and Chang, H.Y. (2006). Anatomic demarcation by positional variation in fibroblast gene expression programs. PLoS Genet *2*, e119.
Roberts, E.W., Broz, M.L., Binnewies, M., Headley, M.B., Nelson, A.E., Wolf, D.M., Kaisho, T., Bogunovic, D., Bhardwaj, N., and Krummel, M.F. (2016). Critical Role for CD103(+)/CD141(+) Dendritic Cells Bearing CCR7 for Tumor Antigen Trafficking and Priming of T Cell Immunity in Melanoma. Cancer Cell *30*, 324-336.
Roberts, E.W., Deonarine, A., Jones, J.O., Denton, A.E., Feig, C., Lyons, S.K., Espeli, M., Kraman, M., McKenna, B., Wells, R.J., et al. (2013). Depletion of stromal cells expressing fibroblast activation protein-alpha from skeletal muscle and bone marrow results in cachexia and anemia. J Exp Med *210*, 1137-1151.
Rock, J.R., Barkauskas, C.E., Cronce, M.J., Xue, Y., Harris, J.R., Liang, J., Noble, P.W., and Hogan, B.L. (2011). Multiple stromal populations contribute to pulmonary fibrosis without evidence for epithelial to mesenchymal transition. Proc Natl Acad Sci U S A *108*, E1475-1483.
Rodda, L.B., Lu, E., Bennett, M.L., Sokol, C.L., Wang, X., Luther, S.A., Barres, B.A., Luster, A.D., Ye, C.J., and Cyster, J.G. (2018). Single-Cell RNA Sequencing of Lymph Node Stromal Cells Reveals Niche-Associated Heterogeneity. Immunity *48*, 1014-1028 e1016.
Rogalla, S., and Contag, C.H. (2015). Early Cancer Detection at the Epithelial Surface. Cancer J *21*, 179-187.

Rosenthal, R., Cadieux, E.L., Salgado, R., Bakir, M.A., Moore, D.A., Hiley, C.T., Lund, T., Tanic, M., Reading, J.L., Joshi, K., et al. (2019). Neoantigen-directed immune escape in lung cancer evolution. Nature *567*, 479-485.

Rosow, D.E., Liss, A.S., Strobel, O., Fritz, S., Bausch, D., Valsangkar, N.P., Alsina, J., Kulemann, B., Park, J.K., Yamaguchi, J., et al. (2012). Sonic Hedgehog in pancreatic cancer: from bench to bedside, then back to the bench. Surgery *152*, S19-32.

Rowe, R.G., Lin, Y., Shimizu-Hirota, R., Hanada, S., Neilson, E.G., Greenson, J.K., and Weiss, S.J. (2011). Hepatocyte-derived Snail1 propagates liver fibrosis progression. Mol Cell Biol *31*, 2392-2403.

Rubiano, A., Delitto, D., Han, S., Gerber, M., Galitz, C., Trevino, J., Thomas, R.M., Hughes, S.J., and Simmons, C.S. (2018). Viscoelastic properties of human pancreatic tumors and in vitro constructs to mimic mechanical properties. Acta Biomater *67*, 331-340.

Rynne-Vidal, A., Jimenez-Heffernan, J.A., Fernandez-Chacon, C., Lopez-Cabrera, M., and Sandoval, P. (2015). The Mesothelial Origin of Carcinoma Associated-Fibroblasts in Peritoneal Metastasis. Cancers (Basel) *7*, 1994-2011.

Saad, A.M., Turk, T., Al-Husseini, M.J., and Abdel-Rahman, O. (2018). Trends in pancreatic adenocarcinoma incidence and mortality in the United States in the last four decades; a SEER-based study. BMC Cancer *18*, 688.

Saatci, O., Kaymak, A., Raza, U., Ersan, P.G., Akbulut, O., Banister, C.E., Sikirzhytski, V., Tokat, U.M., Aykut, G., Ansari, S.A., et al. (2020). Targeting lysyl oxidase (LOX) overcomes chemotherapy resistance in triple negative breast cancer. Nat Commun *11*, 2416.

Sacco, A.M., Belviso, I., Romano, V., Carfora, A., Schonauer, F., Nurzynska, D., Montagnani, S., Di Meglio, F., and Castaldo, C. (2019). Diversity of dermal fibroblasts as major determinant of variability in cell reprogramming. J Cell Mol Med *23*, 4256-4268.

Sahai, E., Astsaturov, I., Cukierman, E., DeNardo, D.G., Egeblad, M., Evans, R.M., Fearon, D., Greten, F.R., Hingorani, S.R., Hunter, T., et al. (2020). A framework for advancing our understanding of cancer-associated fibroblasts. Nat Rev Cancer *20*, 174-186.

Sandbo, N., and Dulin, N. (2011). Actin cytoskeleton in myofibroblast differentiation: ultrastructure defining form and driving function. Transl Res *158*, 181-196.

Sarvaria, A., Madrigal, J.A., and Saudemont, A. (2017). B cell regulation in cancer and anti-tumor immunity. Cell Mol Immunol *14*, 662-674.

Sautes-Fridman, C., Petitprez, F., Calderaro, J., and Fridman, W.H. (2019). Tertiary lymphoid structures in the era of cancer immunotherapy. Nat Rev Cancer *19*, 307-325.

Schonhuber, N., Seidler, B., Schuck, K., Veltkamp, C., Schachtler, C., Zukowska, M., Eser, S., Feyerabend, T.B., Paul, M.C., Eser, P., et al. (2014). A next-generation dual-recombinase system for time- and host-specific targeting of pancreatic cancer. Nat Med *20*, 1340-1347.

Schussler, M.H., Skoudy, A., Ramaekers, F., and Real, F.X. (1992). Intermediate filaments as differentiation markers of normal pancreas and pancreas cancer. Am J Pathol *140*, 559-568.

Schwartz, A.M., and Henson, D.E. (2007). Familial and sporadic pancreatic carcinoma, epidemiologic concordance. Am J Surg Pathol *31*, 645-646.

Serban, M.A., and Prestwich, G.D. (2008). Modular extracellular matrices: solutions for the puzzle. Methods *45*, 93-98.

Shanzer, M., Ricardo-Lax, I., Keshet, R., Reuven, N., and Shaul, Y. (2015). The polyomavirus middle T-antigen oncogene activates the Hippo pathway tumor suppressor Lats in a Src-dependent manner. Oncogene *34*, 4190-4198.

Sheng, G. (2015). The developmental basis of mesenchymal stem/stromal cells (MSCs). BMC Dev Biol *15*, 44.

Sherman, M.H., Yu, R.T., Engle, D.D., Ding, N., Atkins, A.R., Tiriac, H., Collisson, E.A., Connor, F., Van Dyke, T., Kozlov, S., et al. (2014). Vitamin D receptor-mediated stromal reprogramming suppresses pancreatitis and enhances pancreatic cancer therapy. Cell *159*, 80-93.

Shi, Y., Gao, W., Lytle, N.K., Huang, P., Yuan, X., Dann, A.M., Ridinger-Saison, M., DelGiorno, K.E., Antal, C.E., Liang, G., et al. (2019). Targeting LIF-mediated paracrine interaction for pancreatic cancer therapy and monitoring. Nature *569*, 131-135.

Shin, K., Lim, A., Zhao, C., Sahoo, D., Pan, Y., Spiekerkoetter, E., Liao, J.C., and Beachy, P.A. (2014). Hedgehog signaling restrains bladder cancer progression by eliciting stromal production of urothelial differentiation factors. Cancer Cell *26*, 521-533.

Siddiqui, I., Schaeuble, K., Chennupati, V., Fuertes Marraco, S.A., Calderon-Copete, S., Pais Ferreira, D., Carmona, S.J., Scarpellino, L., Gfeller, D., Pradervand, S., et al. (2019). Intratumoral Tcf1(+)PD-1(+)CD8(+) T Cells with Stem-like Properties Promote Tumor Control in Response to Vaccination and Checkpoint Blockade Immunotherapy. Immunity *50*, 195-211 e110.

Silva, E.A., and Mooney, D.J. (2004). Synthetic extracellular matrices for tissue engineering and regeneration. Curr Top Dev Biol *64*, 181-205.

Simoes, F.C., Cahill, T.J., Kenyon, A., Gavriouchkina, D., Vieira, J.M., Sun, X., Pezzolla, D., Ravaud, C., Masmanian, E., Weinberger, M., et al. (2020). Macrophages directly contribute collagen to scar formation during zebrafish heart regeneration and mouse heart repair. Nat Commun *11*, 600.
Simoni, Y., Becht, E., Fehlings, M., Loh, C.Y., Koo, S.L., Teng, K.W.W., Yeong, J.P.S., Nahar, R., Zhang, T., Kared, H., et al. (2018). Bystander CD8(+) T cells are abundant and phenotypically distinct in human tumour infiltrates. Nature *557*, 575-579.
Singh, M., Lima, A., Molina, R., Hamilton, P., Clermont, A.C., Devasthali, V., Thompson, J.D., Cheng, J.H., Bou Reslan, H., Ho, C.C., et al. (2010). Assessing therapeutic responses in Kras mutant cancers using genetically engineered mouse models. Nat Biotechnol *28*, 585-593.
Singhal, P.K., Sassi, S., Lan, L., Au, P., Halvorsen, S.C., Fukumura, D., Jain, R.K., and Seed, B. (2016). Mouse embryonic fibroblasts exhibit extensive developmental and phenotypic diversity. Proc Natl Acad Sci U S A *113*, 122-127.
Somerville, T.D., Biffi, G., Dassler-Plenker, J., Hur, S.K., He, X.Y., Vance, K.E., Miyabayashi, K., Xu, Y., Maia-Silva, D., Klingbeil, O., et al. (2020). Squamous trans-differentiation of pancreatic cancer cells promotes stromal inflammation. Elife *9*.
Sorrell, J.M., and Caplan, A.I. (2004). Fibroblast heterogeneity: more than skin deep. J Cell Sci *117*, 667-675.
Soundararajan, M., and Kannan, S. (2018). Fibroblasts and mesenchymal stem cells: Two sides of the same coin? J Cell Physiol *233*, 9099-9109.
Sousa, C.M., Biancur, D.E., Wang, X., Halbrook, C.J., Sherman, M.H., Zhang, L., Kremer, D., Hwang, R.F., Witkiewicz, A.K., Ying, H., et al. (2016). Pancreatic stellate cells support tumour metabolism through autophagic alanine secretion. Nature *536*, 479-483.
Spaeth, E.L., Labaff, A.M., Toole, B.P., Klopp, A., Andreeff, M., and Marini, F.C. (2013). Mesenchymal CD44 expression contributes to the acquisition of an activated fibroblast phenotype via TWIST activation in the tumor microenvironment. Cancer Res *73*, 5347-5359.
Spitzer, M.H., Carmi, Y., Reticker-Flynn, N.E., Kwek, S.S., Madhireddy, D., Martins, M.M., Gherardini, P.F., Prestwood, T.R., Chabon, J., Bendall, S.C., et al. (2017). Systemic Immunity Is Required for Effective Cancer Immunotherapy. Cell *168*, 487-502 e415.
Spitzer, M.H., and Nolan, G.P. (2016). Mass Cytometry: Single Cells, Many Features. Cell *165*, 780-791.
Stoeckius, M., Hafemeister, C., Stephenson, W., Houck-Loomis, B., Chattopadhyay, P.K., Swerdlow, H., Satija, R., and Smibert, P. (2017). Simultaneous epitope and transcriptome measurement in single cells. Nat Methods *14*, 865-868.
Stoker, M.G., Shearer, M., and O'Neill, C. (1966). Growth inhibition of polyoma-transformed cells by contact with static normal fibroblasts. J Cell Sci *1*, 297-310.
Stratton, M.S., Bagchi, R.A., Felisbino, M.B., Hirsch, R.A., Smith, H.E., Riching, A.S., Enyart, B.Y., Koch, K.A., Cavasin, M.A., Alexanian, M., et al. (2019). Dynamic Chromatin Targeting of BRD4 Stimulates Cardiac Fibroblast Activation. Circ Res *125*, 662-677.
Stuart, T., and Satija, R. (2019). Integrative single-cell analysis. Nat Rev Genet *20*, 257-272.
Su, S., Chen, J., Yao, H., Liu, J., Yu, S., Lao, L., Wang, M., Luo, M., Xing, Y., Chen, F., et al. (2018). CD10(+)GPR77(+) Cancer-Associated Fibroblasts Promote Cancer Formation and Chemoresistance by Sustaining Cancer Stemness. Cell *172*, 841-856 e816.
Subramanian, A., Kuehn, H., Gould, J., Tamayo, P., and Mesirov, J.P. (2007). GSEA-P: a desktop application for Gene Set Enrichment Analysis. Bioinformatics *23*, 3251-3253.
Subramanian, A., Tamayo, P., Mootha, V.K., Mukherjee, S., Ebert, B.L., Gillette, M.A., Paulovich, A., Pomeroy, S.L., Golub, T.R., Lander, E.S., et al. (2005). Gene set enrichment analysis: a knowledge-based approach for interpreting genome-wide expression profiles. Proc Natl Acad Sci U S A *102*, 15545-15550.
Sugawara, S., Sugiyama, A., Nemoto, E., Rikiishi, H., and Takada, H. (1998). Heterogeneous expression and release of CD14 by human gingival fibroblasts: characterization and CD14-mediated interleukin-8 secretion in response to lipopolysaccharide. Infect Immun *66*, 3043-3049.
Sugden, W.W., Meissner, R., Aegerter-Wilmsen, T., Tsaryk, R., Leonard, E.V., Bussmann, J., Hamm, M.J., Herzog, W., Jin, Y., Jakobsson, L., et al. (2017). Endoglin controls blood vessel diameter through endothelial cell shape changes in response to haemodynamic cues. Nat Cell Biol *19*, 653-665.
Sugimoto, H., Mundel, T.M., Kieran, M.W., and Kalluri, R. (2006). Identification of fibroblast heterogeneity in the tumor microenvironment. Cancer Biol Ther *5*, 1640-1646.
Sulzmaier, F.J., Jean, C., and Schlaepfer, D.D. (2014). FAK in cancer: mechanistic findings and clinical applications. Nat Rev Cancer *14*, 598-610.
Sweeney, M., and Foldes, G. (2018). It Takes Two: Endothelial-Perivascular Cell Cross-Talk in Vascular Development and Disease. Front Cardiovasc Med *5*, 154.
Swift, J., Ivanovska, I.L., Buxboim, A., Harada, T., Dingal, P.C., Pinter, J., Pajerowski, J.D., Spinler, K.R., Shin, J.W., Tewari, M., et al. (2013). Nuclear lamin-A scales with tissue stiffness and enhances matrix-directed differentiation. Science *341*, 1240104.

Tabib, T., Morse, C., Wang, T., Chen, W., and Lafyatis, R. (2018). SFRP2/DPP4 and FMO1/LSP1 Define Major Fibroblast Populations in Human Skin. J Invest Dermatol *138*, 802-810.
Takahashi, T., and Morikawa, K. (2006). Vitamin D receptor agonists: opportunities and challenges in drug discovery. Curr Top Med Chem *6*, 1303-1316.
Tape, C.J., Ling, S., Dimitriadi, M., McMahon, K.M., Worboys, J.D., Leong, H.S., Norrie, I.C., Miller, C.J., Poulogiannis, G., Lauffenburger, D.A., et al. (2016). Oncogenic KRAS Regulates Tumor Cell Signaling via Stromal Reciprocation. Cell *165*, 1818.
The 3Rs (2020). Principles of the 3Rs.
The Human Protein Atlas (2020). The Human Protein Atlas, https://www.proteinatlas.org/.
Thommen, D.S., Koelzer, V.H., Herzig, P., Roller, A., Trefny, M., Dimeloe, S., Kiialainen, A., Hanhart, J., Schill, C., Hess, C., et al. (2018). A transcriptionally and functionally distinct PD-1(+) CD8(+) T cell pool with predictive potential in non-small-cell lung cancer treated with PD-1 blockade. Nat Med *24*, 994-1004.
Tian, H., Callahan, C.A., DuPree, K.J., Darbonne, W.C., Ahn, C.P., Scales, S.J., and de Sauvage, F.J. (2009). Hedgehog signaling is restricted to the stromal compartment during pancreatic carcinogenesis. Proc Natl Acad Sci U S A *106*, 4254-4259.
Tiriac, H., Plenker, D., Baker, L.A., and Tuveson, D.A. (2019). Organoid models for translational pancreatic cancer research. Curr Opin Genet Dev *54*, 7-11.
Togashi, Y., Shitara, K., and Nishikawa, H. (2019). Regulatory T cells in cancer immunosuppression - implications for anticancer therapy. Nat Rev Clin Oncol *16*, 356-371.
Torphy, R.J., Wang, Z., True-Yasaki, A., Volmar, K.E., Rashid, N., Yeh, B., Anderson, J.M., Johansen, J.S., Hollingsworth, M.A., Yeh, J.J., et al. (2018). Stromal Content Is Correlated With Tissue Site, Contrast Retention, and Survival in Pancreatic Adenocarcinoma. JCO Precis Oncol *2018*.
Tran, E., Chinnasamy, D., Yu, Z., Morgan, R.A., Lee, C.C., Restifo, N.P., and Rosenberg, S.A. (2013). Immune targeting of fibroblast activation protein triggers recognition of multipotent bone marrow stromal cells and cachexia. J Exp Med *210*, 1125-1135.
Tschumperlin, D.J., Ligresti, G., Hilscher, M.B., and Shah, V.H. (2018). Mechanosensing and fibrosis. J Clin Invest *128*, 74-84.
Tsukui, T., Sun, K.H., Wetter, J.B., Wilson-Kanamori, J.R., Hazelwood, L.A., Henderson, N.C., Adams, T.S., Schupp, J.C., Poli, S.D., Rosas, I.O., et al. (2020). Collagen-producing lung cell atlas identifies multiple subsets with distinct localization and relevance to fibrosis. Nat Commun *11*, 1920.
Tuveson, D., and Clevers, H. (2019). Cancer modeling meets human organoid technology. Science *364*, 952-955.
Umetsu, D.T., Katzen, D., Jabara, H.H., and Geha, R.S. (1986). Antigen presentation by human dermal fibroblasts: activation of resting T lymphocytes. J Immunol *136*, 440-445.
Vaccaro, V., Sperduti, I., and Milella, M. (2011). FOLFIRINOX versus gemcitabine for metastatic pancreatic cancer. N Engl J Med *365*, 768-769; author reply 769.
Valenzi, E., Bulik, M., Tabib, T., Morse, C., Sembrat, J., Trejo Bittar, H., Rojas, M., and Lafyatis, R. (2019). Single-cell analysis reveals fibroblast heterogeneity and myofibroblasts in systemic sclerosis-associated interstitial lung disease. Ann Rheum Dis *78*, 1379-1387.
van Caam, A., Madej, W., Garcia de Vinuesa, A., Goumans, M.J., Ten Dijke, P., Blaney Davidson, E., and van der Kraan, P. (2017). TGFbeta1-induced SMAD2/3 and SMAD1/5 phosphorylation are both ALK5-kinase-dependent in primary chondrocytes and mediated by TAK1 kinase activity. Arthritis Res Ther *19*, 112.
van der Leun, A.M., Thommen, D.S., and Schumacher, T.N. (2020). CD8(+) T cell states in human cancer: insights from single-cell analysis. Nat Rev Cancer *20*, 218-232.
Van Gassen, S., Callebaut, B., Van Helden, M.J., Lambrecht, B.N., Demeester, P., Dhaene, T., and Saeys, Y. (2015). FlowSOM: Using self-organizing maps for visualization and interpretation of cytometry data. Cytometry A *87*, 636-645.
Vennin, C., Chin, V.T., Warren, S.C., Lucas, M.C., Herrmann, D., Magenau, A., Melenec, P., Walters, S.N., Del Monte-Nieto, G., Conway, J.R., et al. (2017). Transient tissue priming via ROCK inhibition uncouples pancreatic cancer progression, sensitivity to chemotherapy, and metastasis. Sci Transl Med *9*.
Vieth, B., Parekh, S., Ziegenhain, C., Enard, W., and Hellmann, I. (2019). A systematic evaluation of single cell RNA-seq analysis pipelines. Nat Commun *10*, 4667.
Von Hoff, D.D., Ervin, T., Arena, F.P., Chiorean, E.G., Infante, J., Moore, M., Seay, T., Tjulandin, S.A., Ma, W.W., Saleh, M.N., et al. (2013). Increased survival in pancreatic cancer with nab-paclitaxel plus gemcitabine. N Engl J Med *369*, 1691-1703.
von Koskull, H., and Virtanen, I. (1987). Induction of cytokeratin expression in human mesenchymal cells. J Cell Physiol *133*, 321-329.
Vorstandlechner, V., Laggner, M., Kalinina, P., Haslik, W., Radtke, C., Shaw, L., Lichtenberger, B.M., Tschachler, E., Ankersmit, H.J., and Mildner, M. (2020). Deciphering the functional heterogeneity of skin fibroblasts using single-cell RNA sequencing. FASEB J *34*, 3677-3692.

Waclaw, B., Bozic, I., Pittman, M.E., Hruban, R.H., Vogelstein, B., and Nowak, M.A. (2015). A spatial model predicts that dispersal and cell turnover limit intratumour heterogeneity. Nature *525*, 261-264.
Wang, W., Wang, Z., Tian, D., Zeng, X., Liu, Y., Fu, Q., Liang, A., Zhang, Y., Gao, Q., Cheng, J., et al. (2018). Integrin beta3 Mediates the Endothelial-to-Mesenchymal Transition via the Notch Pathway. Cell Physiol Biochem *49*, 985.
Wang, Y., Chaffee, T.S., LaRue, R.S., Huggins, D.N., Witschen, P.M., Ibrahim, A.M., Nelson, A.C., Machado, H.L., and Schwertfeger, K.L. (2020). Tissue resident macrophages promote extracellular matrix homeostasis in the mammary gland stroma of nulliparous mice. Elife *9*.
Wang, Y.J., Golson, M.L., Schug, J., Traum, D., Liu, C., Vivek, K., Dorrell, C., Naji, A., Powers, A.C., Chang, K.M., et al. (2016). Single-Cell Mass Cytometry Analysis of the Human Endocrine Pancreas. Cell Metab *24*, 616-626.
Wei, K., Korsunsky, I., Marshall, J.L., Gao, A., Watts, G.F.M., Major, T., Croft, A.P., Watts, J., Blazar, P.E., Lange, J.K., et al. (2020). Notch signalling drives synovial fibroblast identity and arthritis pathology. Nature.
Wei, S.C., Levine, J.H., Cogdill, A.P., Zhao, Y., Anang, N.A.S., Andrews, M.C., Sharma, P., Wang, J., Wargo, J.A., Pe'er, D., et al. (2017). Distinct Cellular Mechanisms Underlie Anti-CTLA-4 and Anti-PD-1 Checkpoint Blockade. Cell *170*, 1120-1133 e1117.
Weissmueller, S., Manchado, E., Saborowski, M., Morris, J.P.t., Wagenblast, E., Davis, C.A., Moon, S.H., Pfister, N.T., Tschaharganeh, D.F., Kitzing, T., et al. (2014). Mutant p53 drives pancreatic cancer metastasis through cell-autonomous PDGF receptor beta signaling. Cell *157*, 382-394.
Werner, S., and Smola, H. (2001). Paracrine regulation of keratinocyte proliferation and differentiation. Trends Cell Biol *11*, 143-146.
Wernig, G., Chen, S.Y., Cui, L., Van Neste, C., Tsai, J.M., Kambham, N., Vogel, H., Natkunam, Y., Gilliland, D.G., Nolan, G., et al. (2017). Unifying mechanism for different fibrotic diseases. Proc Natl Acad Sci U S A *114*, 4757-4762.
Whatcott, C.J., Diep, C.H., Jiang, P., Watanabe, A., LoBello, J., Sima, C., Hostetter, G., Shepard, H.M., Von Hoff, D.D., and Han, H. (2015). Desmoplasia in Primary Tumors and Metastatic Lesions of Pancreatic Cancer. Clin Cancer Res *21*, 3561-3568.
Willis, B.C., duBois, R.M., and Borok, Z. (2006). Epithelial origin of myofibroblasts during fibrosis in the lung. Proc Am Thorac Soc *3*, 377-382.
Wilm, B., Ipenberg, A., Hastie, N.D., Burch, J.B., and Bader, D.M. (2005). The serosal mesothelium is a major source of smooth muscle cells of the gut vasculature. Development *132*, 5317-5328.
Wojciechowicz, K., Gledhill, K., Ambler, C.A., Manning, C.B., and Jahoda, C.A. (2013). Development of the mouse dermal adipose layer occurs independently of subcutaneous adipose tissue and is marked by restricted early expression of FABP4. PLoS One *8*, e59811.
Xie, T., Wang, Y., Deng, N., Huang, G., Taghavifar, F., Geng, Y., Liu, N., Kulur, V., Yao, C., Chen, P., et al. (2018). Single-Cell Deconvolution of Fibroblast Heterogeneity in Mouse Pulmonary Fibrosis. Cell Rep *22*, 3625-3640.
Xiong, X., Kuang, H., Ansari, S., Liu, T., Gong, J., Wang, S., Zhao, X.Y., Ji, Y., Li, C., Guo, L., et al. (2019). Landscape of Intercellular Crosstalk in Healthy and NASH Liver Revealed by Single-Cell Secretome Gene Analysis. Mol Cell *75*, 644-660 e645.
Xu, W., Yang, X.W., Zhao, Z.Y., Dong, B., Guan, X.Y., Tian, X.Y., Qian, H.G., and Hao, C.Y. (2019). Establishment of pancreatic cancer patient-derived xenograft models and comparison of the differences among the generations. Am J Transl Res *11*, 3128-3139.
Yachida, S., Jones, S., Bozic, I., Antal, T., Leary, R., Fu, B., Kamiyama, M., Hruban, R.H., Eshleman, J.R., Nowak, M.A., et al. (2010). Distant metastasis occurs late during the genetic evolution of pancreatic cancer. Nature *467*, 1114-1117.
Yajima, I., Belloir, E., Bourgeois, Y., Kumasaka, M., Delmas, V., and Larue, L. (2006). Spatiotemporal gene control by the Cre-ERT2 system in melanocytes. Genesis *44*, 34-43.
Yamamoto, K., Venida, A., Yano, J., Biancur, D.E., Kakiuchi, M., Gupta, S., Sohn, A.S.W., Mukhopadhyay, S., Lin, E.Y., Parker, S.J., et al. (2020). Autophagy promotes immune evasion of pancreatic cancer by degrading MHC-I. Nature *581*, 100-105.
Yamazaki, T., and Mukouyama, Y.S. (2018). Tissue Specific Origin, Development, and Pathological Perspectives of Pericytes. Front Cardiovasc Med *5*, 78.
Yao, J., Ly, D., Dervovic, D., Fang, L., Lee, J.B., Kang, H., Wang, Y.H., Pham, N.A., Pan, H., Tsao, M.S., et al. (2019). Human double negative T cells target lung cancer via ligand-dependent mechanisms that can be enhanced by IL-15. J Immunother Cancer *7*, 17.
Yost, K.E., Satpathy, A.T., Wells, D.K., Qi, Y., Wang, C., Kageyama, R., McNamara, K.L., Granja, J.M., Sarin, K.Y., Brown, R.A., et al. (2019). Clonal replacement of tumor-specific T cells following PD-1 blockade. Nat Med *25*, 1251-1259.
Zafar, S.N., Siddiqui, A.H., Channa, R., Ahmed, S., Javed, A.A., and Bafford, A. (2019). Estimating the Global Demand and Delivery of Cancer Surgery. World J Surg *43*, 2203-2210.

Zeisberg, E.M., Potenta, S.E., Sugimoto, H., Zeisberg, M., and Kalluri, R. (2008). Fibroblasts in kidney fibrosis emerge via endothelial-to-mesenchymal transition. J Am Soc Nephrol *19*, 2282-2287.
Zeisberg, E.M., Tarnavski, O., Zeisberg, M., Dorfman, A.L., McMullen, J.R., Gustafsson, E., Chandraker, A., Yuan, X., Pu, W.T., Roberts, A.B., et al. (2007). Endothelial-to-mesenchymal transition contributes to cardiac fibrosis. Nat Med *13*, 952-961.
Zeisberg, M., and Duffield, J.S. (2010). Resolved: EMT produces fibroblasts in the kidney. J Am Soc Nephrol *21*, 1247-1253.
Zhang, D., Wang, Y., Shi, Z., Liu, J., Sun, P., Hou, X., Zhang, J., Zhao, S., Zhou, B.P., and Mi, J. (2015). Metabolic reprogramming of cancer-associated fibroblasts by IDH3alpha downregulation. Cell Rep *10*, 1335-1348.
Zhang, X., Liu, H., Hock, T., Thannickal, V.J., and Sanders, Y.Y. (2013). Histone deacetylase inhibition downregulates collagen 3A1 in fibrotic lung fibroblasts. Int J Mol Sci *14*, 19605-19617.
Zheng, B., Ohuchida, K., Chijiiwa, Y., Zhao, M., Mizuuchi, Y., Cui, L., Horioka, K., Ohtsuka, T., Mizumoto, K., Oda, Y., et al. (2016). CD146 attenuation in cancer-associated fibroblasts promotes pancreatic cancer progression. Mol Carcinog *55*, 1560-1572.
Zhou, X., Franklin, R.A., Adler, M., Jacox, J.B., Bailis, W., Shyer, J.A., Flavell, R.A., Mayo, A., Alon, U., and Medzhitov, R. (2018). Circuit Design Features of a Stable Two-Cell System. Cell *172*, 744-757 e717.
Ziegler, C.G.K., Allon, S.J., Nyquist, S.K., Mbano, I.M., Miao, V.N., Tzouanas, C.N., Cao, Y., Yousif, A.S., Bals, J., Hauser, B.M., et al. (2020). SARS-CoV-2 Receptor ACE2 Is an Interferon-Stimulated Gene in Human Airway Epithelial Cells and Is Detected in Specific Cell Subsets across Tissues. Cell *181*, 1016-1035 e1019.
Zunder, E.R., Finck, R., Behbehani, G.K., Amir el, A.D., Krishnaswamy, S., Gonzalez, V.D., Lorang, C.G., Bjornson, Z., Spitzer, M.H., Bodenmiller, B., et al. (2015). Palladium-based mass tag cell barcoding with a doublet-filtering scheme and single-cell deconvolution algorithm. Nat Protoc *10*, 316-333.